



HAL
open science

Optimal measurement strategies for quantum states and quantum channels estimation

Nadia Milazzo

► **To cite this version:**

Nadia Milazzo. Optimal measurement strategies for quantum states and quantum channels estimation. Quantum Physics [quant-ph]. Université Paris-Saclay; Eberhard-Karls-Universität (Tübingen, Allemagne), 2021. English. NNT : 2021UPASP050 . tel-03586181

HAL Id: tel-03586181

<https://theses.hal.science/tel-03586181v1>

Submitted on 23 Feb 2022

HAL is a multi-disciplinary open access archive for the deposit and dissemination of scientific research documents, whether they are published or not. The documents may come from teaching and research institutions in France or abroad, or from public or private research centers.

L'archive ouverte pluridisciplinaire **HAL**, est destinée au dépôt et à la diffusion de documents scientifiques de niveau recherche, publiés ou non, émanant des établissements d'enseignement et de recherche français ou étrangers, des laboratoires publics ou privés.



Optimal measurement strategies for
quantum states and quantum channels
estimation

*Stratégies de mesure optimales pour l'estimation
des états quantiques et des canaux quantiques*

**Thèse de doctorat de l'université Paris-Saclay et de
Eberhard-Karls-Universität Tübingen**

École doctorale n° 564, Physique en Île-de-France (PIF)

Spécialité de doctorat: Physique

Unité de recherche : Université Paris-Saclay, CNRS, LPTMS, 91405, Orsay, France

Référent : Faculté des sciences d'Orsay

**Thèse présentée et soutenue à Tübingen,
le 30/07/2021, par**

Nadia MILAZZO

Composition du Jury

Igor LESANOVSKY

Professeur, Universität Tübingen

Président

Otfried GÜHNE

Professeur, Universität Siegen

Rapporteur & Examineur

Jens SIEWERT

Professeur, Universidad del País
Vasco

Rapporteur & Examineur

Rosa TUALLE-BROURI

Professeure d'université, Institut
d'Optique Graduate School

Examinatrice

Direction de la thèse

Olivier GIRAUD

Directeur de Recherche - CNRS,
Université Paris-Saclay

Directeur de thèse

Daniel BRAUN

Professeur, Universität Tübingen

Co-Directeur de thèse

Acknowledgements

I would like to sincerely thank my supervisors, Prof. Daniel Braun and Dr. Olivier Giraud, for giving me the opportunity of doing this PhD, which was a very enriching experience for me. Their passion for science and for their work gave me great motivation during these years, their support and confidence helped me go through my "mid-PhD" crisis, their understanding in the final months let me taking my time to finish this thesis. It was great meeting them, both as scientists and as persons, and they have all my gratitude for the time they spent working on my project and for always being available for discussions and explanations, every time I needed.

The cotutelle agreement between Universität Tübingen and Université Paris-Saclay gave me the chance of getting to know two different cultures, two different cities, two different languages, two different research environments and finally, double the number of great colleagues and friends that anyone could hope for.

I would like to thank Fabian for all his explanations at the kick-off of this project, Martin for the countless discussions in our office, his precious help in understanding several problems and his proof-reading of the thesis, Lukas for always being happy and ready to help me, scientifically and with my bad German, and for his essential support with "all the cluster stuff", Cornelia and Marcel for welcoming me and for all the coffees together.

I want to thank Hao and Nina for being the perfectly balanced office mates, giving me both the concentration and recreation time I needed, and Mathieu for his patience during our French lessons on the train, the nice work done together and for never believing in my "endless PhD".

I moreover would like to say thank you to my friend and colleague Alessia, for her unconditional support, emotional and scientific, for her deep trust in me and for constantly reminding me how strong one can be, despite everything.

I want to truly thank all my friends, in Tübingen and in Paris, which shared these beautiful, and sometimes difficult, years with me, for all the wonderful experiences we lived together, and my lifelong friends for being close, even when far away.

I would like to thank my family, for making special each of the times I came back home, for all the consolatory "pacchi da giù" in my worst moments and for all their "welcome back" caring acts when I was with them.

Finally, I would like to express my heartfelt thanks to Gabriele, for always believing in me, for helping me with all my problems, from the tiny ones to the bigger ones, and simply for always being with me.

Titre : *Stratégies de mesure optimales pour l'estimation des états quantiques et des canaux quantiques*

Mots clés : intrication quantique, états quantiques, canaux quantiques, optimisation SDP, problème des moments tronqués, inférence bayésienne

Résumé : L'avancée rapide de la technologie de l'information quantique nécessite un contrôle et une manipulation précis des systèmes quantiques. En particulier, il est essentiel de certifier que les processeurs quantiques fonctionnent réellement de manière quantique, afin de valider les expériences et leurs résultats. Les principaux problèmes abordés dans cette thèse concernent la recherche de stratégies optimales pour l'estimation et la caractérisation des états et des canaux quantiques, avec un accent particulier sur les corrélations d'intrication. Nous avons considéré la certification de l'intrication à travers une partition donnée d'un système multi-qubit, lorsque seulement une information partielle sur l'état quantique correspondant est disponible ; nous avons abordé le problème avec un algorithme basé sur le problème des séquences de moments tronqués (tms), identifiant ainsi la séquence de mesure la plus efficace pour détecter l'intrication.

Nous avons également étudié le problème de la séparabilité des canaux quantiques en termes de représentation de la matrice de Choi ; dans ce cas, le cadre tms fournit une condition nécessaire et suffisante unifiée pour les différentes classes de séparabilité des canaux quantiques. Quelques résultats préliminaires sur les "tests fonctionnels quantiques" sont discutés ; nous avons utilisé des stratégies adaptatives bayésiennes pour obtenir une réponse sur le fonctionnement correct ou incorrect d'un dispositif quantique décrit par un seul paramètre dès que possible. Enfin, nous avons également mis en évidence la pertinence des notions d'information quantique par une connexion entre les domaines de l'information quantique, de la condensation de Bose-Einstein (BEC) et de la gravité analogue, en étudiant les propriétés d'intrication d'un BEC analogue à un trou noir.

Title : Optimal measurement strategies for quantum states and quantum channels estimation

Keywords : quantum entanglement, quantum states, quantum channels, SDP programming, truncated moment problem, Bayesian inference

Abstract : The rapid advance of quantum information technology requires precise control and manipulation of quantum systems; in particular, it is essential to certify that quantum processors truly work quantum mechanically, in order to validate experiments and their results. The main problems addressed in this thesis concern finding optimal strategies for the estimation and characterization of quantum states and channels, with a special focus on entanglement correlations. We considered the certification of entanglement across a given partition of a multi-qubit system, when only partial information about the corresponding quantum state is available; we tackled the problem with an algorithm based on the truncated moment sequences (tms) problem, thus identifying the most efficient measurement sequence to detect

entanglement. We furthermore investigated the problem of separability of quantum channels in terms of the Choi matrix representation; in this case, the tms framework provides a unifying necessary and sufficient condition for the different classes of separability of quantum channels. Some preliminary results about "quantum functional testing" are discussed; we used Bayesian adaptive strategies to obtain an answer of correct or wrong functioning of a quantum device described by a single parameter as soon as possible. Finally, we also highlighted the relevance of quantum information notions through a connection between the fields of quantum information, Bose-Einstein condensation (BEC) and analogue gravity, by studying the entanglement properties of a BEC analogue of a black hole.

Synthèse en français

Les progrès rapides de la technologie de l'information quantique exigent un contrôle et une manipulation précis des systèmes quantiques et de leurs propriétés. En particulier, il est essentiel de certifier que les processeurs quantiques fonctionnent réellement de manière quantique, afin de valider les expériences et leurs résultats. Le problème de la certification des états et des dispositifs quantiques est exigeant, et de nombreuses tentatives ont été faites pour trouver des moyens de tester efficacement leurs fonctionnalités de base, telles que leurs propriétés d'intrication. Les principaux problèmes abordés dans cette thèse concernent la recherche de stratégies optimales pour l'estimation et la caractérisation d'états et de canaux quantiques, avec un accent particulier sur les corrélations d'intrication.

Dans notre premier travail, nous avons considéré la certification de l'intrication à travers une partition donnée d'un système multi-qubit, lorsque seule une information partielle sur l'état quantique correspondant est disponible ; nous avons abordé le problème de la recherche de la meilleure stratégie de mesure en introduisant les statistiques des longueurs des séquences de mesure, en choisissant des mesures de Pauli multi-qubit comme observables. En utilisant un échantillon d'états inconnus aléatoires, nous avons pu identifier la séquence de mesure (en moyenne) la plus courte, c'est-à-dire la plus efficace, pour détecter l'intrication. L'étude a été réalisée à l'aide d'un algorithme basé sur le problème des séquences de moments tronqués (tms), qui fournit des conditions nécessaires et suffisantes pour l'intrication ou la séparabilité d'un état quantique d'un système de dimension finie. Cette étude aboutit à une stratégie très efficace, notamment pour les états symétriques, pour lesquels seule une infime fraction (10^{-6}) des états intriqués choisis au hasard ne sont pas détectés pour les systèmes de 6 qubits ou plus.

Dans notre deuxième travail, nous avons poursuivi le problème de la séparabilité des canaux quantiques pour répondre à la question de savoir si un dispositif quantique donné est capable de créer de l'intrication ou non. La représentation de la matrice de Choi, fournie par l'isomorphisme de Choi-Jamiołkowski, pose le problème en termes de systèmes et d'ancillas, donnant différentes classes de séparabilité selon la coupure considérée entre eux. Une fois de plus, le cadre tms s'est avéré bien

adapté à cette étude, donnant une approche unifiée pour les différents problèmes de séparabilité ; une solution a été trouvée en termes de tms associé aux coordonnées de l'état de Choi, dans une base fixe, et la programmation semi-définie a été utilisée pour obtenir un certificat de séparabilité. Nous avons exploré des exemples de familles de canaux à 2 qubits et à un seul qubit, pour lesquels notre algorithme peut donner une réponse dans les cas où d'autres critères ne sont pas concluants. Dans un autre travail, nous avons porté notre attention dans une direction différente, en mettant en évidence une connexion entre les domaines de l'information quantique, de la condensation de Bose-Einstein (BEC) et de la gravité analogique, montrant ainsi la pertinence des notions d'information quantique dans un contexte plus large. Nous avons étudié les propriétés d'intrication d'un BEC analogue à un trou noir, qui est décrit par un état gaussien à trois modes ; nous avons étudié les mesures d'intrication bipartites et tripartites basées sur la description de la matrice de covariance, à la fois à température nulle et à température finie, ce qui fournit la meilleure configuration expérimentale pour la détection d'intrication.

Dans une dernière étape de cette thèse, nous avons commencé à examiner différentes stratégies de mesure pour tester des dispositifs quantiques dont la fonctionnalité peut être décrite par un seul paramètre ; nous avons utilisé une approche bayésienne pour estimer ce paramètre, en exploitant les informations recueillies par les mesures pour mettre à jour une distribution de probabilité conditionnelle, sans avoir besoin d'estimer les valeurs attendues des observables. Le problème de la recherche du plan d'expérience optimal peut dans ce cas se traduire par l'optimisation d'une fonction d'utilité, qui guide habituellement le processus de mise à jour de manière adaptative à chaque étape ; nous avons essayé de surpasser cette approche en regardant non seulement l'étape suivante, mais aussi quelques autres, afin d'obtenir une réponse de bon ou mauvais fonctionnement le plus tôt possible. De plus, nous avons choisi l'état d'entrée du canal quantique en minimisant la probabilité d'erreur donnée par la distance de Chernoff entre les sorties d'un canal idéal et d'un canal défectueux ; enfin, nous avons considéré deux critères de décision finale différents et comparé leur efficacité.

Abstract

English The rapid advance of quantum information technology requires precise control and manipulation of quantum systems and of their properties; in particular, it is essential to certify that quantum processors truly work quantum mechanically, in order to validate experiments and their results. The problem of certification of quantum states and devices is a demanding one, thus many attempts have been put forward to find ways of efficiently test their basic functionalities, such as their entanglement properties. The main problems addressed in this thesis concern indeed finding optimal strategies for the estimation and characterization of quantum states and channels, with a special focus on entanglement correlations. In our first work we considered the certification of entanglement across a given partition of a multi-qubit system, when only partial information about the corresponding quantum state is available; we tackled the problem of finding the best measurement strategy introducing the statistics of lengths of measurement sequences, choosing multi-qubit Pauli-measurements as observables. Using a sample of random unknown states, we were able to identify the (on average) shortest, i.e. most efficient, measurement sequence to detect entanglement. The investigation was carried out with an algorithm based on the truncated moment sequences (tms) problem, which provides necessary and sufficient conditions for entanglement or separability of a quantum state of a finite dimensional system. This study results in a very efficient strategy especially for symmetric states, for which only a tiny fraction (10^{-6}) of randomly chosen entangled states are undetected for systems with 6 qubits or more. We continued in our second work with the problem of separability of quantum channels to answer the question whether a given quantum device is able to create entanglement or not. The Choi matrix representation, provided by the Choi–Jamiołkowski isomorphism, casts the problem in terms of systems and ancillas, giving different classes of separability depending on the cut considered between them. Once again, the tms framework turned out to be well suited for this study, giving a unifying approach for the different separability problems; a solution is found in terms of the tms associated to the coordinates of the Choi state, in a fixed basis, and semidefinite programming is used to get a separability certificate. We explored examples of

families of 2-qubit and single-qutrit channels, for which our algorithm can give an answer in cases where other criteria remain inconclusive.

In a further work we shifted our attention to a different direction, highlighting a connection between the fields of quantum information, Bose-Einstein condensation (BEC) and analogue gravity, thus showing the relevance of quantum information notions in a broader context. We studied the entanglement properties of a BEC analogue of a black hole, which is described by a three-mode Gaussian state; we investigated bipartite and tripartite entanglement measures based on the covariance matrix description, both at zero and finite temperature, providing the best experimental configuration for entanglement detection.

In a final stage of this thesis, we started looking at different measurement strategies for testing quantum devices whose functionality can be described by a single parameter; we used a Bayesian approach to estimate this parameter, exploiting the information collected through measurements to update a conditional probability distribution, without the need of estimating expected values of observables. The problem of finding the optimal experimental design can be in this case translated in the optimization of a utility function, which usually guides the update process adaptively at each step; we tried to outperform this approach looking ahead not only at the next step, but at a few ones, in order to obtain an answer of correct or wrong functioning as soon as possible. Moreover, we chose the input state for the quantum channel considered minimizing the error probability given by the Chernoff distance between the outputs of an ideal and a faulty channel; finally, we considered two different final decision criteria and compared their efficiency.

German Der rasante Fortschritt der Quanteninformationstechnologie erfordert eine präzise Kontrolle und Manipulation von Quantensystemen und deren Eigenschaften. Insbesondere ist es unerlässlich zu zertifizieren, dass Quantenprozessoren wirklich quantenmechanisch arbeiten, um Experimente und deren Ergebnisse zu validieren. Das Problem der Zertifizierung von Quantenzuständen und -geräten ist ein anspruchsvolles, und deshalb wurden viele Versuche unternommen, Wege zu finden, um ihre grundlegenden Funktionalitäten, wie z. B. ihre Verschränkungseigenschaften, effizient zu testen. Die Hauptprobleme, die in dieser Arbeit adressiert werden, betreffen in der Tat das Finden optimaler Strategien für die Schätzung und Charakterisierung von Quantenzuständen und -kanälen, mit einem besonderen Fokus auf Verschränkungskorrelationen.

In unserer ersten Arbeit betrachteten wir den Nachweis von Verschränkung über eine gegebene Partition eines Multi-QuBit Systems, wenn nur partielle Informationen über den entsprechenden Quantenzustand verfügbar sind. Wir beschäftigten uns mit

dem Problem die beste Messstrategie zu finden, indem wir die Statistik der Längen von Messsequenzen einführten und Multi-QuBit-Pauli-Messungen als Observablen wählten. Unter Verwendung einer Stichprobe von zufälligen unbekanntem Zuständen konnten wir die (im Durchschnitt) kürzeste, d.h. effizienteste Messsequenz zum Nachweis von Verschränkung identifizieren. Die Untersuchung wurde mit einem Algorithmus durchgeführt, der auf dem „truncated moment sequences“ (tms)-Problem basiert, das notwendige und hinreichende Bedingungen für Verschränkung oder Separabilität eines Quantenzustands eines endlich dimensional Systems liefert. Das Ergebnis dieser Untersuchung ist eine sehr effiziente Strategie insbesondere für symmetrische Zustände, bei der nur ein winziger Bruchteil (10^{-6}) zufällig gewählter verschränkter Zustände für Systeme mit 6 Qubits oder mehr unentdeckt bleibt.

In unserer zweiten Arbeit haben wir uns mit dem Problem der Separabilität von Quantenkanälen beschäftigt, um die Frage zu beantworten, ob ein gegebenes Quantengerät in der Lage ist, Verschränkung zu erzeugen oder nicht. Die Choi-Matrix-Darstellung, die durch den Choi-Jamiołkowski-Isomorphismus gegeben ist, stellt das Problem in Form von Systemen und Ancillas dar und gibt verschiedene Klassen der Separabilität in Abhängigkeit von dem betrachteten Schnitt zwischen ihnen. Wieder einmal erwies sich der tms-Ansatz als gut geeignet für diese Studie, da er einen vereinheitlichenden Ansatz für die verschiedenen Separabilitätsprobleme bietet. Eine Lösung wird in Form des tms gefunden, das mit den Koordinaten des Choi-Zustands in einer festen Basis verbunden ist, und semidefinite Programmierung wird verwendet, um die Separabilität zu zertifizieren. Wir haben Beispiele für Familien von 2-Qubit- und Ein-Qutrit-Kanälen untersucht, für die unser Algorithmus eine Antwort in Fällen geben kann, in denen andere Kriterien nicht schlüssig sind. In einer weiteren Arbeit lenkten wir unsere Aufmerksamkeit in eine andere Richtung, indem wir eine Verbindung zwischen den Bereichen Quanteninformation, Bose-Einstein-Kondensation (BEC) und analoger Gravitation aufzeigten und damit die Relevanz von Quanteninformationsbegriffen in einem breiteren Kontext zeigten. Wir untersuchten die Verschränkungseigenschaften eines BEC-Analogons eines Schwarzen Lochs, das durch einen dreimodigen Gauß-Zustand beschrieben wird; wir untersuchten für bipartite und tripartite Verschränkungsmaße, die auf der Beschreibung der Kovarianzmatrix basieren, sowohl am Temperatur-Nullpunkt als auch bei endlicher Temperatur, was die beste experimentelle Konfiguration für die Verschränkungsdetektion darstellt.

In einer letzten Phase dieser Arbeit haben wir begonnen, verschiedene Messstrategien für das Testen von Quantengeräten zu untersuchen, deren Funktionalität durch einen einzigen Parameter beschrieben werden kann; wir haben einen Bayes'schen Ansatz verwendet, um diesen Parameter zu schätzen, indem wir die durch Mes-

sungen gesammelten Informationen ausnutzen, um eine bedingte Wahrscheinlichkeitsverteilung zu aktualisieren, ohne die Notwendigkeit, erwartete Werte von Observablen zu schätzen. Das Problem, die optimale Einstellung des Experiments zu finden, kann in diesem Fall in die Optimierung einer Nutzenfunktion übersetzt werden, die normalerweise den Aktualisierungsprozess bei jedem Schritt adaptiv steuert; wir haben versucht, diesen Ansatz zu übertreffen, indem wir nicht nur den nächsten Schritt, sondern einige Schritte vorausschauend betrachtet haben, um so schnell wie möglich eine Antwort zu erhalten, ob die Funktion richtig oder falsch ist. Darüber hinaus wählten wir den Eingangszustand für den Quantenkanal unter Berücksichtigung der Minimierung der Fehlerwahrscheinlichkeit, die durch den Chernoff-Abstand zwischen den Ausgängen eines idealen und eines fehlerhaften Kanals gegeben ist; schließlich betrachteten wir zwei verschiedene endgültige Entscheidungskriterien und verglichen ihre Effizienz.

List of publications and personal contribution

List of publications

1. N. Milazzo, D. Braun, and O. Giraud, *Optimal measurement strategies for fast entanglement detection*, Phys. Rev. A **100**, 012328 (2019)
2. N. Milazzo, D. Braun, and O. Giraud, *Truncated moment sequences and a solution to the channel separability problem*, Phys. Rev. A **102**, 052406 (2020)
3. M. Isoard, N. Milazzo, N. Pavloff, and O. Giraud, *Bipartite and tripartite entanglement in a Bose-Einstein acoustic black hole*, Phys. Rev. A **104**, 063302 (2021)

Personal contribution of the candidate

No.	Author position	Scientific ideas (%)	Data generation (%)	Analysis and interpretation (%)	Paper writing (%)	Status
1	1	50	100	60	80	Accepted
2	1	50	100	70	70	Accepted
3	2	30	10	40	25	Accepted

Contents

1	Framework	1
1.1	Quantum entanglement	1
1.1.1	Entanglement detection	2
1.1.2	Quantum channels	3
1.1.3	Continuous variables	6
1.1.4	Monogamy of entanglement	7
1.2	Truncated moment problem and entanglement	8
1.2.1	Theory	9
1.2.2	Methods	11
2	Results	13
2.1	Optimal measurements for entanglement detection	14
2.2	A solution to the channel separability problem	19
2.3	Entanglement in an acoustic black hole	23
3	Discussion and future directions	28
3.1	Beyond the "myopic" approach: a case study	30
3.1.1	Chernoff distance	35
	Bibliography	39
	Appendix: publications	47

Chapter 1

Framework

1.1 Quantum entanglement

Quantum systems can exhibit properties which have no counterpart in the classical case; the most discussed in the last decades is a type of quantum correlation, called quantum entanglement [82, 72, 58, 20]. The reason for the interest of thousands of works in this quantum feature is not only fundamental, but practical too; indeed, many experiments are now able to generate and exploit entanglement, especially in quantum information and quantum computing tasks. Quantum entanglement came into the scene as a threat raised by the EPR paradox [36] to the completeness of quantum mechanics description of the physical reality through the wave function; this mysterious phenomenon, called initially "Verschränkung" by Schrödinger [86], was then clarified by Bell in [10] with his inequalities, giving start to the great interest around the topic. At present, not only has entanglement been created in laboratory among many qubits (e.g. 18 qubits in [96]) and survived over a distance of 1200 km among two qubits [100], but also it has been used in several applications, such as quantum teleportation [12], quantum cryptography [37] which ensures secure communication, and quantum algorithms, which are faster than their classical counterparts [63]. Finally, entanglement has become of fundamental importance for the ultimate goal of quantum computing, which are large-scale quantum computers [68, 83, 59]; these are expected to perform certain operations exponentially faster than classical computers [40]. Currently, quantum supremacy has been achieved by a quantum processor with 53 qubits in 2019 [5].

We shall now discuss the main ingredients about entanglement which will be useful for the results of this thesis.

1.1.1 Entanglement detection

Let us now discuss more formally how one can define an *entangled* state; in the following, we will consider finite dimensional systems, such as qubits. Let ρ be a mixed state acting on a Hilbert space $\mathcal{H} = \mathcal{H}_A \otimes \mathcal{H}_B$ of a composite system; the state ρ is entangled if it cannot be written as the convex sum of product states, that is

$$\rho \text{ is entangled} \Rightarrow \nexists \omega_i, \rho_i^A, \rho_i^B \text{ s.t. } \rho = \sum_i \omega_i \rho_i^A \otimes \rho_i^B \quad (1.1)$$

where $\omega_i \geq 0$, $\sum_i \omega_i = 1$ and ρ_i^A, ρ_i^B are density matrices acting on \mathcal{H}_A and \mathcal{H}_B respectively. If instead such weights and product states exist, then the state is said to be *separable*. Note that in Eq. (1.1) only two parties are considered, so that in this case one talks about bipartite entanglement. While for bipartite pure states the problem of separability is straightforward [87], for mixed bipartite states more complicated criteria are needed to answer the question of separability or entanglement; moreover, if we allow for more than two parties, that is we consider a multipartite state acting on $\mathcal{H} = \mathcal{H}_1 \otimes \mathcal{H}_2 \dots \otimes \mathcal{H}_N$, the problem of characterizing entanglement gets even more difficult and there is yet no fully general solution to it. Many separability criteria have been formulated [49], both in the bipartite and in the multipartite case; among the most known there are the PPT (positive partial transposition) criterion [80] and entanglement witnesses [73]. The former gives a necessary and sufficient condition for systems of dimensions 2×2 or 2×3 (otherwise it is only necessary) and it states that a state ρ acting on $\mathcal{H}_A \otimes \mathcal{H}_B$ is separable iff $\rho^{T_B} = (\mathbb{1}_A \otimes T_B)\rho \geq 0$, i.e. if the partial transposed state with respect to system B is positive semidefinite; this criterion is simple to apply, but limited in the multipartite case, since PPT entangled states exist (the so-called bound entangled states). Entanglement witnesses instead are based on directly measurable observables and thus are quite used experimentally; an observable W is called a witness if $\text{tr}(W\rho_S) \geq 0$ for all separable states ρ_S and $\text{tr}(W\rho_E) < 0$ for at least one entangled state ρ_E . This approach can be used for detecting both bipartite and multipartite entanglement and provides a clear geometrical picture: the expectation value $\text{tr}(W\rho)$ of an observable W depends linearly on the state and thus the set of states for which $\text{tr}(W\rho) = 0$ holds defines a hyperplane, dividing the set of all states in two parts; separable states lie in the part with $\text{tr}(W\rho) > 0$, while entangled states detected by W lie in the part with $\text{tr}(W\rho) < 0$.

Other criteria are based on algorithmic approaches, in particular on casting the separability problem in terms of convex optimization and semidefinite programming; one of the most known is the method of symmetric extensions [31, 32] which gives a

complete hierarchy of separability criteria and can be formulated as a semidefinite program. This approach was later understood more generally within the theory of truncated moment sequences, which will be further discussed in Sec. 1.2 and applied to get some of the results of this thesis in Sec. 2.1 and 2.2.

Some of the above separability criteria require full or partial a priori knowledge of the state; more precisely, knowledge of the density matrix describing the state corresponds to knowing the outcome of any possible measurement on the system. To estimate an unknown quantum state, a procedure called *quantum tomography* is applied; to do so, several copies of the state are needed, in order to perform different measure on each copy [28]. Full tomography soon becomes impractical; consider e.g. a system of N qubits, whose corresponding Hilbert space has dimension 2^N , then its density matrix, generally a mixed state ρ , is fully specified by $2^N - 1$ entries (because of the trace condition $\text{tr}(\rho) = 1$). Moreover, experimentally it is only possible to perform a finite number of measurements, so the uncertainty associated to the expectation values can yield unphysical states in the inversion procedure. Many attempts to overcome the difficulties of full tomography have been put forward, such as maximum likelihood estimation of the state [60], Bayesian inference [14], compressed sensing [48] or more recently machine learning based approaches [39]. We will see in Sec. 2.1 how partial information about the state of two qubits can suffice when the aim of the experiment is entanglement detection and in Sec. 3.1 how Bayesian inference works (no expectation values needed) in the context of verification of quantum channels; we revise some of the essential concepts of the latter in the next section.

1.1.2 Quantum channels

Quantum channels describe physical operations acting on quantum states; consider a state $\rho \in \mathcal{L}(\mathcal{H})$, where $\mathcal{L}(\mathcal{H})$ is the set of linear operators in \mathcal{H} , then we define a linear map $\Phi : \mathcal{L}(\mathcal{H}) \rightarrow \mathcal{L}(\mathcal{H})$ which acts on the state ρ as $\Phi(\rho) = \rho'$. The image ρ' has to be again a proper quantum state and this imposes some conditions on Φ , such as trace preservation and complete positivity [11]. The last property means that the map Φ is such that $\Phi \otimes \mathbb{1}$ is positive on all states acting on an extended Hilbert space $\mathcal{H} \otimes \mathcal{H}'$; the meaning of it becomes clearer defining the reshuffled matrix $D_\Phi = \Phi^R$, known as the dynamical matrix. The reshuffling operation for a matrix $\mathcal{M} \in \mathbb{M}_k$, with \mathbb{M}_k the set of square $k \times k$ matrices and $k = mn$, is defined as $(\mathcal{M}^R)_{ij} = \text{tr}((E_i \otimes E_j)^\dagger \mathcal{M})$, where $\{E_i\}$ and $\{E_j\}$ are the canonical basis in $\mathbb{M}_m, \mathbb{M}_n$ respectively [75]. In terms of the dynamical matrix, the complete positivity of Φ translates in $D_\Phi \geq 0$, i.e. D_Φ is positive semidefinite; when

written in the canonical basis, the dynamical matrix coincides with the so-called *Choi matrix* [24], defined as

$$C_\Phi = \sum_{i,j} \Phi(|i\rangle\langle j|) \otimes |i\rangle\langle j| \quad (1.2)$$

An important result that we will use in Sec. 2.2 is the *Choi-Jamiołkowski isomorphism* [61], which establishes a channel-state duality: to each map $\Phi : \mathcal{L}(\mathcal{H}) \rightarrow \mathcal{L}(\mathcal{H})$ we can associate an operator acting on an enlarged Hilbert space $\mathcal{H} \otimes \mathcal{H}'$, that is indeed the Choi state $C_\Phi / \dim(\mathcal{H})$, which is a proper density matrix. The Hilbert space \mathcal{H}' is the one of the so-called ancilla system, and in general can have different dimension than \mathcal{H} . The Choi matrix uniquely specifies the channel, and this turns out to be useful for example in studying the separability problem of quantum channels. As it will be motivated later, characterizing single and two-qubit channels is already of great importance for quantum information and quantum computing tasks. Single qubit channels can be parametrized as an affine transformation which maps the Bloch ball ¹ to an ellipsoid; if we indicate with \mathbf{n} the Bloch vector, then we can describe the action of a completely positive map as

$$\mathbf{n}' = \Lambda_\Phi \mathbf{n} + \mathbf{t}_\Phi \quad (1.3)$$

where the matrix Λ_Φ determines the shape of the ellipsoid and the vector t_Φ its center of mass. Positivity conditions of the Choi matrices corresponding to these maps give the well-known Fujiwara-Algoet conditions [42, 18]. As in the multipartite case of states [49], the entanglement problem for quantum channels also defines different classes of entanglement/separability depending on the partition, which in this case we will call cuts, between the systems and the ancillas. We will discuss the problem of entanglement for different examples of channels in Sec. 2.2, exploring the various classes of separability which are depicted in Fig. 1.1; to explain that, let us consider a bipartite system with subsystems A and B , a completely positive map $\Phi : \mathcal{L}(\mathcal{H}_A \otimes \mathcal{H}_B) \rightarrow \mathcal{L}(\mathcal{H}_A \otimes \mathcal{H}_B)$ and the corresponding Choi state $C_\Phi = \sum_{ijkl} \Phi(|ik\rangle\langle jl|) \otimes |ik\rangle\langle jl|$ acting on $\mathcal{H} = \mathcal{H}_A \otimes \mathcal{H}_B \otimes \mathcal{H}_{A'} \otimes \mathcal{H}_{B'}$ (where we assumed, without loss of generality, that the Hilbert space of the system and of the ancilla are equal). Fig. 1.1(a) describes an *entanglement-breaking* channel (EB) [57], which regards separability between the system and the ancilla (note that it can therefore be applied also to systems with only one subsystem); more precisely Φ is EB if $(\Phi \otimes \mathbb{1})(\rho)$ is a separable state across the $H - H'$ cut for any initial

¹Geometrical description of the space of 1-qubit systems, given by positive-semidefiniteness of the density matrix describing a generic 1-qubit mixed state.

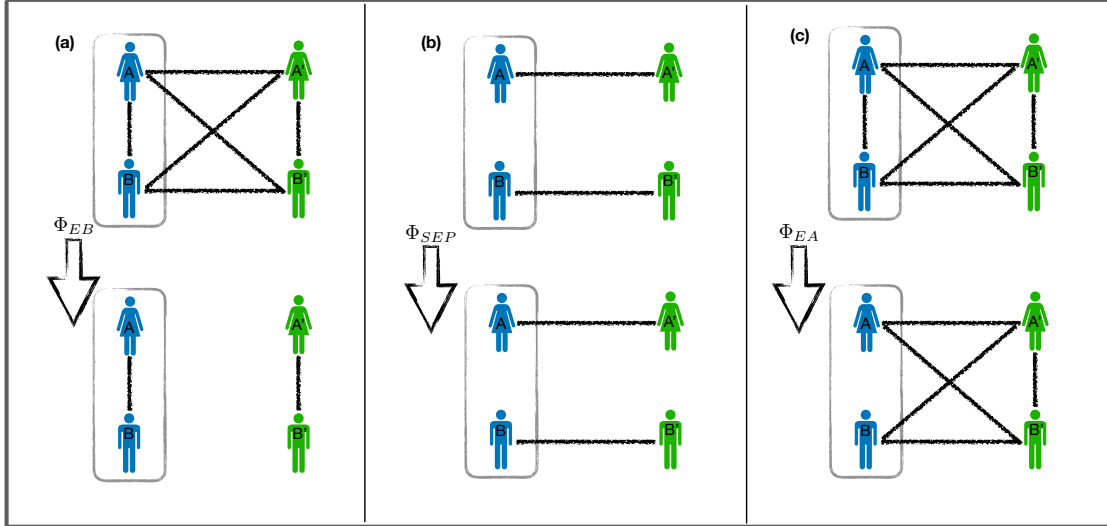


Figure 1.1: Different separability notions for quantum channels for a bipartite system AB with ancillas $A'B'$, where connections represent entanglement. (a) Entanglement-breaking channels destroy entanglement between A and all the ancillas and B and all the ancillas. (b) Separable channels preserve separability between $(A - A')$ and $(B - B')$. (c) Entanglement-annihilating channels destroy entanglement between A and B .

state ρ or if the corresponding C_Φ is separable across the $(A - B) - (A' - B')$ cut. Physically these channels correspond to the case in which the output state is prepared according to the measurement outcomes made by the sender and sent via a classical channel to the receiver. Fig. 1.1(b) corresponds instead to a *separable* map (SEP) [62], which is a channel that maps separable states to separable states; in particular, if we express Φ in terms of Kraus operators [11] as

$$\Phi(\rho) = \sum_m E_m \rho E_m^\dagger \quad \text{with} \quad \sum_m E_m^\dagger E_m = \mathbb{1} \quad (1.4)$$

then Φ is in SEP if $E_m = A_m \otimes B_m$. The corresponding state C_Φ is separable across the $(A - A') - (B - B')$ cut; this can be seen swapping $H_{A'}$ and H_B in C_Φ as

$$C_\Phi = \sum_m \sum_{i,j} A_m |i\rangle\langle j| A_m^\dagger \otimes |i\rangle\langle j| \otimes \sum_{k,l} B_m |k\rangle\langle l| B_m^\dagger \otimes |k\rangle\langle l|. \quad (1.5)$$

where $\sum_{i,j} A_m |i\rangle\langle j| A_m^\dagger \otimes |i\rangle\langle j|$ is the Choi matrix of the completely positive map $\rho \mapsto \sum_m A_m \rho A_m^\dagger$ (same for B). When C_Φ is separable across all possible cuts we call Φ a *fully separable* map (FS). Finally, Φ is called *entanglement-annihilating* [41] if it destroys any entanglement within the system H (but not necessarily between H and H'), as depicted in Fig. 1.1(c).

1.1.3 Continuous variables

In the sections above we have only discussed about finite dimensional systems, but also continuous variable ones are of interest in quantum information [19]; in particular, we summarize here some of the main results about *Gaussian states*, which are defined as those states which have a Gaussian Wigner function [92]. A nice consequence of this definition is that Gaussian states can be fully characterized by their first and second moments and so studied through the covariance matrix and the symplectic formalism [91]. For a N -mode Gaussian state, the $2N \times 2N$ *covariance matrix* (CM) σ , which is a real symmetric positive matrix, has entries

$$\sigma_{ij} = \frac{1}{2} \langle \hat{\xi}_i \hat{\xi}_j + \hat{\xi}_j \hat{\xi}_i \rangle - \langle \hat{\xi}_i \rangle \langle \hat{\xi}_j \rangle \quad (1.6)$$

where $\langle \hat{O} \rangle = \text{tr}(\rho \hat{O})$ and $\boldsymbol{\xi} = \sqrt{2}(\hat{q}_1, \hat{p}_1, \dots, \hat{q}_N, \hat{p}_N)^T$ is the vector of quadrature operators, whose components satisfy the canonical commutation relations

$$[\hat{\xi}_i, \hat{\xi}_j] = 2i\mathfrak{J} \quad \text{with} \quad \mathfrak{J} = \begin{pmatrix} 0 & 1 \\ -1 & 0 \end{pmatrix} \quad (1.7)$$

Since we are only interested in studying entanglement properties of Gaussian states, we can set the mean values of the quadrature operators to 0, as their shifting is given by displacement operators, that are local unitary operations, under which entanglement is unchanged. Positivity of the density matrix together with the canonical commutation relations impose that σ fulfills the inequality $\sigma + i\mathbb{J} \geq 0$ [92, 91], where \mathbb{J} is the direct sum of the N \mathfrak{J} matrices. Unitary operations of the second order in the quadrature operators instead act linearly on the vector of quadrature operators, i.e. $\boldsymbol{\xi} \rightarrow \mathcal{S}\boldsymbol{\xi}$ and \mathcal{S} satisfies $\mathcal{S}\mathbb{J}\mathcal{S}^T = \mathbb{J}$. The latter property implies that $\mathcal{S} \in \text{Sp}(2N, \mathbb{R})$, i.e. is real and *symplectic* [6]; since \mathcal{S} is a linear transformation on $\boldsymbol{\xi}$, from Eq. (1.6) it follows that σ transforms as $\sigma \rightarrow \mathcal{S}\sigma\mathcal{S}^T$. The symplectic framework is important for the analysis of covariance matrices; in particular, a useful result is *Williamson's theorem* [98], which ensures for any σ the existence of a symplectic transformation \mathcal{S} such that

$$\mathcal{S}\sigma\mathcal{S}^T = \text{diag}(\nu_1, \dots, \nu_N, \nu_1, \dots, \nu_N) = \nu \quad (1.8)$$

The matrix ν is called the canonical scaled diagonal form and is unique up to the ordering of the ν_j , which are known as the *symplectic eigenvalues*² of σ and they

²A nice physical interpretation of the symplectic eigenvalues can be seen in the case of a thermal state, for which they can be related with the mean particle number.

can be obtained from the eigenvalues of the matrix $\mathbb{J}\sigma$, which are equal to $\pm i\nu_j$. Moreover, the symplectic eigenvalues give a simple expression for the PPT criterion for continuous variables [90], which was shown to be necessary and sufficient for $1+N$ -mode Gaussian states and $M+N$ -mode bisymmetric Gaussian states [88]; the partial transposition operation on the covariance matrix σ is given by $\sigma^{PT} = \Lambda \sigma \Lambda$ with $\Lambda = \sigma_z \oplus \mathbb{1}_{2N}$ and the PPT criterion reads

$$\nu_j^{PT} \geq 1 \quad j = 1, \dots, N \quad (1.9)$$

as it can be easily derived looking at the condition imposed by the positivity of ρ^{PT} on σ^{PT} . Further applications of this formalism and discussion about entanglement for Gaussian states can be found in Sec. 2.3.

1.1.4 Monogamy of entanglement

Another peculiar feature which differentiates entanglement from classical correlations is its *monogamy*; entanglement being monogamous means that, if systems A and B are maximally entangled, then they cannot share entanglement with a third system C . This holds even if A and B are not in a maximally entangled state, but share anyway some entanglement; then the entanglement shareable with C is limited, meaning that it is possible to get an inequality which regulates how entanglement is distributed among many parties. The first result was given in [25] for the case of three qubits, leading to what is known as the *CKW inequality*:

$$\tau^{(1|2)} + \tau^{(1|3)} \leq \tau^{(1|23)} \quad (1.10)$$

where τ is a proper ³ measure of bipartite entanglement, called the tangle, defined as the square of the concurrence [55, 99]; not all measures of entanglement fulfill the relation in (1.10). This inequality can be extended to $n > 3$ qubits [78], but fails for systems of greater dimension (e.g. qutrits) [79]; it was moreover shown in [38] through a connection with the Minkowski space that strict monogamy laws for quantum correlations exist for all multi-qubit systems. From Eq. (1.10) an equality can be written, defining a residual tangle which quantifies the genuine tripartite entanglement between the three qubits:

$$\tau_{res} = \tau^{(1|23)} - \tau^{(1|2)} - \tau^{(1|3)} \quad (1.11)$$

³A good measure of entanglement needs to satisfy several properties [20], among which there are nonnegativity on inseparable states and monotonicity under LOCC (local operations and classical communications).

Eq. (1.11) is invariant under permutation of the qubits; the latter feature is lost when extending this result to continuous variables. In fact, an equivalent inequality was proved for Gaussian states of three modes [2] and for all n -mode Gaussian states [56]; the proper measure of entanglement in this case is called *Gaussian contangle* G_τ and it is given (for mixed states) by the infimum over all pure Gaussian states of the contangle E_τ , which is equal to the squared logarithmic negativity ⁴

$$G_\tau(\sigma) = \inf_{\sigma^p \leq \sigma} E_\tau(\sigma^p) \quad (1.12)$$

where p stands for pure and $\sigma^p \leq \sigma$ means that the matrix $\sigma - \sigma^p$ is positive semidefinite. The Gaussian contangle $G_\tau(\sigma)$ is an upper bound to the true contangle E_τ and they only coincide for pure Gaussian states. Analogously to Eq. (1.11) one can define a residual contangle G_τ^{res} [4] which this time is partition-dependent:

$$G_\tau^{res} = \min_{i,j,k} \left(G_\tau^{i|jk} - G_\tau^{i|j} - G_\tau^{i|k} \right) \quad (1.13)$$

We will apply definition (1.13) in Sec. 2.3 to quantify tripartite entanglement in an analogue gravity setting.

1.2 Truncated moment problem and entanglement

An interesting mapping of the entanglement problem onto the mathematical problem of truncated moment sequences was recently presented in [16]; the latter is a well-known subject in the mathematical literature [26, 71] which turned out to be very useful for the separability problem of quantum states and channels. Indeed, it allows to obtain necessary and sufficient conditions for deciding whether a state is entangled or separable, thanks to known theorems in the mathematical framework. Moreover, it provides an algorithm which, with known numerical methods, is able to give a definite answer for entanglement or separability of quantum states and channels. We will discuss the theory needed to understand this mapping in the next section, followed by a more detailed description of the resulting algorithm.

⁴The logarithmic negativity is defined as $E_\tau(\rho) \equiv \ln^2 \|\rho^{PT}\|_1$, where $\|\hat{O}\|_1 = \text{Tr} \sqrt{\hat{O}^\dagger \hat{O}}$ is the so-called trace norm.

1.2.1 Theory

Consider a nonnegative measure μ on \mathbb{R}^n and its corresponding moments y_α of order $\alpha = (\alpha_1, \dots, \alpha_n) \in \mathbb{Z}_+^n$ defined as

$$y_\alpha = \int x^\alpha d\mu(x) \quad (1.14)$$

where x^α denotes the monomial $x_1^{\alpha_1} \dots x_n^{\alpha_n}$. A finite set $y = (y_\alpha)_{\alpha \in \mathbb{Z}_+^n}$ of such real numbers is called a *truncated moment sequence* (tms). Suppose now that we are given any set y of real numbers, then we can ask whether it corresponds to the moments of some nonnegative measure μ ; if so, μ is called a *representing measure* for y (note that the measure μ is a probability measure if $y_0 = 1$). The tms problem concerns the characterization of such truncated sequences; solutions to this problem are known, and we are especially interested in the case when the measure μ is constrained to have a finite support K , defined by a semialgebraic set (the reason will be clearer when the correspondence with entanglement is made, as will be detailed below). In this case, which will be referred to as *K-tms* in the following, the moments y_α are given by

$$y_\alpha = \int_K x^\alpha d\mu(x) \quad (1.15)$$

where K is defined by polynomial inequalities as

$$K = \{x \in \mathbb{R}^n \mid g_1(x) \geq 0, \dots, g_m(x) \geq 0\} \quad (1.16)$$

with $g_j(x)$ multivariate polynomials. Necessary and sufficient conditions for the solution of the *K-tms* problem can be obtained in terms of moment matrices, their corresponding flat extensions and localizing matrices, which will all be defined below; for simplicity, we will consider here tms of even degree $2d$. The entries of the *moment matrix* of order t associated to a tms $y = (y_\alpha)_{|\alpha| \leq 2d}$ (with $|\alpha| = \sum_i \alpha_i$) are defined as $M_t(y)_{\alpha\beta} = y_{\alpha+\beta}$, with $|\alpha|, |\beta| \leq t$ [70]; it is a symmetric matrix and its size is given by the number of moments up to order t , that is $\binom{n+t}{t}$. The *localizing matrix* of order t is instead defined as the moment matrix of order t of a shifted sequence $g \star y$, which is given by $(g \star y)_\alpha = \sum_\gamma g_\gamma y_{\alpha+\gamma}$, where g_γ are the expansion coefficients over the basis of monomials x^α of the polynomials g_j in K . The m polynomials defining K give rise to m localizing matrices $M_t(g_j \star y)$; this implies that $t \leq d - d_0$ with

$$d_0 = \max_{1 \leq j \leq m} \{1, \lceil \deg(g_j)/2 \rceil\} \quad (1.17)$$

in order for all of them to be defined. Finally, we define an *extension* of a tms y of degree $2d$ as a tms of degree $2d'$ with $d' > d$, whose moments up to order $2d$ coincides with those of $(y_\alpha)_{|\alpha| \leq 2d}$; analogously, we can say that for $t' > t$, $M_{t'}(y)$ is an extension of $M_t(y)$. $M_{t'}(y)$ is a *flat* extension if its rank is equal to the rank of $M_t(y)$, that is,

$$\text{rk } M_{t'}(y) = \text{rk } M_t(y). \quad (1.18)$$

We will refer to Eq. (1.18) as the rank condition or flatness condition. We then have the following theorem [27]:

Theorem 1: *Let y be a tms and $r = \text{rk } M_t(y)$. Then y has a representing measure μ supported on K if and only if $M_t(y) \geq 0$ and there exists a flat extension $M_{t+d_0}(y)$ (i.e. satisfying the rank condition in Eq. (1.18)) with $M_t(g_j \star y) \geq 0$ for $1 \leq j \leq m$, and d_0 defined in Eq. (1.17).*

The representing measure μ can be written as a sum of r delta functions with positive weights, $d\mu(x) = \sum_j \omega_j \delta(x - x_j)$ and it is said to be *r-atomic*.

We can now apply this theorem to quantum states; consider a multipartite quantum state ρ acting on the tensor product $H = H^{(1)} \otimes \dots \otimes H^{(p)}$ of Hilbert spaces $H^{(i)}$ and let $S_{\mu_1 \mu_2 \dots \mu_p} = S_{\mu_1}^{(1)} \otimes \dots \otimes S_{\mu_p}^{(p)}$ be an orthogonal basis of $\mathcal{L}(H)$ (set of bounded linear operators on H). The state ρ can be expanded as

$$\rho = X_{\mu_1 \mu_2 \dots \mu_p} S_{\mu_1 \mu_2 \dots \mu_p} \quad (1.19)$$

(with implicit summation over repeated indices), where $X_{\mu_1 \mu_2 \dots \mu_p} = \text{tr}(\rho S_{\mu_1 \mu_2 \dots \mu_p})$ are the (real) coordinates of the state. Moreover, a density matrix acting on the single Hilbert space $H^{(i)}$ can be expanded as $\sum_{\mu_i} x_{\mu_i}^{(i)} S_{\mu_i}^{(i)}$, with $x_0^{(i)} = 1$; we can then associate to each $H^{(i)}$ a set of variables $x_{a_i}^{(i)}$, $1 \leq a_i \leq \kappa_i$, where $\kappa_i = \dim \mathcal{L}(H^{(i)}) - 1$. The vector of all these variables can be written as $(x_1, x_2, \dots, x_n) := (x_1^{(1)}, x_2^{(1)}, \dots, x_{\kappa_p}^{(p)})$, with $n = \sum_i \kappa_i$; an arbitrary monomial of these variables reads $x^\alpha \equiv \prod_{k=1}^n x_k^{\alpha_k}$. Finally, one can associate a tms $y = (y_\alpha)_{|\alpha| \leq p}$ of degree p with the coordinates of ρ as $y_\alpha = X_{\mu_1 \mu_2 \dots \mu_p}$, where α is the index such that $x^\alpha = \prod_{i=1}^p x_{\mu_i}^{(i)}$. We can now see that the problem of finding whether ρ is separable across the multipartition $H^{(1)} \otimes \dots \otimes H^{(p)}$ is equivalent to a K -tms problem; a quantum state ρ is separable if it can be written as $\rho = \sum_j \omega_j \rho_j^{(1)} \otimes \rho_j^{(2)} \otimes \dots \otimes \rho_j^{(p)}$. Projecting the separability condition on the basis $S_{\mu_1 \mu_2 \dots \mu_p}$, coordinates of a separable state can be written as

$$X_{\mu_1 \mu_2 \dots \mu_p} = \int_K x_{\mu_1}^{(1)} x_{\mu_2}^{(2)} \dots x_{\mu_p}^{(p)} d\mu(x) \quad (1.20)$$

Eq. (1.20) is equivalent to Eq. (1.15), i.e. to asking whether there exists a positive measure $d\mu$, with support K , for a tms whose moments y_α are given by the coordinates $X_{\mu_1\mu_2\dots\mu_p}$ of the state ρ as explained above. If a solution to this tms problem exists, as stated in Theorem 1, then the state ρ is separable.

1.2.2 Methods

Truncated K -moment problems can be solved numerically with *semidefinite programming* (SDP) [53, 97, 17]; semidefinite approaches have been proposed to test entanglement of quantum states in [32, 50] and then included in the framework of the tms problem in [16]. The advantage of the latter formulation (based on Theorem 1) is that it yields an algorithm which can give a certificate of entanglement or separability for a given quantum state; we recall the main ingredients here. In general, a semidefinite problem can be written as

$$\min_{\mathbf{z}} \mathbf{v}^T \mathbf{z} \quad s.t. \quad F(\mathbf{z}) \geq 0 \quad (1.21)$$

where \mathbf{v} is a vector of real numbers, \mathbf{z} is a vector of real variables and $F(\mathbf{z}) = F_0 + \sum_i z_i F_i$, with F_i real symmetric matrices; the inequality constraint in Eq. (1.21), called linear matrix inequality (LMI), means that the matrix $F(\mathbf{z})$ is positive semidefinite. The objective function to minimize in Eq. (1.21) is a convex function; this means that a local minimum is also a global one [67] and that interior point methods can be used to carry out the optimization [95]. If a solution to the optimization problem which fulfills the constraint in Eq. (1.21) exists, then the SDP is said to be feasible, otherwise is called infeasible.

For a given tms y_α of degree $2d$, we define an extension z_β of degree $2d'$ with $d' > d$, whose entries up to $2d$ are fixed by the ones of y_α . The SDP program associated to Theorem 1 can be defined as [16]

$$\begin{aligned} \min_z \quad & \sum_{\alpha, |\alpha| \leq t_0} v_\alpha z_\alpha \\ s.t. \quad & M_t(z) \geq 0 \\ & M_t(g_j \star y) \geq 0 \quad \text{for } j = 1, \dots, m \\ & z_\alpha = y_\alpha \quad \text{for } |\alpha| \leq 2d \end{aligned} \quad (1.22)$$

where $t_0 = d + d_0$ is the smallest extension order possible and v_α are random coefficients [54]. If the SDP in Eq. (1.22) is feasible, i.e. if it exists an extension z which fulfills the constraints above, then, in order to have a certificate of entanglement or separability, one needs to check the flatness condition in Eq. (1.18). A

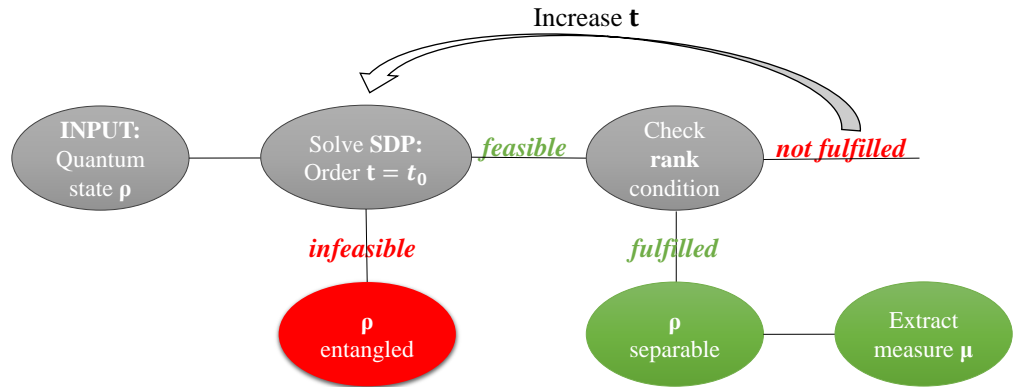


Figure 1.2: Sketch of the algorithm to solve a K -tms problem associated to a quantum state ρ with semidefinite programming. The output is a certificate of entanglement or separability.

sketch can be helpful in understanding how such an algorithm works (see Fig. 1.2). The algorithm takes as input a quantum state ρ , to which a tms y_α is associated, and starts constructing the smallest extension of the tms of order t_0 ; if the SDP is *infeasible*, then the algorithm stops and we can conclude that the state ρ is entangled. Otherwise, when the SDP is *feasible*, the rank condition is checked; if that is satisfied, i.e. if the extension is flat, then the state ρ is separable with respect to the partition of the Hilbert space considered and a representing measure μ can be extracted. If the flatness condition is not met, then the order t is increased and the algorithm is iterated; the only case in which the algorithm remains inconclusive (in a finite number of steps) is when feasible extensions are found for any t and any chosen polynomial v , but the flatness condition is never fulfilled.

We will see in Sec. 2.1 and Sec. 2.2 how the algorithm explained above can be adapted and applied to detect entanglement of quantum states and channels of finite dimensional systems.

Chapter 2

Results

The advance of quantum information technology and the rapid increase of quantum devices availability, together with the need of proper quantum states in experiments, lead the studies and consecutive results of this thesis. In particular, the problem of testing, characterizing and verifying properties of quantum systems is still very challenging. More precisely, one aims at proving that quantum devices truly work in a properly quantum way and that the states they act on are non-classical; moreover, one would like to do this as quickly as possible, since already testing basic quantum functionalities can be very expensive.

First motivation of our works is then the need for optimal experimental designs, whose objective is to reduce the amount of resources needed, trying to overcome the limits imposed by the exponential growth of the Hilbert space in which quantum systems act. Looking at the several efforts made in this direction, one can say that often the problem of stating the quantum nature of states and processors translates in asserting whether the state is entangled or whether the device is able to create entanglement. In fact, the latter is a resource on which quantum technology largely relies, making fast entanglement detection the second main motivation of our investigations, first focused on quantum states.

A quite natural continuation was then to explore how quantum entanglement evolves under physical operations (quantum channels), taking into account the difficulties represented by decoherence over long time scales; in this context, we directed our attention to separability testing, relevant in validation of experiments in which entanglement should be created.

A more general look at entanglement characterization led us also to consider detection and quantification of entanglement in a different area than quantum technology, at the interface between general relativity and quantum physics, revealing the utility of quantum information notions in a wider field.

However, present and future interest and extension of this work can be summarized in pursuing new methods and strategy for fast quantum channel certification, that we started investigating in the final chapter of this thesis; on a long-term basis, this would result in having an efficient framework as the one of classical functional testing, but for quantum devices, with the goal of demonstrating failure of quantum processors as quickly as possible.

We discuss the results obtained in more detail in the following sections.

2.1 Optimal measurements for entanglement detection

What is the most efficient measurement strategy to detect entanglement of a state with only partial information available on it? This question motivated the first application of the tms algorithm described in Sec. 1.2.2; indeed, as we have seen, information on a quantum state is collected performing measurements, each on a different copy of the system. In the mapping with the tms problem, expectation values of measurements correspond to moments of a measure; it is then quite natural to see how the tms framework suits the case of limited knowledge: we can in fact specify only a set \mathcal{A} of the moments up to a certain order and still have a problem which is solvable via a semidefinite program as illustrated in Fig. 1.2. The latter scenario is what is known as the \mathcal{AK} -tms problem [76].

Thanks to the flexibility of this approach, we were able to obtain a statistics of lengths of measurement sequences and to identify among them the best (i.e. fastest on average) to detect entanglement. The states considered here are two-qubit states, with a particular focus on symmetric two-qubit states (defined below), which offer already a quite rich and complex scenario; remarks are made and differences highlighted with the non-symmetric case, and also useful considerations are given for the case of symmetric multi-qubit states.

Symmetric qubit states can be conveniently handled via the so-called tensor representation presented in [44], which generalizes the Bloch sphere picture for spins-1/2; a mixed symmetric state is defined as the mixture of symmetric pure states, each of them being invariant under any permutation of the qubits and expressible as a superposition of Dicke states [30]. The latter can either be seen as symmetric states of $N = 2j$ spins-1/2 or as eigenstates $|j, m\rangle$ of angular momentum operators J_z and J^2 , with total angular momentum quantum number j . The state of a spin- j

can be expanded as

$$\rho = \frac{1}{2^N} \sum_{\mu_1, \mu_2, \dots, \mu_N=0}^3 X_{\mu_1 \mu_2 \dots \mu_N} P_s(\sigma_{\mu_1} \otimes \dots \otimes \sigma_{\mu_N}) P_s^\dagger \quad (2.1)$$

where σ_0 is the 2×2 identity matrix, $\sigma_1, \sigma_2, \sigma_3$ are the Pauli matrices and P_s is the projector onto the symmetric subspace spanned by the Dicke states, with dimension $2j + 1$. The tensor $X_{\mu_1 \mu_2 \dots \mu_N}$ is real, invariant under permutation of indices and can be written as

$$X_{\mu_1 \mu_2 \dots \mu_N} = \text{tr}(\rho \sigma_{\mu_1} \otimes \dots \otimes \sigma_{\mu_N}), \quad 0 \leq \mu_i \leq 3 \quad (2.2)$$

Unit trace of the density matrix translates into $X_{00\dots 0} = 1$ and, moreover, the tensor fulfills the property

$$\sum_{a=1}^3 X_{aa\mu_3\mu_4\dots\mu_N} = X_{00\mu_3\mu_4\dots\mu_N} \quad (2.3)$$

for any choice of the μ_i . We recognize at this point that these are the coordinates of the state to which we associated a tms problem as explained in Sec. 1.2.1 (see in particular Eq. (1.20)); these real entries correspond to the expectation values of the joint measurements $\sigma_{\mu_1} \otimes \dots \otimes \sigma_{\mu_N}$ on the N qubits and thus to the moments of the measure that we want to characterize. It can be shown that a symmetric separable state has the following tensor representation

$$X_{\mu_1 \mu_2 \dots \mu_N} = \sum_i \omega_i n_{\mu_1}^{(i)} n_{\mu_2}^{(i)} \dots n_{\mu_N}^{(i)} \quad (2.4)$$

with $\omega_i \geq 0$, $n_0^{(i)} = 1$ and $\mathbf{n}^{(i)}$ the Bloch vector of the single qubit; in this case, the semialgebraic set K is the unit sphere $K = \{\mathbf{x} \in \mathbb{R}^3 : x_1^2 + x_2^2 + x_3^2 = 1\}$, so that the smallest extension order given by d_0 in Eq. (1.17) is equal to 1.

At this point, we can ask two different questions, both relevant depending on the experimental limitations present: what is the best *set* of measurements, i.e. the most efficient to detect entanglement? On the other hand, what is instead the best *sequence* of measurements? In the first case, the order in which the measurements are performed is not relevant, while in the second case such order matters. We will see how in our case the two strategies converge to equivalent optimality, even if this is not the case in general.

We start by defining $\Omega_{\{M\}}$ as the sample space of outcomes of the \mathcal{AK} -tms algorithm applied to the moments $(y_\alpha)_{\alpha \in \mathcal{A}}$ of an entangled state, which contains two possible outcomes with the following probabilities: we denote with $p^{(k)} \equiv P(E, \{M\})$ the probability of detecting a state as entangled when the outcomes of a set of k

observables $\{M\}$ are known and with $1 - p^{(k)} \equiv P(\bar{E}, \{M\})$ the probability of not detecting the state as entangled. The outcome "E" corresponds to an infeasible SDP, while the outcome \bar{E} to a feasible SDP, meaning that the state with such moments fixed is still compatible with a separable state.

On the other hand, we can also define the probability of detecting entanglement at step k given that no entanglement was detected up to the step $k - 1$ when going down a certain ordered sequence of measurements, which we call a path γ ; we denote these probabilities with $q^{(k)}(\gamma)$. At last, we denote with $r^{(k)}(\gamma)$ the probability of stopping exactly at the k th step when measurements are taken along the path γ , which is relevant in terms of running or not the tms calculations.

The three probabilities are linked by simple relations of probability theory; in fact, e.g. for a set with $k = 2$ measurements, starting from the theorem of total probability we have

$$\begin{aligned} P(E, \{M_1, M_2\}) &= P(E, \{M_1\})P(E, \{M_1, M_2\}|E, \{M_1\}) \\ &\quad + P(\bar{E}, \{M_1\})P(E, \{M_1, M_2\}|\bar{E}, \{M_1\}) \\ \Rightarrow P(E, \{M_1, M_2\}|\bar{E}, \{M_1\}) &= \frac{P(E, \{M_1, M_2\}) - P(E, \{M_1\})}{1 - P(E, \{M_1\})} \\ \Rightarrow q^{(2)}(\gamma) &= \frac{p^{(2)}(\gamma) - p^{(1)}(\gamma)}{1 - p^{(1)}(\gamma)} \end{aligned} \quad (2.5)$$

where we used $P(\bar{E}, \{M_1\}) = 1 - P(E, \{M_1\})$ and $P(E, \{M_1, M_2\}|E, \{M_1\}) = 1$. Then in general we have $q^{(k)}(\gamma) = \frac{p^{(k)}(\gamma) - p^{(k-1)}(\gamma)}{1 - p^{(k-1)}(\gamma)}$.

We remark that $p^{(0)} = 0$ (as nothing is measured) and thus $q^{(1)} = p^{(1)}$; then, inverting Eq. (2.5) we obtain that $p^{(k)}(\gamma) = \sum_{j=1}^k q^{(j)}(\gamma) \prod_{n=j+1}^k (1 - q^{(n)}(\gamma))$.

The probabilities $r^{(k)}(\gamma)$ are instead the joint probability $P(E, \{M_1, \dots, M_k\} \cap \bar{E}, \{M_1, \dots, M_{k-1}\})$, which by means of the identity $P(A \cap B) = P(A|B)P(B)$, can be rewritten as $r^{(k)}(\gamma) = q^{(k)}(\gamma)(1 - p^{(k-1)}(\gamma))$ and so as

$$r^{(k)}(\gamma) = q^{(k)}(\gamma) \prod_{j=1}^{k-1} (1 - q^{(j)}(\gamma)) = p^{(k)}(\gamma) - p^{(k-1)}(\gamma) \quad (2.6)$$

Considering Pauli spin operators as observables, full tomography of a symmetric two-qubit state can be carried out with 8 measurements of the type $\sigma_i \otimes \sigma_j$; indeed, the tensor $X_{\mu_1 \mu_2}$ is in this case a symmetric 4×4 matrix with 10 unique entries, from which we discard $\mathbb{1} \otimes \mathbb{1}$ and the third diagonal $\sigma_z \otimes \sigma_z$ because of the property in Eq. (2.3), which reads $\sum_{a=1}^3 X_{aa} = X_{00}$. The probability to detect a state as entangled when only the outcomes of a subset of these 8 observables are known

must not depend on the choice of the reference frame for the axes along which the measurement is performed; this means that we can reduce the number of possible sets of measurements considering invariance with respect to the exchange of two axes or cyclic permutations of them. The number of the unique ones can be calculated and it reaches its maximum (26 unique sets) for sets of 4 measurements. To find the most efficient set at fixed length we tested a sample of 5×10^4 random states, generated according to [101]; we report the best set at each length in Table 2.1. These results served in making a simplification in the case of ordered sequences, in which we decided to fix the first measurement of the path to be the most efficient for $k = 1$, in order to reduce computational times. For the same reason, we considered that also the $8!$ sequence of measurements can be reduced defining a canonical representation of a path γ of length k : it is constructed starting from its equivalent list of k sets of length k' and then keeping the first one in lexicographical order among the ones that are obtained by relabelling of the axes; two paths are then equivalent if they have the same canonical representation. Again, the best path can be found testing a sample of thousands of random states; it is defined as the one that detects as quickly as possible (on average) whether the state is entangled. This can be expressed via the average depth at which the tms algorithm stops, and thus in terms of the $r^{(k)}(\gamma)$ probabilities as

$$d(\gamma) = \sum_{k=1}^8 k r^{(k)}(\gamma) \quad \Rightarrow \quad \gamma_{best} = \arg \min_{\gamma \in S} d(\gamma) \quad (2.7)$$

where S is the ensemble of all the inequivalent paths of length 8, which result to be 3228; $d(\gamma)$ corresponds to the number of measurements needed on average to detect a state as entangled, following the path γ . The minimum is found at $d = 3.07$ and it corresponds to measure first two of the diagonal entries $\sigma_i \otimes \sigma_i$ of the moment matrix (which for the property in Eq. (2.3) automatically give also the third) and then an off diagonal one $\sigma_i \otimes \sigma_j$. Note that, as for entanglement witnesses, we can give a geometrical picture of performing measurements in sequence, with the difference that our aim is not to choose an optimal entanglement witness, but to determine whether the hyperplane given by fixing a moment, or equivalently by the expectation value of the corresponding observable, cuts the convex set of separable states or not. If it does, it means that it is still not enough to detect entanglement; we then need to perform a second measurement, which fixes another hyperplane. If the region defined by the intersection of the two hyperplanes falls outside the set of separable states, then it means that measuring those two observables is sufficient for detecting the states in the intersection region as entangled.

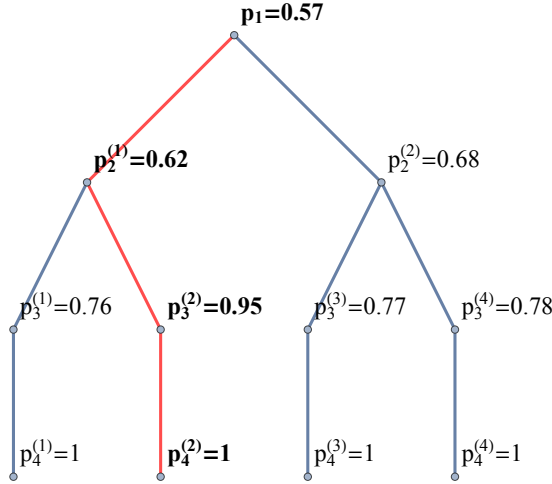


Figure 2.1: Counter-example showing that the best path does not always coincide with the one with highest probability at each level; in this binary tree of depth 4 the random probabilities satisfy the same constraint as in our case, i.e. $p^{(k-1)}(\gamma) \leq p^{(k)}(\gamma)$. It is easily verified that the best path, with $d(\gamma) = 1.8$, is the red one, even if at depth 2 it does not have the highest $p^{(2)}(\gamma)$.

Rewriting $d(\gamma)$ in terms of $p^{(k)}(\gamma)$, we can see the correspondence for the two optimal strategies (sets or paths): $d(\gamma) = 8p^{(8)}(\gamma) - p^{(7)}(\gamma) - p^{(6)}(\gamma) - \dots - p^{(1)}(\gamma)$; in our case, choosing the optimal set at each step k coincides with selecting the best path, which is not obvious, as can be confirmed by the counter example we found, illustrated in Fig. 2.1. We have seen how obtaining a distribution of lengths $d(\gamma)$ for a symmetric two-qubit system is already quite demanding; we started a similar investigation for the non-symmetric case, as the tms algorithm can deal in principle with any state, with no special symmetry and any number of subsystems. The semialgebraic set K is now defined by the product of two Bloch spheres and, while the order of the smallest extension stays the same, the size of the corresponding moment matrix increases, slowing down the computation (we will discuss more about the complexity of the algorithm in Sec. 2.2). The complexity of the non-symmetric case limited our study to partial knowledge up to 5 observables measured; full tomography involves now 15 observables in total and this time the maximum in the number of inequivalent sets is reached at $k = 7$ with 254 unique sets; the main difference with the symmetric case is the efficiency in detecting entanglement of the best set of measurement at same k , as we report in Table 2.1. Conversely, we were able to find a surprisingly efficient strategy for symmetric multi-qubit states, for which it suffices to look at the diagonal tensor entries, that are entries of the form $X_{\mu_1 \dots \mu_j \mu_1 \dots \mu_j}$ with $0 \leq \mu_i \leq 3$. As seen above, for a separable state they correspond to terms of the form $\sum_j \omega_j (n_{\mu_1} \dots n_{\mu_j})^{2j}$ and they are positive, since the n_{μ_i} are real and $\omega_j \geq 0$; this means that a negative value for any of

	k	Best set	P(E, {M₁, ..., M_k})
Symmetric	1	$\{M_{xx}\}$	~ 0.18
Symmetric Non-symmetric	2	$\{M_{xx}, M_{yy}\}$ $\{M_{x_1x_2}, M_{y_1y_2}\}$	~ 0.45 ~ 0.01
Symmetric Non-symmetric	3	$\{M_{xx}, M_{xy}, M_{yy}\}$ $\{M_{x_1x_2}, M_{y_1y_2}, M_{z_1z_2}\}$	~ 0.65 ~ 0.1
Symmetric Non-symmetric	4	$\{M_{xx}, M_{xz}, M_{yy}, M_{yz}\}$ $\{M_{x_1x_2}, M_{x_1y_2}, M_{y_1x_2}, M_{z_1z_2}\}$	~ 0.8 ~ 0.12
Symmetric Non-symmetric	5	$\{M_x, M_{xx}, M_{xz}, M_{yy}, M_{yz}\}$ $\{M_{x_1x_2}, M_{x_1y_2}, M_{y_1x_2}, M_{y_1y_2}, M_{z_1z_2}\}$	~ 0.82 ~ 0.23
Symmetric	6	$\{M_x, M_z, M_{xx}, M_{xz}, M_{yy}, M_{yz}\}$	~ 0.87
Symmetric	7	$\{M_x, M_z, M_{xx}, M_{xy}, M_{xz}, M_{yy}, M_{yz}\}$	~ 0.98

Table 2.1: Best set of measurements of length k for symmetric (up to $k = 7$) and non-symmetric states ($2 \leq k \leq 5$). In the symmetric case the notation M_{ij} denotes the joint measurement $\sigma_i \otimes \sigma_j$, while M_i stands for $\mathbb{1} \otimes \sigma_i$. In the non-symmetric case the notation $M_{i_1j_2}$ denotes the joint measurement $\sigma_{i_1} \otimes \sigma_{j_2}$.

the corresponding measurement operators translates into entanglement detection. Restricting the investigation to integer spin- j states (for $1 \leq j \leq 5$), the number of not detected entangled states (among the 10^6 random states tested) decreases with the spin size j , and already for $j = 4$ all the states in the sample are detected. Finally, we also highlighted the connection between the rate of detected entangled states and how quantum a state is, quantified by the quantumness as in [43]: we see that, the more quantum a state is, the faster it is detected as entangled.

2.2 A solution to the channel separability problem

Thanks to the generality offered by the tms approach, we were able to extend the results obtained for quantum states to the field of quantum channels, providing a necessary and sufficient condition for the separability problem; the latter translates again in the application of the tms algorithm, which gives a definite answer to the question whether a quantum channel is able to create entanglement or not. We exploit the Choi matrix representation of quantum channels and the channel-state duality described by the Choi-Jamiołkowski isomorphism, and explore three different classes of separability across different cuts between systems and ancillas, as discussed in Sec. 1.1.2. We recall that we consider a completely positive map

$\Phi : \mathcal{L}(\mathcal{H}_A \otimes \mathcal{H}_B) \rightarrow \mathcal{L}(\mathcal{H}_A \otimes \mathcal{H}_B)$ whose corresponding Choi state reads

$$C_\Phi = \sum_{ijkl} \Phi(|ik\rangle \langle jl|) \otimes |ik\rangle \langle jl| \quad (2.8)$$

It acts on $\mathcal{H} = \mathcal{H}_A \otimes \mathcal{H}_B \otimes \mathcal{H}_{A'} \otimes \mathcal{H}_{B'}$, with $S_{\mu_A \mu_B \mu_{A'} \mu_{B'}} = S_{\mu_A}^{(A)} \otimes S_{\mu_B}^{(B)} \otimes S_{\mu_{A'}}^{(A')} \otimes S_{\mu_{B'}}^{(B')}$ an orthogonal basis for \mathcal{H} ($S_\mu^{(\bullet)}$ are Hermitian matrices forming an orthogonal basis of the set of bounded linear operators on H_\bullet). Theorem 1 in Sec. 1.2.1 can be translated in a necessary and sufficient condition on the Choi matrix to be separable, according to the different cuts seen in Sec. 1.1.2 (EB, SEP and FS). We remark that the entanglement annihilating maps do not fit our setting, since only entanglement between the subsystems A and B is broken; such a scenario gives a necessary and sufficient condition in terms of the partial trace of the Choi state, which cannot be cast in a tms form. In fact, we want to decompose the Choi matrix as $\sum_k P_k \otimes Q_k$, where P_k and Q_k are positive operators acting on a different partition of the Hilbert space, depending on which cut is considered; also the semialgebraic set K is defined according to the decomposition we are interested in. We consider e.g. the EB case: conditions for K are obtained expanding P_k over a basis of operators S_λ^{AB} and Q_k over $S_{\lambda'}^{A'B'}$; then K is given by the positivity of the real expansion coefficients $c_\lambda, d_{\lambda'}$ as

$$\begin{aligned} \sum_{\lambda} c_{\lambda} S_{\lambda}^{AB} &\geq 0 \\ \sum_{\lambda'} d_{\lambda'} S_{\lambda'}^{A'B'} &\geq 0 \end{aligned} \quad (2.9)$$

Moreover, the Choi matrix can be written as $C_\Phi = \sum_{\lambda, \lambda'} X_{\lambda \lambda'} S_{\lambda}^{AB} \otimes S_{\lambda'}^{A'B'}$; the coordinates $X_{\lambda \lambda'}$ are then mapped to a tms of degree 2 (since we look for separability across a bipartition) $(y_\alpha)_{\alpha \leq 2}$, from which we can obtain necessary and sufficient conditions for channels as in Theorem 1:

Theorem 2:

(i) The channel Φ is EB if and only if, considering extensions $(y_\beta)_{\beta \leq 2t}$ of $(y_\beta)_{\beta \leq 2}$, there exists a flat extension $(y_\beta)_{\beta \leq 2(t+d_0)}$ of $(y_\beta)_{\beta \leq 2t}$ (possibly with $t = 1$), with $M_t(y) \geq 0$ and $M_t(g_j \star y) \geq 0$ for $j = 1, \dots, m$, where the g_j are polynomials of variables c_λ and $d_{\lambda'}$ defined by the conditions $\sum_{\lambda} c_{\lambda} S_{\lambda}^{AB} \geq 0$, $\sum_{\lambda'} d_{\lambda'} S_{\lambda'}^{A'B'} \geq 0$, and $d_0 = \max_{1 \leq j \leq m} \{1, \lceil \deg(g_j)/2 \rceil\}$.

(ii) The channel Φ is SEP if and only if, considering extensions $(y_\beta)_{\beta \leq 2t}$ of $(y_\beta)_{\beta \leq 2}$, there exists a flat extension $(y_\beta)_{\beta \leq 2(t+d_0)}$ of $(y_\beta)_{\beta \leq 2t}$ (possibly with $t = 1$), with $M_t(y) \geq 0$ and $M_t(g_j \star y) \geq 0$ for $j = 1, \dots, m$, where the g_j are polynomials of

variables c_λ and $d_{\lambda'}$ defined by the conditions $\sum_\lambda c_\lambda S_\lambda^{AA'} \geq 0$, $\sum_{\lambda'} d_{\lambda'} S_{\lambda'}^{BB'} \geq 0$, and $d_0 = \max_{1 \leq j \leq m} \{1, \lceil \deg(g_j)/2 \rceil\}$.

Finally, in the case of fully separable channels, the Choi matrix must be separable across any cut; it can be expanded as $C_\Phi = X_{\mu_A \mu_B \mu_{A'} \mu_{B'}} S_{\mu_A}^{(A)} \otimes S_{\mu_B}^{(B)} \otimes S_{\mu_{A'}}^{(A')} \otimes S_{\mu_{B'}}^{(B')}$, such that the coefficients $X_{\mu_A \mu_B \mu_{A'} \mu_{B'}}$ are mapped to a tms of order 4.

Theorem 2 gave us the possibility to investigate different examples of quantum channels through a tms algorithm analogous to the one for states; once one fixes the channel Φ , the algorithm takes only two inputs, the Choi state and the polynomials defining K . Moreover, keeping the second input fixed, we can easily go from one separability problem (SEP or EB) to another one swapping Hilbert spaces. Differently from the states case, specifying the coordinates of the Choi state does not directly correspond to fixing the expectation values of some physical observables, since the latter are now relative to the enlarged space system-ancilla. To get again that correspondence, we need to switch to the superoperator representation $\Phi_{ij,kl}$, obtained through a reshuffling operation in the computational basis; this results in measurements on the output state $\Phi(\rho_{input})$ (note that for another basis this results in general in a linear combination of physical measurements on the system).

We studied examples of 2-qubit and single qutrit channels, for which the set K is now different than the state case seen in Sec. 2.1, since it is not relative to single qubit, unless the FS case is considered. The polynomial inequalities in K can be written starting from the characteristic polynomials of the matrices in Eq. (2.9); they have degree 4 and thus $d_0 = 2$, as defined in Eq. (1.17). Our investigation was limited by the complexity of the SDP program applied to separability of quantum channels; in fact, while the fully separable case is still tractable for a generic 2-qubit channel, the EB and SEP problems become too complex. This can be quantified looking at the decision variables of the SDP, given by the number of free entries of the extension of the moment matrix $M_t(y)$ of order t , which corresponds to the number of monomials from n variables up to degree $2t$, that is $\binom{n+2t}{2t}$ (while the size of the moment matrix is $\binom{n+t}{t}$). Since the variables of the tms in Eq. (1.20) are $(x_\mu)_{1 \leq \mu \leq 15}$ for the system, $(x'_\mu)_{1 \leq \mu \leq 15}$ for the ancilla and the smallest extension possible is given by $t = 3$, the number of decision variables exceeds 10^6 and the numerics require too much time and memory. Moreover, the most common method to solve SDP is the Interior Point Method, which at each iteration requires the solution of a linear system with $O(N^3)$ complexity, where N is the number of linear constraints in the SDP involving all the n variables; finally, the number of semidefinite constraints is given by $\binom{n+t}{t} + m \binom{n+t-1}{t-1} + m \binom{n+t-2}{t-2}$, where m is the number of inequalities in the semialgebraic set for each set of variables. Even

though these figures make the complexity of the problem grow very fast, we were able to study three different families of channels:

Fully symmetric Choi states These are channels whose corresponding Choi matrix is a fully symmetric state, i.e.

$$(\mathbb{1} - P)C_\Phi(\mathbb{1} - P) = (\mathbb{1} - P)C_\Phi P = PC_\Phi(\mathbb{1} - P) = 0 \quad (2.10)$$

where for a 2-qubit channel P is the projection operator onto the symmetric subspace spanned by the Dicke states $P = \sum_{m=-2}^2 |D_4^{(m)}\rangle\langle D_4^{(m)}|$. If a fully symmetric state is separable with respect to an arbitrary partition, then it is fully separable; it follows that in this case we only need to explore the FS separability problem. We obtained results for symmetric states of 4 qubits (i.e. spin-2 states) in Sec. 2.1.

Planar channels These channels are given by a linear combination of tensor products of single-qubit planar channels, such as

$$\Phi = a\phi_{pl}^{(1)} \otimes \phi_{pl}^{(1)} + b\phi_{pl}^{(2)} \otimes \phi_{pl}^{(2)} \quad (2.11)$$

Recalling the definition of a single qubit channel in Eq. (1.3), planar channels are those that map the Bloch ball to a disk; more precisely, the matrix Λ_Φ can be rewritten, up to unitary rotations, as $diag(\lambda_1, \lambda_2, \lambda_3)$. Planar channels are the ones with one of the $\lambda_i = 0$; in Eq. (2.11) ϕ_{pl} can be either unital ($\mathbf{t}_\Phi=0$) or not, and positivity conditions depending on the λ_i s can be calculated accordingly. We chose to expand the corresponding Choi matrix over tensor products of Pauli matrices, resulting in a matrix invariant under partial transposition with respect to any qubit; this entails separability across the 1×3 bipartition as found in [65]. We can then still explore the three different classes of separability with the tms algorithm and the results for the $\sim 10^3$ tests done gave all full separability of the Choi states, leading us to conjecture that all the states corresponding to channels as in Eq. (2.11) are fully separable (this made investigation of the SEP and EB cases superfluous).

Qutrit channels Finally we considered damping qutrit channels defined as

$$\Phi_D : \zeta \rightarrow \zeta' = \Lambda \zeta \quad \text{with} \quad \Lambda = \text{diag}(\Lambda_1, \dots, \Lambda_8) \quad (2.12)$$

where $\zeta_i = \frac{3}{2} \text{tr}(\rho \lambda_i)$, $\rho = \frac{1}{3}(\mathbb{1} + \sum_{i=1}^8 \zeta_i \lambda_i)$ and the $\{\lambda_i\}$ are the Gell-Mann matrices. As done in [22], we set $\Lambda_{i \neq 3,8} = x$, $\Lambda_{i=3} = y$, $\Lambda_{i=8} = y^2$; the corresponding Choi state is a maximally mixed state for $x = y = 0$, while it corresponds to a maximally entangled state of two qutrits for $x = y = 1$. In this case only the EB problem is defined and the tms problem has degree 2; we compare the results obtained through the tms algorithm with the ones obtained in [22] via the negativity

	Rank condition	Size biggest moment matrices	Run-time
Fully symmetric	$\text{rk } M_3(y) = \text{rk } M_2(y)$	20×20	1s
Planar	$\text{rk } M_3(y) = \text{rk } M_2(y)$ $\text{rk } M_4(y) = \text{rk } M_3(y)$	165×165 495×495	10s/6min
Damping single-qutrit	$\text{rk } M_3(y) = \text{rk } M_1(y)$	969×969	5h

Table 2.2: Complexity of the moment problem in terms of the rank condition for the extensions explored and of the size of the highest order moment matrices involved. For the first two examples, the corresponding run-time for a single run of the algorithm refers to a standard computer with a 64bit Windows operating system, 4GB RAM and Intel Core i7 CPU 2.00GHz-2.60GHz, while for the third example a more powerful machine was used (a single run required between 150 and 300 GB of RAM).

$N(\rho) = \frac{1}{2}(\|\rho^{PT}\|_1 - 1)$, where $\|\rho^{PT}\|_1$ is the trace norm of the partial transpose with respect to the system qutrit. The negativity $N(\rho)$ cannot detect PPT-entangled states (meaning that there are entangled states with $N(\rho) = 0$). Our algorithm is instead able to give a certificate of separability (in the class EB) for states for which the negativity criterion remains inconclusive.

We give some more detailed figures of complexity and run-time for these three different examples in Table 2.2.

2.3 Entanglement in an acoustic black hole

Entanglement is a benchmark for the quantum nature of physical systems and for this reason is sometimes relevant also in settings apparently very far from the quantum information or quantum computing field. Here we considered the study of entanglement in an *analogue gravity* platform, such as a Bose-Einstein condensate (BEC), which is experimentally implementable; an extensive discussion of the background theory of analogue gravity and BECs (see e.g. [9] and [47]) is beyond the scope of this thesis, so we will limit ourselves to the essential notions needed to lay the ground for investigating entanglement, both its detection and quantification.

The idea of analogue black holes came from Unruh [94] after the prediction of Hawking radiation in [51, 52]; this radiation is so faint that it cannot be detected in our universe, so Unruh suggested that an acoustic analogue of a black hole may be implemented in a pipe: if the flow happens to be supersonic in some region of space, an acoustic wave emitted from this region will not be able to propagate

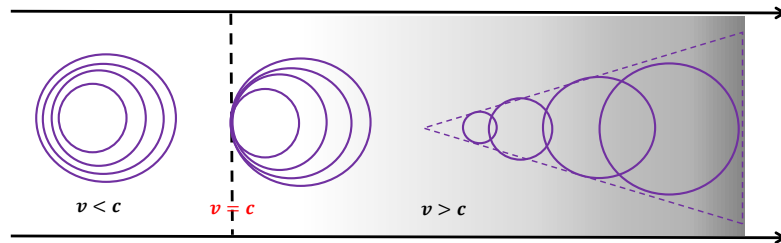


Figure 2.2: Sound waves propagation in a transonic flow which moves from left to right. In the subsonic region on the left the velocity v of the fluid is less than the speed of sound c and the sound waves propagate in all directions. v then reaches c at the sonic horizon (dashed line) and overcomes it on the right, in the supersonic region. The latter is indicated with a gray background to recall the analogy with the interior of the black hole; in this region, sound waves are dragged by the flow.

upstream and will be trapped, see Fig. 2.2. Therefore, sound waves play here the role of light, trapped in the interior of gravitational black holes. Unruh showed that these acoustic black holes should emit a faint sonic radiation, analogous to the Hawking radiation of gravitational black holes. This analogue radiation emerges from the *sonic horizon*, which corresponds to the boundary between the subsonic and the supersonic regions of the flow, as schematically depicted by the vertical dashed line in Fig. 2.2. Any sound wave crossing this horizon from the subsonic area to the supersonic region will be trapped, in analogy with a light wave passing through the "event horizon" of a gravitational black hole.

Beyond this kinematic picture, the analogy with the gravitational case becomes complete looking at the hydrodynamic equations for sound waves, which indeed in [94] were shown to correspond to the wave equation of a massless scalar field in a curved spacetime; moreover, once the sound field is quantized, it can be shown that the presence of a sonic horizon, which disconnects the subsonic and the supersonic region, leads to the spontaneous creation of particles (i.e. phonons) from the horizon, as in the Hawking radiation case.

Bose-Einstein condensates of atomic vapor are good candidates for studying analogue Hawking radiation, since they are quantum systems, thus they present quantum fluctuations that can lead to spontaneous emission of particles at the sonic horizon, and because the interactions between the atoms are well described

by *Bogoliubov theory* [15]; he suggested a perturbation theory which takes into account the interactions and which predicts the emergence of sound-like excitations from quantum fluctuations in the condensate. A one-dimensional analogue black hole configuration using a BEC has been experimentally realized [93, 29]; in order to obtain a sonic horizon, a proper external potential can be used to change the density profile and thus the velocity at which the excitations propagate along the condensate. It is then possible to modulate the flow velocity in order to create a subsonic and a supersonic region.

We considered a stationary flow of a one-dimensional BEC which is upstream subsonic and downstream supersonic in the so-called "*waterfall configuration*", in which the external potential used is a step function; in this case, analytical results can be obtained [69] and sound-like excitations propagate in the BEC according to a dispersion relation for the frequency ω of Bogoliubov type [81], which give rise to a scattering process onto the sonic horizon. In particular, in this setting, we have three different modes describing three different scattering processes which involve one or more propagation channels, both ingoing (towards the horizon) and outgoing (away from the horizon); any wave propagating along an ingoing channel will scatter at the horizon and be transmitted or reflected along different outgoing channels.

Each mode can be described by a quantum boson operator (i.e. the propagating modes behave as bosons satisfying the canonical commutation relations), resulting in two annihilation and one creation operators (the latter is due to negative norm of some of the channels [69, 84]); we denote the "*incoming*" modes with $(\hat{b}_0(\omega), \hat{b}_1(\omega), \hat{b}_2(\omega))$, corresponding to scattering processes initiated by a wave incident along one of the "in" channels directed towards the horizon, and analogously the "*outgoing*" ones with $(\hat{c}_0(\omega), \hat{c}_1(\omega), \hat{c}_2(\omega))$. In our picture, the mode associated with $\hat{c}_0(\omega)$ is denoted as the Hawking outgoing mode; indeed, it corresponds to a sound-like excitation travelling in the subsonic region and escaping from the sonic black hole, in analogy with the Hawking particle which escapes from the gravitational field of a black hole. The other two, associated with operators $\hat{c}_1(\omega)$ and $\hat{c}_2(\omega)$, are instead denoted as the companion and the partner respectively; the latter carries a negative energy and thus represents the counterpart of the partner particle involved in the Hawking pair produced in the gravitational case. Due to dispersive effects in the system, the presence of mode 2 is limited to a range of frequencies ω up to a frequency threshold Ω ; moreover, such a waterfall configuration is uniquely determined once the downstream (corresponding to the supersonic region) or upstream (subsonic region) Mach number is fixed. The latter is defined as $m_\alpha = \frac{V_\alpha}{c_\alpha}$, where V_α is the upstream ($\alpha = u$ and $m_u \leq 1$) or downstream

($\alpha = d$ and $m_d \geq 1$) velocity and c_α is the speed of sound in the BEC, which reads $c_\alpha = \sqrt{gn_\alpha/m}$, with g the coupling constant between the atoms of the condensate, n_α the atomic density of the BEC and m their mass.

The two sets of operators $\hat{\mathbf{b}}(\omega)$ and $\hat{\mathbf{c}}(\omega)$ can be expressed as linear combinations of each other, so a Bogoliubov transformation relating them can be found; in particular, the Bogoliubov transformation associated with this scattering process leads to a *three-mode Gaussian pure state*, given by the vacuum of the b modes $|0\rangle_b$ expanded over the Fock basis for excitations of c type.

This allowed us to explore entanglement of such state by means of the known results for Gaussian states discussed in Sec. 1.1.3 and Sec. 1.1.4. Bipartite entanglement of the three reduced two mode states can equally be detected by the PPT criterion in Eq. (1.9) or by the criterion found in [35], which is equivalent in this case to the violation of a Cauchy-Schwarz inequality for entangled modes pairs. We found that both criteria detect entanglement in the reduced states $0|2$ (Hawking-partner) and $1|2$ (companion-partner), while the reduced state $0|1$ is separable (Hawking-companion).

Nonetheless, the three modes share genuine tripartite entanglement, which we could quantify, since in the case of a three-mode pure Gaussian state explicit expressions for the residual contangle in Eq. (1.13) were found (see [4]); it results that the residual contangle only depends on the *local mixedness* a_i , which are defined as the inverse of the purity for the single-mode reduced states. In particular, the minimum in Eq. (1.13) is given by taking as reference mode i the one with the smallest a_i ; in our setting, at fixed $m_u = 0.59$ (corresponding to the experimental value found in Ref. [29]), this is realized by mode 1 up to a threshold frequency ω_c , above which a_0 becomes the smallest. The residual contangle diverges at $\omega \rightarrow 0$, while for higher frequencies rapidly decreases to zero and vanishes at the upper-bound frequency Ω ; this is expected since above this threshold mode 2 disappears and the tripartite state no longer exists. Moreover, we explored the behaviour of the residual contangle as a function of the Mach number; in fact, integrating $G_\tau^{\text{res}}(\omega)$ over all frequencies, we found that the amount of tripartite entanglement is maximal for $m_u = 0.14$, thus suggesting which is the best choice of parameters for an experimental measure of tripartite entanglement in the waterfall configuration of this one-dimensional condensate. Finally, tripartite entanglement of our state can be *unitarily localized* in a two-mode squeezed state [89] via a Bogoliubov transformation; this can be described via a simple equivalent optical setup using non-degenerate parametric down-conversion to create a two-mode squeezed state. If we identify one of the modes as the partner, then the other one, directed to a beam-splitter, generates the two other outgoing channels, respectively the companion and the Hawking mode.

We could extend the study of the bipartite entanglement for the Hawking-partner pair to the case in which the BEC has a *finite temperature*; in this case, our state is no more the vacuum and it is no more pure, but it is instead a mixed state, whose modes have a finite occupation number. Once again, the PPT and the Cauchy-Schwarz criterion gave the same results about the detection of bipartite entanglement, as a function of the frequency ω of the excitations and of the temperature T_{BEC} of the condensate, at fixed $m_u = 0.59$; as the temperature increases, the range of frequencies at which entanglement is present decreases, until $T_{BEC} \sim 1.8 g n_u$, above which entanglement is destroyed, thus suggesting experimentally a maximum temperature of the Bose gas when observation of entanglement is of interest. As before, we also explored the dependency on the Mach number at fixed T_{BEC} ; for low temperatures of the condensate, entanglement persists for a larger fraction of the frequency domain when m_u approaches 1, while this region is a lot reduced for temperatures $T_{BEC} \sim 1.8 g n_u$ and shifted to lower Mach numbers ($m_u < 0.6$).

At last, we moved our attention to the quantification at finite temperatures of bipartite entanglement of the Hawking pair, to underline the relevance of the approach based on the symplectic spectrum, and thus of the PPT criterion, instead of the Cauchy-Schwarz one, the latter being more often used in the context of analogue gravity setups. We defined as the "*PPT measure*" the quantity $1 - \nu_-^{PT}$, where ν_- is the smallest symplectic eigenvalue¹, and as the "*Cauchy-Schwarz parameter*" Δ_{CS} the quantity $\Delta_{CS} \equiv |\langle \hat{c}_0 \hat{c}_2 \rangle|^2 - \frac{(a_0-1)(a_2-1)}{4}$, where the mean value is taken over the mixed state at finite temperature; both quantities are nonnegative for entangled states. We show that, while the PPT measure is an entanglement monotone at any temperature, the Cauchy-Schwarz parameter is not, except for $T_{BEC} = 0$. The PPT approach should then be preferred for quantifying entanglement in the transsonic flow of a BEC at finite temperature.

¹see [3] for further explanations on the reason why only the smallest symplectic eigenvalue is enough.

Chapter 3

Discussion and future directions

The problem of efficient channel certification remains an open and expensive one; several methods have been proposed (see e.g. [64] for a recent review), such as randomized benchmarking or cross-entropy benchmarking (the latter was used in [5] for showing quantum supremacy of the latest processor mentioned in Sec. 1.1). Any certification protocol aims at obtaining an output which accepts or rejects the hypothesis that the quantum device is working correctly, providing also a corresponding level of confidence. In principle, since we are dealing with quantum processes, i.e. quantum maps acting on states, one could deal with this problem by certifying output states on a large set of input states or by considering the correspondence with the Choi state, as we did in Sec. 2.2 for entanglement properties of quantum maps. Nevertheless, these methods are not efficient enough and suffer of the so-called state preparation and measurement (SPAM) errors. More often certification problems can be translated into estimation problems, in which the functioning of the quantum device can be described by a finite number of parameters and one seeks estimating them with a certain precision. Especially suited for this type of processes are Bayesian updating methods, whose advantage is that single outcomes of experiments can be exploited (no need for mean values from many measurements). Core of these methods is the Bayes rule for conditional probabilities; suppose we perform the experiments $\mathbf{e} = \{e_1, e_2, \dots, e_n\}$ to infer the vector of unknown parameters \mathbf{x} and throughout the experimental process we collect the data $\mathbf{D} = \{d_1, d_2, \dots, d_n\}$, then we can write:

$$Pr(\mathbf{x}|\mathbf{D}) = \frac{Pr(\mathbf{D}|\mathbf{x})Pr(\mathbf{x})}{Pr(\mathbf{D})} \quad (3.1)$$

where the probability on the left hand side is referred to as the *posterior*, while $Pr(\mathbf{x})$ is called the *prior* and it contains any a priori knowledge on the parameters. $Pr(\mathbf{D}|\mathbf{x})$

is the *likelihood*, which in this context is represented by the Born rule, and finally $Pr(\mathbf{D})$ is a normalization factor. Analytic calculation of the probability distribution in (3.1) soon becomes impractical (after few experiments/updates), thus numerical methods, often involving Monte Carlo algorithms, have been implemented to overcome these difficulties; in the following we will consider the so-called *sequential* Monte Carlo algorithms (SMC) [33], where sequential indicates that data are processed sequentially, since the role of the prior for each successive datum is taken by the posterior from the last. The latter method, also known as particle filtering, approximates the prior continuous probability distribution $Pr(\mathbf{x})$ with a discrete approximation that can be written as $\sum_i \omega_i \delta(\mathbf{x} - \mathbf{x}_i)$, where the $\{\mathbf{x}_i\}$ are the locations of a set of "particles" (samples) and ω_i the corresponding "weights" (probabilities). From this expression, a particle filter $\{\omega'_i, \mathbf{x}'_i\}$ for the posterior probability distribution $Pr(\mathbf{x}|\mathbf{D})$ can be obtained, setting $\mathbf{x}'_i = \mathbf{x}_i$ and updating the weights as $\omega'_i = \omega_i Pr(\mathbf{D}|\mathbf{x}_i) / \sum_j \omega_j Pr(\mathbf{D}|\mathbf{x}_j)$. This update method suffers of numerical instability as data is collected, a problem known as impoverishment of the filter; solutions to it are known as resampling algorithms [34] which substitutes the impoverished filter with a new one that is not, but still approximates the same probability distribution, modifying the choice of particle locations.

This way of including new knowledge into the process of estimation naturally suggests adaptive strategies to perform at each update the best experiment possible; a lot of effort has been put in the context of Bayesian experimental design [21], which casts the problem of choosing the best experiment into the theoretical problem of optimizing a *utility function*. The latter quantity depends on the possible future designs/experiments $\mathbf{e}' = \{e_{n+1}, e_{n+2}, \dots, e_{n+m}\}$, the possible future data $\mathbf{D}' = \{d_{n+1}, d_{n+2}, \dots, d_{n+m}\}$ and the model parameters \mathbf{x} ; the optimal Bayesian design \mathbf{e}'^* , among the ones in the design space \mathbf{E} , is then the one that maximises the expected utility function [85, 45]:

$$\mathbf{e}'^* = \arg \max_{\mathbf{e}' \in \mathbf{E}} E[U(\mathbf{e}', \mathbf{x}, \mathbf{D}')] \quad (3.2)$$

where $E[\dots]$ denotes the expected value (which is taken over different variables depending on the choice of U) and $U(\mathbf{e}', \mathbf{x}, \mathbf{D}')$ is the utility function, which optimized at each step gives indeed a *sequential* or *adaptive* design (we will see that a step in the optimization can consist in one or more experiments, i.e. $m \geq 1$); if instead a unique \mathbf{e}'^* is used throughout the whole experiment, it is called a *static* design. In the former case, common choices of utility functions for parameter estimation problems are functions of the posterior covariance matrix or information-based utilities [85, 45], as e.g. the information gain (IG) [74] defined via the

Kullback-Leibler divergence (KLD) between the prior and the posterior distribution; omitting the dependence on \mathbf{e} and \mathbf{D} to simplify notation, we have:

$$IG(\mathbf{e}', \mathbf{D}') \equiv E_{\mathbf{x}|\mathbf{e}', \mathbf{D}'} \left[\log \frac{Pr(\mathbf{x}|\mathbf{e}', \mathbf{D}')}{Pr(\mathbf{x})} \right] = \int_{\mathbf{x}} Pr(\mathbf{x}|\mathbf{e}', \mathbf{D}') \log \frac{Pr(\mathbf{x}|\mathbf{e}', \mathbf{D}')}{Pr(\mathbf{x})} d\mathbf{x} \quad (3.3)$$

where the index of E indicates the variable for the expectation to be taken over. In the following we will consider two different options for the utility function U and see how they perform for a specific example of parameter estimation for a quantum channel.

3.1 Beyond the "myopic" approach: a case study

We consider the problem of testing a single-qubit quantum channel which rotates the input state of an angle θ around the \hat{z} axis; the action of such a device is completely characterized by the single parameter θ . We conceive of a scenario in which a company provides us with a device as described above and our aim is to verify, as soon as possible, whether it performs as the company states; more formally, we want to establish whether the true parameter θ_t characterizing the channel lies in the *confidence region* given by the company. In the case of a single parameter this region is simply an interval centered around the mean value θ_c estimated by the company; in the following we will refer to this interval as SPEC. The certification process consists then of two different stages; in the first one, we update the posterior probability distribution following an adaptive strategy, and in the second one we use a *decision criterion* to accept or reject the value θ_c given by the company.

Many adaptive experimental designs involve going only one step ahead in the future, which in terms of the notation used in Sec. 3 means to consider only one experiment and one outcome $\{e_{n+1}, d_{n+1}\}$; this is called the *myopic* approach and it is in general not optimal, since one should look ahead to *all* future observations and decisions that can be made at each step in the experiment. The last approach is known as *backward induction* [13] and it is computationally very expensive, so it remains limited to simple design problems, making myopic approaches more appealing for more complex problems. In the following we will use a strategy which goes beyond the single step optimization, but is anyway limited to a finite number of steps ahead ($1 \leq m \leq 4$) in the future observations. To this end, we use in Eq. (3.2) two different utility functions, the negative variance of the posterior distribution and the

expected information gain, which is usually addressed as the mutual information¹; considering a finite number l of possible outcomes for each experiment, the mutual information at fixed m is given by:

$$E_{\mathbf{x}, \mathbf{D}' | \mathbf{e}'} [IG] \equiv \overline{IG}^{(m)} = \sum_k w_k IG_k(\mathbf{e}', \mathbf{D}') \quad (3.4)$$

where k runs up to the total number of possible outcome sequences l^m , w_k is the probability of obtaining the k th sequence of outcomes of length m and IG_k is the information gain of the k th sequence. Note that in this case the prior distribution in Eq. (3.3) is not the one relative to the previous single step, but rather the one of m steps back.

Once we stop the update process (we will discuss below when it is reasonable to stop it in the case here considered) we can apply a decision criterion which allows us to express agreement or disagreement with the company; again, we consider two different options. The first criterion only relies on the position of the mean of the posterior distribution obtained, looking whether it falls inside or outside the SPEC; the second one instead compares the SPEC interval with a chosen *credible region* for the posterior distribution. We took the *highest posterior density* (HPD) region as the credible one, which in our case contains 95% of the probability mass; the overlap of this credible interval with the SPEC gives the decision method used in [66], which we will call the "HPD+SPEC" criterion. According to the latter, we accept the value θ_c estimated by the company if the 95% HPD credible region falls inside the SPEC, we reject it if it entirely falls outside. If the overlap is partial, this criterion remains inconclusive.

To start with the above certification process for the single-qubit rotation channel considered, which we denote as Φ^{rot} , we need to fix an initial input state $\rho_{in}^{(0)}$; we chose it as $\rho_{in}^{(0)} = |+\rangle\langle +|$ along the \hat{x} axis, as this state is more affected by a rotation around the \hat{z} axis and, moreover, since it maximises the Chernoff distance, as will be explained in Sec. 3.1.1. The experiment is carried out performing 2-outcome measurements, given by two POVM elements, e.g. projectors $\Pi_1^{(i)} = (\mathbb{I} + \sigma_i)/2$ ($\Pi_2^{(i)} = \mathbb{I} - \Pi_1^{(i)}$), with σ_i the Pauli matrices σ_x and σ_y (the one with σ_z gives no information in this case). The likelihood of obtaining one of the two outcomes is given by the Born rule $Tr(\Pi_{1,2}^{(i)} \rho_{out}^{(i)})$, where at the first update $\rho_{out} = \Phi^{rot}(\rho_{in}^{(0)})$.

To simulate an experiment, we choose as initial prior a uniform distribution over the $[-\pi, \pi]$ interval, we fix the true angle θ_t , the company angle θ_c and a SPEC

¹Formally, the mutual information corresponds to the KLD between the joint distribution $Pr(\mathbf{x}, \mathbf{D}' | \mathbf{e}')$ and the product of the marginal distributions for \mathbf{x} and \mathbf{D}' [85].

around it as $[\theta_c - \Delta\theta_c, \theta_c + \Delta\theta_c]$, where $\Delta\theta_c$ represents the uncertainty associated to the parameter θ_c given by the company. Moreover, we also introduce the possibility of choosing a third action besides the two measurements mentioned above, which consists in applying the channel again over the output state without measuring (this is practically implemented including the identity operator as possible measurement). The choice of this third action entails that the input state is not always reset to $\rho_{in}^{(0)}$ between the single experiments and, furthermore, that the likelihood will depend on $M\theta_t$, where M is equal to the number of times we chose the third action, with $M \leq m$.² Indeed, quantum mechanically, if one e.g. applies twice the rotation channel and then measures the qubit or measures twice the qubit after applying the rotation only once, they will get different outcome probabilities (for a small rotation angles θ , the leading term in the likelihood function increases to $\sim \theta^2$ from $\sim \frac{\theta^2}{2}$).

Assuming that there is only one true parameter, according to the central limit theorem (or to the Bernstein-von Mises theorem in the context of Bayesian inference), the posterior distribution tends toward a normal distribution for $N \gg 1$ measurements. In this case the width of the posterior distribution decreases as SD_{prior}/\sqrt{N} , where SD is the standard deviation. Using this information we can estimate after how many measurements it becomes reasonable to stop the update process, i.e. when the width of the posterior becomes comparable with that of a uniform distribution inside the SPEC. This is given by $N = \frac{\sigma_{prior}^2}{\sigma_{SPEC}^2}$, where σ^2 is the variance.

We show in the following some preliminary results obtained for $\theta_t = \pi/10$ and several values of θ_c with a fixed $\Delta\theta_c = \frac{\pi}{18}$; the fixed width of the SPEC gives $N \approx 300$. We find that the optimization over sequences of measurements using both the negative variance and the mutual information over a sequence gives an advantage, i.e. the final posterior distribution is narrower than the one obtained with the same number of measurements (but different number of updates) with the myopic approach. After few initial oscillations, the best sequence of measurements always coincides with the one which contains $M = m - 1$ times the identity, while in the myopic approach the third possible action is never chosen. We present the average values (over 2000 random samples) of the final posterior variance and the number of steps needed on average to reach the optimal measurement in Table 3.1, for sequences of measurements of length 1 to 4 and for both the utility functions considered. To compare the efficiencies of the different optimization methods, we calculate the probability of success (i.e. the probability of reaching the right

²It is actually possible to show that even without including this third possible action the joint probability of obtaining two outcomes successively is not always factorizable.

Measurement sequence length	Utility function	Average variance	Number of steps before optimal measurement sequence
1	MI	0.0033	
	VAR	0.0034	
2	MI	0.0017	5
	VAR	0.0017	8
3	MI	0.0012	12
	VAR	0.0012	7
4	MI	0.0012	14
	VAR	0.0009	8

Table 3.1: Average values (over 2000 random samples) of the final posterior variance and number of steps needed on average to reach the optimal measurement, for sequences of measurements of length 1 to 4 and for both the utility functions considered.

conclusion agreeing or disagreeing with the company) for the two different decision criteria; we recall that for the "HPD+SPEC" criterion we cannot in fact define a probability of error, since the cases of no success are actually inconclusive cases and one should continue the experiment doing more measurements³. Nonetheless, we consider here a fixed number of measurements ($N = 300$) and compare the success probabilities in this case.

We present the results for each utility function and decision method in Fig. 3.1, comparing sequences of 1, 2, 3 and 4 measurements. The calculations are performed with the Qinfer package [46] which uses SMC methods; in particular, we consider the credible region as there implemented, i.e. particles in the returned region are selected by including the highest-weight particles first until the desired credibility level (95%) is reached. Moreover, using a particle filter with 2000 particles, we found good agreement when comparing the numerical values of the MI for all length of the measurement sequences with the analytical ones, relative to the first update. We can see that the probability of success decreases and reaches the minimum value when the true angle θ_t almost coincides with one of the boundary of SPEC (here $\theta_t \simeq \theta_c - \Delta\theta_c$). Looking at the results for the decision criterion based on the position of the mean, we can estimate the statistical fluctuations looking at these minimum values of the probabilities, which in this case should all be equal to 1/2; in this way we get fluctuations of $\sim 5\%$. We can see that the probability of success for both criteria grow going from sequences of measurements of length 1 (myopic approach) to length 4; a deviation from this behaviour can be seen in

³Numerical tests show that the overlap between the posterior HPD and the SPEC does not decrease regularly as the variance; indeed the credible regions still oscillate after 350 updates (for an example download animation at [1]).

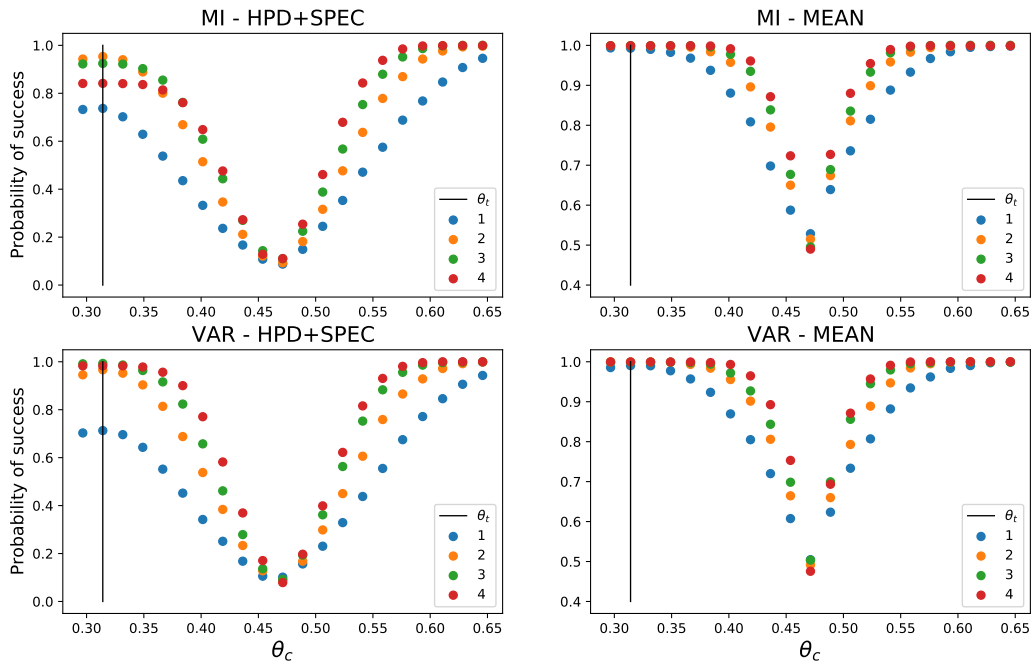


Figure 3.1: Success probabilities for different lengths of measurement sequences for the two utility functions considered, here indicated with MI and VAR, and for the two different final decision criterion, denoted as HPD+SPEC and MEAN. The calculations are performed with QInfer and the probabilities are averaged over 2000 random particle filters with 2000 particles. The probabilities increase going from length 1 to 4, with a deviation from this behaviour only of sequences of 4 measurements for MI with HPD+SPEC (first few points). The minimum is reached when $\theta_t \simeq \theta_c - \Delta\theta_c$ and fluctuations amount to $\sim 5\%$.

the case of mutual information optimization over sequences of length 4 with the HPD+SPEC criterion; indeed, the first few corresponding probabilities (see the upper-left panel in Fig. 3.1) are smaller than the ones for sequences of length 2 and 3. This deviation would require further investigation.

Finally, we compare in Fig. 3.2 the results presented in Fig. 3.1 only for sequences of length 4 to highlight which is the most efficient combination of adaptive measurement strategy and final decision criterion. We can conclude that both utility functions give greater and equal success probabilities using the position of the mean as final decision criterion.

Future directions of this study would include similar investigation for different rotation angles, extensions to $M > 4$ of the length of measurements sequence and generalizations to multi-parameter estimation problems.

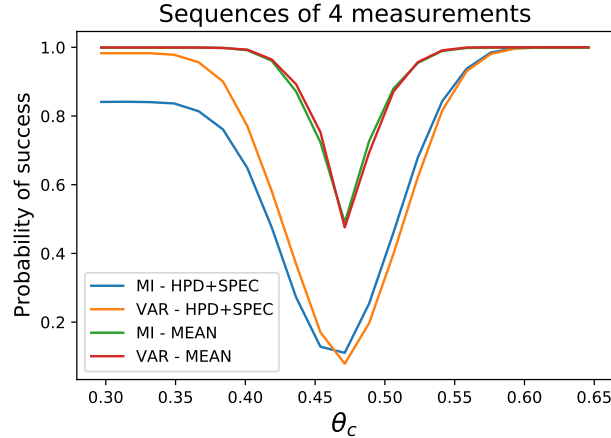


Figure 3.2: Success probabilities for measurement sequences of length 4 for the two utility functions considered, here indicated with MI and VAR, and for the two different final decision criterion, denoted as HPD+SPEC and MEAN. The calculations are performed with QInfer and the probabilities are averaged over 2000 random particle filters with 2000 particles. The position of the mean as final decision criterion results more efficient than HPD+SPEC and equally efficient for both utility functions.

3.1.1 Chernoff distance

Lastly, we investigated the problem of discriminating two different quantum channels; to this end, we considered the results obtained in the context of quantum hypothesis testing for quantum states (see e.g. [8]) and applied them to the output states returned by the channels considered. As in the previous section, we are interested in knowing whether a channel performs as intended more than estimating the characterizing parameters with high precision. In particular, we want to estimate the probability of error in stating that a given device does or does not work correctly (correct functioning corresponds to the one of an ideal channel). We considered here a special class of quantum channels, i.e. those which square to the identity operator, such as e.g. the Hadamard, the Not and the Z channels; the reason is that we want to answer the question:

Given e.g. a faulty Hadamard channel, is it easier (smaller probability of error) to conclude that the "squared" channel (applied twice to the input) does or does not act as the identity operator than saying whether it does or does not act as an ideal Hadamard channel?

To clarify the above statement, consider an input qubit channel prepared in the pure state $\psi_{in} = \frac{1}{\sqrt{2}}(|0\rangle + |1\rangle)$; the application of an ideal Hadamard gate will rotate it to the pure state $|0\rangle$. If one now measures the Pauli observable σ_x , they

will get the two possible outcomes $(+, -)$, each with probability $1/2$. If instead the Hadamard gate is applied twice to the input (equivalent to applying the identity) before measuring σ_x , the qubit is left in the state ψ_{in} and one will get the $+$ outcome with probability 1. When the two experiments are repeated several times, one will get a sequence of $(+, -, -, +, +, \dots)$ and one of $(+, +, +, +, +, \dots)$. If now instead the application of a faulty Hadamard gate is considered, one can see that it is easier to notice a deviation from the expected sequence of all $+$ than from the one of $+$ and $-$ with probability $1/2$.

Following the reasoning above, let us consider two quantum states ρ and τ acting on a finite-dimensional Hilbert space and occurring with prior probabilities π_0 and π_1 respectively; the probability of error P_e in distinguish two probability distributions decreases exponentially in the number of draws from the distributions, which we indicate with N . We thus have

$$P_{e,N} \sim e^{-N\xi} \quad (3.5)$$

The approximation in Eq. (3.5) becomes more and more precise when going to the asymptotic limit; in the classical case, the asymptotic error exponent was found by Chernoff in [23] and later generalized to the quantum case in [7, 77]. In the latter case, ξ corresponds to the quantum *Chernoff distance* ξ_{QCB} defined as

$$\xi_{QCB} = -\log\left(\inf_{0 \leq s \leq 1} \text{Tr}(\rho^{1-s}\tau^s)\right) = \lim_{N \rightarrow \infty} -\frac{1}{N} \log P_{e,N} \quad (3.6)$$

The quantity $\text{Tr}(\rho^{1-s}\tau^s)$ in Eq. (3.6) is real and non-negative for every $0 \leq s \leq 1$. We set τ as the output of the ideal channel and ρ as the output of the faulty channel; we can then maximize the Chernoff distance ξ_{QCB} over the possible input states to maximize the distinguishability of the outputs and thus obtain the fastest decay of $P_{e,N}$ possible. This always resulted in choosing pure states as input states.

The Hadamard (H), Not (X) and Z channels can all be explained as rotations on the Bloch sphere, which are in general written as $R_{\hat{n}}(\theta) = \exp\left(-i\frac{\theta}{2}\hat{n} \cdot \vec{\sigma}\right)$, where θ is the rotation angle, \hat{n} is the rotation axis and $\vec{\sigma}$ is the vector of Pauli matrices; H , X and Z all perform rotation of $\theta = \pi$, with $\hat{n} = \hat{x} + \hat{z}$, $\hat{n} = \hat{x}$ and $\hat{n} = \hat{z}$ respectively.

We considered both the case of a narrow distribution of the faultiness ε (i.e. $\delta(\varepsilon)$ corresponding to only one fixed value of ε) and of a broader distribution of errors, uniform on the interval $[0, 1/2]$, to see how the probabilities compare also when we are far from the ideal case.

We show in Fig. 3.3 the results for $P_{e,N}$ for the Z gate in the two scenarios above.

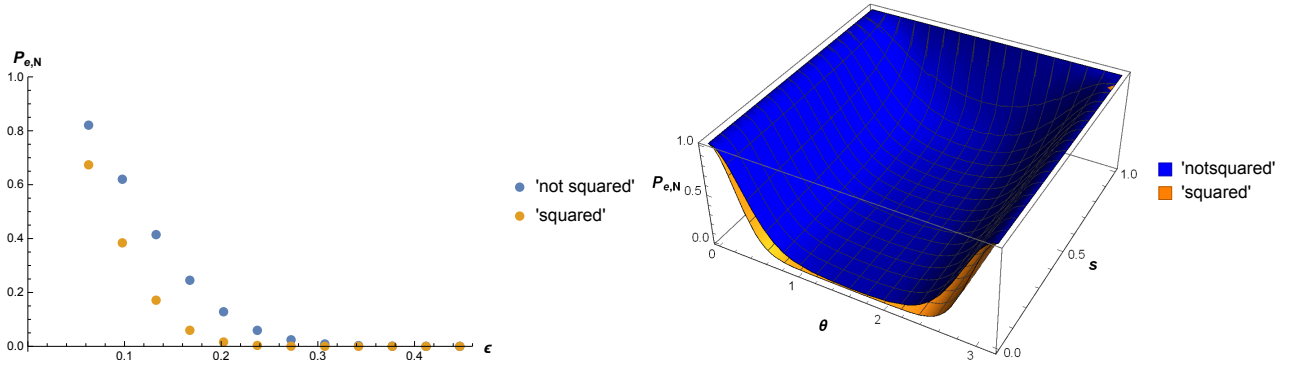


Figure 3.3: (left) Probabilities of error $P_{e,2N}$ ("not squared" case) and $P_{e,N}$ ("squared" case) as a function of ϵ ($N = 100$). Output states of the faulty and ideal Z gate are more distinguishable in the "squared" case; the minimum is reached for pure qubit states on the xy -plane. (right) Same probabilities for a uniform distribution $P(\epsilon)$ over $[0, 1/2]$ as a function of the exponent s in Eq. (3.6) and of the angle $\theta \in [0, \pi]$ in the usual representation of the Bloch sphere for one qubit states; the minimum probabilities of error are 1.6×10^{-2} and 4×10^{-4} for the "not squared" and "squared" case respectively.

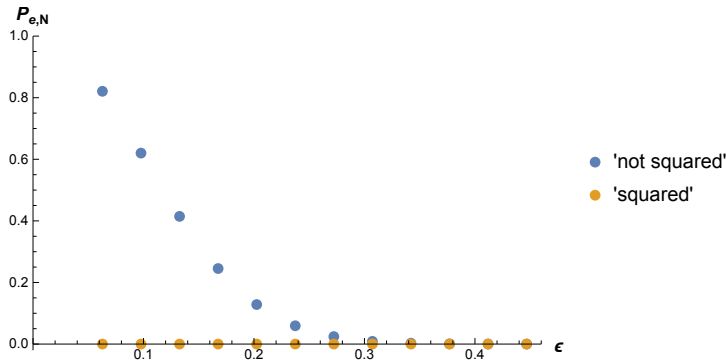


Figure 3.4: Probabilities of error $P_{e,2N}$ ("not squared" case) and $P_{e,N}$ ("squared" case) as a function of ϵ ($N = 100$). $P_{e,N}$ in the "squared" case decreases to zero faster than $P_{e,2N}$ in the "not squared" one.

We find that the Chernoff distance in Eq. (3.6) is always greater (states more distinguishable) in the "squared" case than in the "not squared" one; this means that the probability of error in discriminating the two channel outputs goes to zero faster in the "squared" case, i.e. they are more easily distinguishable. We remark that in order to make a fair comparison between the "squared" and "not squared" case we need to allow for a double number of draws N in the latter one. We see how the advantage of the "squared" case holds also in the case of a uniform distribution of errors. Analogous results are obtained for the Hadamard and Not gates. If we consider instead a channel which does not square to the identity operator, (e.g. a rotation channel with small rotation angle $\theta = \pi/10$ as in Sec. 3.1), the same behaviour for the error probabilities as for the Z channel can be seen only when the

distribution of errors is narrow and we are still close to the ideal case, while it is lost otherwise and it makes no difference to compare the ideal and faulty channel in the "not squared" or "squared" case. To conclude, we present the results in Fig. 3.4.

Bibliography

- [1] URL: https://unitc-my.sharepoint.com/:f:/g/personal/ptinm01_cloud_uni-tuebingen_de/EkvIMmgoiSxHseZbV8hq1ZMB4tcRUldc0v1FwQdGtg4v8g?e=tc0LaT.
- [2] Gerardo Adesso and Fabrizio Illuminati. “Continuous variable tangle, monogamy inequality, and entanglement sharing in Gaussian states of continuous variable systems”. In: *New Journal of Physics* 8 (Jan. 2006), pp. 15–15. DOI: [10.1088/1367-2630/8/1/015](https://doi.org/10.1088/1367-2630/8/1/015).
- [3] Gerardo Adesso, Alessio Serafini, and Fabrizio Illuminati. “Extremal entanglement and mixedness in continuous variable systems”. In: *Phys. Rev. A* 70 (2 Aug. 2004), p. 022318. DOI: [10.1103/PhysRevA.70.022318](https://doi.org/10.1103/PhysRevA.70.022318).
- [4] Gerardo Adesso, Alessio Serafini, and Fabrizio Illuminati. “Multipartite entanglement in three-mode Gaussian states of continuous-variable systems: Quantification, sharing structure, and decoherence”. In: *Phys. Rev. A* 73 (3 Mar. 2006), p. 032345. DOI: [10.1103/PhysRevA.73.032345](https://doi.org/10.1103/PhysRevA.73.032345).
- [5] Frank Arute et al. “Quantum supremacy using a programmable superconducting processor”. In: *Nature* 574.7779 (2019), pp. 505–510.
- [6] Arvind et al. “The real symplectic groups in quantum mechanics and optics”. In: *Pramana* 45.6 (1995), pp. 471–497. ISSN: 0973-7111. DOI: [10.1007/BF02848172](https://doi.org/10.1007/BF02848172).
- [7] K. M. R. Audenaert et al. “Discriminating States: The Quantum Chernoff Bound”. In: *Phys. Rev. Lett.* 98 (16 Apr. 2007), p. 160501. DOI: [10.1103/PhysRevLett.98.160501](https://doi.org/10.1103/PhysRevLett.98.160501).
- [8] Koenraad MR Audenaert et al. “Asymptotic error rates in quantum hypothesis testing”. In: *Communications in Mathematical Physics* 279.1 (2008), pp. 251–283.
- [9] Carlos Barceló, Stefano Liberati, and Matt Visser. “Analogue gravity”. In: *Living reviews in relativity* 14.1 (2011), pp. 1–159.

- [10] John S Bell. “On the einstein podolsky rosen paradox”. In: *Physics Physique Fizika* 1.3 (1964), p. 195.
- [11] Ingemar Bengtsson and Karol Zyczkowski. *Geometry of Quantum States: An Introduction to Quantum Entanglement*. Cambridge University Press, 2006. DOI: [10.1017/CB09780511535048](https://doi.org/10.1017/CB09780511535048).
- [12] Charles H. Bennett et al. “Teleporting an unknown quantum state via dual classical and Einstein-Podolsky-Rosen channels”. In: *Phys. Rev. Lett.* 70 (13 Mar. 1993), pp. 1895–1899. DOI: [10.1103/PhysRevLett.70.1895](https://doi.org/10.1103/PhysRevLett.70.1895).
- [13] José M Bernardo and Adrian FM Smith. *Bayesian theory*. Vol. 405. John Wiley & Sons, 2009.
- [14] Robin Blume-Kohout. “Optimal, reliable estimation of quantum states”. In: *New Journal of Physics* 12.4 (Apr. 2010), p. 043034. DOI: [10.1088/1367-2630/12/4/043034](https://doi.org/10.1088/1367-2630/12/4/043034).
- [15] N Bogoliubov. “On the theory of superfluidity”. In: *J. Phys* 11.1 (1947), p. 23.
- [16] F Bohnet-Waldraff, D Braun, and O Giraud. “Entanglement and the truncated moment problem”. In: *Phys. Rev. A* 96.3 (2017), p. 32312. DOI: [10.1103/PhysRevA.96.032312](https://doi.org/10.1103/PhysRevA.96.032312).
- [17] S. Boyd and L. Vandenberghe. *Convex Optimization*. Cambridge University Press, 2004.
- [18] Daniel Braun et al. “A universal set of qubit quantum channels”. In: *Journal of Physics A: Mathematical and Theoretical* 47.13 (Mar. 2014), p. 135302. DOI: [10.1088/1751-8113/47/13/135302](https://doi.org/10.1088/1751-8113/47/13/135302).
- [19] Samuel L. Braunstein and Peter van Loock. “Quantum information with continuous variables”. In: *Rev. Mod. Phys.* 77 (2 June 2005), pp. 513–577. DOI: [10.1103/RevModPhys.77.513](https://doi.org/10.1103/RevModPhys.77.513).
- [20] Dagmar Bruß. “Characterizing entanglement”. In: *Journal of Mathematical Physics* 43.9 (2002), pp. 4237–4251. ISSN: 00222488. DOI: [10.1063/1.1494474](https://doi.org/10.1063/1.1494474). arXiv: [0110078 \[quant-ph\]](https://arxiv.org/abs/0110078).
- [21] Kathryn Chaloner and Isabella Verdinelli. “Bayesian experimental design: A review”. In: *Statistical Science* (1995), pp. 273–304.
- [22] Agata Checińska and Krzysztof Wódkiewicz. “Fidelity and entanglement breaking properties of qutrit channels”. In: *Optics Communications* 283.5 (2010). Quo vadis Quantum Optics?, pp. 795–804. ISSN: 0030-4018. DOI: <https://doi.org/10.1016/j.optcom.2009.10.046>.

- [23] Herman Chernoff et al. “A measure of asymptotic efficiency for tests of a hypothesis based on the sum of observations”. In: *The Annals of Mathematical Statistics* 23.4 (1952), pp. 493–507.
- [24] Man-Duen Choi. “Completely positive linear maps on complex matrices”. In: *Linear Algebra and its Applications* 10.3 (1975), pp. 285–290. ISSN: 0024-3795. DOI: [https://doi.org/10.1016/0024-3795\(75\)90075-0](https://doi.org/10.1016/0024-3795(75)90075-0).
- [25] Valerie Coffman, Joydip Kundu, and William K. Wootters. “Distributed entanglement”. In: *Phys. Rev. A* 61 (5 Apr. 2000), p. 052306. DOI: [10.1103/PhysRevA.61.052306](https://doi.org/10.1103/PhysRevA.61.052306).
- [26] Raúl E. Curto and Lawrence A. Fialkow. “Truncated K-moment problems in several variables”. In: *Journal of Operator Theory* 54.1 (2005), pp. 189–226. ISSN: 03794024. arXiv: [0507067](https://arxiv.org/abs/0507067) [math].
- [27] Raul Curto and Lawrence Fialkow. “Solution of the truncated complex moment problem for flat data”. In: *Mem. Amer. Math. Soc* 568 (Jan. 1996). DOI: [10.1090/memo/0568](https://doi.org/10.1090/memo/0568).
- [28] G. Mauro D’Ariano, Matteo G.A. Paris, and Massimiliano F. Sacchi. “Quantum tomography”. In: *Advances in Imaging and Electron Physics* 128 (2003), pp. 205–308. ISSN: 10765670. DOI: [10.1016/S1076-5670\(03\)80065-4](https://doi.org/10.1016/S1076-5670(03)80065-4). arXiv: [0302028](https://arxiv.org/abs/0302028) [quant-ph].
- [29] Juan Ramon Munoz De Nova et al. “Observation of thermal Hawking radiation and its temperature in an analogue black hole”. In: *Nature* 569.7758 (2019), pp. 688–691.
- [30] R. H. Dicke. “Coherence in Spontaneous Radiation Processes”. In: *Phys. Rev.* 93 (1 Jan. 1954), pp. 99–110. DOI: [10.1103/PhysRev.93.99](https://doi.org/10.1103/PhysRev.93.99).
- [31] A. C. Doherty, Pablo A. Parrilo, and Federico M. Spedalieri. “Distinguishing Separable and Entangled States”. In: *Phys. Rev. Lett.* 88 (18 Apr. 2002), p. 187904. DOI: [10.1103/PhysRevLett.88.187904](https://doi.org/10.1103/PhysRevLett.88.187904).
- [32] Andrew C Doherty, Pablo A Parrilo, and Federico M Spedalieri. “Complete family of separability criteria”. In: *Phys. Rev. A* 69.2 (Feb. 2004), p. 22308.
- [33] Arnaud Doucet, Simon Godsill, and Christophe Andrieu. “On sequential Monte Carlo sampling methods for Bayesian filtering”. In: *Statistics and computing* 10.3 (2000), pp. 197–208.
- [34] Arnaud Doucet and Adam M Johansen. “A tutorial on particle filtering and smoothing: Fifteen years later”. In: *Handbook of nonlinear filtering* 12.656-704 (2009), p. 3.

- [35] Lu-Ming Duan et al. “Inseparability Criterion for Continuous Variable Systems”. In: *Phys. Rev. Lett.* 84 (12 Mar. 2000), pp. 2722–2725. DOI: [10.1103/PhysRevLett.84.2722](https://doi.org/10.1103/PhysRevLett.84.2722).
- [36] A. Einstein, B. Podolsky, and N. Rosen. “Can Quantum-Mechanical Description of Physical Reality Be Considered Complete?” In: *Phys. Rev.* 47 (10 May 1935), pp. 777–780. DOI: [10.1103/PhysRev.47.777](https://doi.org/10.1103/PhysRev.47.777).
- [37] Artur K. Ekert. “Quantum cryptography based on Bell’s theorem”. In: *Phys. Rev. Lett.* 67 (6 Aug. 1991), pp. 661–663. DOI: [10.1103/PhysRevLett.67.661](https://doi.org/10.1103/PhysRevLett.67.661).
- [38] Christopher Eltschka and Jens Siewert. “Monogamy Equalities for Qubit Entanglement from Lorentz Invariance”. In: *Phys. Rev. Lett.* 114 (14 Apr. 2015), p. 140402. DOI: [10.1103/PhysRevLett.114.140402](https://doi.org/10.1103/PhysRevLett.114.140402).
- [39] Christopher Ferrie. “Self-Guided Quantum Tomography”. In: *Phys. Rev. Lett.* 113 (19 Nov. 2014), p. 190404. DOI: [10.1103/PhysRevLett.113.190404](https://doi.org/10.1103/PhysRevLett.113.190404).
- [40] Richard P Feynman. “Simulating physics with computers”. In: *Int. J. Theor. Phys* 21.6/7 (1982).
- [41] Sergey N Filippov, Tomáš Rybár, and Mário Ziman. “Local two-qubit entanglement-annihilating channels”. In: *Physical Review A* 85.1 (2012), p. 012303.
- [42] Akio Fujiwara and Paul Algoet. “One-to-one parametrization of quantum channels”. In: *Phys. Rev. A* 59 (5 May 1999), pp. 3290–3294. DOI: [10.1103/PhysRevA.59.3290](https://doi.org/10.1103/PhysRevA.59.3290).
- [43] Olivier Giraud, Petr Braun, and Daniel Braun. “Quantifying quantumness and the quest for Queens of Quantum”. In: *New Journal of Physics* 12.6 (2010), p. 63005.
- [44] O. Giraud et al. “Tensor Representation of Spin States”. In: *Phys. Rev. Lett.* 114 (8 Feb. 2015), p. 080401. DOI: [10.1103/PhysRevLett.114.080401](https://doi.org/10.1103/PhysRevLett.114.080401).
- [45] Christopher E Granade et al. “Robust online Hamiltonian learning”. In: *New Journal of Physics* 14.10 (2012), p. 103013.
- [46] Christopher Granade et al. “QInfer: Statistical inference software for quantum applications”. In: *Quantum* 1 (Apr. 2017), p. 5. ISSN: 2521-327X. DOI: [10.22331/q-2017-04-25-5](https://doi.org/10.22331/q-2017-04-25-5).
- [47] Allan Griffin, David W Snoke, and Sandro Stringari. *Bose-einstein condensation*. Cambridge University Press, 1996.

- [48] David Gross et al. “Quantum State Tomography via Compressed Sensing”. In: *Phys. Rev. Lett.* 105 (15 Oct. 2010), p. 150401. DOI: [10.1103/PhysRevLett.105.150401](https://doi.org/10.1103/PhysRevLett.105.150401).
- [49] Otfried Gühne and Géza Tóth. “Entanglement detection”. In: *Physics Reports* 474.1-6 (2009), pp. 1–75. ISSN: 03701573. DOI: [10.1016/j.physrep.2009.02.004](https://doi.org/10.1016/j.physrep.2009.02.004). arXiv: [0811.2803](https://arxiv.org/abs/0811.2803).
- [50] Aram W Harrow, Anand Natarajan, and Xiaodi Wu. “An Improved Semidefinite Programming Hierarchy for Testing Entanglement”. In: *Communications in Mathematical Physics* 352.3 (2017), pp. 881–904. ISSN: 1432-0916. DOI: [10.1007/s00220-017-2859-0](https://doi.org/10.1007/s00220-017-2859-0).
- [51] Stephen W Hawking. “Black hole explosions?” In: *Nature* 248.5443 (1974), pp. 30–31.
- [52] Stephen W Hawking. “Particle creation by black holes”. In: *Communications in mathematical physics* 43.3 (1975), pp. 199–220.
- [53] J William Helton and Jiawang Nie. “A semidefinite approach for truncated K-moment problems”. In: *Found. Comput. Math.* 12.6 (2012), pp. 851–881.
- [54] Didier Henrion and Jean-Bernard Lasserre. “Detecting global optimality and extracting solutions in GloptiPoly”. In: *Positive polynomials in control*. Springer, 2005, pp. 293–310.
- [55] Scott Hill and William K. Wootters. “Entanglement of a Pair of Quantum Bits”. In: *Phys. Rev. Lett.* 78 (26 June 1997), pp. 5022–5025. DOI: [10.1103/PhysRevLett.78.5022](https://doi.org/10.1103/PhysRevLett.78.5022).
- [56] Tohya Hiroshima, Gerardo Adesso, and Fabrizio Illuminati. “Monogamy Inequality for Distributed Gaussian Entanglement”. In: *Phys. Rev. Lett.* 98 (5 Feb. 2007), p. 050503. DOI: [10.1103/PhysRevLett.98.050503](https://doi.org/10.1103/PhysRevLett.98.050503).
- [57] Michael Horodecki, Peter W. Shor, and Mary Beth Ruskai. “Entanglement Breaking Channels”. In: *Reviews in Mathematical Physics* 15.06 (2003), pp. 629–641. DOI: [10.1142/S0129055X03001709](https://doi.org/10.1142/S0129055X03001709).
- [58] Ryszard Horodecki et al. “Quantum entanglement”. In: *Rev. Mod. Phys.* 81 (2 June 2009), pp. 865–942. DOI: [10.1103/RevModPhys.81.865](https://doi.org/10.1103/RevModPhys.81.865).
- [59] He-Liang Huang et al. “Superconducting quantum computing: a review”. In: *Science China Information Sciences* 63.8 (2020), pp. 1–32.
- [60] Daniel F. V. James et al. “Measurement of qubits”. In: *Phys. Rev. A* 64 (5 Oct. 2001), p. 052312. DOI: [10.1103/PhysRevA.64.052312](https://doi.org/10.1103/PhysRevA.64.052312).

- [61] A. Jamiołkowski. “Linear transformations which preserve trace and positive semidefiniteness of operators”. In: *Reports on Mathematical Physics* 3.4 (1972), pp. 275–278. ISSN: 0034-4877. DOI: [https://doi.org/10.1016/0034-4877\(72\)90011-0](https://doi.org/10.1016/0034-4877(72)90011-0).
- [62] N. Johnson. “Norms and Cones in the Theory of Quantum Entanglement”. PhD thesis. University of Guelph, July 2012.
- [63] Richard Jozsa. “Entanglement and quantum computation”. In: *arXiv preprint quant-ph/9707034* (1997).
- [64] Martin Kliesch and Ingo Roth. “Theory of Quantum System Certification”. In: *PRX Quantum* 2 (1 Jan. 2021), p. 010201. DOI: [10.1103/PRXQuantum.2.010201](https://doi.org/10.1103/PRXQuantum.2.010201).
- [65] B. Kraus et al. “Separability in $2 \times N$ composite quantum systems”. In: *Phys. Rev. A* 61 (6 May 2000), p. 062302. DOI: [10.1103/PhysRevA.61.062302](https://doi.org/10.1103/PhysRevA.61.062302).
- [66] John K Kruschke and Torrin M Liddell. “The Bayesian New Statistics: Hypothesis testing, estimation, meta-analysis, and power analysis from a Bayesian perspective”. In: *Psychonomic Bulletin & Review* 25.1 (2018), pp. 178–206.
- [67] Roy H Kwon. *Introduction to linear optimization and extensions with MATLAB®*. CRC Press, 2013.
- [68] Thaddeus D Ladd et al. “Quantum computers”. In: *Nature* 464.7285 (2010), pp. 45–53.
- [69] P.-É. Larré et al. “Quantum fluctuations around black hole horizons in Bose-Einstein condensates”. In: *Phys. Rev. A* 85 (1 Jan. 2012), p. 013621. DOI: [10.1103/PhysRevA.85.013621](https://doi.org/10.1103/PhysRevA.85.013621).
- [70] Jean B. Lasserre. “Global Optimization with Polynomials and the Problem of Moments”. In: *SIAM Journal on Optimization* 11.3 (2001), pp. 796–817. DOI: [10.1137/S1052623400366802](https://doi.org/10.1137/S1052623400366802).
- [71] Monique Laurent. “Revisiting two theorems of Curto and Fialkow on moment matrices”. In: *Proc. Amer. Math. Soc* 133.10 (2005), pp. 2965–2976.
- [72] M Lewenstein. “Quantum-information-theory wintersemester 2000/2001”. In: *Institute for Theoretical Physics, University of Hannover* (2004).
- [73] M. Lewenstein et al. “Characterization of separable states and entanglement witnesses”. In: *Phys. Rev. A* 63 (4 Mar. 2001), p. 044304. DOI: [10.1103/PhysRevA.63.044304](https://doi.org/10.1103/PhysRevA.63.044304).

- [74] Dennis V Lindley. “On a measure of the information provided by an experiment”. In: *The Annals of Mathematical Statistics* (1956), pp. 986–1005.
- [75] Jarosław Adam Miszcza. “Singular value decomposition and matrix reorderings in quantum information theory”. In: *International Journal of Modern Physics C* 22.09 (2011), pp. 897–918.
- [76] Jiawang Nie. “The A-Truncated K-Moment Problem”. In: *Foundations of Computational Mathematics* 14.6 (2014), pp. 1243–1276. ISSN: 16153383. DOI: [10.1007/s10208-014-9225-9](https://doi.org/10.1007/s10208-014-9225-9). arXiv: [1210.6930](https://arxiv.org/abs/1210.6930).
- [77] Michael Nussbaum, Arleta Szkoła, et al. “The Chernoff lower bound for symmetric quantum hypothesis testing”. In: *The Annals of Statistics* 37.2 (2009), pp. 1040–1057.
- [78] Tobias J. Osborne and Frank Verstraete. “General Monogamy Inequality for Bipartite Qubit Entanglement”. In: *Phys. Rev. Lett.* 96 (22 June 2006), p. 220503. DOI: [10.1103/PhysRevLett.96.220503](https://doi.org/10.1103/PhysRevLett.96.220503).
- [79] Yong-Cheng Ou. “Violation of monogamy inequality for higher-dimensional objects”. In: *Phys. Rev. A* 75 (3 Mar. 2007), p. 034305. DOI: [10.1103/PhysRevA.75.034305](https://doi.org/10.1103/PhysRevA.75.034305).
- [80] Asher Peres. “Separability Criterion for Density Matrices”. In: *Phys. Rev. Lett.* 77 (8 Aug. 1996), pp. 1413–1415. DOI: [10.1103/PhysRevLett.77.1413](https://doi.org/10.1103/PhysRevLett.77.1413).
- [81] Lev Pitaevskii and Sandro Stringari. *Bose-Einstein Condensation and Superfluidity*. eng. Oxford: Oxford University Press, 2016, p. 576. ISBN: 9780198758884. DOI: [10.1093/acprof:oso/9780198758884.001.0001](https://doi.org/10.1093/acprof:oso/9780198758884.001.0001).
- [82] John Preskill. “Lecture notes for physics 229: Quantum information and computation”. In: *California Institute of Technology* 16 (1998), p. 10.
- [83] John Preskill. “Quantum Computing in the NISQ era and beyond”. In: *Quantum* 2 (Aug. 2018), p. 79. ISSN: 2521-327X. DOI: [10.22331/q-2018-08-06-79](https://doi.org/10.22331/q-2018-08-06-79).
- [84] Scott J Robertson. “The theory of Hawking radiation in laboratory analogues”. In: *Journal of Physics B: Atomic, Molecular and Optical Physics* 45.16 (2012), p. 163001.
- [85] Elizabeth G Ryan et al. “A review of modern computational algorithms for Bayesian optimal design”. In: *International Statistical Review* 84.1 (2016), pp. 128–154.

- [86] E Schrödinger. “Die gegenwärtige Situation in der Quantenmechanik”. In: *Naturwissenschaften* 23.48 (1935), pp. 807–812. ISSN: 1432-1904. DOI: [10.1007/BF01491891](https://doi.org/10.1007/BF01491891).
- [87] Aditi Sen De et al. “The Separability versus Entanglement Problem”. In: *Lectures on Quantum Information*. John Wiley & Sons, Ltd, 2006. Chap. 8, pp. 123–146. ISBN: 9783527618637. DOI: <https://doi.org/10.1002/9783527618637.ch8>.
- [88] Alessio Serafini. “Multimode Uncertainty Relations and Separability of Continuous Variable States”. In: *Phys. Rev. Lett.* 96 (11 Mar. 2006), p. 110402. DOI: [10.1103/PhysRevLett.96.110402](https://doi.org/10.1103/PhysRevLett.96.110402).
- [89] Alessio Serafini, Gerardo Adesso, and Fabrizio Illuminati. “Unitarily localizable entanglement of Gaussian states”. In: *Phys. Rev. A* 71 (3 Mar. 2005), p. 032349. DOI: [10.1103/PhysRevA.71.032349](https://doi.org/10.1103/PhysRevA.71.032349).
- [90] R Simon. “Peres-Horodecki Separability Criterion for Continuous Variable Systems”. In: *Phys. Rev. Lett.* 84 (2000), pp. 2726–2729. DOI: [10.1103/PhysRevLett.84.2726](https://doi.org/10.1103/PhysRevLett.84.2726).
- [91] R. Simon, N. Mukunda, and Biswadeb Dutta. “Quantum-noise matrix for multimode systems: U(n) invariance, squeezing, and normal forms”. In: *Phys. Rev. A* 49 (3 Mar. 1994), pp. 1567–1583. DOI: [10.1103/PhysRevA.49.1567](https://doi.org/10.1103/PhysRevA.49.1567).
- [92] R. Simon, E. C. G. Sudarshan, and N. Mukunda. “Gaussian-Wigner distributions in quantum mechanics and optics”. In: *Phys. Rev. A* 36 (8 Oct. 1987), pp. 3868–3880. DOI: [10.1103/PhysRevA.36.3868](https://doi.org/10.1103/PhysRevA.36.3868).
- [93] Jeff Steinhauer. “Observation of quantum Hawking radiation and its entanglement in an analogue black hole”. In: *Nature Physics* 12.10 (2016), pp. 959–965.
- [94] W. G. Unruh. “Experimental Black-Hole Evaporation?” In: *Phys. Rev. Lett.* 46 (21 May 1981), pp. 1351–1353. DOI: [10.1103/PhysRevLett.46.1351](https://doi.org/10.1103/PhysRevLett.46.1351).
- [95] Lieven Vandenbergh and Stephen Boyd. “Semidefinite programming”. In: *SIAM review* 38.1 (1996), pp. 49–95.
- [96] Xi-Lin Wang et al. “18-Qubit Entanglement with Six Photons’ Three Degrees of Freedom”. In: *Phys. Rev. Lett.* 120 (26 June 2018), p. 260502. DOI: [10.1103/PhysRevLett.120.260502](https://doi.org/10.1103/PhysRevLett.120.260502).
- [97] John Watrous. “Semidefinite Programs for Completely Bounded Norms”. In: *Theory of Computing* 5.11 (2009), pp. 217–238. DOI: [10.4086/toc.2009.v005a011](https://doi.org/10.4086/toc.2009.v005a011).

- [98] John Williamson. “On the algebraic problem concerning the normal forms of linear dynamical systems”. In: *American journal of mathematics* 58.1 (1936), pp. 141–163.
- [99] William K. Wootters. “Entanglement of Formation of an Arbitrary State of Two Qubits”. In: *Phys. Rev. Lett.* 80 (10 Mar. 1998), pp. 2245–2248. DOI: [10.1103/PhysRevLett.80.2245](https://doi.org/10.1103/PhysRevLett.80.2245).
- [100] Juan Yin et al. “Satellite-based entanglement distribution over 1200 kilometers”. In: *Science* 356.6343 (2017), pp. 1140–1144. ISSN: 0036-8075. DOI: [10.1126/science.aan3211](https://doi.org/10.1126/science.aan3211).
- [101] Karol Życzkowski et al. “Generating random density matrices”. In: *Journal of Mathematical Physics* 52.6 (2011), p. 062201. DOI: [10.1063/1.3595693](https://doi.org/10.1063/1.3595693).

Optimal measurement strategies for fast entanglement detectionN. Milazzo,^{1,2,*} D. Braun,¹ and O. Giraud²¹*Institut für theoretische Physik, Universität Tübingen, 72076 Tübingen, Germany*²*LPTMS, CNRS, Université Paris-Sud, Université Paris-Saclay, 91405 Orsay, France*

(Received 25 February 2019; published 17 July 2019)

With the advance of quantum information technology, the question of how to most efficiently test quantum circuits is becoming of increasing relevance. Here we introduce the statistics of lengths of measurement sequences that allows one to certify entanglement across a given bipartition of a multiqubit system over the possible sequence of measurements of random unknown states and identify the best measurement strategies in the sense of the (on average) shortest measurement sequence of (multiqubit) Pauli measurements. The approach is based on the algorithm of truncated moment sequences, which allows one to deal naturally with incomplete information, i.e., information that does not fully specify the quantum state. We find that the set of measurements corresponding to diagonal matrix elements of the moment matrix of the state are particularly efficient. For symmetric states their number increases only like the third power of the number N of qubits. Their efficiency increases rapidly with N , leaving already for $N = 4$ less than a fraction 10^{-6} of randomly chosen entangled states undetected.

DOI: [10.1103/PhysRevA.100.012328](https://doi.org/10.1103/PhysRevA.100.012328)**I. INTRODUCTION**

With the availability of the first small quantum processors, the task of characterizing such processors has become a key challenge. Indeed, long before proving full functionality, one of the major questions that faces a quantum processor is whether it “truly” works quantum mechanically—or could rather be explained by classical processes. Similar questions arise already at the level of a quantum state: Given a physical system in an unknown quantum state, can the statistics arising from it be explained by a classical state? If the state is fully characterized, one can apply nonclassicality measures to find out, but since a mixed quantum state of N qubits is specified by $d = 2^{2N} - 1$ real parameters, it is clear that an answer based on full quantum state tomography quickly becomes impractical. In addition, one can only estimate expectation values based on averages over finitely many measurements that are themselves imperfect, and the resulting uncertainty can lead to nonphysical states in the inversion procedure underlying full quantum state tomography. More robust approaches to state tomography are maximum likelihood estimation of the state [1–4] and Bayesian inference [5,6], which output estimates of the state that are by construction *bona fide* physical states, as well as “self-consistent quantum tomography,” which does not necessarily rely on perfect measurements [7], but none of these approaches remedies the efficiency problem.

Recent developments based on compressed sensing make use of prior information on states. They provide a large gain in efficiency, in particular, for the typically low-rank states relevant for quantum information tasks [8–12] or matrix-product states that describe interacting condensed-matter systems in low dimensions [13,14]. Machine learning aimed at

determining by itself what the best measurements are for a certain task, or to recognize entanglement from measurement data, was considered, e.g., in [15–18], but the efficiency of such approaches needs further study. Other proposals include few-copy multiparticle entanglement detection based on probabilistic verification [19,20].

For testing quantum circuits, the approach of randomized benchmarking has emerged [21–24]. Key to this approach is that for estimating fidelities between actual and ideal gate sets, only low moments of the matrix elements are required. In this case, averaging over the full unitary group can be replaced by averaging over a unitary t design [25] or producing required input states by random quantum circuits (see also [26]). References [27] and [28] showed that a small number of parameters of a quantum process can be efficiently obtained, but it is not as clear what the most relevant parameters that should be chosen are.

It is often stated that quantum states and quantum processors are much harder to test and characterize than their classical analogs because of the exponential growth of the Hilbert space [13,29,30]. However, also classically the number of possible memory configurations of N bits increases exponentially as 2^N —and with N of order 10^{13} for a standard laptop computer, it is completely out of the question to test all possible configurations. Costs of integration itself have decreased exponentially according to Moore’s law; for the same reason, functional testing of classical memory devices has evolved to the most expensive (because time-consuming) part of the production of integrated memory chips. Functional testing of classical memories has therefore evolved to *testing the most critical known configurations with the goal of demonstrating failure of memory cells as quickly as possible*. “Most critical” depends on the architecture of the chip, and information on its design goes into the design of memory patterns to be tested. For example, a cell on a given bit line

*nadia.milazzo@u-psud.fr

might resist storing a “0,” most likely if all other cells on the same bit line contain a “1.” In MRAM devices, magnetic stray fields from a set of cells can destabilize others in the vicinity when uniformly polarized, etc.

Quantum information processing may still have a long way to go before such economical pressure on functional testing will be felt. At the moment, rather than showing failure, one would like to prove basic quantum functionalities as quickly as possible. Nevertheless, the principles of classical functional testing can also provide guidance in the current state of affairs on characterizing quantum processors and states: rather than aiming at full quantum tomography, one may want to focus on producing states that are likely to be particularly unstable and show their “functionality” as quickly as possible. In practice, this will require information about the physical realization of the quantum processor, but in the absence of such input, a reasonable target is highly entangled states or, more generally, highly nonclassical states known to be prone to decoherence. Indeed, experimental efforts have early on concentrated on producing such states (see, e.g., [31–35] for states with large numbers of entangled particles).

The question then arises: What is the most efficient measurement strategy to prove that such a state is entangled (or, more generally, nonclassical)? That is, What would you choose to measure first, second, and so on, in order to be able to prove as quickly as possible, with the limited knowledge about the state that you will gain from those measurements, chosen from a given set, that the state is entangled? What are the minimum and average numbers of measurements needed to prove entanglement or, more generally, the statistics on the length of measurement sequences when going down a certain path of measurements?

These are the questions that we start to answer in the present paper. Note that this is not about choosing optimal entanglement witnesses but, rather, about deciding whether or not the intersection of hyperplanes defined by the expectation values of certain observables cuts the set of separable states (see Fig. 4). Perfectly suited for answering these questions is the formalism of *truncated moment sequences* (TMSs) that we introduced in [36] for the analysis of entanglement. The TMS problem aims at finding a probability measure for which only some moments are known. If the probability measure is, furthermore, constrained to be supported on a compact set K , the problem is known as the K -TMS problem. As reviewed below, it can be solved with a hierarchy of flat extensions that maps onto a convex optimization algorithm, using a semidefinite relaxation procedure. Each expectation value can be associated with a moment of a measure, and instead of fixing all moments up to a certain order as in the standard TMS algorithm, one might just specify any set \mathcal{A} of moments. The problem of deciding whether a classical measure that reproduces all these moments exists is then known as the “ $\mathcal{A}K$ -TMS” problem [37]. It can still be solved with a convex optimization algorithm.

In the present work we exploit this approach in order to obtain the statistics of lengths of measurement sequences in the simplest case of two qubits depending on the chosen measurement strategy. For larger numbers of qubits, the full numerical solution of the $\mathcal{A}K$ -TMS problem becomes too demanding, but it turns out that surprisingly efficient sufficient

conditions for entanglement can be obtained for symmetric states from the diagonal matrix elements of the moment matrix used in the approach (see below for a definition). These correspond to certain linear combinations of expectation values of (possibly multipartite) measurements in the Pauli basis and have to be positive for a solution of the $\mathcal{A}K$ -TMS problem to exist. Checking the positivity of moment matrices is in fact the first step in the TMS algorithm, and negativity of any of the diagonal matrix elements hence witnesses entanglement. With these we can find numerical estimates of the fraction of randomly drawn states that are already detected as entangled by just measuring the observables corresponding to the diagonal matrix elements of the moment matrix.

Similar ideas for certifying entanglement with incomplete measurements were considered in [38] for continuous variable systems. Here we focus on the statistics of lengths of sequences of measurements for multiqubit systems and the insights that can be drawn from the TMS algorithm, which we review in the next section, before applying it to incomplete measurements.

II. FRAMEWORK AND NOTATION

We now briefly summarize the TMS algorithm approach described in detail in [36], which is the framework for the following sections. The basic idea is to map the quantum entanglement problem onto the mathematically well-studied truncated moment problem. Indeed, finding out whether an arbitrary multipartite state can be decomposed into product states corresponds to finding out about the existence of a probability distribution whose lowest-order moments are fixed. Analytically, the mapping allows one to make use of theorems from the TMS literature providing necessary and sufficient separability conditions; numerically, semidefinite optimization techniques yield an algorithm which gives a certificate of entanglement or separability. The algorithm applies—at least in principle—to arbitrary quantum states with an arbitrary number of constituents and arbitrary symmetries between the subparts. The general case is dealt with in [36]; we only recall here the main key points for the case of symmetric states of qubits, defined as mixtures of symmetric pure states (the latter are invariant under any permutation of the qubits). To do so, we use a convenient representation in terms of symmetric tensors which was introduced in [39], generalizing the Bloch sphere picture of spins-1/2. We can write a generic state ρ of a spin- j state as

$$\rho = \frac{1}{2^N} \sum_{\mu_1, \mu_2, \dots, \mu_N=0}^3 X_{\mu_1 \mu_2 \dots \mu_N} P_S(\sigma_{\mu_1} \otimes \dots \otimes \sigma_{\mu_N}) P_S^\dagger, \quad (1)$$

where σ_0 is the 2×2 identity matrix, σ_1 , σ_2 , and σ_3 are the Pauli matrices, and P_S is the projector onto the symmetric subspace spanned by the Dicke states $|j, m\rangle$ (eigenstates of pseudoangular momentum component J_z and with total angular momentum quantum number j). They can also be seen as symmetric states of $N = 2j$ spins-1/2 (or qubits). The tensor $X_{\mu_1 \mu_2 \dots \mu_N}$ is then given by

$$X_{\mu_1 \mu_2 \dots \mu_N} = \text{tr}(\rho \sigma_{\mu_1} \otimes \dots \otimes \sigma_{\mu_N}), \quad (2)$$

with $0 \leq \mu_i \leq 3$. It is real and invariant under permutation of indices and verifies $X_{00\dots 0} = \text{tr}(\rho) = 1$. Moreover, it has the property that

$$\sum_{a=1}^3 X_{aa\mu_3\mu_4\dots\mu_N} = X_{00\mu_3\mu_4\dots\mu_N} \quad (3)$$

for any choice of the μ_i . A separable pure state can be seen as a spin-coherent state, which in representation (2) has tensor entries $X_{\mu_1\mu_2\dots\mu_N} = n_{\mu_1}n_{\mu_2}\dots n_{\mu_N}$, with $n_0 = 1$ and (n_1, n_2, n_3) the unit vector giving the direction of the coherent state on the Bloch sphere. In terms of this tensor representation, a symmetric state is separable if and only if its tensor representation can be written as

$$X_{\mu_1\mu_2\dots\mu_N} = \sum_i \omega_i n_{\mu_1}^{(i)} n_{\mu_2}^{(i)} \dots n_{\mu_N}^{(i)}, \quad \omega_i \geq 0, \quad (4)$$

where $n_0^{(i)} = 1$ and $\mathbf{n}^{(i)}$ is the Bloch vector of the single qubit. If we express (4) in the equivalent integral form,

$$X_{\mu_1\mu_2\dots\mu_N} = \int_K x_{\mu_1} x_{\mu_2} \dots x_{\mu_N} d\mu(\mathbf{x}), \quad (5)$$

with $x_0 = 1$, $K = \{\mathbf{x} \in \mathbb{R}^3 : x_1^2 + x_2^2 + x_3^2 = 1\}$ the unit sphere, and $d\mu(\mathbf{x}) = \sum_i \omega_i \delta(\mathbf{x} - \mathbf{n}^{(i)})$ a positive measure on K , we can say that a symmetric state is separable if and only if there exists a positive measure $d\mu$ supported by K such that all entries of the tensor $X_{\mu_1\mu_2\dots\mu_N}$ are given by moments of that measure.

Problems of this type are known as K -TMS problems, or \mathcal{AK} -TMS problems in the case of partial knowledge of a state where only a subset of the moments, specified by set \mathcal{A} , is known. They can be solved by a semidefinite relaxation procedure. The algorithm proposed in [36] uses indeed semidefinite programming (SDP) and the concept of “extensions,” introduced in [40], but based on a matrix of moments and a theorem in the theory of moment sequences. In order to present more clearly the mathematical setting for the \mathcal{AK} -TMS problem, we introduce a more compact notation for Eq. (5). For any N -tuple (μ_1, \dots, μ_N) we define a triplet $\alpha = (\alpha_1, \alpha_2, \alpha_3)$ of integers such that $x_{\mu_1} x_{\mu_2} \dots x_{\mu_N} = x^\alpha$, where we use the notation $x^\alpha = x_1^{\alpha_1} x_2^{\alpha_2} x_3^{\alpha_3}$. The degree of the monomial x^α is $|\alpha| = \sum_i \alpha_i$. We then set $y_\alpha \equiv X_{\mu_1\mu_2\dots\mu_N}$. The $(y_\alpha)_{|\alpha| \leq d}$ is a TMS, that is, a sequence of moments of μ truncated at degree d . When only a subset $\alpha \in \mathcal{A}$ of these moments is known, we consider the TMS $(y_\alpha)_{\alpha \in \mathcal{A}}$. With this notation we can rewrite (5) as

$$y_\alpha = \int_K x^\alpha d\mu(\mathbf{x}). \quad (6)$$

To a TMS y of degree d , for any integer $k \leq d/2$, we can associate a matrix $M_k(y)$ defined by $M_k(y)_{\alpha\beta} = y_{\alpha+\beta}$ with $|\alpha|, |\beta| \leq k$, which we call the k th-order moment matrix. A necessary condition for a TMS to admit a representing measure is that the moment matrix of any order be positive semidefinite. A second necessary condition can be obtained from the polynomial constraint $x_1^2 + x_2^2 + x_3^2 = 1$, which defines set K . For even degree d we define a “shifted TMS” of degree $d - 2$, and its moment matrix of order $k - 1$ is called the k th-order localizing matrix of y . It is necessarily positive semidefinite if a TMS admits a representing measure.

Beyond these two necessary conditions, a sufficient condition was obtained in [41] for an even-degree TMS. Namely, if a TMS z of even degree $2k$ is such that

$$\text{rank} M_k(z) = \text{rank} M_{k-1}(z), \quad (7)$$

then the TMS z admits a representing measure. As the above condition is only sufficient, a TMS admitting a representing measure does not necessarily fulfill it, but one can always search for an extension of it which does. An extension of a TMS y of degree d is defined as any TMS z of degree $2k$ with $2k > d$, such that $z_\alpha = y_\alpha$ for all $\alpha \in \mathcal{A}$. An extension z is called flat if it satisfies Eq. (7). If z verifies the sufficient conditions above, then it has a representing measure, and so does y as a restriction of z . Then it is possible to formulate a necessary and sufficient condition for the existence of a representing measure as follows.

Theorem. A state ρ is separable if and only if its coordinates $X_{\mu_1\mu_2\dots\mu_N}$ are mapped to a TMS $(y_\alpha)_{\alpha \in \mathcal{A}}$ such that there exists a flat extension $(z_\beta)_{|\beta| \leq 2k}$ with $2k > d$ and whose corresponding k th-order moment and localizing matrices are positive semidefinite.

This necessary and sufficient condition can be translated into an algorithm looking for flat extensions of the TMS y associated with a quantum state ρ . One runs the algorithm with the input of the state ρ (which means fixing y_α for all $\alpha \in \mathcal{A}$), starting from the lowest possible extension order k . If the corresponding SDP is “infeasible,” then the conditions of the theorem are not satisfied and the TMS admits no representing measure $d\mu$, which means that the quantum state whose coordinates are given by y_α is entangled. If, on the contrary, the SDP problem is “feasible,” then the TMS admits a representing measure, and the corresponding quantum state is separable. The algorithm also extends to the case of nonsymmetric states (see [36] for further detail).

III. UNORDERED MEASUREMENTS

A. Goal

Let us now consider the question raised in Sec. I. Our goal is to identify the smallest set of measurements that should be performed on an unknown spin state to detect that it is entangled. This is possible in a real experiment when many identical copies of the same state are available, so that a different measurement can be performed on each copy. We first discuss the case of symmetric two-qubit states, which, as we see in detail, already presents some complexity. In this case the positive-partial-transpose criterion [42,43] applied to a partially known density matrix would also provide a way of detecting entanglement via SDP. Nevertheless, we use our TMS approach, since it allows for a straightforward generalization to an arbitrary number of qubits, and moreover, it applies SDP to the matrix of moments, whose entries are directly given by measurement results.

B. Symmetries and measurements

For a symmetric two-qubit state ρ , Eq. (2) with $N = 2$ gives

$$X_{\mu_1\mu_2} = \text{tr}(\rho \sigma_{\mu_1} \otimes \sigma_{\mu_2}) \quad (8)$$

with $0 \leq \mu_i \leq 3$ and $(\sigma_0, \sigma_1, \sigma_2, \sigma_3) \equiv (\mathbb{1}, \sigma_x, \sigma_y, \sigma_z)$. In this case the tensor $X_{\mu_1\mu_2}$ reduces to a 4×4 real symmetric matrix. Its 10 entries $X_{\mu_1\mu_2}$ with $\mu_1 \leq \mu_2$ can be seen as the result of the measurement of the joint operator $\sigma_{\mu_1} \otimes \sigma_{\mu_2}$. We now ask which are the possible measurements that we can perform and how many there are; the observables considered are the simplest, i.e., Pauli spin operators. Let us denote these inequivalent measurement operators

$$\mathcal{M} = \{M_x, M_y, M_z, M_{xx}, M_{xy}, M_{xz}, M_{yy}, M_{yz}, M_{zz}\} \quad (9)$$

(we omit the identity operator corresponding to $X_{00} = \mathbb{1}$, and we always order sets of measurements in degree-lexicographic order). For instance, M_x is the measurement of $\mathbb{1}$ on the first qubit and of σ_x on the second one (or the reverse), while M_{xx} is the measurement of the joint operator $\sigma_x \otimes \sigma_x$. Since the tensor $X_{\mu_1\mu_2}$ is such that

$$\sum_{i=1}^3 X_{ii} = X_{00}, \quad (10)$$

only two of the three diagonal entries are independent, and measuring two of three of the observables M_{xx} , M_{yy} , and M_{zz} yields the third value. Thus, carrying a tomography to its end for a single spin-1 state consists in measuring eight observables in total.

Our aim is to find the probability that a state is detected as entangled if only the result of measurements of a certain subset of these eight observables is known. Let us first observe that these probabilities should not depend on the choice of the reference frame for the axes along which the measurement is performed. As a consequence, the results for equivalent measurements in different directions should be the same. We therefore consider only sets which are nonequivalent under transpositions $\{P_{xy}, P_{xz}, P_{yz}\}$, which exchange two axes, and cyclic permutations P_{yzx} and P_{zxy} .

We consider all possible nonequivalent sets of k measurements, with $1 \leq k \leq 8$, disregarding the order of measurements within a set. For sets of length $k = 1$ we can easily see that the nonequivalent measurements are only three: M_x , M_{xx} , and M_{xy} . Indeed, the local measurements M_x , M_y , and M_z are equivalent, as well as the two-qubit ‘‘diagonal’’ measurements M_{xx} , M_{yy} , and M_{zz} [giving the diagonal entries of matrix $(X_{\mu\nu})_{1 \leq \mu, \nu \leq 3}$] and, also, the two-qubit ‘‘off-diagonal’’ measurements M_{xy} , M_{xz} , and M_{yz} (giving its off-diagonal entries). For $k = 2$, there are 28 possible pairs, among which only 9 are inequivalent, namely, $\{M_x, M_y\}$, $\{M_x, M_{xx}\}$, $\{M_x, M_{xy}\}$, $\{M_x, M_{yy}\}$, $\{M_x, M_{yz}\}$, $\{M_{xx}, M_{xy}\}$, $\{M_{xx}, M_{yy}\}$, $\{M_{xx}, M_{yz}\}$, $\{M_{xy}, M_{xz}\}$. We denote by m_k the number of nonequivalent sets of k measurements, and we list them in Table I. The corresponding complete lists of measurements for all k are given in Appendix A.

For each k , our question reduces to finding out which set of measurements, among the m_k possible ones, yields the highest entanglement detection probability. Note that performing k measurements is not exactly equivalent to having k fixed moments. Indeed, since moments are related by Eq. (10), measuring M_{xx} and M_{yy} fixes the three moments X_{11} , X_{22} , and

TABLE I. First row of data: Number m_k of nonequivalent unordered sets of measurements for $1 \leq k \leq 8$. Second row of data: Number m'_k of nonequivalent ordered sequences of measurements for $1 \leq k \leq 8$.

	k							
	1	2	3	4	5	6	7	8
m_k (unordered)	3	9	19	26	23	14	5	1
m'_k (ordered; M_{xx} fixed)	1	5	26	128	524	1604	3228	3228

X_{33} . Any measurement set of length k containing both M_{xx} and M_{yy} will in fact correspond to a TMS with $k + 1$ moments fixed. We therefore always discard M_{zz} from the measurement sets.

C. Set probabilities

In terms of the TMS algorithm, performing a measurement means obtaining a value of a tensor entry $X_{\mu_1\mu_2\dots\mu_N}$ or, equivalently, of a moment y_α . Performing k measurements means that the k moments y_α corresponding to these measurements are fixed, as well as all moments obtained via relation (3).

For a given number k of measurements, we indicate a specific set of measurements among the m_k possible ones as $\{M\}_I$. For instance, if $k = 3$, we could have $I = \{x, y, zz\}$, which corresponds to the set of measurements $\{M_x, M_y, M_{zz}\}$.

If we consider a fixed k and a fixed subset $\{M\}_I$ of the set of observables \mathcal{M} , we denote the sample space of outcomes of the \mathcal{AK} -TMS algorithm applied to the moments $(y_\alpha)_{\alpha \in A}$ of an entangled state as Ω_I . It contains two possible outcomes, to which a probability can be assigned: detecting the state as entangled (if the associated SDP is infeasible, i.e., if the state is entangled), with probability $P(E, \{M\}_I)$; or *not* detecting it as entangled (if the SDP is feasible, i.e., if the state with such moments fixed is still compatible with a separable state), with probability $P(\bar{E}, \{M\}_I)$. To shorten the notation we may denote $P(E, \{M\}_I)$ as $p_I^{(k)}$, which entails $P(\bar{E}, \{M\}_I) = 1 - p_I^{(k)}$.

These probabilities can be estimated by running the TMS algorithm for each k and each I , testing all the m_k possible sets of measurements. Note that $p_I^{(k)}$ always increases, in the sense that $p_J^{(k)} \leq p_I^{(k)}$ for $J \subset I$. Indeed, the probability of not detecting entanglement with more and more measurements decreases with the number of measurements. In other words, fixing more moments y_α reduces the probability of finding a measure μ with such moments. Once all eight measurements are done the state is fixed uniquely, so that for entangled states $p_I^{(8)} = 1$. To estimate the values for the probabilities $p_I^{(k)}$, we sample states from the set of symmetric two-qubit states. We generated 5×10^4 random states drawn from the Hilbert-Schmidt ensemble of matrices $\rho = \frac{GG^\dagger}{\text{tr}(GG^\dagger)}$, with G a complex matrix with independent Gaussian entries (following [44]). Among them were 1843 separable states that we discarded, implying the normalization condition $p_I^{(8)} = 1$ for full tomography. For each measurement set $\{M\}_I$ and each entangled state in our sample the TMS algorithm was run with the corresponding moments fixed; the results for the probabilities $p_I^{(k)}$ are reported in Figs. 1 and 2.

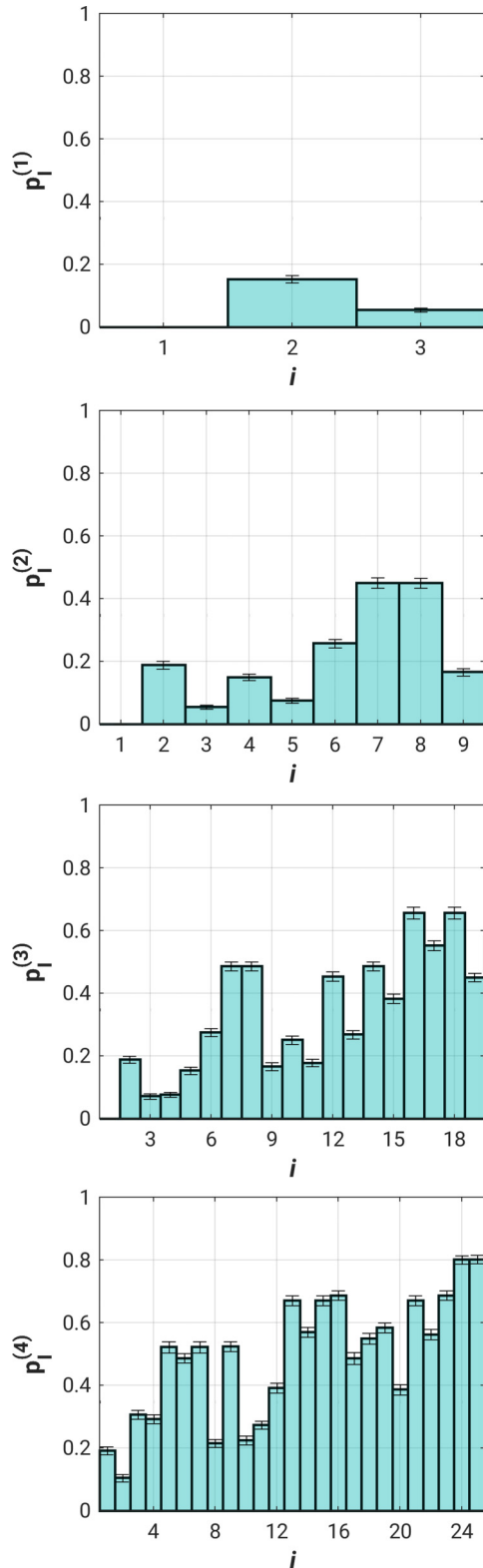


FIG. 1. Probabilities $p_I^{(k)}$ of detecting entanglement in a symmetric state of two qubits with measurement set I of cardinality k , $1 \leq k \leq 4$, as a function of the label i of set I ($1 \leq i \leq m_k$). The associated error bars represent the difference between the maximum and the minimum of the fluctuations observed for 1000 different samples of size 4×10^4 randomly extracted from the initial sample considered. The set of measurements $\{M\}_I$ corresponding to each label is listed in Appendix A.

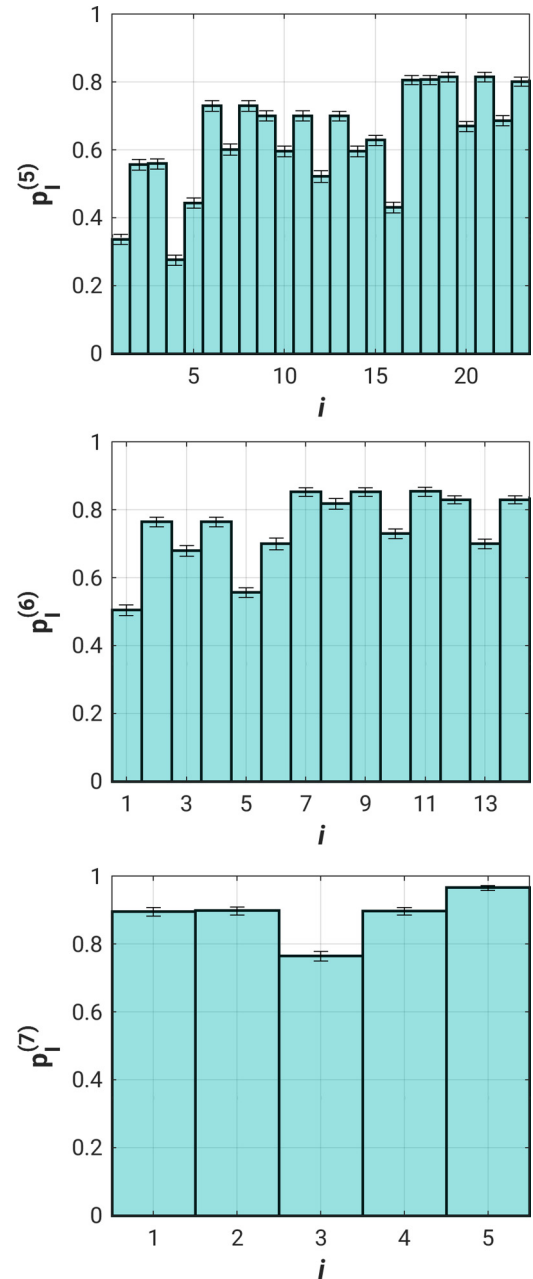


FIG. 2. Probabilities $p_I^{(k)}$ for $5 \leq k \leq 7$; same as Fig. 1.

Some probabilities appear to be equal. This is, for instance, the case for probabilities labeled 16 and 18 for $k = 3$. This is a consequence of an additional symmetry due to the linear equations that measurement results must satisfy. In the case where $k = 3$, labels 16 and 18 correspond to $\{M_{xx}, M_{xy}, M_{yy}\}$ and $\{M_{xx}, M_{xz}, M_{yy}\}$, respectively. Since, as we have mentioned, knowing the result of any two diagonal measurements gives the third one because of Eq. (10), the information acquired by measuring the observables corresponding to labels 16 and 18 is equivalent, and therefore the probabilities must be equal.

The optimal choice of measurements $\{M\}_{I_{\text{opt}}}$ at fixed k corresponds to the sets giving the highest probability of detecting entanglement. For $k = 1$ the highest value of $p_I^{(1)}$ corresponds to measurement 2, $\{M_{xx}\}$. For $k = 2$ it corresponds to 7,

$\{M_{xx}, M_{yy}\}$. For $k = 3$ the highest values correspond to two measurements: 16, $\{M_{xx}, M_{xy}, M_{yy}\}$, and 18, $\{M_{xx}, M_{xz}, M_{yy}\}$. For $k = 4$ it corresponds to 23, $\{M_{xx}, M_{xy}, M_{xz}, M_{yy}\}$, 24, $\{M_{xx}, M_{xy}, M_{xz}, M_{yz}\}$, and 25, $\{M_{xx}, M_{xz}, M_{yy}, M_{yz}\}$. Again, the degeneracy of the optimal set reflects the equivalence of the corresponding sets once (10) is taken into account. For $k \geq 2$, the sets $\{M\}_{I_{\text{opt}}}$ in fact correspond to cases where measuring two observables fixes three moments.

D. Quantumness

For a fixed set of measurements M_I one can ask whether the rate of detected entangled states depends on *how quantum* a state is. For an arbitrary state ρ , quantumness may be defined in several different ways; we follow here the definition given in [45], based on spin-coherent states. These are a generalization of the usual coherent states of the harmonic oscillator used in quantum optics to spins; they correspond to spin states which minimize a particular uncertainty relation, and they move as classical phase space points under a Hamiltonian linear in the angular momentum operators [46,47]. As any spin-1/2 pure state $|\phi\rangle$ has this property, an arbitrary N -qubit spin-coherent state can be defined as $|\phi\rangle^{\otimes N}$ with $|\phi\rangle$ a one-qubit state.

Quantumness is then defined as the Hilbert-Schmidt distance to the convex set \mathcal{C} of classical spin states [48], that is, the ensemble of all density matrices which can be expressed as a mixture of spin-coherent states with positive weights (or in other words the set \mathcal{C} is the convex hull of spin-coherent states). Namely, the quantumness $Q(\rho)$ is given by

$$Q(\rho) = \min_{\rho_c \in \mathcal{C}} \|\rho - \rho_c\|, \tag{11}$$

where $\|O\| = \sqrt{\text{Tr}(O^\dagger O)}$ is the Hilbert-Schmidt norm. For all ρ the property $Q(\rho) \geq 0$ holds, with equality for classical states $\rho \in \mathcal{C}$. Results are reported in Fig. 3, up to $k = 4$ for the optimal sets of measurements $\{M\}_{I_{\text{opt}}}$ given above. We can observe that the rate of detected entangled states increases with the quantumness of the states; in other words, the more quantum a state is, the faster it is detected as entangled.

IV. ORDERED MEASUREMENTS

A. The setting

In the previous section we assumed that k observables are measured among the eight possible ones and that the TMS algorithm is subsequently run. Of course, we can imagine a different experimental protocol where we would perform a measurement, run the TMS algorithm with a single moment fixed, and then, only in the case where the state is not detected as entangled, perform a second measurement and run the TMS algorithm again with two moments fixed, and so on, until entanglement is detected or full tomography is achieved. In this setting, we need to distinguish the $k!$ different ordered arrangements of each k -element subset of \mathcal{M} .

In the following, we call an ordered sequence of measurements a *path*, and we denote it γ . To distinguish it from a set, we denote it as a tuple with parentheses, such as (M_x, M_y, M_{xz}) . A path of length k can be alternatively seen as a list of k sets of increasing size given by the restriction

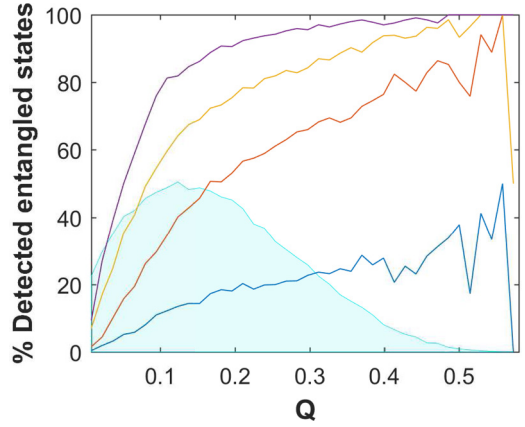


FIG. 3. Percentage of detected entangled states for the optimal sets of measurements $\{M\}_I$ for $k = 1$ to 4 (solid lines from bottom to top), as a function of the quantumness for symmetric states of two qubits. The shaded area in the background represents the distribution of the quantumness Q (bin width, 0.015) of the total number of states (multiplied by a factor of 2×10^{-2}); the first bin contains entangled states with Q between 10^{-4} and 10^{-2} . The distribution shows that there are very few states for the highest values of quantumness, which explains the large statistical errors at maximum quantumness.

of the path to the first k' observables with $1 \leq k' \leq k$. For instance, for $k = 3$ the path (M_x, M_{xz}, M_y) can be seen as the list $\{M_x\}$, $\{M_x, M_{xz}\}$, $\{M_x, M_y, M_{xz}\}$ (as usual we write sets in lexicographical order since the order within a set does not matter).

Considering all $8!$ paths of length 8 would require an exceedingly long computational time. For this reason, we slightly simplify the problem by fixing the first measurement to perform. The most reasonable choice, looking at the results in Fig. 1, is to fix it as a diagonal observable M_{xx}, M_{yy} , or

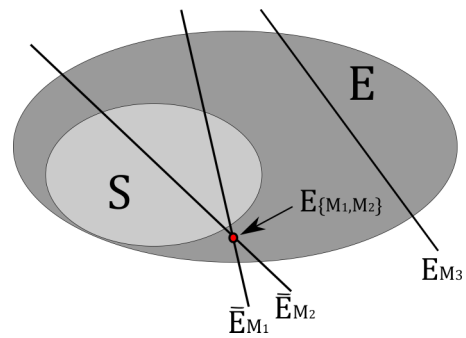


FIG. 4. Two-dimensional sketch of the sets involved. S , separable states; E , entangled states. We consider an arbitrary state in region E . Fixing one moment means restricting the set of compatible states to a hyperplane (one of the three lines in the sketch). Hyperplanes which cross the set of separable states contain both entangled and separable states, thus measuring the observable M_1 or M_2 alone is not enough to detect entanglement. Fixing both, on the other hand, restricts the set of compatible states to a region (a point in the sketch) outside S , i.e., observables $\{M_1, M_2\}$ together detect a fraction of states as entangled (E). The third line instead does not cross the set of separable states, meaning that measuring M_3 suffices to detect entanglement (which we denote E_{M_3}).

M_{zz} , since for $k = 1$ it detects the largest fraction of entangled states. Up to relabeling of the axes, we can take M_{xx} as the first element since, as before, we only keep nonequivalent paths. To find these paths, we define a canonical representation of a path γ of length k by considering its equivalent list of k sets of length k' . For each of these sets we choose the first one in lexicographical order among the ones that are obtained by relabeling of the axes. The list of k sets obtained in this way is the canonical representation of γ . Two paths are equivalent if they have the same canonical representation. We report the number m'_k of nonequivalent paths of length k in Table I, where, e.g., for $k = 2$ the nonequivalent sequences will be (M_{xx}, M_x) , (M_{xx}, M_y) , (M_{xx}, M_{xy}) , (M_{xx}, M_{yy}) , and (M_{xx}, M_{yz}) .

B. Path probabilities

We now show how to retrieve the results for this more general case from the $p_l^{(k)}$ obtained in the previous section. The probability of detecting a state as entangled after the first measurement, say M_1 , is $P(E, \{M_1\})$, given in the previous section. The probability of detecting a state as entangled after the second measurement, say M_2 , is then $P(E, \{M_1, M_2\}|\bar{E}, \{M_1\})$, which is the probability of detecting entanglement with the second measurement given that it was not detected with the first one. This quantity now depends on which measurement is performed first. This is illustrated in Fig. 4. Using the theorem of total probability, we have

$$P(E, \{M_1, M_2\}) = P(E, \{M_1\})P(E, \{M_1, M_2\}|E, \{M_1\}) + P(\bar{E}, \{M_1\})P(E, \{M_1, M_2\}|\bar{E}, \{M_1\}). \quad (12)$$

Since $P(\bar{E}, \{M_1\}) = 1 - P(E, \{M_1\})$ and $P(E, \{M_1, M_2\}|E, M_1) = 1$ we get

$$P(E, \{M_1, M_2\}|\bar{E}, \{M_1\}) = \frac{P(E, \{M_1, M_2\}) - P(E, \{M_1\})}{1 - P(E, \{M_1\})}. \quad (13)$$

Thus, the conditional probability we are looking for can be expressed solely in terms of the $p_l^{(k)}$ from the previous section.

Then let $\gamma = (M_1, \dots, M_8)$ be a path of length $k = 8$. We define

$$q^{(k)}(\gamma) = P(E, \{M_1, \dots, M_k\}|\bar{E}, \{M_1, \dots, M_{k-1}\}) \quad (14)$$

as the probability of detecting entanglement at step k in γ given that no entanglement was detected up to step $k - 1$. By a reasoning similar to the one leading to Eq. (13), we can express $q^{(k)}(\gamma)$ in terms of the $p^{(k)}(\gamma) \equiv P(E, \{M_1, \dots, M_k\})$, as

$$q^{(k)}(\gamma) = \frac{p^{(k)}(\gamma) - p^{(k-1)}(\gamma)}{1 - p^{(k-1)}(\gamma)}. \quad (15)$$

In particular, since $p^{(0)} = 0$ (as nothing is measured, and hence detected as entangled, at level 0), we have $q^{(1)} = p^{(1)}$. Inverting (15) one obtains $p^{(k)}(\gamma)$ in terms of $q^{(k)}(\gamma)$ as $p^{(k)}(\gamma) = \sum_{j=1}^k q^{(j)}(\gamma) \prod_{n=j+1}^k (1 - q^{(n)}(\gamma))$.

A third natural probability to consider is related to our measurement algorithm, where we perform TMS calculations at step k only if the state was compatible with a

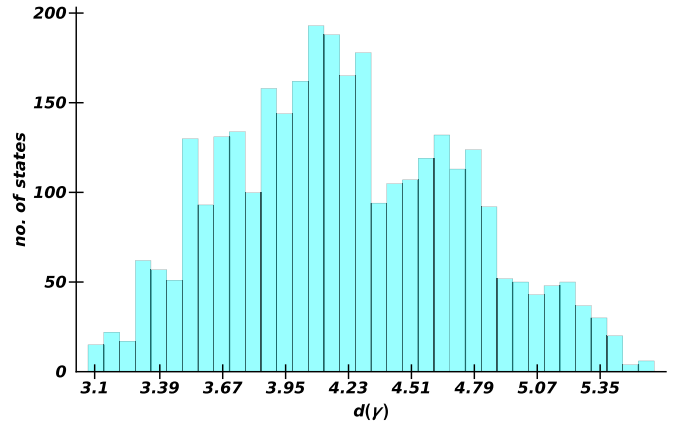


FIG. 5. Distribution (with bin width 0.07) of lengths $d(\gamma)$ of measurement sequences γ of symmetric states of two qubits resulting in detection of entanglement between the minimum value of 3.07 and the maximum one of 5.61.

separable state. We define $r^{(k)}(\gamma)$ as the probability of stopping exactly at the k th level when measurements are taken along path γ . It can be written as the joint probability $P(E, \{M_1, \dots, M_k\} \cap \bar{E}, \{M_1, \dots, M_{k-1}\})$. Using the identity $P(A \cap B) = P(A|B)P(B)$, $r^{(k)}(\gamma)$ can be expressed as $q^{(k)}(\gamma)(1 - p^{(k-1)}(\gamma))$. It can be rewritten in terms of $q^{(k)}(\gamma)$ or $p^{(k)}(\gamma)$ as

$$r^{(k)}(\gamma) = q^{(k)}(\gamma) \prod_{j=1}^{k-1} (1 - q^{(j)}(\gamma)) = p^{(k)}(\gamma) - p^{(k-1)}(\gamma). \quad (16)$$

C. The best path

Using (15) and (16) and the numerical results in the previous section, we can obtain a numerical estimate of the $q^{(k)}(\gamma)$ and the $r^{(k)}(\gamma)$ for all possible paths. The optimal path γ_{best} is the one that detects as quickly as possible (on average) whether the state is entangled. To identify γ_{best} among all possible ones we define the average depth at which our algorithm stops as

$$d(\gamma) = \sum_{k=1}^8 kr^{(k)}(\gamma). \quad (17)$$

Expressing Eq. (17) in words, $d(\gamma)$ gives the number of measurements that one needs to perform, on average, to detect a state as entangled, following the path γ . Each path will be characterized by this number, and in particular, the shortest path will be given by

$$\gamma_{\text{best}} = \arg \min_{\gamma \in S} d(\gamma). \quad (18)$$

The distribution of $d(\gamma)$ over all 3228 paths of length 8 for symmetric states of two qubits is reported in Fig. 5. The minimum value found for $d(\gamma)$ is $d = 3.07$, while the maximum value is 5.61. The minimum value is degenerate and corresponds to three optimal paths. Although these three paths do not have the same canonical representation they lead to the same value because of condition (10).

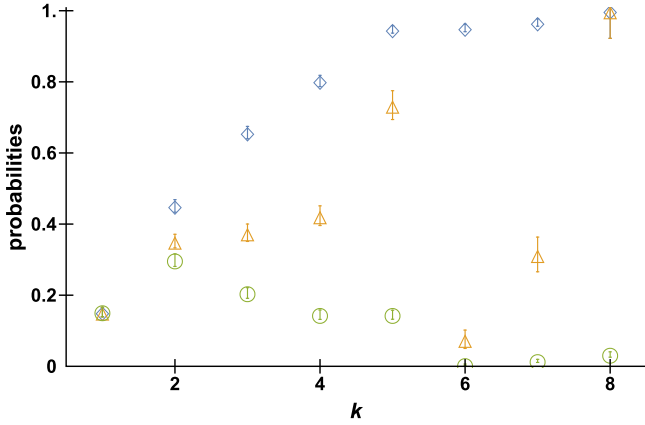


FIG. 6. Probabilities $p^{(k)}(\gamma_{\text{best}})$ (blue diamonds), $q^{(k)}(\gamma_{\text{best}})$ (orange triangles), and $r^{(k)}(\gamma_{\text{best}})$ (green circles). Error bars represent the statistical errors derived from those of the $p_i^{(k)}$; see Fig. 1.

If one considered that knowing two diagonal moments is equivalent to knowing them all and included in the symmetrization the third diagonal moment once the first two are measured, there would be a unique optimal path. We report here one of the three equivalent optimal paths, $\gamma_{\text{best}} = (M_{xx}, M_{yy}, M_{xz}, M_{yz}, M_{xy}, M_x, M_y, M_z)$; choosing this path, one only needs to perform (on average) three measurements to detect a state as entangled. These three measurements give access to the two diagonal moments [and thus all of them via (10)] and one of the off-diagonal ones. The probabilities relative to this best path are shown in Fig. 6.

Rewriting $d(\gamma)$ in terms of $p^{(k)}(\gamma)$ we get

$$d(\gamma) = 8p^{(8)}(\gamma) - p^{(7)}(\gamma) - p^{(6)}(\gamma) - \dots - p^{(1)}(\gamma). \quad (19)$$

It turns out that choosing measurements according to γ_{best} coincides (within the error bars) with choosing for each k , $1 \leq k \leq 8$, the best set of measurements, i.e., the one with the highest probability of detecting entanglement at a given level (highest $p_i^{(k)}$ among the m_k possibilities for each k). This is not obvious, and it is not always the case: a counterexample is given by a binary tree of depth 4 in which the random probabilities satisfy the same constraint as in our case, i.e., $p^{(k-1)}(\gamma) \leq p^{(k)}(\gamma)$, and the four paths have probabilities (0.57, 0.62, 0.76), (0.57, 0.62, 0.95), (0.57, 0.68, 0.77), (0.57, 0.68, 0.78). It is easily verified that the best path, with $d(\gamma) = 1.8$, is the second one, which at depth 2 does not have the highest $p^{(2)}(\gamma)$, so the minimal $d(\gamma)$ does not always correspond to the path with the highest $p^{(k)}(\gamma)$ at each step.

In practice, joint measurements such as M_{xx} might be more challenging to implement than two single measurements M_x , as qubits need first a unitary operation to entangle them and then two local measurements. In such a case, one might modify (17) with another factor for each path that takes such additional costs into account. Also, we base our analysis on average values of measurement outcomes which we took as known with arbitrary precision. This is, of course, an idealization. In practice, only a finite number of measurements can be performed, leading to statistical error bars for each moment. These can, in principle, be taken into account in

TABLE II. Number m_k of nonequivalent unordered sets of measurements of two qubits for $1 \leq k \leq 15$.

k	1	2	3	4	5	6	7	8	9	10	11	12	13	14	15
m_k	3	10	30	69	132	205	254	254	205	132	69	30	10	3	1

the TMS algorithm, but they increase the computational time. Both of these points are beyond the scope of the present paper.

V. NONSYMMETRIC CASE

So far we have restricted ourselves to symmetric states of two qubits. Let us now consider the generic case of arbitrary two-qubit nonsymmetric states. In this case we can still exploit the TMS algorithm, with the following differences [36]. The bipartite state acts on the tensor product $\mathcal{H}_1 \otimes \mathcal{H}_2$ of Hilbert spaces and each of them now has its own set of variables x, y , and z ; we label these variables (x_i, y_i, z_i) , with $i = 1, 2$. The compact set K is now the product of two Bloch spheres. The set \mathcal{M} of possible measurements is

$$\mathcal{M} = \{M_{x_1}, M_{y_1}, M_{z_1}, M_{x_2}, M_{x_1x_2}, M_{y_1y_2}, M_{z_1z_2}, M_{y_2}, M_{x_1y_2}, M_{y_1y_2}, M_{z_1y_2}, M_{z_2}, M_{x_1z_2}, M_{y_1z_2}, M_{z_1z_2}\}. \quad (20)$$

For example, M_{x_1} is the measurement of $\sigma_x \otimes \mathbb{1}$ and $M_{x_1x_2}$ is the measurement of the joint operator $\sigma_x \otimes \sigma_x$. Up to relabeling the variables for each qubit, some sets of measurement operators are equivalent. The number m_k of nonequivalent sets of measurements is obtained by applying the 36 possible permutations on the (x_i, y_i, z_i) . This number is reported in Table II for $1 \leq k \leq 15$.

The number m_k increases rapidly with k , and so does the size of the moment matrices considered in the TMS algorithm: indeed, because of condition (7), the algorithm always searches at least for the first extension; in both cases (symmetric and nonsymmetric) the smallest extension corresponds to the moment matrix of order 2. In the symmetric case it is a 10×10 matrix, while in the nonsymmetric case it already becomes a 28×28 matrix which contains all the monomials up to degree 4 for the set of six variables x_i, y_i, z_i , with $i = 1, 2$, i.e., 210 moments, versus 35 in the symmetric case. For the previous reasons computational times become an issue in the nonsymmetric case. Nevertheless, we could estimate probabilities up to $k = 5$, running the TMS algorithm over a database of 50 000 nonsymmetric two-qubit random states. What we observe is that no state is detected as entangled with only one measurement, a tiny fraction ($\sim 1\%$) is detected as entangled by the combination of two measurements $\{M_{x_1x_2}, M_{y_1y_2}\}$, and the largest fraction of states detected as entangled for $3 \leq k \leq 5$ is given, respectively, by the set of measurements $\{M_{x_1x_2}, M_{y_1y_2}, M_{z_1z_2}\}$ ($\sim 10\%$), $\{M_{x_1x_2}, M_{x_1y_2}, M_{y_1x_2}, M_{z_1z_2}\}$ ($\sim 12\%$), $\{M_{x_1x_2}, M_{x_1y_2}, M_{y_1x_2}, M_{y_1y_2}, M_{z_1z_2}\}$ ($\sim 23\%$). This is a big difference compared to the symmetric case, in which we could detect $\sim 15\%$ of the states as entangled with a single measurement, $\sim 40\%$ already with two measurements, and almost all states with five measurements.

VI. HIGHER SPIN-*j*

Going back to the case of symmetric states, we can also get an idea of how complexity changes for higher spin sizes; indeed, the size of the set \mathcal{M} in the symmetric case corresponds to the sum of the number of monomials in three variables up to degree $d = 2j + 1$, where j is the spin size. These numbers form the sequence of triangular numbers $T_n = \sum_{i=1}^n i = \frac{n(n+1)}{2}$; we can then write that m_k for any spin- j is

$$m_k = \binom{\sum_{n=1}^{2j+1} T_n - 1}{k}, \tag{21}$$

where we subtract 1 since the first element of \mathcal{M} is always the identity. However, in this case, we can still have some information looking at the expression for the tensor representation of a separable state in (4). Indeed, for an even number of qubits (integer spins) we can look at the diagonal tensor entries, which are defined as the entries of the form $X_{\mu_1 \dots \mu_j \mu_1 \dots \mu_j}$ with $0 \leq \mu_i \leq 3$. These correspond to terms of the form $\sum_j \omega_j (n_{\mu_1} \dots n_{\mu_j})^{2j}$; it follows that for a separable state these entries are positive, since the n_{μ_i} are real and $\omega_j \geq 0$. Therefore measuring a negative value for any of the corresponding measurement operators means detecting entanglement; we indicate the operators corresponding to the diagonal entries of the tensor $X_{\mu_1 \mu_2 \dots \mu_N}$ with $\{D\}_I$. We can then restrict our investigation for an integer spin- j to these 4^j observables, which are further reduced by symmetry to $\binom{j+3}{3}$. We report in Fig. 7 the number of entangled states that are not detected by any of the observables $\{D\}_I$ for spin size $1 \leq j \leq 5$ (for each j we used a sample of 10^6 random states from which we again removed the separable ones). The number of undetected entangled states decreases with the spin size j and already at $j = 4$ all the states in the sample are detected; we can also observe that restricting the analysis to these observables already gives significant information for spin-1 and spin-2 and almost-complete information for spin-3. Moreover, we can also compare these observables to see which is the most efficient measurement to perform as we did for the spin-1 case; to estimate the corresponding $p_I^{(1)}$, we again only consider sets which are nonequivalent

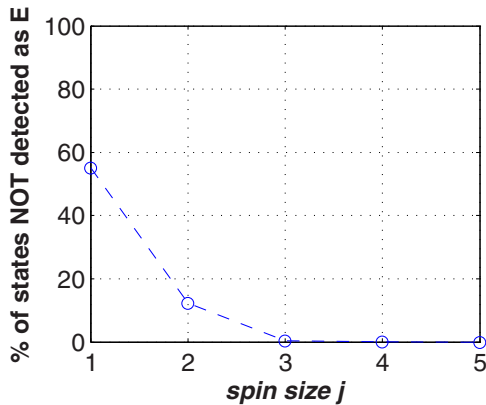


FIG. 7. Percentage of entangled states not detected by any of the negative outcomes of the measurements $\{D\}_I$ corresponding to the diagonal entries of the tensor $X_{\mu_1 \mu_2 \dots \mu_N}$ as a function of the spin size j .

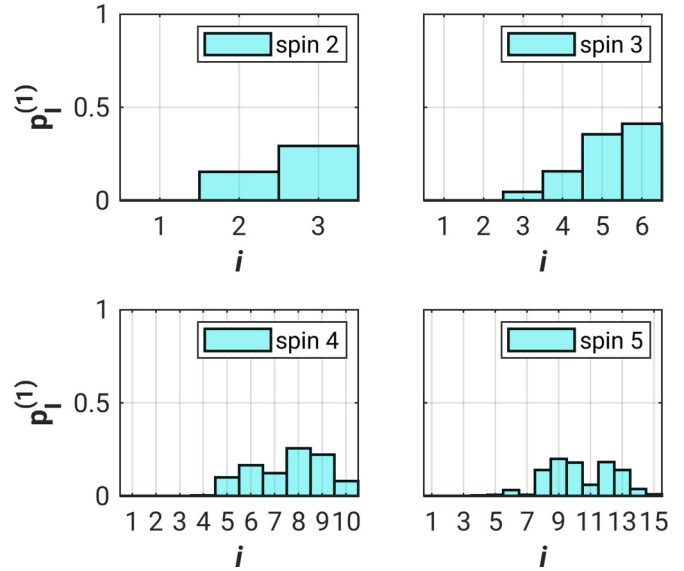


FIG. 8. Comparison of the nonequivalent diagonal observables $\{D\}_I$ for spin- j , $2 \leq j \leq 5$: probabilities $p_I^{(1)}$ as a function of the label i of set I . The highest values are reached, respectively, for D_{xxxxy} , D_{xyyyz} , $D_{xxxxxyy}$, and $D_{xxxxxyyy}$ (where the last term corresponds to the measurement of $\mathbb{1}^{\otimes 2} \otimes \sigma_x^{\otimes 4} \otimes \sigma_y^{\otimes 4}$; see Appendix B for the full list).

under permutation of the axes, performing the transformations $\{P_{xy}, P_{xz}, P_{yz}, P_{yzx}, P_{zxy}\}$ described in Sec. III B. The results are shown in Fig. 8. The question arises whether similarly efficient measurements can be found for half-integer spin- j . It was recently shown in [49] how the positive-partial-transpose separability criterion for symmetric states of multiqubit systems can be formulated in terms of matrix inequalities based on the tensor representation in Eq. (2). It is possible to construct a matrix T from the tensor representation of the state and show that it is similar to the partial transpose of the density matrix written in the computational basis. In the case of spin-3/2 this matrix is an 8×8 Hermitian matrix given

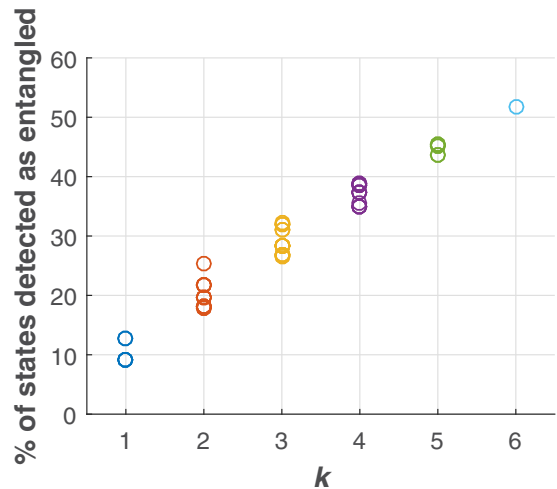


FIG. 9. Entanglement detection probabilities based on the negativity of the $\binom{6}{k}$ subsets of the set $\{X_{011} - X_{113}, X_{011} + X_{113}, X_{022} - X_{223}, X_{022} + X_{223}, X_{033} - X_{333}, X_{033} + X_{333}\}$ for $k = 1, \dots, 6$, where the tensor $X_{\mu_1 \mu_2 \mu_3}$ represents a spin-3/2.

by $T_{\mu_i, \nu_i'} = \sum_{\tau=0}^3 X_{\tau\mu\nu} \sigma_{i,i'}^\tau$, where $\sigma_{i,i'}^\tau$ are the Pauli-matrix components, and its positivity is a necessary and sufficient classicality criterion; as a consequence, the positivity of the diagonal entries is a necessary condition for a separable state. We can again restrict our investigation to the corresponding observables $\{D\}_I$, but this time it implies the measurement of sets of two observables. Indeed, in terms of the tensor entries $X_{\mu_1\mu_2\mu_3}$, the diagonal entries in T are $X_{000} \pm X_{003}$, $X_{011} \pm X_{113}$, $X_{022} \pm X_{223}$, $X_{033} \pm X_{333}$, so we need to compare pairs of outcomes. Recalling that $X_{000} = 1$, we can neglect the first entry, since the condition $-1 \leq X_{003} \leq 1$ is always satisfied. The results of such investigation for the other six pairs and for their combinations [all the $\binom{6}{k}$ sets, with $2 \leq k \leq 6$] are reported in Fig. 9. As before, we can gain already relevant information from this restricted analysis.

VII. CONCLUSIONS

In summary, we have studied the statistics of lengths of measurement sequences for multiqubit systems that allow one to detect entanglement without any prior information about the state, for both unordered sets of measurements and ordered ones (i.e., measurement paths). For symmetric states of two qubits, we have identified the best measurement path that results, on average over all randomly chosen entangled states, in a proof of entanglement with 3.07 measurements (compared to the 8 measurements needed for full tomography in this case). For larger numbers N of qubits in symmetric states, we found that measurements based on the diagonal matrix elements of the moment matrix of the state become very efficient in detecting entanglement. Their number increases like N^3 , and already at $N = 8$ qubits the number of states *not* detected as entangled has decreased to about 10^{-6} or smaller. For nonsymmetric states, substantially larger numbers of measurements are needed to detect entanglement with certainty: at least two measurements are needed for two-qubit states, resulting in only about a 1% detection probability, however. With five measurements the probability increases to about 23%. The work is based on the truncated moment sequence algorithm that naturally allows one to deal with missing data. It is very flexible and can be easily adapted to experimentally relevant ensembles of states and other side conditions, such as sets of measurements that can be implemented or more elaborate cost functions.

ACKNOWLEDGMENTS

D.B. thanks O.G., the LPTMS, and the Université Paris-Saclay for hospitality.

APPENDIX A: UNORDERED MEASUREMENT SETS

We list here all the m_k unique sets of k measurements for $1 \leq k \leq 8$.

<hr/> <hr/>	
$k = 1$	
1	M_x
2	M_{xx}
3	M_{xy}
<hr/> <hr/>	

(Continued).

<hr/> <hr/>	
$k = 1$	
<hr/>	
$k = 2$	
1	$\{M_x, M_y\}$
2	$\{M_x, M_{xx}\}$
3	$\{M_x, M_{xy}\}$
4	$\{M_x, M_{yy}\}$
5	$\{M_x, M_{yz}\}$
6	$\{M_{xx}, M_{xy}\}$
7	$\{M_{xx}, M_{yy}\}$
8	$\{M_{xx}, M_{yz}\}$
9	$\{M_{xy}, M_{xz}\}$
$k = 3$	
1	$\{M_x, M_y, M_z\}$
2	$\{M_x, M_y, M_{xx}\}$
3	$\{M_x, M_y, M_{xy}\}$
4	$\{M_x, M_y, M_{xz}\}$
5	$\{M_x, M_z, M_{yy}\}$
6	$\{M_x, M_{xx}, M_{xy}\}$
7	$\{M_x, M_{xx}, M_{yy}\}$
8	$\{M_x, M_{xx}, M_{yz}\}$
9	$\{M_x, M_{xy}, M_{xz}\}$
10	$\{M_x, M_{xy}, M_{yy}\}$
11	$\{M_x, M_{xy}, M_{yz}\}$
12	$\{M_x, M_{xz}, M_{yy}\}$
13	$\{M_x, M_{yy}, M_{yz}\}$
14	$\{M_z, M_{xx}, M_{yy}\}$
15	$\{M_{xx}, M_{xy}, M_{xz}\}$
16	$\{M_{xx}, M_{xy}, M_{yy}\}$
17	$\{M_{xx}, M_{xy}, M_{yz}\}$
18	$\{M_{xx}, M_{xz}, M_{yy}\}$
19	$\{M_{xy}, M_{xz}, M_{yz}\}$
$k = 4$	
1	$\{M_x, M_y, M_z, M_{xx}\}$
2	$\{M_x, M_y, M_z, M_{xy}\}$
3	$\{M_x, M_y, M_{xx}, M_{xy}\}$
4	$\{M_x, M_y, M_{xx}, M_{xz}\}$
5	$\{M_x, M_y, M_{xx}, M_{yy}\}$
6	$\{M_x, M_y, M_{xx}, M_{yz}\}$
7	$\{M_x, M_z, M_{xx}, M_{yy}\}$
8	$\{M_x, M_y, M_{xy}, M_{xz}\}$
9	$\{M_x, M_z, M_{xz}, M_{yy}\}$
10	$\{M_x, M_y, M_{xz}, M_{yz}\}$
11	$\{M_x, M_z, M_{xy}, M_{yy}\}$
12	$\{M_x, M_{xx}, M_{xy}, M_{xz}\}$
13	$\{M_x, M_{xx}, M_{xy}, M_{yy}\}$
14	$\{M_x, M_{xx}, M_{xy}, M_{yz}\}$
15	$\{M_x, M_{xx}, M_{xz}, M_{yy}\}$
16	$\{M_x, M_{xx}, M_{yy}, M_{yz}\}$
17	$\{M_x, M_{xy}, M_{xz}, M_{yy}\}$
18	$\{M_x, M_{xy}, M_{xz}, M_{yz}\}$
19	$\{M_x, M_{xy}, M_{yy}, M_{yz}\}$
20	$\{M_z, M_{xx}, M_{yy}, M_{yz}\}$
21	$\{M_x, M_{xz}, M_{yy}, M_{yz}\}$
22	$\{M_z, M_{xx}, M_{xz}, M_{yy}\}$
23	$\{M_{xx}, M_{xy}, M_{xz}, M_{yy}\}$
24	$\{M_{xx}, M_{xy}, M_{xz}, M_{yz}\}$
25	$\{M_{xx}, M_{xz}, M_{yy}, M_{yz}\}$
$k = 5$	
1	$\{M_x, M_y, M_z, M_{xx}, M_{xy}\}$
2	$\{M_x, M_y, M_z, M_{xx}, M_{yy}\}$
<hr/> <hr/>	

(Continued).

$k = 5$	
3	$\{M_x, M_y, M_z, M_{xx}, M_{yz}\}$
4	$\{M_x, M_y, M_z, M_{xy}, M_{xz}\}$
5	$\{M_x, M_y, M_{xx}, M_{xy}, M_{yz}\}$
6	$\{M_x, M_y, M_{xx}, M_{xy}, M_{yy}\}$
7	$\{M_x, M_y, M_{xx}, M_{xy}, M_{yz}\}$
8	$\{M_x, M_z, M_{xx}, M_{xz}, M_{yy}\}$
9	$\{M_x, M_y, M_{xx}, M_{xz}, M_{yy}\}$
10	$\{M_x, M_y, M_{xx}, M_{xz}, M_{yz}\}$
11	$\{M_x, M_z, M_{xx}, M_{xy}, M_{yy}\}$
12	$\{M_x, M_z, M_{xx}, M_{yy}, M_{yz}\}$
13	$\{M_x, M_y, M_{xy}, M_{xz}, M_{yy}\}$
14	$\{M_x, M_z, M_{xy}, M_{xz}, M_{yy}\}$
15	$\{M_x, M_z, M_{xy}, M_{yy}, M_{yz}\}$
16	$\{M_x, M_{xx}, M_{xy}, M_{xz}, M_{yy}\}$
17	$\{M_x, M_{xx}, M_{xy}, M_{xz}, M_{yz}\}$
18	$\{M_x, M_{xx}, M_{xy}, M_{yy}, M_{yz}\}$
19	$\{M_x, M_{xx}, M_{xz}, M_{yy}, M_{yz}\}$
20	$\{M_x, M_{xy}, M_{xz}, M_{yy}, M_{yz}\}$
21	$\{M_z, M_{xx}, M_{xz}, M_{yy}, M_{yz}\}$
22	$\{M_z, M_{xx}, M_{xy}, M_{yy}, M_{yz}\}$
23	$\{M_{xx}, M_{xy}, M_{xz}, M_{yy}, M_{yz}\}$
$k = 6$	
1	$\{M_x, M_y, M_z, M_{xx}, M_{xy}, M_{xz}\}$
2	$\{M_x, M_y, M_z, M_{xx}, M_{xy}, M_{yy}\}$
3	$\{M_x, M_y, M_z, M_{xx}, M_{xy}, M_{yz}\}$
4	$\{M_x, M_y, M_z, M_{xx}, M_{xz}, M_{yy}\}$
5	$\{M_x, M_y, M_z, M_{xy}, M_{xz}, M_{yz}\}$
6	$\{M_x, M_y, M_{xx}, M_{xy}, M_{xz}, M_{yy}\}$
7	$\{M_x, M_y, M_{xx}, M_{xy}, M_{xz}, M_{yz}\}$
8	$\{M_x, M_z, M_{xx}, M_{xy}, M_{xz}, M_{yy}\}$
9	$\{M_x, M_z, M_{xx}, M_{xz}, M_{yy}, M_{yz}\}$
10	$\{M_x, M_y, M_{xx}, M_{xz}, M_{yy}, M_{yz}\}$
11	$\{M_x, M_z, M_{xx}, M_{xy}, M_{yy}, M_{yz}\}$
12	$\{M_x, M_z, M_{xy}, M_{xz}, M_{yy}, M_{yz}\}$
13	$\{M_x, M_{xx}, M_{xy}, M_{xz}, M_{yy}, M_{yz}\}$
14	$\{M_z, M_{xx}, M_{xy}, M_{xz}, M_{yy}, M_{yz}\}$
$k = 7$	
1	$\{M_x, M_y, M_z, M_{xx}, M_{xy}, M_{xz}, M_{yy}\}$
2	$\{M_x, M_y, M_z, M_{xx}, M_{xy}, M_{xz}, M_{yz}\}$
3	$\{M_x, M_y, M_z, M_{xx}, M_{xz}, M_{yy}, M_{yz}\}$
4	$\{M_x, M_y, M_{xx}, M_{xy}, M_{xz}, M_{yy}, M_{yz}\}$
5	$\{M_x, M_z, M_{xx}, M_{xy}, M_{xz}, M_{yy}, M_{yz}\}$
$k = 8$	
1	$\{M_x, M_y, M_z, M_{xx}, M_{xy}, M_{xz}, M_{yy}, M_{yz}\}$

APPENDIX B: NONEQUIVALENT DIAGONAL OBSERVABLES

We list here all the nonequivalent observables D_I for spin- j , $2 \leq j \leq 5$.

$j = 2$	
1	D_{xx}
2	D_{xxxx}
3	D_{xxyy}
$j = 3$	
1	D_{xx}
2	D_{xxxx}
3	D_{xxyy}
4	D_{xxxxx}
5	D_{xxxxyy}
6	D_{xxyyzz}
$j = 4$	
1	D_{xx}
2	D_{xxxx}
3	D_{xxyy}
4	D_{xxxxxx}
5	D_{xxxxyy}
6	D_{xxyyzz}
7	$D_{xxxxxxxx}$
8	$D_{xxxxxyy}$
9	$D_{xxxxyyy}$
10	$D_{xxxxyyzz}$
$j = 5$	
1	D_{xx}
2	D_{xxxx}
3	D_{xxyy}
4	D_{xxxxxx}
5	D_{xxxxyy}
6	D_{xxyyzz}
7	$D_{xxxxxxxx}$
8	$D_{xxxxxyy}$
9	$D_{xxxxyyy}$
10	$D_{xxxxyyzz}$
11	$D_{xxxxxxxxxx}$
12	$D_{xxxxxyyy}$
13	$D_{xxxxyyyy}$
14	$D_{xxxxyyzz}$
15	$D_{xxxxyyyzz}$

[1] D. F. V. James, P. G. Kwiat, W. J. Munro, and A. G. White, *Phys. Rev. A* **64**, 052312 (2001).
 [2] R. Blume-Kohout, *Phys. Rev. Lett.* **105**, 200504 (2010).
 [3] Z. Hradil, *Phys. Rev. A* **55**, R1561 (1997).
 [4] T. Baumgratz, A. Nüßeler, M. Cramer, and M. B. Plenio, *New J. Phys.* **15**, 125004 (2013).
 [5] R. Blume-Kohout, *New J. Phys.* **12**, 043034 (2010).
 [6] J. Rau, *Phys. Rev. A* **82**, 012104 (2010).
 [7] S. T. Merkel, J. M. Gambetta, J. A. Smolin, S. Poletto, A. D. Corcoles, B. R. Johnson, C. A. Ryan, and M. Steffen, *Phys. Rev. A* **87**, 062119 (2013).

[8] D. Gross, Y.-K. Liu, S. T. Flammia, S. Becker, and J. Eisert, *Phys. Rev. Lett.* **105**, 150401 (2010).
 [9] M. Ohliger, V. Nesme, D. Gross, Y.-K. Liu, and J. Eisert, [arXiv:1111.0853](https://arxiv.org/abs/1111.0853).
 [10] M. Ohliger, V. Nesme, and J. Eisert, *New J. Phys.* **15**, 015024 (2013).
 [11] M. Kliesch, R. Kueng, J. Eisert, and D. Gross, [arXiv:1701.03135](https://arxiv.org/abs/1701.03135).
 [12] S. T. Flammia, D. Gross, Y.-K. Liu, and J. Eisert, *New J. Phys.* **14**, 095022 (2012).

- [13] M. Cramer, M. B. Plenio, S. T. Flammia, R. Somma, D. Gross, S. D. Bartlett, O. Landon-Cardinal, D. Poulin, and Y.-K. Liu, *Nat. Commun.* **1**, 149 (2010).
- [14] B. P. Lanyon, C. Maier, M. Holzäpfel, T. Baumgratz, C. Hempel, P. Jurcevic, I. Dhand, A. S. Buyskikh, A. J. Daley, M. Cramer *et al.*, *Nat. Phys.* **13**, 1158 (2017).
- [15] C. Ferrie, *Phys. Rev. Lett.* **113**, 190404 (2014).
- [16] B. Wang, [arXiv:1709.03617](https://arxiv.org/abs/1709.03617).
- [17] S. Lu, S. Huang, K. Li, J. Li, J. Chen, D. Lu, Z. Ji, Y. Shen, D. Zhou, and B. Zeng, *Phys. Rev. A* **98**, 012315 (2018).
- [18] G. Torlai, G. Mazzola, J. Carrasquilla, M. Troyer, R. Melko, and G. Carleo, *Nat. Phys.* **14**, 447 (2018).
- [19] V. Saggio, A. Dimić, C. Greganti, L. A. Rozema, P. Walther, and B. Dakić, [arXiv:1809.05455](https://arxiv.org/abs/1809.05455).
- [20] A. Dimić and B. Dakić, *npj Quantum Info.* **4**, 11 (2018).
- [21] E. Knill, D. Leibfried, R. Reichle, J. Britton, R. B. Blakestad, J. D. Jost, C. Langer, R. Ozeri, S. Seidelin, and D. J. Wineland, *Phys. Rev. A* **77**, 012307 (2008).
- [22] E. Magesan, J. M. Gambetta, B. R. Johnson, C. A. Ryan, J. M. Chow, S. T. Merkel, M. P. da Silva, G. A. Keefe, M. B. Rothwell, T. A. Ohki *et al.*, *Phys. Rev. Lett.* **109**, 080505 (2012).
- [23] J. P. Gaebler, A. M. Meier, T. R. Tan, R. Bowler, Y. Lin, D. Hanneke, J. D. Jost, J. P. Home, E. Knill, D. Leibfried *et al.*, *Phys. Rev. Lett.* **108**, 260503 (2012).
- [24] G. Chiribella, G. M. D'Ariano, and M. Roetteler, *New J. Phys.* **15**, 103019 (2013).
- [25] C. Dankert, R. Cleve, J. Emerson, and E. Livine, *Phys. Rev. A* **80**, 012304 (2009).
- [26] L. Arnaud and D. Braun, *Phys. Rev. A* **75**, 062314 (2007).
- [27] C. T. Schmiegelow, A. Bendersky, M. A. Larotonda, and J. P. Paz, *Phys. Rev. Lett.* **107**, 100502 (2011).
- [28] A. Bendersky, F. Pastawski, and J. P. Paz, *Phys. Rev. A* **80**, 032116 (2009).
- [29] A. I. Lvovsky and M. G. Raymer, *Rev. Mod. Phys.* **81**, 299 (2009).
- [30] J. G. Titchener, M. Gräfe, R. Heilmann, A. S. Solntsev, A. Szameit, and A. A. Sukhorukov, *npj Quantum Info.* **4**, 19 (2018).
- [31] H. Häffner, W. Hansel, C. F. Roos, J. Benhelm, D. Chek-al kar, M. Chwalla, T. Körber, U. D. Rapol, M. Riebe, P. Schmidt *et al.*, *Nature* **438**, 643 (2005).
- [32] T. Monz, P. Schindler, J. T. Barreiro, M. Chwalla, D. Nigg, W. A. Coish, M. Harlander, W. Hansel, M. Hennrich, and R. Blatt, *Phys. Rev. Lett.* **106**, 130506 (2011).
- [33] T. S. Iskhakov, I. N. Agafonov, M. V. Chekhova, and G. Leuchs, *Phys. Rev. Lett.* **109**, 150502 (2012).
- [34] R. McConnell, H. Zhang, J. Hu, S. Čuk, and V. Vuletić, *Nature* **519**, 439 (2015).
- [35] J. G. Bohnet, B. C. Sawyer, J. W. Britton, M. L. Wall, A. M. Rey, M. Foss-Feig, and J. J. Bollinger, *Science* **352**, 1297 (2016).
- [36] F. Bohnet-Waldraff, D. Braun, and O. Giraud, *Phys. Rev. A* **96**, 032312 (2017).
- [37] J. Nie, *Found. Comput. Math.* **14**, 1243 (2014).
- [38] A. Mari, K. Kieling, B. M. Nielsen, E. S. Polzik, and J. Eisert, *Phys. Rev. Lett.* **106**, 010403 (2011).
- [39] O. Giraud, D. Braun, D. Baguette, T. Bastin, and J. Martin, *Phys. Rev. Lett.* **114**, 080401 (2015).
- [40] A. C. Doherty, P. A. Parrilo, and F. M. Spedalieri, *Phys. Rev. A* **71**, 032333 (2005).
- [41] L. Fialkow and J. Nie, *J. Funct. Anal.* **263**, 1682 (2012).
- [42] A. Peres, *Phys. Rev. Lett.* **77**, 1413 (1996).
- [43] M. Horodecki, P. Horodecki, and R. Horodecki, *Phys. Lett. A* **223**, 1 (1996).
- [44] K. Zyczkowski, K. A. Penson, I. Nechita, and B. Collins, *J. Math. Phys.* **52**, 062201 (2011).
- [45] O. Giraud, P. Braun, and D. Braun, *New J. Phys.* **12**, 063005 (2010).
- [46] R. H. Dicke, *Phys. Rev.* **93**, 99 (1954).
- [47] F. T. Arecchi, E. Courtens, R. Gilmore, and H. Thomas, *Phys. Rev. A* **6**, 2211 (1972).
- [48] O. Giraud, P. Braun, and D. Braun, *Phys. Rev. A* **78**, 042112 (2008).
- [49] F. Bohnet-Waldraff, D. Braun, and O. Giraud, *Phys. Rev. A* **94**, 042343 (2016).

Truncated moment sequences and a solution to the channel separability problemN. Milazzo ^{1,2}, D. Braun,¹ and O. Giraud²¹*Institut für theoretische Physik, Universität Tübingen, 72076 Tübingen, Germany*²*Université Paris-Saclay, CNRS, LPTMS, 91405 Orsay, France*

(Received 3 July 2020; accepted 15 October 2020; published 6 November 2020)

We consider the problem of separability of quantum channels via the Choi matrix representation given by the Choi-Jamiołkowski isomorphism. We explore three classes of separability across different cuts between systems and ancillae, and we provide a solution based on the mapping of the coordinates of the Choi state (in a fixed basis) to a truncated moment sequence (tms) y . This results in an algorithm which gives a separability certificate using semidefinite programming. The computational complexity and the performance of it depend on the number of variables n in the tms and on the size of the moment matrix $M_t(y)$ of order t . We exploit the algorithm to numerically investigate separability of families of two-qubit and single-qutrit channels; in the latter case we can provide an answer for examples explored earlier through the criterion based on the negativity N , a criterion which remains inconclusive for Choi matrices with $N = 0$.

DOI: [10.1103/PhysRevA.102.052406](https://doi.org/10.1103/PhysRevA.102.052406)**I. INTRODUCTION**

Entanglement properties of quantum states have been at the center of many investigations in recent years. Meanwhile, first small-scale quantum processors have become available, and the problem of verifying that such devices work in a properly “quantum” way has become center stage. In that context, it is of high relevance to understand the way entanglement evolves under physical operations acting on quantum states [1–6]. Many contributions to tomography and benchmarking of quantum devices or, more generally, quantum channels can be found in the literature, e.g., recent approaches in the framework of resource and device-independent theories [7,8], schemes which aim at reducing the resources required for entanglement verification [9], methods based on quantum process tomography [10,11], approaches that detect inseparability based on witness operators [12] or separability based on theorems exploiting local operations and classical communication [13,14]. An uncontroversial requirement for a proper quantum operation is that the device is able to create entanglement, a resource on which quantum technology largely relies. In particular it is well known that a quantum computer that generates only limited amounts of entanglement can be simulated efficiently classically [15]. On the other hand the properties of devices which break entanglement turned out to be useful for proving relevant conjectures [16] for obtaining results for the problem of additivity of capacity [17,18] and for their connection with different types of quantum correlations [19]. The problem of deciding whether a quantum *state* is entangled or not has been solved in the sense of its reduction to matrix extensions and semidefinite programming [20], an approach that was later understood more generally within the theory of truncated moment sequences [21]. However, no corresponding algorithm that gives a definite outcome for quantum *channels* was known, i.e., an algorithm that takes as input an arbitrary quantum channel and outputs a

definite answer whether the quantum channel can generate entanglement for some initial separable state. Although one might argue that with modern technology it is quite easy to entangle, e.g., two qubits and verify their entanglement, the entanglement is typically lost on relatively short timescales. The way entanglement is created and possibly destroyed again by the full channel, including storage and decoherence processes over longer times, depends on the input state. When trying to verify entanglement creation one would, thus, have to search for suitable input states. In such a situation it would be much more convenient to assess the possibility of entanglement creation directly on the level of the quantum channel. In the present paper we present such an algorithm for the channel separability problem. It generalizes to quantum channels the hierarchy of Refs. [20,21]. The resulting algorithm provides definiteness in the answer to the question whether a quantum channel is entangling or separable, even in cases where more straightforward separability criteria based on positive but not completely positive maps fail as we will demonstrate with explicit examples in Sec. IV C.

The mathematical object associated with a physical operation is a quantum channel, which acts on the joint state of a system \mathcal{A} and its environment to produce an output state. The environment can be seen as an ancilla system \mathcal{A}' with which the system \mathcal{A} is possibly entangled. The system \mathcal{A} itself may be bipartite and made of two subsystems A and B which may or may not be entangled with one another or with their respective ancillae A' and B' . Since a channel acts on both the system and its ancilla, the output state may be entangled in different ways, which leads to different definitions of separability of quantum channels [22–26]. These definitions depend on whether the total state of the system and ancilla is separable for instance across the cut $\mathcal{A} - \mathcal{A}'$ or across the cut $A - B$. The algorithm that we present in Sec. III D allows one to investigate all different notions of separability with only small modifications needed in the input to go from one

definition to the other, thus, giving a unifying framework for the separability problem in the case of quantum channels.

The Choi-Jamiołkowski isomorphism relates completely positive trace-preserving maps with density matrices or equivalently completely positive maps with positive operators. Characterizing separability for channels can be investigated in the light of results obtained for quantum states. Many theoretical results have been obtained for states in terms of separability criteria [27]. One of the most well-known necessary conditions for separability is the positive partial transpose (PPT) criterion, which states that if a state ρ is separable then $\rho^{\text{PT}} \geq 0$ with ρ^{PT} the partial transpose with respect to one of the subsystems [28,29].

As was shown recently [30], the separability problem for states can be recast as a “truncated moment” problem, a problem well studied in recent years in the mathematical literature. The truncated moment problem consists of finding conditions under which a given sequence of numbers corresponds to moments of a probability distribution. The moment problem corresponds to the case where an infinite sequence is given, whereas in the truncated moment problem only the lowest moments are fixed and the aim is to find a measure matching these moments. Of relevance for the separability problem as we will see is the K -truncated moment problem where the measure is additionally required to have the set K as support. In Ref. [30] we showed that asking whether a quantum state is separable along an arbitrary partition of Hilbert space can be cast in the form of a K -truncated moment problem, and we applied this approach to symmetric multiqubit states.

In the present paper our goal is to apply this formalism to the more general situation of the separability of quantum channels. Even though the problem of separability of channels can be related to the one of states through the Choi-Jamiołkowski isomorphism, it is still relevant to explicitly formulate the mapping with the moment problem since it allows us to provide theorems that give necessary and sufficient conditions for a channel to be separable or entanglement breaking; moreover, the resulting necessary and sufficient criterion is also practically usable thanks to a quite simple algorithm that implements the theorems numerically. The paper is organized as follows. In Sec. II we recall some useful definitions about quantum channels and the various notions of separability. In Sec. III we explain in detail how the truncated moment problem maps to these separability problems, and we provide a theoretical solution in the form of a set of theorems (Sec. III C) and a numerical solution in terms of an algorithm (Sec. III D). In Sec. IV we consider various examples of application of this algorithm, which allow detection of separability in quantum channels. Finally we conclude in Sec. V.

II. DEFINITIONS

We start by recalling some elementary definitions.

A. Quantum channels

Let ρ be a quantum state acting on a tensor product $H = H^{(1)} \otimes \dots \otimes H^{(d)}$ of Hilbert spaces $H^{(i)}$ of finite dimension. Any physical transformation can be described by a completely positive map, that is, a map Φ such that $\Phi \otimes \mathbb{1}$ is positive on all states acting on an extended Hilbert space $H \otimes H'$ (where

H' is the Hilbert space of an ancillary system of arbitrary size). A quantum channel Φ is, therefore, defined as a completely positive trace-preserving linear map, which maps ρ to a state $\rho' = \Phi(\rho)$ acting on some Hilbert space (that for simplicity we consider here equal to H so that $\Phi: \mathcal{L}(H) \rightarrow \mathcal{L}(H)$, where $\mathcal{L}(H)$ is the set of linear operators on H).

Let N be the dimension of the Hilbert space H . A density matrix can be expanded as $\rho = \sum_{i,j} \rho_{ij} |i\rangle \langle j|$, with $|i\rangle$ as the vectors of the canonical basis of H . To any linear map Φ mapping ρ to ρ' one can associate a superoperator M of size N^2 such that $\rho'_{ij} = M_{ij,kl} \rho_{kl}$ (with summation over repeated indices), and a dynamical matrix D_Φ defined [31] by a reshuffling of entries of M , namely, $(D_\Phi)_{ij,kl} = M_{ik,jl}$ [27]. Alternatively one can define the Choi matrix,

$$C_\Phi = \sum_{i,j} \Phi(|i\rangle \langle j|) \otimes |i\rangle \langle j|, \quad (1)$$

[32], which coincides with D_Φ when written in the canonical basis. The Choi matrix C_Φ is Hermitian. The map Φ is positive if and only if the corresponding Choi matrix C_Φ is block positive (that is, positive on product states in $H \otimes H$) [33]. According to Choi’s theorem [32], Φ is completely positive if and only if its Choi matrix is positive semidefinite. Finally, Φ is trace preserving if and only if the N^2 conditions $\sum_i (C_\Phi)_{ij,il} = \delta_{jl}$ are fulfilled. These conditions imply that $\text{tr} C_\Phi = N$.

As a consequence, if Φ is a quantum channel, then $\frac{1}{N} C_\Phi$ can be seen as a density matrix acting on $H \otimes H$. Any completely positive trace-preserving map can be associated with a density matrix in that way. The Choi-Jamiołkowski isomorphism is a bijection between a quantum channel Φ and its Choi matrix C_Φ [27,33]. We will also make use of the fact that a quantum channel can be written in Kraus form as

$$\Phi(\rho) = \sum_l E_l \rho E_l^\dagger, \quad \sum_l E_l^\dagger E_l = \mathbb{1}. \quad (2)$$

The Kraus operators E_l are not unique, but a canonical form can be found by diagonalizing the Choi matrix and reshuffling its eigenvectors into square matrices in which case a set of at most N^2 Kraus operators suffices [27].

B. Separability of channels

A bipartite quantum state ρ acting on a Hilbert space $H_A \otimes H_B$ is separable if it admits a decomposition,

$$\rho = \sum_i w_i \rho_i^{(A)} \otimes \rho_i^{(B)}, \quad (3)$$

with $w_i \geq 0$ and $\rho_i^{(A)}, \rho_i^{(B)}$ acting on H_A, H_B respectively. More generally, a positive semidefinite matrix M is said to be separable if it can be written as

$$M = \sum_k P_k \otimes Q_k, \quad (4)$$

with P_k and Q_k positive semidefinite matrices.

Various kinds of channel separability have been introduced in the literature. Consider the Hilbert space $H = H_A \otimes H_B$ describing a system partitioned into two subsystems A and B and let $\Phi: \mathcal{L}(H_A \otimes H_B) \rightarrow \mathcal{L}(H_A \otimes H_B)$ be a completely positive map. As a criterion for complete positivity one must

consider the extended Hilbert state $H \otimes H'$ with $H' = H$ where here and in the following the prime is used to denote the ancilla system. The corresponding Choi matrix C_Φ can be seen as a density matrix acting on Hilbert space $\mathcal{H} = H_A \otimes H_B \otimes H_{A'} \otimes H_{B'}$. Following Eq. (1) it can be expressed as $C_\Phi = \sum_{ijrs} \Phi(|ir\rangle \langle js|) \otimes |ir\rangle \langle js|$.

1. Separable channels

Φ is called separable (SEP) if it takes the form $\Phi(\rho) = \sum_l (A_l \otimes B_l) \rho (A_l \otimes B_l)^\dagger$ [22]. In other words, the Kraus operators for the channel Φ in (2) can be factored as $E_l = A_l \otimes B_l$. Such channels map separable states to separable states. In terms of these Kraus operators, the Choi matrix of a separable map Φ is given by

$$C_\Phi = \sum_{i,j,r,s} \sum_l A_l |i\rangle \langle j| A_l^\dagger \otimes B_l |r\rangle \langle s| B_l^\dagger \otimes |i\rangle \langle j| \otimes |r\rangle \langle s|. \quad (5)$$

Swapping $H_{A'}$ and H_B we can interpret C_Φ as an operator in $H = H_A \otimes H_{A'} \otimes H_B \otimes H_{B'}$ and reexpress it as

$$C_\Phi = \sum_l \sum_{i,j} A_l |i\rangle \langle j| A_l^\dagger \otimes |i\rangle \langle j| \otimes \sum_{r,s} B_l |r\rangle \langle s| B_l^\dagger \otimes |r\rangle \langle s|. \quad (6)$$

It is clear that $\sum_{i,j} A_l |i\rangle \langle j| A_l^\dagger \otimes |i\rangle \langle j|$ is positive semidefinite for all l 's because it is the Choi matrix of the completely positive map $\rho \mapsto A_l \rho A_l^\dagger$; and the same holds for B . Therefore, C_Φ can be written as a sum $\sum_l M_A^{(l)} \otimes M_B^{(l)}$ with $M_A^{(l)}$ and $M_B^{(l)}$ positive semidefinite: It is, thus, a separable matrix across the $(A - A') - (B - B')$ cut. It was shown in Ref. [6] that the converse is true, namely, C_Φ is separable across the $(A - A') - (B - B')$ cut if and only if Φ is a separable map. We will use this characterization of separable channels in Sec. III C.

We will call Φ fully separable (FS) if the corresponding C_Φ is separable across all possible cuts.

2. Entanglement-breaking channels

Φ is called entanglement breaking (EB) [23] if $(\Phi \otimes \mathbb{1})(\rho)$ is a separable state across the $H - H'$ cut whatever the initial state $\rho \in \mathcal{L}(\mathcal{H})$. It does not address the separability of the bipartite system H into A and B but rather the separability between the system and its environment (it can, therefore, be defined for one-qubit channels). Various necessary and sufficient conditions for entanglement breaking have been obtained in Ref. [23]. One necessary and sufficient criterion is that there exist a Kraus form where all Kraus operators have rank 1. In terms of the Choi matrix, a necessary and sufficient condition for EB is that C_Φ be separable across the $(A - B) - (A' - B')$ cut. Physically these channels correspond to the case in which the output state is prepared according to the measurement outcomes made by the sender and sent via a classical channel to the receiver. We point out the difference between separable and entanglement-breaking channels in Fig. 1.

Channels which become entanglement breaking after a sufficient number of compositions with themselves are called eventually entanglement-breaking channels [25,26].

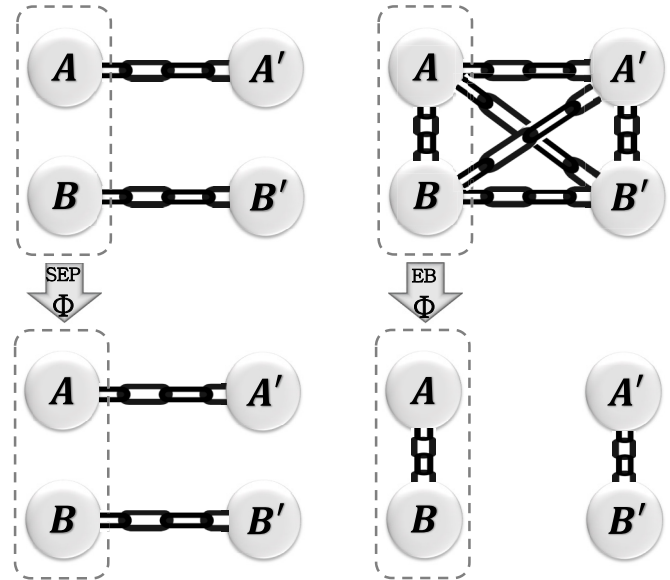


FIG. 1. Difference between separable (left) and entanglement-breaking (right) channels for a bipartite system AB with ancillae $A'B'$. The chains represent entanglement. A separable channel preserves separability between $(A - A')$ and $(B - B')$, whereas an entanglement-breaking channel destroys entanglement between A and all the ancillae and B and all the ancillae, giving separability between $(A - B)$ and $(A' - B')$.

3. Entanglement annihilating channels

Φ is called entanglement annihilating [34] if it destroys any entanglement within the system H (but it does not necessarily destroy entanglement between H and H'). A necessary and sufficient condition for entanglement annihilating channels in terms of the Choi matrix is that $C_\Phi \geq 0$ and that its partial trace over A and B is proportional to the identity matrix (see Corollary 1 of Ref. [24]). Such a condition on partial trace is not implementable in truncated moment sequence (tms) form, so we will not address this type of separability.

III. TRUNCATED MOMENT SEQUENCES

In the present section, we introduce the mathematical framework of truncated moment sequences (Sec. III A) and then apply it to quantum states (Sec. III B) and channels (Sec. III C). In general, to some nonnegative measure μ on \mathbb{R}^n one can associate its moments, which are the average values of the monomials $x_1^{\alpha_1} \cdots x_n^{\alpha_n}$. The moment y_α of order $\alpha = (\alpha_1, \dots, \alpha_n) \in \mathbb{Z}_+^n$ is defined as $y_\alpha = \int x^\alpha d\mu(x)$, where x^α denotes the monomial $x_1^{\alpha_1} \cdots x_n^{\alpha_n}$. If we are given a finite set y of real numbers, i.e., a *truncated sequence*, a natural question is to ask whether these numbers are the moments of a certain probability distribution. If the measure μ is constrained to be supported by a semialgebraic set K , the moment y_α is given as

$$y_\alpha = \int_K x^\alpha d\mu(x). \quad (7)$$

The tms problem deals with the characterization of the truncated sequences $y = (y_\alpha)_{\alpha \in \mathbb{Z}_+^n}$ that are sequences of moments of a measure μ . Solutions to this problem have been put forward in the mathematical literature. As we will see, the

separability problem can be expressed exactly in the form of Eq. (7). The reader interested in the mathematical results for the solution of the moment problem should continue with the next section; otherwise, jumping to Secs. III B and III C will directly give its connection with the physical problem of separability of quantum states and quantum channels, respectively.

A. The tms problem

In order to be as self-contained and pedagogical as possible for a physics-oriented audience, we start by reviewing and explaining some results from the mathematical literature [35–41]. We follow the nice presentation from Ref. [42]. We then recall the theorems obtained in Ref. [30] for quantum states and formulate them in the case of quantum channels.

A tms $y = (y_\alpha)_{|\alpha| \leq 2d}$ of degree $2d$ is a finite set of real numbers indexed by n -tuples $\alpha = (\alpha_1, \dots, \alpha_n)$ of integers $\alpha_i \geq 0$ such that $|\alpha| = \sum_i \alpha_i \leq 2d$ (here we only consider tms of even degree: indeed, although the definition would extend trivially to odd-degree tms, even-degree tms are the only ones involved in the theorems below, so this slightly simplifies notations). We denote by S_{2d} the set of n -tuples $\alpha = (\alpha_1, \dots, \alpha_n)$ with $|\alpha| \leq 2d$ so that y is a vector in $\mathbb{R}^{S_{2d}}$. The number of such n tuples is

$$\sum_{k=0}^{2d} \binom{k+n-1}{n-1} = \binom{n+2d}{2d}. \quad (8)$$

A moment sequence corresponds to a situation where all y_α are known to arbitrary order, which we denote by $y \in \mathbb{R}^{S_\infty}$.

The truncated moment problem (tms problem) is the problem of finding whether there exists a representing measure for a given sequence y , that is, a positive measure $d\mu$ such that $y_\alpha = \int x^\alpha d\mu(x)$ for all α with $|\alpha| \leq 2d$. Here the notation x^α stands for $\prod_{i=1}^n x_i^{\alpha_i}$.

The K -tms problem addresses the case where the measure $d\mu$ is additionally required to be supported by a semialgebraic set K , that is, a set defined by polynomial inequalities. We will use the notation $K = \{x \in \mathbb{R}^n | g_1(x) \geq 0, \dots, g_m(x) \geq 0\}$ with $g_j(x)$ multivariate polynomials. The sequence y has a representing measure for the K -tms problem if for all α 's with $|\alpha| \leq 2d$, Eq. (7) holds.

Necessary and sufficient conditions for the solution of the tms problem can be obtained in terms of moment matrices. Given a tms $(y_\alpha)_{|\alpha| \leq 2d}$, its moment matrix of order t is the matrix $M_t(y)$ indexed by α, β with $|\alpha|, |\beta| \leq t$ and defined as $M_t(y)_{\alpha\beta} = y_{\alpha+\beta}$. The entries of the matrix involve indices of y up to order $2t$ and since the highest index of y is $2d$ (by definition of the tms) such a matrix is defined only if $t \leq d$. The size of $M_t(y)$ is given by the number of moments up to order t , that is, $\binom{n+t}{t}$. In the case of an infinite moment sequence, the matrix $M(y)$ is infinite.

Necessary and sufficient conditions for the solution of the K -tms problem additionally involve the localizing matrices associated with polynomials g_j specifying K , which are defined as follows. Any polynomial g of n variables x_1, \dots, x_n can be decomposed over monomials as $g = \sum_{|\alpha| \leq \deg(g)} g_\alpha x^\alpha$, where $\deg(g)$ is the degree of the multivariate polynomial g . It can, thus, be seen as a vector in $\mathbb{R}^{S_{\deg(g)}}$. For a tms $(y_\alpha)_{|\alpha| \leq 2d}$ and a polynomial g , we define a shifted sequence $g \star y$ by

setting $(g \star y)_\alpha = \sum_\gamma g_\gamma y_{\alpha+\gamma}$. The localizing matrix of order t associated with g is defined as the moment matrix of order t of the shifted sequence, that is, $M_t(g \star y)$. Explicitly, its components read $M_t(g \star y)_{\alpha\beta} = \sum_\gamma g_\gamma y_{\alpha+\beta+\gamma}$. The highest index of y involved here is $2t + \deg(g)$ so that the matrix is defined only for $2t + \deg(g) \leq 2d$, that is, $t \leq d - \deg(g)/2$. The m polynomials defining K give rise to m -localizing matrices $M_t(g_j \star y)$. In order that all of them be defined, the order t has to be such that $t \leq d - d_0$ with

$$d_0 = \max_{1 \leq j \leq m} \{1, \lceil \deg(g_j)/2 \rceil\}, \quad (9)$$

that is, the degree of y has to be greater than or equal to $2(t + d_0)$.

The three theorems below give necessary and sufficient conditions for a tms (or a full moment sequence) to have a representing measure, supported on K or not. In all cases, the representing measure is r atomic, meaning that it is a sum of r δ functions with positive weights, $d\mu(x) = \sum_j \omega_j \delta(x - x_j)$. The central criterion is the existence of extensions. An extension of a tms y of degree $2d$ is a tms of degree $2d'$ with $d' > d$ whose restriction to indices of order $2d$ or less coincides with y . We denote it again by y . One can define the moment matrix of order t of such an extension for all $t \leq d'$, and we then say that for $t' > t$, $M_{t'}(y)$ is an extension of $M_t(y)$. An extension $M_{t'}(y)$ is said to be a flat extension of $M_t(y)$ if it satisfies the condition that its rank is equal to the rank of $M_t(y)$, that is,

$$\text{rk } M_{t'}(y) = \text{rk } M_t(y). \quad (10)$$

In particular, if (10) holds then $M_{t'}(y) \geq 0 \Leftrightarrow M_t(y) \geq 0$ (see Appendix B). Theorem 1 below deals with the moment problem, Theorem 2 with the tms problem, and Theorem 3 with the K -tms problem.

Theorem 1. (Ref. [35]; see Theorem 1.2 of Ref. [42]) Let $y \in \mathbb{R}^{S_\infty}$. If $M(y) \geq 0$ and $\text{rk } M(y) = r$ is finite, then y has a unique representing measure, which is r atomic.

Theorem 2. (Ref. [35]; see Theorem 1.3 and Corollary 1.4 of Ref. [42]) Let $y \in \mathbb{R}^{S_{2d}}$. If $M_t(y) \geq 0$ and $M_t(y)$ is a flat extension of $M_{t-1}(y)$, then y can be extended to $y \in \mathbb{R}^{S_{2d+2}}$ in such a way that $M_{t+1}(y)$ is a flat extension of $M_t(y)$.

From induction and using Theorem 1, one concludes that the tms in $\mathbb{R}^{S_{2d}}$ can be, in fact, extended to $y \in \mathbb{R}^{S_\infty}$ and has a unique representing measure, which is r atomic with $r = \text{rk } M_t(y)$. Moreover one can show (see Ref. [42] for detail) that the r atoms x_i which support the measure can be obtained from the kernel of $M_t(y)$, that is, the set of polynomials $p = \sum_\alpha p_\alpha x^\alpha$ such that $\sum_\beta M_t(y)_{\alpha\beta} p_\beta = 0$. More specifically, the set of x_i is the variety $\mathcal{V}[\ker M_t(y)] = \{x \in \mathbb{C}^n; f(x) = 0 \forall f \in \ker M_t(y)\}$, that is, the set of common roots of polynomials in the kernel of $M_t(y)$. In words, what the above results say is that in order to find a representing measure for $y \in \mathbb{R}^{S_{2d}}$ one has to start from the moment matrix $M_{t=d}(y)$ (which is the smallest moment matrix containing all the data) and look for extensions of higher and higher order, until for some order t one has $\text{rk } M_t(y) = \text{rk } M_{t-1}(y)$. If such an extension exists then the representing measure exists and is supported by the common roots of polynomials of $\ker M_t(y)$.

Theorem 3. (Ref. [35]; see Theorem 1.6 of Ref. [42]) Let $y \in \mathbb{R}^{S_{2d}}$ and $r = \text{rk } M_t(y)$. Then y has a r atomic representing measure supported on K if and only if $M_t(y) \geq 0$ and there

exists a flat extension $M_{t+d_0}(y)$ with $M_t(g_j \star y) \geq 0$ for $1 \leq j \leq m$ and d_0 defined in (9).

This theorem can be decrypted as follows. Starting from the moment matrix of order d and looking for higher-order extensions of order t , if there exists an extension $M_{t+d_0}(y)$ with $\text{rk } M_{t+d_0}(y) = \text{rk } M_t(y) = r$ then all its submatrices $M_{t+1}(y), M_{t+2}(y), \dots$ are also flat extensions of $M_t(y)$. From Theorems 1 and 2 one readily concludes that there exists a unique r -atomic representing measure; the atoms are given by the variety associated with the kernel of the first extension where the flatness condition is achieved. However these atoms may not be located on K . The conditions $M_t(g_j \star y) \geq 0$ on the localizing matrices precisely enforce that additional condition (see Appendix A for an insight into the proof). As mentioned above, these matrices are only defined if the degree of y is greater than $2(t + d_0)$, which is why, in order to fulfill these conditions, one has to find extensions in $y \in \mathbb{R}^{S_{2(t+d_0)}}$. Therefore, although an extension to $M_{t+1}(y)$ is enough to guarantee the existence of a r -atomic representing measure, an extension to $M_{t+d_0}(y)$ is required so that it is supported by K . As a consequence, achieving the flatness condition requires to go quickly to matrices of high order, which has an impact in terms of computational complexity.

B. Tms for quantum states

Let us now apply these theorems to quantum states, following Ref. [30]. Consider a quantum state ρ acting on the tensor product $H = H^{(1)} \otimes \dots \otimes H^{(p)}$ of Hilbert spaces $H^{(i)}$ with $\dim \mathcal{L}(H^{(i)}) = \kappa_i + 1$. Let $S_{\mu_i}^{(i)}$ ($0 \leq \mu_i \leq \kappa_i$) be a set of Hermitian matrices forming an orthogonal basis for $\mathcal{L}(H^{(i)})$, and $S_{\mu_1 \mu_2 \dots \mu_p} = S_{\mu_1}^{(1)} \otimes \dots \otimes S_{\mu_p}^{(p)}$ an orthogonal basis of $\mathcal{L}(H)$. We expand ρ as

$$\rho = X_{\mu_1 \mu_2 \dots \mu_p} S_{\mu_1 \mu_2 \dots \mu_p} \tag{11}$$

(with implicit summation over repeated indices), where $X_{\mu_1 \mu_2 \dots \mu_p} = \text{tr}(\rho S_{\mu_1 \mu_2 \dots \mu_p})$ are the (real) coordinates of the state. Here each index μ_i runs from 0 to κ_i , and we will use latin letters a_i for indices running from 1 to κ_i . It will prove convenient to take $S_0^{(i)}$ as the identity matrix of size the dimension of $H^{(i)}$. Actually, as detailed in Ref. [30], the matrices $S_{\mu_1 \mu_2 \dots \mu_p}$ need not be an orthogonal basis: It suffices that they be a tight frame (a mathematical structure bearing some analogy with orthogonal bases), which proves useful, for example, in the case of symmetric states where some redundancy of the matrices in the expansion (11) is handy.

One can associate with ρ a tms $y = (y_\alpha)_{|\alpha| \leq p}$ of degree p in the following way. A density matrix acting on Hilbert space $H^{(i)}$ can be expanded as $\sum_{\mu_i=0}^{\kappa_i} x_{\mu_i}^{(i)} S_{\mu_i}^{(i)}$. We associate to $H^{(i)}$ a set of κ_i variables $x_{a_i}^{(i)}$, $1 \leq a_i \leq \kappa_i$. Let $x = (x_1, x_2, \dots, x_n)$ be the vector of all these variables. In the general case $(x_1, x_2, \dots, x_n) := (x_1^{(1)}, x_2^{(1)}, \dots, x_{\kappa_p}^{(p)})$ and $n = \sum_i \kappa_i$, and each x_k corresponds to a certain $x_{a_i}^{(i)}$, whereas if we consider symmetric states (i.e., mixtures of pure states invariant under permutation of the $H^{(i)}$) only one set of variables, say $x_{a_1}^{(1)}$, should be considered, and then n is the common value $\kappa_1 = \kappa_2 = \dots$.

An arbitrary monomial of these variables x_k can be written as $x^\alpha \equiv \prod_{k=1}^n x_k^{\alpha_k}$, where α_k counts the number of variables

x_k in the monomial. We then define a tms by $y_\alpha = X_{\mu_1 \mu_2 \dots \mu_p}$, where α is the index such that $x^\alpha = \prod_{i=1}^p x_{\mu_i}^{(i)}$. Since X has p indices we have $|\alpha| \leq p$ so that y_α is a tms of degree p . In fact, in order to define a moment matrix, an even-degree tms is required. Thus, we set $p = 2d$ if p is even or $p = 2d - 1$ if p is odd. Thus, $X_{\mu_1 \mu_2 \dots \mu_p}$ is mapped to a tms $(y_\alpha)_{|\alpha| \leq 2d}$ (and in the case where p is odd the moments of order exactly $2d$ remain unspecified).

As an example, let us consider the case of a state of two spins 1. We expand it as $\rho = X_{\mu_1 \mu_2} S_{\mu_1 \mu_2}$, where indices μ_i run from 0 to 8 (since a spin-1 density matrix is a 3×3 Hermitian matrix and can be described by nine real numbers). We then introduce the vector of variables $x = (x_1, x_2, \dots, x_{16})$, where x_1, \dots, x_8 are associated with the first spin and x_9, \dots, x_{16} with the second. Entries $X_{\mu_1 \mu_2}$ define a tms y_α of degree 2 where each α is a vector of integers of length 16 with all entries equal to 0 if $\mu_1 = \mu_2 = 0$, a single nonzero entry $\alpha_{\mu_1} = 1$ if $\mu_1 \neq 0$ and $\mu_2 = 0$, a single entry $\alpha_{\mu_2+8} = 1$ if $\mu_2 \neq 0$ and $\mu_1 = 0$, and two entries equal to 1 if both μ_1 and μ_2 are nonzero. Each of these α 's is associated with a monomial, for instance, $X_{3;8}$ corresponds to $\alpha = (0, 0, 1, 0, 0, 0, 0, 0, 0, 0, 0, 0, 0, 0, 0, 1)$ or to $x_3 x_{16}$.

As shown in Ref. [30], the problem of finding whether ρ is separable across the multipartition $H^{(1)} \otimes \dots \otimes H^{(p)}$ is equivalent to a K -tms problem. Indeed, projecting the separability condition on the basis $S_{\mu_1 \mu_2 \dots \mu_p}$, coordinates of a separable state can be written as

$$X_{\mu_1 \mu_2 \dots \mu_p} = \int_K x_{\mu_1}^{(1)} x_{\mu_2}^{(2)} \dots x_{\mu_p}^{(p)} d\mu(x), \tag{12}$$

with $x_0^{(i)} = 1$, $x = (x^{(1)}, x^{(2)}, \dots, x^{(p)}) \in \mathbb{R}^n$ ($n = \sum_i \kappa_i$), $x^{(i)} = (x_a^{(i)})_{1 \leq a \leq \kappa_i} \in \mathbb{R}^{\kappa_i}$, and $d\mu(x) = \sum_j \omega_j \delta(x - z_j)$ a measure supported on a semialgebraic set $K \subset \mathbb{R}^n$ defined by the positivity of the density matrices on each local Hilbert space (that is, the measure is an atomic measure with atoms $z_j \in K$). This tms problem is equivalent to asking whether there exists a positive measure $d\mu$ with support K for a tms whose moments are the y_α given as explained above by the coordinates $X_{\mu_1 \mu_2 \dots \mu_p}$ of the state ρ . In this language, Eq. (12) precisely takes the form (7). As a consequence, separability of ρ can be addressed in the following way: Given a state ρ , we can map its coordinates $X_{\mu_1 \mu_2 \dots \mu_p}$ to a tms $(y_\alpha)_{|\alpha| \leq 2d}$ and look for extensions $(y_\alpha)_{|\alpha| \leq 2t}$, starting from $t = d$. State ρ is separable if and only if there exists a flat extension $(y_\alpha)_{|\alpha| \leq 2(t+d_0)}$ of $(y_\alpha)_{|\alpha| \leq 2t}$ with $M_t(y) \geq 0$ and $M_t(g_j \star y) \geq 0$ for $j = 1, \dots, m$.

C. Tms for quantum channels

We will now reformulate the theorem above to give a necessary and sufficient criterion for the separability of quantum channels. Let $\Phi: \mathcal{L}(H_A \otimes H_B) \rightarrow \mathcal{L}(H_A \otimes H_B)$ be a completely positive map and C_Φ its corresponding Choi matrix acting on $\mathcal{H} = H_A \otimes H_B \otimes H_{A'} \otimes H_{B'}$; an orthogonal basis of \mathcal{H} is then given by matrices $S_{\mu_A \mu_B \mu_{A'} \mu_{B'}} = S_{\mu_A}^{(A)} \otimes S_{\mu_B}^{(B)} \otimes S_{\mu_{A'}}^{(A')} \otimes S_{\mu_{B'}}^{(B')}$, where $S_{\mu}^{(\bullet)}$ are Hermitian matrices forming an orthogonal basis of the set of bounded linear operators on H_\bullet . Let us translate the above tms theorems as necessary and sufficient conditions on the Choi matrix to be separable.

The compact K is defined according to the decomposition we are interested in. In the EB case, one wants to decompose the Choi matrix as $\sum_k P_k \otimes Q_k$, where P_k and Q_k are positive operators acting on $H_A \otimes H_B$ and $H_{A'} \otimes H_{B'}$, respectively. Expanding the P_k over a basis of operators S_λ^{AB} (these S_λ^{AB} could be taken as the $S_{\mu_A}^{(A)} \otimes S_{\mu_B}^{(B)}$) and Q_k over a basis $S_{\lambda'}^{A'B'}$ and expressing the condition that they must be positive, we obtain a definition of the compact K as the set of real expansion coefficients $c_\lambda, d_{\lambda'}$ such that

$$\sum_\lambda c_\lambda S_\lambda^{AB} \geq 0, \quad (13)$$

$$\sum_{\lambda'} d_{\lambda'} S_{\lambda'}^{A'B'} \geq 0. \quad (14)$$

These positivity conditions can be rewritten as inequalities on the coefficients of the corresponding characteristic polynomials using the Descartes sign rule (see Sec. III D below). In the SEP case, the Choi matrix now has to be decomposed as $\sum_k P_k \otimes Q_k$ with P_k and Q_k acting on $H_A \otimes H_{A'}$ and $H_B \otimes H_{B'}$, respectively. The same reasoning applies for the positivity conditions as in the EB case.

Given a channel Φ , we expand the corresponding Choi matrix as

(1) for EB, $C_\Phi = \sum_{\lambda, \lambda'} X_{\lambda\lambda'} S_\lambda^{AB} \otimes S_{\lambda'}^{A'B'}$ (with S_λ^{AB} a basis of operators for the system and $S_{\lambda'}^{A'B'}$ for the ancilla)

(2) for SEP, $C_\Phi = \sum_{\lambda, \lambda'} \tilde{X}_{\lambda\lambda'} S_\lambda^{AA'} \otimes S_{\lambda'}^{BB'}$ (with $S_\lambda^{AA'}$ a basis of operators for the Hilbert space $H_A \otimes H_{A'}$, and $S_{\lambda'}^{BB'}$ for the Hilbert space $H_B \otimes H_{B'}$).

We can then map either the coordinates $X_{\lambda\lambda'}$ or the coordinates $\tilde{X}_{\lambda\lambda'}$ to a tms $(y_\alpha)_{\alpha \leq 2}$ (indeed, since we look for separability across a bipartition, the degree of the tms is 2). The necessary and sufficient conditions for channels are then given as follows:

Theorem 4.

(i) The channel Φ is EB if and only if, considering extensions $(y_\beta)_{\beta \leq 2t}$ of $(y_\beta)_{\beta \leq 2}$, there exists a flat extension $(y_\beta)_{\beta \leq 2(t+d_0)}$ of $(y_\beta)_{\beta \leq 2t}$ (possibly with $t = 1$) with $M_t(y) \geq 0$ and $M_t(g_j \star y) \geq 0$ for $j = 1, \dots, m$ where the g_j 's are polynomials of variables c_λ and $d_{\lambda'}$ defined by the conditions $\sum_\lambda c_\lambda S_\lambda^{AB} \geq 0$, $\sum_{\lambda'} d_{\lambda'} S_{\lambda'}^{A'B'} \geq 0$, and $d_0 = \max_{1 \leq j \leq m} \{1, \lceil \deg(g_j)/2 \rceil\}$.

(ii) The channel Φ is SEP if and only if, considering extensions $(y_\beta)_{\beta \leq 2t}$ of $(y_\beta)_{\beta \leq 2}$, there exists a flat extension $(y_\beta)_{\beta \leq 2(t+d_0)}$ of $(y_\beta)_{\beta \leq 2t}$ (possibly with $t = 1$), with $M_t(y) \geq 0$ and $M_t(g_j \star y) \geq 0$ for $j = 1, \dots, m$ where the g_j 's are polynomials of variables c_λ and $d_{\lambda'}$ defined by the conditions $\sum_\lambda c_\lambda S_\lambda^{AA'} \geq 0$, $\sum_{\lambda'} d_{\lambda'} S_{\lambda'}^{BB'} \geq 0$, and $d_0 = \max_{1 \leq j \leq m} \{1, \lceil \deg(g_j)/2 \rceil\}$.

In the case of fully separable channels, the Choi matrix must be separable across any cut. We expand the matrix C_Φ as $C_\Phi = X_{\mu_A \mu_B \mu_{A'} \mu_{B'}} S_{\mu_A}^{(A)} \otimes S_{\mu_B}^{(B)} \otimes S_{\mu_{A'}}^{(A')} \otimes S_{\mu_{B'}}^{(B')}$. The coefficients $X_{\mu_A \mu_B \mu_{A'} \mu_{B'}}$ are now mapped to a tms of order 4, and the set K is given by positivity conditions on each Hilbert space. The channel Φ is fully separable if and only if, looking for extensions of that tms, we find a flat extension (with positivity conditions on the moment and localizing matrices).

D. The algorithm

Theorem 4 can be translated into an algorithm that characterizes separable or entangling channels with respect to a chosen partition. The algorithm is based on semidefinite programming (SDP). The inputs to the algorithm are the following. The first input is the Choi matrix of the specific channel that one wants to test; it acts on the system-ancilla Hilbert space $H = H_A \otimes H_B \otimes H_{A'} \otimes H_{B'}$, and its coordinates (in a basis depending on the partition chosen) provide a tms y_α . The second input is the set of polynomials g_j defining the compact K via polynomial inequalities [as in Eqs. (13) and (14)], which allows one to define the localizing matrices. Keeping the second input fixed, we can change the Choi matrix by swapping Hilbert spaces so as to explore different separability problems (SEP, EB, or FS) as defined in Sec. II B. The SDP algorithm minimizes a linear function of the moments y_α under the constraints that the moment matrix and the localizing matrices are positive semidefinite.

Let W be a matrix as in (13) and (14). It depends on the set of variables associated with each Hilbert space, for instance, the variables c_λ in Eq. (13). To derive an explicit expression for the g_j , we express the coefficients of the characteristic polynomial $p(z) = \sum_{k=0}^n (-1)^{n-k} a_k z^k$ of W through the recursive Faddeev-LeVerrier algorithm, i.e., for $1 \leq m \leq n$,

$$a_{n-m} = -\frac{1}{m} \sum_{k=1}^m (-1)^k a_{n-m+k} \text{tr}(W^k), \quad (15)$$

with $a_n = 1$ and $a_0 = \det(W)$. From Descartes sign rule, positivity of W is equivalent to having $a_k \geq 0$ for all k 's. Let us consider, for example, the case of two-qubit channels for which i, j go from 0 to 1 in Eq. (6) and C_Φ is a 16×16 matrix and look for its separability as a tensor product of two 4×4 matrices. The characteristic polynomial for each factor is then of degree 4 [$n = 4$ in Eq. (15)], and the inequalities for positivity are given by Newton's identities (also known as Girard-Newton formulas). Besides $a_4 = 1$ and $a_3 = \text{tr } W = 1$ (since W is a density matrix), we get the conditions,

$$\begin{aligned} a_2 &= \frac{1}{2}(1 - \text{tr } W^2) \geq 0, \\ a_1 &= \frac{1}{6}(2 \text{tr } W^3 - 3 \text{tr } W^2 + 1) \geq 0, \\ a_0 &= \frac{1}{24}(-6 \text{tr } W^4 + 8 \text{tr } W^3 + 3(\text{tr } W^2)^2 - 6 \text{tr } W^2 + 1) \geq 0, \end{aligned} \quad (16)$$

which yield polynomial inequalities on the c_λ .

The tms y_α associated with C_Φ is obtained from its coordinates in a certain basis. In the case of states (see Sec. III B), specifying the coordinates of the density matrix was equivalent to fixing some moments of the measure $d\mu(x)$ as being the expectation values of some physical observables, given by $\text{tr}(\rho S_{\mu_A}^{(1)} \otimes \dots \otimes S_{\mu_p}^{(p)})$. In the case of channels instead, the observables are relative to the enlarged space system ancilla, so in order to perform physical measurements on the system only one needs to express the values $\text{tr}(C_\Phi S_{\mu_A}^{(A)} \otimes S_{\mu_B}^{(B)} \otimes S_{\mu_{A'}}^{(A')} \otimes S_{\mu_{B'}}^{(B')})$ in terms of the entries of the superoperator M specifying the channel as $\rho'_{ij} = M_{ij,kl} \rho_{kl}$. This gives a direct relation with the input-output representation, i.e., the quantum channel Φ is seen as a dynamical process: If ρ is the initial (input) state before the process, then $\Phi(\rho)$ is the final (output) state

after the process occurs. We can go from one representation to the other considering that M and C_Φ are related by the reshuffling operation in the computational basis; for a generic basis this will, in general, result in a linear combination of physical measurements on the system. The number of physical measurements needed to fix one entry of the moment matrix relative to C_Φ can be used, for instance, as a cost function to decide between efficiency of entanglement detection and experimental convenience. The system-ancilla approach is what is used in the so-called ancilla-assisted process tomography (see, e.g., Ref. [43]), whereas the input-output one is the standard quantum process tomography (see, e.g., Ref. [44]).

The SDP algorithm then consists of minimizing a function $\sum_\alpha R_\alpha y_\alpha$ with R_α an arbitrary polynomial under the constraint that $M_t(y)$ and the localizing matrices $M_t(g_j \star y)$ are positive semidefinite and look for an extension such that the flatness condition is fulfilled. The algorithm is implemented using GLOPTIPOLY [45] and the MOSEK optimization toolbox [46]. Note that if the rank condition is not met the SDP can still yield a solution to the minimization problem [47], but it does not tell us anything *a priori* on the representing measure problem. To describe all the ingredients in the algorithm, to study its complexity and its efficiency, we will apply it in the next section to different examples: the spin-1 channels mentioned already above, and specific two-qubit channels, which are relevant in many experimental settings.

IV. EXAMPLES

In the general case, the number of moments involved, and, thus, the size of the moment matrices, scales very fast with the extension order t so that numerically the SDP soon becomes intractable. More specifically, whereas full separability of two-qubit channels is a problem that is still tractable numerically, already the SEP and EB cases turn out to be too complex if we consider arbitrary qubit channels. Indeed, in that case the variables involved are $(x_\mu)_{1 \leq \mu \leq 15}$ for the system and $(x'_\mu)_{1 \leq \mu \leq 15}$ for the ancilla. The number of decision variables in the SDP is the number of free entries of the extension of the moment matrix we are looking for; in the order- t extension $M_t(y)$, it is the number of monomials from 30 variables up to degree $2t$, given by $\binom{30+2t}{2t}$ [see Eq. (8)]. Moreover, the polynomials defining the compact K for a two-qubit Hilbert space (of dimension 4) are the ones given in Eq. (17), that is, their degree is 4, and, thus, $d_0 = 2$. Since the smallest moment matrix containing all given moments is $M_1(y)$, the smallest extension we have to consider in Theorem 4 is $M_3(y)$. The size of this matrix is $\binom{33}{3} = 5456$, and the number of decision variables is $\binom{36}{6} \geq 10^6$. Therefore, the size of the SDP grows very quickly, and, thus, the number of semidefinite constraints requires too much time and memory.

Nevertheless, the algorithm can still be applied to families of channels for which the number of variables involved is smaller than in the general case. In the following we present different examples of such families. We highlight their complexities and computational cost, and explain in more detail the role of the different factors mentioned above. We finally outline some numerical results on their entangling or separable properties.

A. Fully symmetric Choi matrix

We start with a simple example which allows us to highlight the connection between the TMS algorithm for channels and for states. We consider quantum channels Φ such that the Choi matrix C_Φ has components only on the symmetric subspace. In other words, we impose that the four-qubit state associated with the two-qubit channel Φ via the Choi-Jamiołkowski isomorphism be fully symmetric under permutation of the qubits (in the sense that it is a mixture of fully symmetric pure states). In that case, the Choi matrix only has components on the subspace spanned by Dicke states $|D_j^{(m)}\rangle$, which are the symmetrized tensor products of $2j$ qubits with $j = 2$ (four qubits) and $-j \leq m \leq j$. This means that

$$(\mathbb{1} - P)C_\Phi(\mathbb{1} - P) = (\mathbb{1} - P)C_\Phi P = PC_\Phi(\mathbb{1} - P) = 0, \quad (17)$$

where $P = \sum_{m=-2}^2 |D_4^{(m)}\rangle\langle D_4^{(m)}|$ is the projection operator onto the symmetric subspace. The constraints in Eq. (17) fix conditions on the superoperator M of which C_Φ is a reshuffling. For $j = 2$, only $(2j + 1)^2$ real independent parameters remain.

Such a restriction has a clear physical interpretation in the case of one-qubit channels. Indeed, the Choi matrix of a nonunital one-qubit channel can be put in the form

$$\frac{1}{2} \begin{pmatrix} 1 + \lambda_3 + t_3 & 0 & t_1 + it_2 & \lambda_1 + \lambda_2 \\ 0 & 1 - \lambda_3 + t_3 & \lambda_1 - \lambda_2 & t_1 + it_2 \\ t_1 - it_2 & \lambda_1 - \lambda_2 & 1 - \lambda_3 - t_3 & 0 \\ \lambda_1 + \lambda_2 & t_1 - it_2 & 0 & 1 + \lambda_3 - t_3 \end{pmatrix}, \quad (18)$$

in the canonical basis [27]. Imposing that the matrix is associated with a symmetric state is equivalent to imposing that it has no component over the singlet state; this leads to the conditions $t_1 = t_2 = t_3 = 0$ (i.e., the channel is unital) and $\lambda_1 - \lambda_2 + \lambda_3 = 1$, which correspond to a face of the tetrahedron of admissible values of the λ_i corresponding to unital channels, given by the Fujiwara-Algoet conditions $1 \pm \lambda_3 \geq |\lambda_1 \pm \lambda_2|$ [48]. Such points on a face of the tetrahedron correspond to channels whose Kraus rank is 3, which are characterized by the fact that they are the only indivisible channels (that is, they cannot be written as the composition of two nonunitary channels) [49,50].

In the two-qubit channel case there is no such clear geometrical picture of the fully symmetric Choi matrix. However, since the Choi state is a fully symmetric state of $N = 4$ qubits, if it is separable with respect to an arbitrary partition, then it is fully separable, and it can be written as a convex sum of N projectors on pure symmetric states (see, e.g., Ref. [51]). This means that in this case we only need to consider the fully separable case, which coincides with exploring the case of spin-2 states (since those states can be seen as symmetric states of four qubits). The tms algorithm for states was exploited in Ref. [21] to investigate multipartite entanglement of such states. The problem can be formulated as in Eq. (7) with a tms of degree 4 [thus, the smallest moment matrix to consider in Theorem 4 is $M_2(y)$] and a vector of variables (x_1, x_2, x_3) (as explained in Sec. III B since the state is fully symmetric we only need the three variables associated with a single

qubit). The semialgebraic set K is the Bloch sphere so that $d_0 = 1$. Thus, the first flatness condition in Theorem 4 reads $\text{rk } M_3(y) = \text{rk } M_2(y)$ with $M_2(y)$ and $M_3(y)$ of sizes 10×10 and 20×20 , respectively. The algorithm usually stops at the first extension, and it takes at about 1 s to give a certificate of separability or entanglement of the channel (the time here reported refers to running the algorithm on a standard computer with a 64-bit Windows operating system, 4-GB RAM and Intel Core i7 CPU 2.00–2.60 GHz). We refer to the results obtained for states in Refs. [21,30] for more detail on the implementation in that case.

B. Two-qubit planar channels

We now consider the case where the two-qubit channel is a linear combination of tensor products of single-qubit planar channels. Such one-qubit channels ϕ_{pl} send the (three-dimensional) Bloch ball into a (two-dimensional) ellipse. Note that, according to the so-called “no-pancake theorem” a planar channel cannot map the Bloch ball to a disk touching the sphere unless it reduces to a point or a line (see Refs.[49,52]).

Any one-qubit channel can be described by a 4×4 matrix of the form

$$M = \begin{pmatrix} 1 & 0 & 0 & 0 \\ t_1 & \lambda_1 & 0 & 0 \\ t_2 & 0 & \lambda_2 & 0 \\ t_3 & 0 & 0 & \lambda_3 \end{pmatrix}, \quad (19)$$

where $\lambda = (\lambda_1, \lambda_2, \lambda_3)$ with $\lambda_i \geq 0$ is the distortion vector and $\mathbf{t} = (t_1, t_2, t_3)$ is the translation vector. Geometrically, the channel maps the Bloch vector \mathbf{r} to $M\mathbf{r} + \mathbf{t}$, that is, the sphere becomes an ellipsoid whose half-axes are given by the λ_i and centered at \mathbf{t} .

Planar channels are those where one of the λ_i is zero. Geometrically, this means that they map the Bloch ball to a disk. In Ref. [53] this type of channel was investigated, but with focus on their entanglement-annihilating properties. In what follows, we consider planar channels ϕ_{pl} with $\lambda_2 = 0$. We investigate whether linear combinations, such as

$$\Phi = a\phi_{\text{pl}}^{(1)} \otimes \phi_{\text{pl}}^{(1)} + b\phi_{\text{pl}}^{(2)} \otimes \phi_{\text{pl}}^{(2)}, \quad (20)$$

with $a, b \in \mathbb{R}$ result in separable channels. We consider the case in which both $\phi_{\text{pl}}^{(1)}$ and $\phi_{\text{pl}}^{(2)}$ are unital, one unital, the other nonunital, and both nonunital. Note that states (20) are not symmetric states, in general, as they are symmetrizations of mixed states but not mixtures of symmetric pure states. The condition of complete positivity in the case of a unital planar channel ($\mathbf{t} = 0$) is given by $|\lambda_1| \leq 1 - |\lambda_3|$ with $|\lambda_1|, |\lambda_3|$ the half-axes of the ellipse. In the case of nonunital channels the conditions for complete positivity can be found in Theorem IV.1 of Ref. [49]. Here for simplicity we consider the case where $\lambda_2 = 0$ and $\mathbf{t} = (0, 0, t_3)$. In such a case these conditions simplify to

$$\begin{aligned} 1 + \lambda_1 + \lambda_3 &\geq 0, & 1 + \lambda_1 - \lambda_3 &\geq 0 \\ 1 - \lambda_1 - \lambda_3 &\geq 0, & 1 - \lambda_1 + \lambda_3 &\geq 0, \\ t_3^2 &\leq 1 - \lambda_1^2 + \lambda_3^2 - 2|\lambda_3|. \end{aligned} \quad (21)$$

The Choi matrix C_Φ is then properly normalized ($b = \frac{1}{16} - a$) in order to obtain a valid quantum state with trace 1, giving the Choi state on which we apply our algorithm. The basis over which C_Φ is expanded is chosen as the tensor product $\sigma_{\mu_1} \otimes \sigma_{\mu_2} \otimes \sigma_{\mu_3} \otimes \sigma_{\mu_4}$ with $0 \leq \mu_i \leq 2$ and $\{\sigma_{\mu_i}\} = \{\mathbb{1}, \sigma_x, \sigma_z\}$, σ_x, σ_z being the usual Pauli matrices (this is also reasonable from the experimental point of view since Pauli physical measurements are often used for multiqubit channels). The Choi states associated with states (20) turn out to be equal to their partial transpose with respect to any qubit. Invariance under partial transposition with respect to the first qubit in $2 \times N$ systems was shown in Ref. [54] to entail separability. Therefore, the four-qubit Choi state is separable across any bipartition into sets of one and three qubits.

Separability for the bipartitions into two sets of two qubits, required from the definition of EB and SEP channels, corresponds to the situation of Theorem 4 and can be explored with our algorithm as follows. In contrast to the symmetric case addressed in Subsec. IV A, there are now different variables x_i in Eq. (12) for the system A and the ancilla A' (and equivalently for B and B')

Let us first consider the question of full separability. In that case, since each system qubit and ancilla qubit, respectively, is described by two variables $(x_\mu^A)_{1 \leq \mu \leq 2}, (x_\mu^B)_{1 \leq \mu \leq 2}$ and $(x_\mu^{A'})_{1 \leq \mu \leq 2}, (x_\mu^{B'})_{1 \leq \mu \leq 2}$, the vector of variables has length 8. The moments y_α are given by entries of the Choi matrix, the tms has degree 4, so that formula (8) applies with $n = 8$ and $2d = 4$. The semialgebraic set is given by the choice of basis matrices for the Choi matrix. Since we expanded it over Pauli matrices, the constraint for each set of variable is the one for qubits, i.e., the vector of variables is restricted to the Bloch ball. The compact K is, therefore, the product of four unit disks.

Since all polynomials defining K are of degree 2, we have $d_0 = 1$, and, thus, the first rank condition reads $\text{rk } M_3(y) = \text{rk } M_2(y)$ where the moment matrices have size $\binom{n+t}{t}$, i.e., respectively 165 and 45. A first hint on the computational complexity of the SDPs we need to solve is given by the number of decision variables of the optimization, which in our case corresponds to the number of monomials from eight variables up to degree 6, the latter being the degree of the extension of the tms needed to construct $M_3(y)$. Moreover, SDP are usually solved with the interior point method; each iteration in the primal-dual interior point algorithm requires the solution of a linear system, which is the most expensive operation with $O(N^3)$ complexity, solvable using Gaussian elimination. Here N is the number of linear constraints in the SDP, and efficiency drops with the growing number of semidefinite terms involved in these linear constraints, which in the case here considered are $\sim 10^3$. This, in general, has a big impact on the time and memory requested for a single run of the algorithm [46]. Nevertheless, we could run our algorithm in that case, which allowed us to test for separability of channels of the form (20). The algorithm still performs very well (on a machine with same characteristics as described above in Sec. IV A); for all the examples tested a certificate of separability was found either at the first relaxation order $\text{rk } M_3 = \text{rk } M_2$ (with a time of ~ 10 s for a single run) or at the second relaxation order $\text{rk } M_4 = \text{rk } M_3$ (with a running time of ~ 6 min).

We tested $\sim 10^3$ cases, which were chosen uniformly at random in the range of parameters $(\lambda_1^{(1)}, \lambda_3^{(1)}, \lambda_1^{(2)}, \lambda_3^{(2)}, t_3^{(1)}, t_3^{(2)}, \text{ and } a)$ allowed by the complete-positivity conditions of the quantum channels considered [see Eq. (22) and above it]. All the Choi states tested result fully separable for all the three cases listed above (where channels ϕ_{p_i} can be unital or not); as a consequence, all these states are both EB and SEP. Based on the available numerical evidence we conjecture that all states of the form (20) are fully separable.

C. Qutrit channels

We now study the case of qutrit channels. More specifically, we apply our algorithm to a family of channels presented in Ref. [55] where EB properties of qutrit gates were studied through the negativity $N(\rho) = \frac{1}{2}(\|\rho^{T_H}\|_1 - 1)$ with $\|\rho^{T_H}\|_1$ the trace norm of the partial transpose with respect to the system qutrit. The negativity $N(\rho)$ cannot detect PPT-entangled states; in other words there exist entangled states with $N(\rho) = 0$. For such states, our algorithm is able to give a certificate of separability as we illustrate below. Note that, even though in this case the system is not bipartite, the definition of entanglement breaking still applies since it involves the presence of an ancilla, as explored for one-qubit channels in Ref. [52]; on the other hand, the definition of SEP separability cannot be applied to this example.

As a basis for qutrit density operators, we use Gell-Mann matrices $\{\lambda_i\}_{i=1}^8$ together with $\lambda_0 = \sqrt{\frac{2}{3}}\mathbb{1}$. In this basis, an arbitrary qutrit density matrix can be written as

$$\rho = \frac{1}{3} \left(\mathbb{1} + \sum_{i=1}^8 \zeta_i \lambda_i \right), \quad (22)$$

with $\zeta_i = \frac{3}{2} \text{tr}(\rho \lambda_i)$.

The channel we consider is a damping qutrit channel, i.e., a channel that can be written as an affine transformation on the generalized (qutrit) Bloch vector as $\Phi_D: \xi \rightarrow \xi' = \Lambda \xi$, where $\Lambda = \text{diag}(\Lambda_1, \dots, \Lambda_8)$ is the damping matrix. The Λ_i cannot take any arbitrary value because Φ_D has to be completely positive, thus, leading to the constraints $|\Lambda_i| \leq 1$. More specifically, we consider the family of damping channels given in Ref. [55] and parametrized by $\Lambda_{i \neq 3,8} = x$, $\Lambda_{i=3} = y$, $\Lambda_{i=8} = y^2$. The Choi state corresponding to Φ_D can be written by transforming the propagator to the canonical basis, then reshuffling and normalizing (it corresponds to a maximally mixed state for $x = y = 0$ and to a maximally entangled state of two qutrits for $x = y = 1$). The region of parameters for which C_{Φ_D} is positive semidefinite together with the values of the corresponding negativity is shown in Fig. 2.

Any two-qutrit state can be expanded over the basis formed by tensor products of Gell-Mann matrices [56]. This setting is analogous to the one described in Sec. III B for two spin-1 states. The vector of variables is $x = (x_1, x_2, \dots, x_{16})$, where x_1, \dots, x_8 are the coordinates α_i associated with the system qutrit, and x_9, \dots, x_{16} are associated with the ancilla qutrit. Since there are two subsystems, and the tms has degree 2. The characteristic polynomial for a qutrit density matrix has

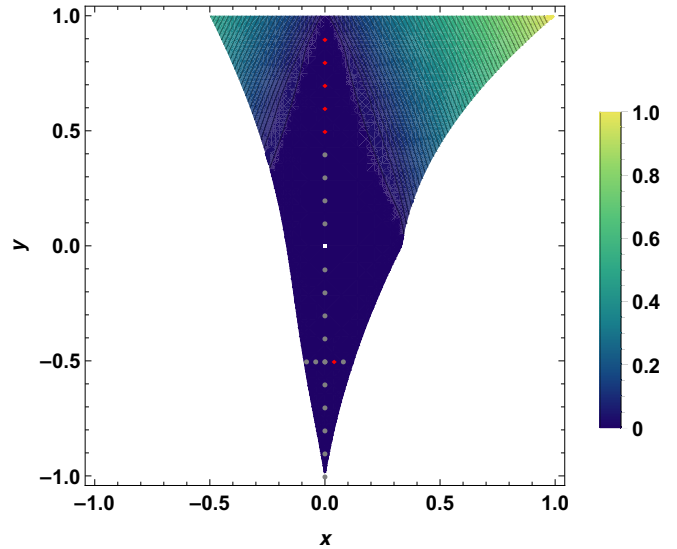


FIG. 2. Region of x and y parameters for which C_{Φ_D} of the damping qutrit channel is positive semidefinite; the color function corresponds to the negativity values in the range of $[0, 1]$ with steps for the contour lines of 0.02. The central plateau corresponds to the region of zero negativity where the PPT criterion remains inconclusive. Gray points correspond to states found separable by our algorithm, signifying entanglement breaking channels; red points correspond to states where the algorithm needs to go to a higher extension order and remains inconclusive with our numerical resources. The white point marks the maximally mixed state.

degree 3, therefore, the semialgebraic set is given by the conditions $\text{tr} \rho^2 \leq 1$ and $\det \rho \geq 0$ with ρ as the density operator in Eq. (22). It follows that the corresponding polynomials of the variable x_i have maximal degree 3, and, thus, $d_0 = 2$. This gives the rank shift in Theorem 4: At the first iteration of the algorithm the flatness condition reads $\text{rk } M_3(y) = \text{rk } M_1(y)$. These moment matrices have size 969 and 17, respectively. The number of decision variables in the SDP corresponds to the number of monomials from 16 variables up to degree 6 ($\sim 7 \times 10^4$) and the number of semidefinite constraints is given by $\binom{n+t}{t} + m \binom{n+t-1}{t-1} + m \binom{n+t-2}{t-2}$, that is, the size of the moment matrix of the first extension ($t = 3$) and the size of the localizing matrices multiplied by the number m of inequalities in the semialgebraic set for each set of variables.

The tms algorithm can be exploited to investigate, in particular, the Choi states with zero negativity for which the PPT criterion alone is inconclusive. The results for some pairs of parameters with $(x = 0, y \in [-1, 1])$ and $(x \in [-\frac{2}{25}, \frac{2}{25}], y = -\frac{1}{2})$ are explored and they are shown in Fig. 2. The points highlighted in gray are the points tested with the algorithm which give a certificate of separability, including the white point which corresponds to a Choi state equal to the maximally mixed state of two qutrits. In the latter cases the SDP is feasible and the flatness condition $\text{rk } M_3(y) = \text{rk } M_1(y)$ is satisfied, meaning that the corresponding Φ_D 's are EB; on the other hand, the algorithm remains inconclusive for the red points at the first iteration, leading to the necessity for higher-order extensions, which are beyond our computational resources. We did not detect PPT entangled states among the tests performed; the algorithm confirms

entanglement for negativity greater than zero for all the states tested. A single run of the algorithm in this case takes about 5h and between 150 and 300 GB of RAM.

V. CONCLUSIONS

In this paper we have discussed an algorithm that deterministically detects whether a quantum channel is separable or not, or whether it is entanglement breaking or not. Such an algorithm finds its motivation in important questions relative to modern quantum technology as the verification of devices which should work in a properly quantum way, often leading to the necessity of detecting whether a quantum channel is able to generate entanglement or not also over a certain time (as explained in the Introduction). We were able to explore in a unifying framework three classes of separability across different cuts between systems and ancillae (SEP, EB, or FS); indeed, with only a small modification in the input we can switch between these different classes. This algorithm is the numerical counterpart of a theorem that provides a necessary and sufficient separability criterion based on a mapping between coordinates of the Choi matrix of the channel, expressed in a given basis and a truncated moment sequence. Low-order moments are fixed by measurements performed on the channel, and the separability problem is equivalent to finding whether these moments are those of a measure supported on a certain compact set.

In the case of fully symmetric Choi matrices for qubit channels where the aim is to find a decomposition over the Bloch sphere, the number of variables in the tms is $n = 3$ so that the size of a moment matrix of order t is $\binom{n+t}{t} \sim t^3/6$. On the other hand, in the simplest case of detection of EB or SEP in a generic two-qubit channel, there are $n = 30$ variables involved, and, thus, the size of the moment matrix is $\binom{n+t}{t} = 5456$ for $t = 3$. Moreover, the number of independent entries in $M_t(y)$ is given by $\binom{n+2t}{2t} \sim 2 \times 10^6$ for $t = 3$. Nevertheless, we can consider families of channels for which the number of free parameters in each subsystem is smaller than in the general case. Then, the number of variables involved in the mapping to tms is reduced and the matrices in the SDP become amenable to numerical investigation. As we showed here, this is the case for planar channels (where one dimension is suppressed) or qutrit channels (which live in the symmetric space of two qubits). Our algorithm is then able to decide whether the channel is EB or SEP. For instance, in the case of qutrit channels we were able to provide a certificate of separability in cases where the negativity of the Choi matrix vanishes and, thus, is unable to yield a conclusion. Since calculations are costly, this approach could be used as a numerical tool to explore possible conjectures or produce counterexamples.

APPENDIX A: SKETCH OF THE PROOF OF THEOREM 3

Suppose $\text{rk } M_t(y) = r$ with $M_t(y) \geq 0$ and there exists a flat extension $M_{t+d_0}(y)$ with $M_t(g_j \star y) \geq 0$ for $1 \leq j \leq m$. Then $M_{t+1}(y)$ is also a flat extension of $M_t(y)$, and we then know from Theorem 2 that y admits a (unique) r -atomic representing measure supported by $x_k \in \mathcal{V}[\ker M_t(y)]$. All what remains to show is that positivity of the localizing matrices

enforces that the x_j belong to K , that is, $g_j(x_k) \geq 0$ for $1 \leq j \leq m$ and $1 \leq k \leq r$.

This can be performed as follows. First, observe that since $M_t(y)$ is of rank r , one can find a nonsingular $r \times r$ principal submatrix of $M_t(y)$. If \mathcal{B} is the set of labels α of the rows of that matrix, then the image of $M_t(y)$ is spanned by the x^α , $\alpha \in \mathcal{B}$, and by definition these x^α are on the order less than or equal to t . Since the whole vector space of polynomials can be decomposed as a direct sum of the image and the kernel of $M_t(y)$, an arbitrary polynomial p can be decomposed as $p = q + \tilde{p}$ with $q = \sum_{\alpha \in \mathcal{B}} q_\alpha x^\alpha \in \text{Im } M_t(y)$ and $\tilde{p} \in \ker M_t(y)$.

Now let p_k be interpolating polynomials of the $x_{k'}$, which are the atoms supporting the representing measure of y . That is, $p_k(x_{k'}) = \delta_{kk'}$ for $1 \leq k, k' \leq r$. One can decompose them as above as $p_k = q_k + \tilde{p}_k$ with $\tilde{p}_k \in \ker M_t(y)$ and q_k of degree less than t . By definition, the $x_{k'}$ are roots of all polynomials in $\ker M_t(y)$, and, thus, one has $\tilde{p}_k(x_{k'}) = 0$, which implies $q_k(x_{k'}) = \delta_{kk'}$ for $1 \leq k, k' \leq r$.

Now, for $y = \int x^\alpha d\mu(x)$ and for arbitrary polynomials represented by vectors $p, q \in \mathbb{R}^S$,

$$\begin{aligned} q^T M_t(y) p &= q_\alpha M_{\alpha\beta} p_\beta \\ &= q_\alpha y_{\alpha+\beta} p_\beta \\ &= \int q_\alpha x^{\alpha+\beta} p_\beta d\mu(x) \\ &= \int p(x) q(x) d\mu(x) \end{aligned} \quad (\text{A1})$$

(with Einstein summation convention) and

$$\begin{aligned} q^T M_t(g \star y) p &= q_\alpha g_\gamma y_{\alpha+\beta+\gamma} p_\beta \\ &= \int q_\alpha g_\gamma p_\beta x^{\alpha+\beta+\gamma} d\mu(x) \\ &= \int p(x) q(x) g(x) d\mu(x). \end{aligned} \quad (\text{A2})$$

Thus, $M_t(g_j \star y) \geq 0$ and $d\mu(x) = \sum_i \omega_i \delta(x - x_i) dx$ entail $\forall k, j$,

$$\begin{aligned} 0 &\leq q_k^T M_t(g_j \star y) q_k \\ &= \int q_k(x)^2 g_j(x) d\mu(x) \\ &= \sum_{i=1}^r \omega_i \int dx q_k(x)^2 g_j(x) \delta(x - x_i) \\ &= \sum_{i=1}^r \omega_i q_k(x_i)^2 g_j(x_i) \\ &= \omega_k g_j(x_k), \end{aligned} \quad (\text{A3})$$

since $q_k(x_i) = \delta_{ki}$. As all $\omega_k > 0$ this implies that $g_j(x_k) \geq 0$ and, thus, $x_k \in K$, which completes the proof.

APPENDIX B: RANK PROPERTY OF EXTENSIONS





Let us show that the rank condition $\text{rk } M_{t'}(y) = \text{rk } M_t(y)$ implies the fact that positivity of $M_t(y)$ and $M_{t'}(y)$ are equivalent.

Since $M_t(y)$ is a principal submatrix of $M_{t'}(y)$ one direction is obvious. To show the converse, suppose

$M_t(y) \geq 0$ and $\text{rk } M_t(y) = r = \text{rk } M_{t'}(y)$. Then, as in Appendix A, there exists a nonsingular $r \times r$ principal submatrix of $M_t(y)$ indexed by labels $\alpha \in \mathcal{B}$ with $|\alpha| \leq t$. This $r \times r$ submatrix is also a nonsingular principal sub-

matrix of $M_{t'}(y)$. Since $M_{t'}(y)$ has rank r , the corresponding r monomials x^α are, therefore, a basis of $\text{Im } M_{t'}(y)$. Since the submatrix is positive because $M_t(y)$ is, then so is $M_{t'}(y)$.

-
- [1] F. Verstraete and H. Verschelde, [arXiv:quant-ph/0202124](https://arxiv.org/abs/quant-ph/0202124).
- [2] M. Arsenijević, J. Jeknić-Dugić, and M. Dugić, *Braz. J. Phys.* **48**, 242 (2018).
- [3] F.-Z. Kong, H.-Z. Xia, M. Yang, Q. Yang, and Z.-L. Cao, *Sci. Rep.* **6**, 25958 (2016).
- [4] V. Gheorghiu and G. Gour, *Phys. Rev. A* **86**, 050302(R) (2012).
- [5] W. Wen, Y.-K. Bai, and H. Fan, *Eur. Phys. J. D* **64**, 557 (2011).
- [6] J. I. Cirac, W. Dür, B. Kraus, and M. Lewenstein, *Phys. Rev. Lett.* **86**, 544 (2001).
- [7] D. Rosset, F. Buscemi, and Y.-C. Liang, *Phys. Rev. X* **8**, 021033 (2018).
- [8] Y. Mao, Y.-Z. Zhen, H. Liu, M. Zou, Q.-J. Tang, S.-J. Zhang, J. Wang, H. Liang, W. Zhang, H. Li *et al.*, *Phys. Rev. Lett.* **124**, 010502 (2020).
- [9] H. Häselser, T. Moroder, and N. Lütkenhaus, *Phys. Rev. A* **77**, 032303 (2008).
- [10] J. F. Poyatos, J. I. Cirac, and P. Zoller, *Phys. Rev. Lett.* **78**, 390 (1997).
- [11] M. Mohseni, A. T. Rezakhani, and D. A. Lidar, *Phys. Rev. A* **77**, 032322 (2008).
- [12] C. Macchiavello and M. Rossi, *Phys. Rev. A* **88**, 042335 (2013).
- [13] S. M. Cohen, *J. Math. Phys.* **55**, 062202 (2014).
- [14] S. M. Cohen, *Phys. Rev. A* **87**, 052135 (2013).
- [15] R. Jozsa and N. Linden, *Proc. R. Soc. London, Ser. A* **459**, 2011 (2003).
- [16] J. Bae and A. Acín, *Phys. Rev. Lett.* **97**, 030402 (2006).
- [17] M. E. Shirokov, *Commun. Math. Phys.* **262**, 137 (2006).
- [18] P. W. Shor, *J. Math. Phys.* **43**, 4334 (2002).
- [19] K. P. Seshadreesan and M. M. Wilde, *Phys. Rev. A* **92**, 042321 (2015).
- [20] A. C. Doherty, P. A. Parrilo, and F. M. Spedalieri, *Phys. Rev. A* **69**, 022308 (2004).
- [21] N. Milazzo, D. Braun, and O. Giraud, *Phys. Rev. A* **100**, 012328 (2019).
- [22] N. Johnson, Ph.D. thesis, University of Guelph, 2012.
- [23] M. Horodecki, P. W. Shor, and M. B. Ruskai, *Rev. Math. Phys.* **15**, 629 (2003).
- [24] S. N. Filippov and M. Ziman, *Phys. Rev. A* **88**, 032316 (2013).
- [25] M. Rahaman, S. Jaques, and V. I. Paulsen, *J. Math. Phys.* **59**, 062201 (2018).
- [26] M. Christandl, A. Müller-Hermes, and M. M. Wolf, in *Annales Henri Poincaré* (Springer, Berlin, 2019), Vol. 20, pp. 2295–2322.
- [27] I. Bengtsson and K. Życzkowski, *Geometry of Quantum States: An Introduction to Quantum Entanglement* (Cambridge University Press, Cambridge, U.K., 2006).
- [28] A. Peres, *Phys. Rev. Lett.* **77**, 1413 (1996).
- [29] M. Horodecki, P. Horodecki, and R. Horodecki, *Phys. Lett. A* **223**, 1 (1996).
- [30] F. Bohnet-Waldraff, D. Braun, and O. Giraud, *Phys. Rev. A* **96**, 032312 (2017).
- [31] E. C. G. Sudarshan, P. M. Mathews, and J. Rau, *Phys. Rev.* **121**, 920 (1961).
- [32] M.-D. Choi, *Linear Algebra Appl.* **10**, 285 (1975).
- [33] A. Jamiołkowski, *Rep. Math. Phys.* **3**, 275 (1972).
- [34] L. Moravčíková and M. Ziman, *J. Phys. A: Math. Theor.* **43**, 275306 (2010).
- [35] R. Curto and L. Fialkow, *Mem. Amer. Math. Soc.* **568** (1996).
- [36] R. Curto and L. Fialkow, *Trans. Amer. Math. Soc.* **352**, 2825 (2000).
- [37] R. E. Curto and L. A. Fialkow, *J. Operator Theory* **54**, 189 (2005).
- [38] M. Laurent, in *Emerging Applications of Algebraic Geometry* (Springer, Berlin, 2009), pp. 157–270.
- [39] J. W. Helton and J. Nie, *Found. Comput. Math.* **12**, 851 (2012).
- [40] J. Nie, *Found. Comput. Math.* **14**, 1243 (2014).
- [41] J. Nie and X. Zhang, *SIAM J. Optim.* **26**, 1236 (2016).
- [42] M. Laurent, *Proc. Am. Math. Soc.* **133**, 2965 (2005).
- [43] J. B. Altepeter, D. Branning, E. Jeffrey, T. C. Wei, P. G. Kwiat, R. T. Thew, J. L. O’Brien, M. A. Nielsen, and A. G. White, *Phys. Rev. Lett.* **90**, 193601 (2003).
- [44] C. Zu, W.-B. Wang, L. He, W.-G. Zhang, C.-Y. Dai, F. Wang, and L.-M. Duan, *Nature (London)* **514**, 72 (2014).
- [45] D. Henrion, J.-B. Lasserre, and J. Löfberg, *Optim. Methods Softw.* **24**, 761 (2009).
- [46] M. ApS, *The MOSEK Optimization Toolbox for MATLAB Manual*, Version 8.1 (2018), <http://docs.mosek.com/8.1/toolbox/index.html>.
- [47] D. Henrion and J.-B. Lasserre, *Positive Polynomials in Control* (Springer, Berlin, 2005), pp. 293–310.
- [48] A. Fujiwara and P. Algoet, *Phys. Rev. A* **59**, 3290 (1999).
- [49] D. Braun, O. Giraud, I. Nechita, C. Pellegrini, and M. Žnidarič, *J. Phys. A: Math. Theor.* **47**, 135302 (2014).
- [50] M. M. Wolf and J. I. Cirac, *Commun. Math. Phys.* **279**, 147 (2008).
- [51] L. Chen, D. Chu, L. Qian, and Y. Shen, *Phys. Rev. A* **99**, 032312 (2019).
- [52] M. B. Ruskai, *Rev. Math. Phys.* **15**, 643 (2003).
- [53] S. N. Filippov, T. Rybár, and M. Ziman, *Phys. Rev. A* **85**, 012303 (2012).
- [54] B. Kraus, J. I. Cirac, S. Karnas, and M. Lewenstein, *Phys. Rev. A* **61**, 062302 (2000).
- [55] A. Che and K. Wódkiewicz, *Opt. Commun.* **283**, 795 (2010).
- [56] C. M. Caves and G. J. Milburn, *Opt. Commun.* **179**, 439 (2000).

Bipartite and tripartite entanglement in a Bose-Einstein acoustic black holeMathieu Isoard ^{1,2}, Nadia Milazzo ^{1,3}, Nicolas Pavloff ¹ and Olivier Giraud ¹¹*Université Paris-Saclay, CNRS, LPTMS, 91405, Orsay, France*²*Physikalisches Institut, Albert-Ludwigs-Universität Freiburg, D-79104 Freiburg, Germany*³*Institut für theoretische Physik, Universität Tübingen, 72076 Tübingen, Germany*

(Received 15 February 2021; accepted 8 October 2021; published 1 December 2021)

We investigate quantum entanglement in an analog black hole realized in the flow of a Bose-Einstein condensate. The system is described by a three-mode Gaussian state and we construct the corresponding covariance matrix at zero and finite temperature. We study associated bipartite and tripartite entanglement measures and discuss their experimental observation. We identify a simple optical setup equivalent to the analog Bose-Einstein black hole which suggests a different way of determining the Hawking temperature and gray-body factor of the system.

DOI: [10.1103/PhysRevA.104.063302](https://doi.org/10.1103/PhysRevA.104.063302)**I. INTRODUCTION**

Analog gravity aims at providing platforms making it possible to conduct laboratory studies of phenomena at the interface between general relativity and quantum physics, such as Hawking radiation [1] and black hole superradiance [2], for which in the gravitational context direct observation is not possible or no complete theory exists. It has also been suggested that analog models can bring some insight on the information loss paradox [3,4]. The concept has now broadened so as to include experimental tests of physical effects of relevance in cosmological scenarios, such as dynamical Casimir effect, Kibble-Zurek mechanism, Zakharov oscillations, Hubble friction, etc.; see, e.g., [5] and references therein.

In order to reach meaningful results based on the study of an analog model, it is important to precisely characterize the experimental system supporting the analysis and to correctly circumscribe the phenomenon under scrutiny. The present work aims at following this line of research in the case of an analog of event horizon realized in a Bose-Einstein condensed (BEC) ultracold atomic vapor. The use of a BEC as an analog model has been first suggested by Garay *et al.* [6], followed by many others. This motivated Steinhauer and his group to develop and then ameliorate an experimental setup making it possible to realize an acoustic horizon in a quasi one-dimensional BEC [7–11]. Particular attention has been devoted to the study of the analogous Hawking radiation, which corresponds to the emission of a pair of quasiparticles consisting of a “Hawking quantum” and a “Partner.” Concomitantly, the theoretical study of this system by means of a Bogoliubov decomposition has been first suggested in [12], then gradually refined [13–15] until a point where a detailed comparison with experiments has been possible [16]. There is now compelling evidence that analog Hawking radiation has been observed in different systems [10,11,17,18] but the crucial question of the quantum nature of the phenomenon has been debated: is the phenomenon mostly triggered by noise

or does it correspond to spontaneous quantum emission as in Hawking’s original scenario? A natural test of the latter consists in demonstrating entanglement of the Hawking pair. Indeed, experimental observation of correlated pairs of excitations does not suffice to demonstrate the quantum nature of the Hawking process, since the phenomenon also exists, e.g., in the nonquantum setting of water waves [19]. Also, as can be inferred from the quantitative results presented in Ref. [16], in BEC systems the corresponding signal is robust with respect to temperature: its observation therefore does not rule out the possibility that the analog Hawking radiation is mostly triggered by thermal and not quantum fluctuations. By contrast, the presence of entanglement between the Hawking quantum and its Partner demonstrates the presence of quantum effects. Additionally, a quantitative measure of entanglement is necessary for evaluating the respective impacts of quantum and thermal effects. However, it has not always been checked whether the measures used up to now in the literature provide good quantitative estimates of entanglement in the system. An important goal of the present work is to identify which, among different measures of entanglement, enable a quantitative, monotone, experimentally relevant determination of the degree of bipartite entanglement in a finite-temperature BEC analog of black hole.

Several theoretical works have addressed the issue of entanglement in analog gravity systems. Most of them [20–27] discuss qualitative measures such as the Peres-Horodecki or Cauchy-Schwarz criteria, which indicate if a state is entangled or not but—as shown below—do not provide good estimates of its degree of entanglement. In the present work we follow Refs. [28–31] and focus on *quantitative* measures. It is important to take into account the specificities of BEC physics in order to conduct the corresponding theoretical analysis. In particular, dispersive effects and the lack of Lorentz invariance complexify the standard Hawking quantum-Partner picture by introducing new propagation channels; accordingly the system is described by a three-mode Gaussian state. Its detailed

description makes it possible to quantify its bipartite and also tripartite entanglement. We advocate for the use of a measure of entanglement based on the Gaussian contangle, and we show that this is an experimentally accessible quantity which can provide a signature of the quantum nature of Hawking radiation. We also show how entanglement can be localized in our system in an effective two-mode state, which makes it possible to propose a simple and appealing equivalent optical model. This description suggests an alternative definition of the analog Hawking temperature and of the associated gray-body factor, in closer agreement with the gravitational paradigm. Another interesting outcome of this construction is the understanding that genuine tripartite entanglement may occur between the three modes, although two of them are not entangled.

The paper is organized as follows. In Sec. II we present the theoretical description of an acoustic black hole realized in an ultracold atomic vapor. In Sec. III we review the basics of Bogoliubov transformations and apply it to our situation. The description of Gaussian states appearing in the scattering processes involved in black hole analogs is discussed in Sec. IV. Section V is dedicated to the investigation of two-mode and three-mode entanglement in the Gaussian states we are considering here. The case of a finite-temperature setting is examined in Sec. VI, where we also provide a proof of principle of the measurability of the quantities we use for assessing the degree of entanglement. Concluding remarks are presented in Sec. VII. Some technical points are given in the Appendixes. In Appendix A we recall some properties of Bogoliubov transformations. In Appendix B we give some useful explicit expressions of the elements of the covariance matrix. In Appendix C we recall the low frequency behavior of the coefficients describing the scattering of linear waves by the acoustic horizon. Appendix D details the construction making it possible to localize entanglement in our system. In Appendix E we establish a formula making it possible to compute the Gaussian contangle at finite temperature.

II. ANALOG BLACK HOLE IN BECS

We consider a stationary flow of a one-dimensional (1D) BEC which is upstream subsonic and downstream supersonic. This “transonic” configuration mimics a black hole since acoustic excitations generated in the downstream supersonic region are dragged by the flow, and not detected in the upstream region.

A. The background flow

The complex quantum field $\hat{\Psi}$ describing the bosonic gas is decomposed into a classical part Φ (describing the stationary flow of the condensate) supplemented by small quantum fluctuations (described by an operator $\hat{\psi}$) according to

$$\hat{\Psi}(x, t) = \exp(-i\mu t/\hbar)[\Phi(x) + \hat{\psi}(x, t)], \quad (1)$$

where μ is the chemical potential [32]. The function Φ is solution of a classical Gross-Pitaevskii equation, with the addition of an external potential $U(x)$ used to implement the transonic

flow:

$$\mu\Phi(x) = -\frac{\hbar^2}{2m}\Phi_{xx} + [g|\Phi|^2 + U(x)]\Phi, \quad (2)$$

where $g > 0$ is a nonlinear coefficient accounting for repulsion between the atoms in a mean-field approach. The operator $\hat{\psi}$ describes the quantum fluctuations on top of the background Φ .

The experimental implementation of the 1D configuration (2) is obtained by a tight transverse confinement of a guided BEC. In the large density limit the transverse degrees of freedom cannot be discarded and the 1D reduction fails. Also, the so-called Bogoliubov decomposition (1) implies a long-range coherence (off-diagonal long-range order; see, e.g., [32]) which, in one dimension, is destroyed by phase fluctuations. Nonetheless a description of the system relying on Eqs. (1) and (2) can be ascribed a domain of applicability in the so-called 1D mean field regime [33]. For a Bose gas with s-wave scattering length a transversely confined by a harmonic trap of angular frequency ω_{\perp} , this regime corresponds to the range of densities

$$\frac{ma^2\omega_{\perp}}{\hbar} \ll n_{\text{typ}}a \ll 1, \quad (3)$$

where n_{typ} is a typical order of magnitude of the linear density $n(x) = |\Phi(x)|^2$. For ^{87}Rb or ^{23}Na atoms, the domain of validity (3) ranges over four orders of magnitude in density¹ and in this case $g = 2\hbar\omega_{\perp}a$ [34].

Several configurations realizing an analog black hole have been proposed in the past [13–15, 35–38]. The approach we use in this work is valid in a general setting, but for the sake of illustration we will present numerical results for the so-called “waterfall configuration” [15] which has been experimentally realized in [9, 10] and which has been shown to lead to a significant violation of the Cauchy-Schwarz criterion in [26]. In this configuration $U(x) = -U_0\Theta(x)$, where $U_0 > 0$ and Θ is the Heaviside step function. The corresponding solution of Eq. (2) is a plane wave flow of density n_d and velocity $V_d > 0$ in the downstream region ($x > 0$) and half a dark soliton in the upstream region ($x < 0$) with asymptotic density n_u and velocity $V_u > 0$, meaning that

$$\begin{aligned} \Phi(x > 0) &= \sqrt{n_d} \exp(imV_d x/\hbar) \exp(i\beta_d), \\ \Phi(x \rightarrow -\infty) &= \sqrt{n_u} \exp(imV_u x/\hbar) \exp(i\beta_u), \end{aligned} \quad (4)$$

where β_u and β_d are constant phase factors. This setting is illustrated in Fig. 1 (see details in [15]).

In the following we will loosely state that the horizon is located at $x = 0$. However, it is important to note that, in any dispersive analog model, the location of the horizon is ill-defined, as it depends on frequency. A commonly accepted way to circumvent this difficulty is to take the zero-frequency value: the analog horizon is then the point where the velocity of the flow $v(x) = \frac{\hbar}{m}\text{Im}(\Phi^*\Phi_x)/n(x)$ is equal to the local sound velocity $c(x)$. This definition makes sense because it has been shown that the characteristics of analog Hawking

¹A more detailed discussion of the domain of applicability of the Bogoliubov decomposition (1) can be found, e.g., in [26].

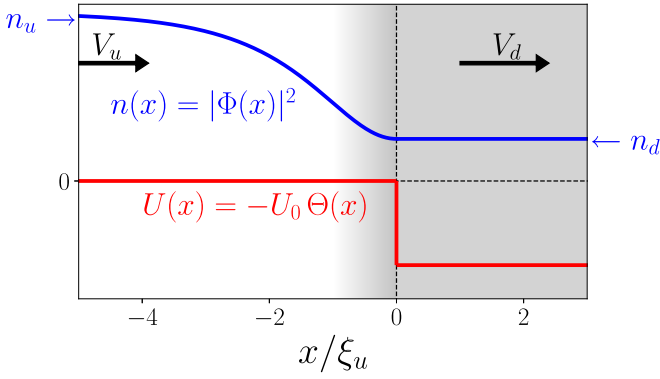


FIG. 1. Waterfall configuration. The flow is directed from left to right. The downstream classical field $\Phi(x > 0)$ is exactly a plane wave of density n_d and velocity V_d . $\Phi(x < 0)$ is the half profile of a dark soliton which is asymptotically a plane wave of density n_u and velocity V_u ; see Eqs. (4). The far upstream flow is subsonic, with a velocity $0 < V_u < c_u$, and the downstream flow is supersonic with a velocity $V_d > c_d > 0$, where $c_\alpha = (gn_\alpha/m)^{1/2}$ is the speed of sound in region $\alpha = u$ (upstream) or d (downstream). The shaded region $x > 0$ corresponds to the interior of the analog black hole; the gradient of gray around $x \lesssim 0$ depicts the (ill-defined; see text) position of the horizon. The coordinate x is plotted in units of the upper healing length $\xi_u = \hbar/(mc_u)$.

radiation are governed by long wave-length physics; see, e.g., [39–41]. However, in the BEC context, the definition of a local sound velocity $c(x)$ is only legitimate in regions where the density varies over a length scale large compared to the healing length. This is not the case around $x \lesssim 0$ for the waterfall configuration and this forbids a rigorous definition of an horizon. Nevertheless, the system still emits a spontaneous analog Hawking radiation, because the feature that triggers this process is the mismatch between the left subsonic asymptotic flow and the right supersonic one (this is at the heart of the Bogoliubov transform discussed in Sec. III). One may wonder, however, if the concept of Hawking temperature is still meaningful in the absence of a proper location of the horizon, since, strictly speaking, the widely used semiclassical result (C5) which defines the Hawking temperature as the analog surface gravity is not valid here.² The solution lies in the study of the low-frequency behavior of the spectrum of the analog Hawking radiation which is thermal-like. This makes it possible to determine an effective Hawking temperature; see, e.g., [13–15]. We will come to this point in more detail in Secs. IV D and V C.

B. Elementary excitations

Since the far upstream and downstream background flows are uniform, the elementary excitations which form a basis set for the quantum operator $\hat{\psi}$ are plane waves in these two regions, with dispersion relations of Bogoliubov type (see, e.g., [32]):

$$(\omega - qV_\alpha)^2 = \omega_{\text{B},\alpha}^2(q), \quad \alpha = u \text{ or } d, \quad (5)$$

where V_u and V_d are the upstream and downstream velocities, and $\omega_{\text{B},\alpha}$ is the Bogoliubov dispersion relation

$$\omega_{\text{B},\alpha}(q) = c_\alpha q \sqrt{1 + \xi_\alpha^2 q^2 / 4}, \quad (6)$$

$c_\alpha = (gn_\alpha/m)^{1/2}$ being the speed of sound and $\xi_\alpha = \hbar/(mc_\alpha)$ the “healing length,” in the far upstream region if $\alpha = u$ and in the downstream region if $\alpha = d$. The left-hand side of Eq. (5) includes a Doppler shift caused by the velocity V_α of the background.

It will be useful in the following to define the quantities

$$m_\alpha = \frac{V_\alpha}{c_\alpha}, \quad \alpha = u \text{ or } d, \quad (7)$$

known as the upstream ($\alpha = u$) and downstream ($\alpha = d$) Mach numbers. It was shown in [15] that the waterfall configuration, which we use below to exemplify our results, is uniquely characterized once the value of m_u , say, is fixed. In particular the parameters of the flow are related by the following relations:

$$\frac{V_d}{V_u} = \frac{n_u}{n_d} = \frac{1}{m_u^2} = m_d = \left(\frac{\xi_d}{\xi_u}\right)^2 = \left(\frac{c_u}{c_d}\right)^2. \quad (8)$$

The flow being upstream subsonic ($V_u < c_u$, i.e., $m_u < 1$) and downstream supersonic ($V_d > c_d$, i.e., $m_d > 1$), the graphs of the corresponding dispersion relations are of different types, as illustrated in Fig. 2. In the upstream region the spectrum has two branches which we label as 0|in and 0|out. In the downstream supersonic region there are four branches: 1|in, 1|out, 2|in and 2|out, the last two branches being limited to $\omega \in [0, \Omega]$, where Ω is the frequency at which these two branches coalesce, and whose value is given by

$$\Omega = q^* V_d - \omega_{\text{B},d}(q^*) \quad \text{with} \quad q^* \xi_d = \left(-2 + \frac{m_d^2}{2} + \frac{m_d}{2} \sqrt{8 + m_d^2}\right)^{\frac{1}{2}}. \quad (9)$$

For future convenience (see Sec. VI) we define functions $q_{0|\text{in}}(\omega)$, $q_{1|\text{in}}(\omega)$ and $q_{2|\text{in}}(\omega)$ as the reciprocal of the Bogoliubov dispersion relation (5) along some of these branches; $q_{0|\text{in}}(\omega)$ and $q_{1|\text{in}}(\omega)$ are defined for $\omega > 0$ and $q_{2|\text{in}}(\omega)$ only for $\omega \in [0, \Omega]$. A number of previous works [15,16,20,26,37] followed the convention introduced in [14], in which indices u , $d1$, and $d2$ are employed instead of the indices 0, 1, and 2 we use here. We changed convention in order to simplify the manipulation of the matrix notation introduced below.

The particular transonic configuration we consider corresponds, for angular frequencies ω lower than the threshold Ω , to a specific scattering process of elementary excitations onto the analog event horizon. For instance, a wave issued from the interior region along the channel identified as 1|in in Fig. 2 is transmitted to the exterior along the 0|out channel and reflected back along the 1|out and 2|out channels. The corresponding (complex) transmission and reflection amplitudes are denoted as $S_{10}(\omega)$, $S_{11}(\omega)$, and $S_{12}(\omega)$, respectively. They are obtained by imposing matching conditions at $x = 0$, as explained in Ref. [15]. The quantum boson operator corresponding to this whole process is denoted as $\hat{b}_1(\omega)$. Similarly, a wave incident along the 0|in channel is transmitted towards

²Note that this issue is also encountered in profiles smoother than that of the waterfall; see, e.g., [13].

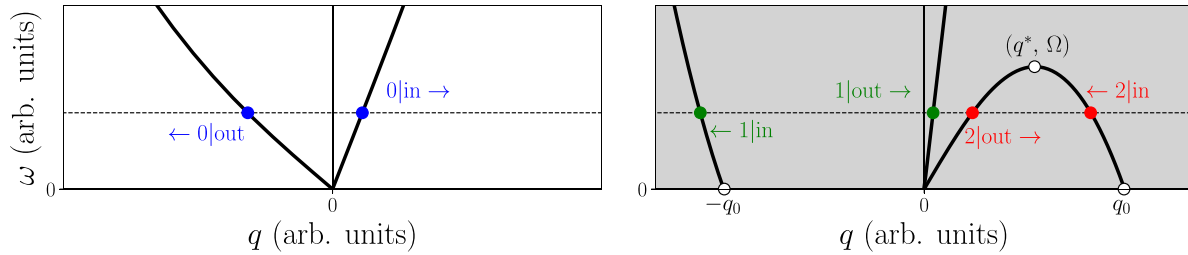


FIG. 2. Graphical representation of the positive frequency part of the dispersion relation (5) in the far upstream (left plot) and downstream (right plot) regions. The downstream region (gray background) is the interior of the analog black hole, while the upstream region (white background) is the exterior. In the upstream region, to any given ω (represented by a horizontal dashed line) correspond two channels of propagation denoted as $0|in$ and $0|out$. In the downstream region there are four or two channels, depending if ω is smaller or larger than Ω . The arrows indicate the direction of propagation of the corresponding waves, and the channels are labeled 1 or 2, with an additional “in” (or “out”) indicating if the wave propagates towards (or away from) the horizon.

the interior of the black hole along channels $1|out$ [amplitude $S_{01}(\omega)$] and $2|out$ [amplitude $S_{02}(\omega)$] and reflected along $0|out$ [amplitude $S_{00}(\omega)$]; the corresponding quantum mode is associated with operator $\hat{b}_0(\omega)$.³ A third mode describes the scattering of a wave issued from the channel $2|in$ onto the outgoing channels $0|out$, $1|out$, and $2|out$. The channels labeled $2|in$ and $2|out$ are particular, in the sense that they have a negative norm, i.e., a negative energy in the rest frame of the fluid [42–45]. As a result, the mode initiated by the incoming channel $2|in$ should be quantized using an operator $\hat{b}_2^\dagger(\omega)$, i.e., inverting the role of the creation and annihilation operators used for the two other modes. Only in this way do the propagating modes behave as bosons satisfying the usual commutation relations

$$\begin{aligned} [\hat{b}_i(\omega), \hat{b}_j^\dagger(\omega')] &= \delta_{i,j} \delta(\omega - \omega'), \\ [\hat{b}_i(\omega), \hat{b}_j(\omega')] &= [\hat{b}_i^\dagger(\omega), \hat{b}_j^\dagger(\omega')] = 0, \end{aligned} \quad (10)$$

for i and $j \in \{0, 1, 2\}$. Another consequence is that the 3×3 scattering matrix $S(\omega)$ whose elements are the $S_{ij}(\omega)$ obeys a skew-unitarity relation [14]:

$$S^\dagger \eta S = \eta = S \eta S^\dagger, \quad \eta = \text{diag}(1, 1, -1). \quad (11)$$

For $\omega > \Omega$ the situation is drastically different: the channels $2|in$ and $2|out$ disappear (cf. Fig. 2), as well as the operator $\hat{b}_2(\omega)$, and the S -matrix becomes 2×2 and unitary.

We denote the b modes as “incoming” since they correspond to scattering processes initiated by a single wave incident along one of the three “in” channels directed towards the horizon: $0|in$, $1|in$, and $2|in$. One could equivalently choose to work with “outgoing modes” [12] describing processes each resulting in the emission of a single wave along one of the three “out” channels $0|out$, $1|out$, and $2|out$. We denote the corresponding quantum operators as $\hat{c}_0(\omega)$, $\hat{c}_1(\omega)$,

and $\hat{c}_2(\omega)$. They relate to the incoming operators *via* [14]

$$\begin{pmatrix} \hat{c}_0 \\ \hat{c}_1 \\ \hat{c}_2^\dagger \end{pmatrix} = \begin{pmatrix} S_{00} & S_{01} & S_{02} \\ S_{10} & S_{11} & S_{12} \\ S_{20} & S_{21} & S_{22} \end{pmatrix} \begin{pmatrix} \hat{b}_0 \\ \hat{b}_1 \\ \hat{b}_2^\dagger \end{pmatrix}, \quad (12)$$

where for legibility we omit the ω dependence of all the terms. The definition (12), together with the property (11), ensures that the \hat{c} operators obey the same commutation relations (10) as the \hat{b} operators and thus describe bosonic quasiparticles.

In the setting we consider, the analog of the Hawking radiation spectrum is the number of excitations emitted per unit time and per unit frequency into the subsonic region ($x < 0$), that is, the expectation value of $\hat{c}_0^\dagger(\omega)\hat{c}_0(\omega)$ over the state vector. From relation (12) one sees that this current is nonzero when the state vector is the vacuum $|0\rangle_b$ of incoming modes: ${}_b\langle 0|\hat{c}_0^\dagger(\omega)\hat{c}_0(\omega)|0\rangle_b = |S_{02}(\omega)|^2$; this is the analogous Hawking effect [13,14,45,46]. The mode associated with operator \hat{c}_0 is thus denoted the Hawking outgoing mode. The other outgoing modes, associated with operators \hat{c}_1 and \hat{c}_2 , are denoted the Companion and the Partner, respectively.

As can be seen from expression (12), the *outgoing* operators \hat{c} and \hat{c}^\dagger are expressed as a combination of the *ingoing* annihilation and creation operators \hat{b} and \hat{b}^\dagger . Therefore, it is possible to associate a Bogoliubov transformation with our analog system. This is the aim of the next section.

III. BOGOLIUBOV TRANSFORMATIONS

Bogoliubov transformations are linear transformations of creation and annihilation operators that preserve the canonical commutation rules [47]. In the context of quantum field theory in curved spacetime, these transformations are at the heart of the Hawking process; indeed, since they mix annihilation and creation operators they can give rise to spontaneous emission of particles from vacuum [48–53]. This mixing of operators also occurs for analog black holes, as is clear from Eq. (12). This way of viewing the emergence of the analog Hawking radiation through a Bogoliubov transformation makes a direct connection with the gravitational case: as shown by Hawking in 1974 [48,49], one of the parameters involved in the Bogoliubov transformation, the so-called β -coefficient, is directly related to the number of particles created by black holes. In our case, we can derive such a parameter and

³In the terminology we use, it is important to make a distinction between the “quantum modes” and the “propagation channels”: a mode corresponds to a whole process typically involving one or several incoming channels and one or several outgoing channels.

compare its properties with Hawking's β -coefficient; in particular, through this approach, we will be able to question the thermality of the analog Hawking radiation (see Sec. IV C). Furthermore, identifying the Bogoliubov transformation will be an important step to understand and study the entanglement properties of the analog Hawking radiation (see Sec. V).

The present section is divided into two parts. First, we consider an arbitrary (but unitary) Bogoliubov transformation and derive its properties. Then, we apply these results to the particular case of analog black holes in BECs starting from expression (12).

A. General setting

We start by briefly recalling some well-known facts concerning unitary Bogoliubov transformations [42,47,54]. Some useful intermediate results are given in Appendix A.

Let us consider N boson operators $\hat{b}_1, \dots, \hat{b}_N$ satisfying the usual commutation relations $[\hat{b}_i, \hat{b}_j^\dagger] = \delta_{i,j}$. Defining the column vector

$$\mathbf{b} = (\hat{b}_1, \dots, \hat{b}_N, \hat{b}_1^\dagger, \dots, \hat{b}_N^\dagger)^\top, \quad (13)$$

the Bose commutation relations can be rewritten as

$$[\mathbf{b}_i, \mathbf{b}_j] = \tilde{\mathbb{J}}_{ij}, \quad \text{with} \quad \tilde{\mathbb{J}} = \begin{pmatrix} 0 & \mathbb{1}_N \\ -\mathbb{1}_N & 0 \end{pmatrix}, \quad (14)$$

where $\mathbb{1}_N$ is the $N \times N$ identity matrix. A (unitary) Bogoliubov transformation is a linear transformation mapping the operators \hat{b}_i onto new operators \hat{c}_i defined through

$$\mathbf{c} = \sum_{j=1}^{2N} \mathcal{T}_{ij} \mathbf{b}_j, \quad \text{or equivalently} \quad \mathbf{c} = \mathcal{T} \mathbf{b}. \quad (15)$$

For unitary Bogoliubov transformations \mathbf{c} has the form

$$\mathbf{c} = (\hat{c}_1, \dots, \hat{c}_N, \hat{c}_1^\dagger, \dots, \hat{c}_N^\dagger)^\top, \quad (16)$$

i.e., $\mathbf{c}_{i+N} = \mathbf{c}_i^\dagger$. In this case the matrix \mathcal{T} admits the block decomposition

$$\mathcal{T} = \begin{pmatrix} \alpha^* & -\beta^* \\ -\beta & \alpha \end{pmatrix}, \quad (17)$$

where α and β are $N \times N$ matrices. Operators \hat{c}_i and \hat{b}_i can then be related by a unitary operator T such that

$$\hat{c}_i = T^\dagger \hat{b}_i T, \quad (18)$$

whose explicit construction from matrix \mathcal{T} is detailed in Appendix A.

In general, the transformation \mathcal{T} in (15) mixes creation and annihilation operators, so that the vacua $|0\rangle_b$ and $|0\rangle_c$, defined by

$$\hat{b}_i |0\rangle_b = 0, \quad \text{and} \quad \hat{c}_i |0\rangle_c = 0, \quad i \in \{1, \dots, N\}, \quad (19)$$

differ. These vacua are related via the identity

$$|0\rangle_b = T |0\rangle_c, \quad (20)$$

as is clear from the fact that $\hat{b}_i T |0\rangle_c = T \hat{c}_i |0\rangle_c = 0$.

Defining the $N \times N$ matrix $X = -\beta^* \alpha^{-1}$ and using the decomposition (A6), it is possible to write Eq. (20) under the

explicit form

$$|0\rangle_b = \frac{1}{(\det \alpha)^{\frac{1}{2}}} e^{\frac{1}{2} \sum_{i,j} X_{ij} \hat{c}_i^\dagger \hat{c}_j^\dagger} |0\rangle_c. \quad (21)$$

A simple example of a Bogoliubov transformation is the one leading to two-mode squeezed states [55,56]. For a real squeezing parameter r , a two-mode squeezed state is obtained by applying the two-mode squeezing operator

$$T = \exp[r(\hat{c}_1^\dagger \hat{c}_2^\dagger - \hat{c}_1 \hat{c}_2)] \quad (22)$$

to the vacuum state $|0\rangle_c$. The corresponding Bogoliubov transformation is of the form (17) with $N = 2$ and α, β given by

$$\alpha = \begin{pmatrix} \cosh r & 0 \\ 0 & \cosh r \end{pmatrix}, \quad \beta = -\begin{pmatrix} 0 & \sinh r \\ \sinh r & 0 \end{pmatrix}. \quad (23)$$

In this case (21) reads

$$|0\rangle_b = (\cosh r)^{-1} \exp(\tanh r \hat{c}_1^\dagger \hat{c}_2^\dagger) |0\rangle_c. \quad (24)$$

B. Bogoliubov transformation in a transonic BEC

In the case described in Sec. II of a transonic flow realized in a BEC, \mathbf{b} and \mathbf{c} correspond to sets of ingoing and outgoing modes. The associated column vectors $\mathbf{b} = (\hat{b}_0, \hat{b}_1, \hat{b}_2, \hat{b}_0^\dagger, \hat{b}_1^\dagger, \hat{b}_2^\dagger)^\top$ and $\mathbf{c} = (\hat{c}_0, \hat{c}_1, \hat{c}_2, \hat{c}_0^\dagger, \hat{c}_1^\dagger, \hat{c}_2^\dagger)^\top$ are related by Eq. (12). One can express this relation equivalently as $\mathbf{c} = \mathcal{T} \mathbf{b}$, with \mathcal{T} a Bogoliubov transformation of the form (17) with

$$\alpha = \begin{pmatrix} S_{00}^* & S_{01}^* & 0 \\ S_{10}^* & S_{11}^* & 0 \\ 0 & 0 & S_{22} \end{pmatrix}, \quad \beta = -\begin{pmatrix} 0 & 0 & S_{02}^* \\ 0 & 0 & S_{12}^* \\ S_{20} & S_{21} & 0 \end{pmatrix}, \quad (25)$$

where for legibility we do not write the ω -dependence of the scattering amplitudes. This yields

$$X = \frac{1}{S_{22}} \begin{pmatrix} 0 & 0 & S_{02} \\ 0 & 0 & S_{12} \\ S_{02} & S_{12} & 0 \end{pmatrix}. \quad (26)$$

From relation (11) one can show that $\det \alpha = |S_{22}|^2$, and thus (21) takes the simple form

$$|0\rangle_b = \frac{1}{|S_{22}|} e^{(X_{02} \hat{c}_0^\dagger + X_{12} \hat{c}_1^\dagger) \hat{c}_2^\dagger} |0\rangle_c. \quad (27)$$

A word of caution is in order here. The case we consider in the present section is different from the discussion of the previous Sec. III A because, as explained in Sec. II B, the modes are here continuously distributed along the energy axis [compare, for instance, the commutation relations (10) and (14)]. A natural way to set up a framework encompassing both situations consists in discretizing the energies with a small mesh $\Delta\omega$ and to define coarse-grained operators

$$\hat{B}_{i,p} = \frac{1}{\sqrt{\Delta\omega}} \int_{\omega_p}^{\omega_{p+1}} d\omega \hat{b}_i(\omega) \quad (28)$$

and

$$\hat{C}_{i,p} = \frac{1}{\sqrt{\Delta\omega}} \int_{\omega_p}^{\omega_{p+1}} d\omega \hat{c}_i(\omega), \quad (29)$$

where $i \in \{0, 1, 2\}$, $p \in \mathbb{N}$ and $\omega_p = p \Delta\omega$. It is easy to check that these operators obey the standard Bose commutation rules, such as $[\hat{B}_{i,p}, \hat{B}_{j,q}^\dagger] = \delta_{i,j}\delta_{p,q}$ for instance. If $\Delta\omega$ is small compared to the typical scale of variation of the elements of the S -matrix, then the $\hat{C}_{i,p}$ and the $\hat{B}_{j,p}$ are related by a relation analogous to (12):

$$\begin{pmatrix} \hat{C}_{0,p} \\ \hat{C}_{1,p} \\ \hat{C}_{2,p}^\dagger \end{pmatrix} = \begin{pmatrix} S_{00} & S_{01} & S_{02} \\ S_{10} & S_{11} & S_{12} \\ S_{20} & S_{21} & S_{22} \end{pmatrix} \begin{pmatrix} \hat{B}_{0,p} \\ \hat{B}_{1,p} \\ \hat{B}_{2,p}^\dagger \end{pmatrix}, \quad (30)$$

where the S_{ij} should be evaluated at ω_p . Thus the relation (27) should be replaced by

$$|0\rangle_b = \frac{1}{\prod_{p=0}^{\infty} |S_{22}(\omega_p)|} \times e^{\sum_{p=0}^{\infty} (X_{02}(\omega_p)\hat{C}_{0,p}^\dagger + X_{12}(\omega_p)\hat{C}_{1,p}^\dagger)\hat{C}_{2,p}^\dagger} |0\rangle_c. \quad (31)$$

This remark being made, in the following we favor legibility over formal rigor: We will continue to write relations of the type (27), instead of the more rigorous but cumbersome Eq. (31), keeping in mind that the correction of “naive” expressions—such as Eq. (32), (33), (38), or (97) below—is straightforward.

From (27), if we define the Fock state basis of quasiparticles of type c by

$$|n\rangle_i = \frac{1}{\sqrt{n!}} (\hat{c}_i^\dagger)^n |0\rangle_c, \quad (32)$$

where i is the mode number, then the explicit expansion of the vacuum $|0\rangle_b$ reads

$$|0\rangle_b = \frac{1}{|S_{22}|} \sum_{n,n'=0}^{\infty} \sqrt{\binom{n+n'}{n}} X_{02}^n X_{12}^{n'} |n\rangle_0 |n'\rangle_1 |n+n'\rangle_2. \quad (33)$$

It is convenient for future use in Secs. **IV D** and **V C** to introduce a new set of operators $\mathbf{e} = (\hat{e}_0, \hat{e}_1, \hat{e}_2, \hat{e}_0^\dagger, \hat{e}_1^\dagger, \hat{e}_2^\dagger)^\top$. By writing

$$S_{ij}(\omega) = v_{ij}(\omega) e^{i\varphi_{ij}(\omega)}, \quad v_{ij} \geq 0, \quad 0 \leq i, j \leq 2, \quad (34)$$

we define the operators \hat{e}_0, \hat{e}_1 and \hat{e}_2 as

$$\hat{e}_0 = e^{-i\varphi_{02}} \hat{c}_0, \quad \hat{e}_1 = e^{-i\varphi_{12}} \hat{c}_1, \quad \hat{e}_2 = e^{i\varphi_{22}} \hat{c}_2 \quad (35)$$

(note the + sign in front of φ_{22}). This defines a local unitary Bogoliubov transformation, as it does not mix annihilation and creation operators. In particular $|0\rangle_e = |0\rangle_c$. Using the notations of Sec. **III A**, this transformation can be cast in the form

$$\mathbf{e} = \mathcal{R} \mathbf{c}, \quad (36)$$

where

$$\mathcal{R} = \text{diag}(e^{-i\varphi_{02}}, e^{-i\varphi_{12}}, e^{i\varphi_{22}}, e^{i\varphi_{02}}, e^{i\varphi_{12}}, e^{-i\varphi_{22}}). \quad (37)$$

Then, using expression (26) and this new set of creation and annihilation operators \mathbf{e} , Eq. (27) becomes

$$|0\rangle_b = \frac{1}{v_{22}} e^{v_{22}^{-1} (v_{02} \hat{e}_0^\dagger + v_{12} \hat{e}_1^\dagger) \hat{e}_2^\dagger} |0\rangle_e. \quad (38)$$

IV. THREE-MODE GAUSSIAN STATES

In the context of analog gravity, the general description of the system by means of a Gaussian state has been presented in the monograph [46]. The importance of Gaussianity has been implicitly or explicitly assumed in many articles, but it has been thoroughly discussed only in Ref. [25]. In the present work we will extend in Secs. **V** and **VI** the analysis of [25] to build *quantitative and monotone* measures of bipartite and tripartite entanglement. Since Gaussianity is a central point in our approach, in the present section we briefly present general properties of Gaussian states, then construct the covariance matrix of the three-mode Gaussian pure state which describes our system $[|0\rangle_b$ defined by Eq. (33)] and discuss in more detail the covariance matrix of the reduced state $\rho^{(0)}$, in connection with the determination of the Hawking temperature.

A. Gaussian states

In order to set up notations we start by reviewing the formalism for Gaussian states (see [57] for a review). Gaussian states are states whose Wigner function is a Gaussian. A Gaussian state ρ can be entirely described by its first and second moments. We define the covariance matrix σ of ρ as the real symmetric positive-definite matrix

$$\sigma_{ij} \equiv \frac{1}{2} \langle \hat{\xi}_i \hat{\xi}_j + \hat{\xi}_j \hat{\xi}_i \rangle - \langle \hat{\xi}_i \rangle \langle \hat{\xi}_j \rangle, \quad (39)$$

where $\hat{\xi}_i$ are components of the vector $\hat{\xi} = \sqrt{2} (\hat{q}_1, \hat{p}_1, \dots, \hat{q}_N, \hat{p}_N)^\top$ of quadratures relative to mode i , defined so that $[\hat{q}_i, \hat{p}_j] = i \delta_{i,j}$. In the definition (39) and in all the following the averages $\langle \dots \rangle$ are taken over the density matrix ρ characterizing the state of the system, which, in the simpler case, is the projector onto the vacuum state $|0\rangle_b$. We shall discuss in Sec. **VI** how to generalize to a finite-temperature configuration.

The commutation relations between the $\hat{\xi}_i$ can be expressed as $[\hat{\xi}_i, \hat{\xi}_j] = 2i \mathbb{J}_{ij}$, $\forall i, j \in \{1, \dots, 2N\}$ with

$$\mathbb{J} = \bigoplus_1^N J_i, \quad J_i = \begin{pmatrix} 0 & 1 \\ -1 & 0 \end{pmatrix}. \quad (40)$$

Entanglement properties of a quantum state are unchanged by local unitary (LU) operations, so that the mean values of position and momentum operators can be set to 0. An N -mode Gaussian state is then entirely specified by its $2N \times 2N$ covariance matrix, which can be rewritten in terms of 2×2 blocks as

$$\sigma = \begin{pmatrix} \sigma_1 & \varepsilon_{12} & \cdots & \varepsilon_{1N} \\ \varepsilon_{12}^\top & \ddots & \ddots & \vdots \\ \vdots & \ddots & \ddots & \varepsilon_{N-1N} \\ \varepsilon_{1N}^\top & \cdots & \varepsilon_{N-1N}^\top & \sigma_N \end{pmatrix}, \quad (41)$$

with

$$\varepsilon_{ij} = 2 \begin{pmatrix} \langle \hat{q}_i \hat{q}_j \rangle & \langle \hat{q}_i \hat{p}_j \rangle \\ \langle \hat{p}_i \hat{q}_j \rangle & \langle \hat{p}_i \hat{p}_j \rangle \end{pmatrix} \quad (42)$$

and

$$\sigma_i = \begin{pmatrix} \langle 2\hat{q}_i^2 \rangle & \langle \{\hat{q}_i, \hat{p}_i\} \rangle \\ \langle \{\hat{q}_i, \hat{p}_i\} \rangle & \langle 2\hat{p}_i^2 \rangle \end{pmatrix}, \quad (43)$$

$\{.,.\}$ denoting the anticommutator. A covariance matrix σ satisfies the inequality

$$\sigma + i\mathbb{J} \geq 0, \tag{44}$$

which is a consequence of the canonical commutation relations and positivity of the density matrix [58,59]. In particular, σ is a positive matrix.

B. Transformations of Gaussian states

Partial tracing a Gaussian state is particularly simple. The covariance matrix of the reduced state is simply obtained by discarding the lines and columns corresponding to the modes over which the partial trace is done (see, e.g., [60]). For instance, the two-mode state obtained from (41) by tracing out all modes but i and j has covariance matrix

$$\sigma_{ij} = \begin{pmatrix} \sigma_i & \varepsilon_{ij} \\ \varepsilon_{ij}^\dagger & \sigma_j \end{pmatrix}, \tag{45}$$

where the 2×2 blocks are the same as the ones in (41). In the same way, the reduced density matrix $\rho^{(i)}$ of mode i obtained by tracing out all the other modes is a single-mode Gaussian state entirely specified by the covariance matrix σ_i .

Let us now turn to the modification of the covariance matrix under a Bogoliubov transformation. It is important to stress here that we change operators but keep the same quantum state over which the averages $\langle \dots \rangle$ are performed. For the vector of creation and annihilation operators \mathbf{b} , we denote by ξ_b the corresponding vector of position and momentum operators $\xi_b = \sqrt{2}(\hat{q}_1, \hat{p}_1, \dots, \hat{q}_N, \hat{p}_N)^\top$ with $\hat{q}_j = (\hat{b}_j + \hat{b}_j^\dagger)/\sqrt{2}$ and $\hat{p}_j = i(\hat{b}_j^\dagger - \hat{b}_j)/\sqrt{2}$. We thus have $\xi_b = U\mathbf{b}$, with

$$U = \begin{pmatrix} \frac{1}{\sqrt{2}} & 0 & 0 & \dots & \frac{1}{\sqrt{2}} & 0 & 0 & \dots \\ -\frac{i}{\sqrt{2}} & 0 & 0 & \dots & \frac{i}{\sqrt{2}} & 0 & 0 & \dots \\ 0 & \frac{1}{\sqrt{2}} & 0 & \dots & 0 & \frac{1}{\sqrt{2}} & 0 & \dots \\ 0 & -\frac{i}{\sqrt{2}} & 0 & \dots & 0 & \frac{i}{\sqrt{2}} & 0 & \dots \\ 0 & 0 & \ddots & \dots & 0 & 0 & \ddots & \dots \end{pmatrix} \tag{46}$$

a $2N \times 2N$ unitary matrix. Similarly, $\xi_c = U\mathbf{c}$. The Bogoliubov transformation $\mathbf{c} = \mathcal{S}\mathbf{b}$ then entails that $\xi_c = \mathcal{S}_{\mathcal{S}}\xi_b$ with

$$\mathcal{S}_{\mathcal{S}} = U\mathcal{S}U^\dagger. \tag{47}$$

It can be proved that the matrix $\mathcal{S}_{\mathcal{S}} \in \text{Sp}(2N, \mathbb{R})$ is real and symplectic [59]. Since this transformation is linear, we get from Eq. (39) that a Gaussian state with covariance matrix σ_b in mode b is a Gaussian state in mode c with covariance matrix

$$\sigma_c = \mathcal{S}_{\mathcal{S}} \sigma_b \mathcal{S}_{\mathcal{S}}^\top \tag{48}$$

in mode c .

As guaranteed by Williamson theorem [61], it is always possible to find a symplectic transform that brings any covariance matrix σ to a canonical diagonal matrix $\text{diag}(v_1, \dots, v_N, v_1, \dots, v_N)$, which is unique up to the ordering of the v_j . The v_j are called the *symplectic eigenvalues* of σ . They can be directly obtained from the eigenvalues of the matrix $\mathbb{J}\sigma$, which are given by $\pm iv_j$ [62]. In terms of the

v_j , given the uncertainty relation (44), the positivity of ρ is equivalent to

$$v_j \geq 1, \quad j = 1, \dots, N. \tag{49}$$

C. Thermal states

The symplectic eigenvalues have an appealing physical interpretation. Indeed, they can be related with the mean particle number of a thermal state.

Recall that a generic (single-mode) thermal state is a state whose density matrix in the Fock space spanned by vectors $|n\rangle$ is of the form

$$\rho^{\text{th}}(a) = \frac{2}{a+1} \sum_{n=0}^{\infty} \left(\frac{a-1}{a+1}\right)^n |n\rangle\langle n|, \tag{50}$$

with a some parameter. Denoting as \hat{n} the corresponding number operator, since $\bar{n} \equiv \langle \hat{n} \rangle = \text{tr}(\rho^{\text{th}}\hat{n}) = \frac{1}{2}(a-1)$, the parameter a is simply related with the mean particle number as $a = 2\bar{n} + 1$. The state $\rho^{\text{th}}(a)$ is in fact a Gaussian state with 2×2 covariance matrix $\sigma^{\text{th}} = a\mathbb{1}_2$. This means that a single-mode covariance matrix in diagonal form describes a thermal state with mean particle number $\bar{n} = (a-1)/2$ and symplectic eigenvalue $v = a$. Another way of representing a thermal state is to set $\bar{n} = \sinh^2 r$, which yields

$$\rho^{\text{th}}(a) = \frac{1}{\cosh^2 r} \sum_{n=0}^{\infty} (\tanh r)^{2n} |n\rangle\langle n|, \quad a = \cosh(2r). \tag{51}$$

The purity of $\rho^{\text{th}}(a)$ can be readily calculated from (50) or (51); it reads $\text{tr}[\rho^{\text{th}}(a)]^2 = 1/\cosh(2r) = 1/a$. The quantity a being the inverse of the purity of a single-mode reduced density matrix, it is referred to as the *local mixedness* [63]. Note that the vacuum state is a thermal state $\rho^{\text{th}}(1)$ with mean occupation numbers $\bar{n}_j = 0$ and local mixedness unity.

More generally [64], an N -mode Gaussian state with arbitrary covariance matrix σ can be brought to a product of thermal states

$$\rho_v = \bigotimes_{j=1}^N \rho^{\text{th}}(v_j). \tag{52}$$

Indeed, if \mathcal{S} is the symplectic transformation that diagonalizes σ as $\text{diag}(v_1, v_1, \dots, v_N, v_N) = \mathcal{S}\sigma\mathcal{S}^\top$, then it can be realized on the Gaussian state by a unitary evolution generated by a quadratic Hamiltonian (see, e.g., [59]). Therefore Williamson's theorem ensures that any Gaussian state can be decomposed into a product of thermal states whose mean occupation number in mode j is obtained from the symplectic eigenvalue v_j as $\bar{n}_j = (v_j - 1)/2$ [59]. The condition $v_j \geq 1$ in (49) simply corresponds to the fact that the mean occupation numbers have to be positive. Note that the purity of state (52) is simply given in terms of the covariance matrix by $\text{tr}(\rho_v)^2 = 1/\sqrt{\det \sigma}$.

D. Vacuum as a three-mode Gaussian state

The Bogoliubov transformation associated with the scattering process (12) leads to a three-mode Gaussian pure state, given by (33). The covariance matrix of the vacuum $|0\rangle_b$ is the identity matrix $\mathbb{1}_6$. Applying (48) we thus get that the

covariance matrix of state (33) is

$$\sigma_c = \mathcal{S}_{\mathcal{T}} \mathcal{S}_{\mathcal{T}}^{\dagger}. \quad (53)$$

Using the explicit expression of \mathcal{F} derived from (25), and the explicit expression (46) for U , we obtain the 6×6 matrix given in Eq. (B1) of Appendix B. Note that using (42) and (43) the 2×2 matrices σ_i and ε_{ij} , $i \in \{0, 1, 2\}$, simply read

$$\sigma_i = (1 + 2 \langle \hat{c}_i^{\dagger} \hat{c}_i \rangle) \mathbb{1}_2 \quad (54)$$

and (for $i \neq 2$)

$$\varepsilon_{i2} = \begin{pmatrix} 2 \operatorname{Re} \langle \hat{c}_i \hat{c}_2 \rangle & 2 \operatorname{Im} \langle \hat{c}_i \hat{c}_2 \rangle \\ 2 \operatorname{Im} \langle \hat{c}_i \hat{c}_2 \rangle & -2 \operatorname{Re} \langle \hat{c}_i \hat{c}_2 \rangle \end{pmatrix},$$

$$\varepsilon_{01} = \begin{pmatrix} 2 \operatorname{Re} \langle \hat{c}_0 \hat{c}_1^{\dagger} \rangle & 2 \operatorname{Im} \langle \hat{c}_0 \hat{c}_1^{\dagger} \rangle \\ -2 \operatorname{Im} \langle \hat{c}_0 \hat{c}_1^{\dagger} \rangle & 2 \operatorname{Re} \langle \hat{c}_0 \hat{c}_1^{\dagger} \rangle \end{pmatrix}. \quad (55)$$

In the two-mode and three-mode cases, it is known [65,66] that all pure Gaussian states can be brought by LLUBOs (local linear unitary Bogoliubov transformations) to a *standard form* where matrices σ_i are proportional to the identity and matrices ε_{ij} are diagonal. In order to get such a standard form, we use the set of operators \hat{e}_j related with the \hat{c}_j by $\mathbf{e} = \mathcal{R} \mathbf{c}$, where \mathcal{R} has been defined in (37). Using the results of Sec. IV B and applying Eq. (48), the covariance matrix of state (38) in mode e is

$$\sigma_e = \mathcal{S}_{\mathcal{R}} \mathcal{S}_{\mathcal{T}} \mathcal{S}_{\mathcal{T}}^{\dagger} \mathcal{S}_{\mathcal{R}}^{\dagger}. \quad (56)$$

Note that $\mathcal{S}_{\mathcal{R}}$ is a rotation operator. Indeed, one can easily show that $\mathcal{S}_{\mathcal{R}} = \operatorname{diag}\{R(\varphi_{02}), R(\varphi_{12}), R(-\varphi_{22})\}$, where

$$R(\phi) = \begin{pmatrix} \cos \phi & \sin \phi \\ -\sin \phi & \cos \phi \end{pmatrix}. \quad (57)$$

Then, one proves that the covariance matrix σ_e defined by (56) is in the standard form, with σ_i given by (54) and

$$\varepsilon_{ij} = 2 |\langle \hat{c}_i \hat{c}_j^{\dagger} \rangle| \mathbb{1}_2 = 2 v_{i2} v_{j2} \mathbb{1}_2, \quad i, j = 0, 1, \quad (58)$$

$$\varepsilon_{i2} = 2 |\langle \hat{c}_i \hat{c}_2 \rangle| \sigma_z = 2 v_{i2} v_{22} \sigma_z, \quad i = 0, 1,$$

where σ_z is the third Pauli matrix. Following the notation introduced in Sec. IV C for thermal states, we define real parameters $r_i \geq 0$ and $a_i \geq 1$ such that

$$\bar{n}_i = \langle \hat{c}_i^{\dagger} \hat{c}_i \rangle = \sinh^2(r_i) = \frac{a_i - 1}{2}. \quad (59)$$

To be completely accurate, we recall that the operators $\hat{c}_i = \hat{c}_i(\omega)$ all depend on the energy $\hbar \omega$ of the elementary excitations. Therefore, the above defined quantities a_i also depend on ω . They can be written explicitly as functions of the coefficients of the scattering matrix:

$$a_0(\omega) = 1 + 2 |S_{02}(\omega)|^2,$$

$$a_1(\omega) = 1 + 2 |S_{12}(\omega)|^2,$$

$$a_2(\omega) = -1 + 2 |S_{22}(\omega)|^2 \quad (60)$$

(see Appendix B). From the solution of the scattering problem in the waterfall configuration, we calculate the scattering amplitudes $S_{ij}(\omega)$ following [15]. This makes it possible to compute the three local mixednesses a_0 , a_1 , and a_2 as functions of the frequency. In particular we have

$$a_0(\omega) + a_1(\omega) = a_2(\omega) + 1, \quad (61)$$

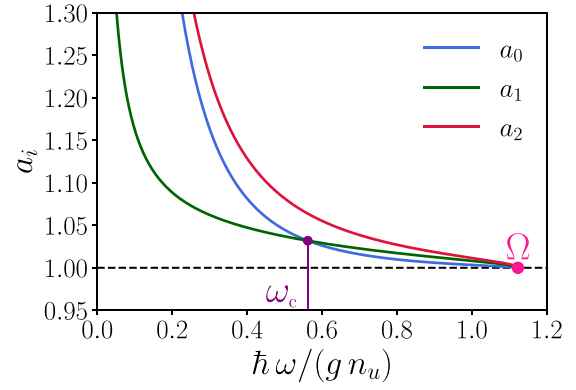


FIG. 3. Local mixedness $a_i(\omega)$ [see Eqs. (60)] for each mode 0, 1, and 2 as functions of the dimensionless quantity $\hbar \omega / (g n_u)$, for a waterfall configuration with $m_u = 0.59$. The frequency ω_c indicates the turning point above which a_0 becomes lower than a_1 . The upper-bound frequency Ω corresponds to the vanishing of the mode 2 [see Eq. (9)].

which stems from relations (60) and (11). Figure 3 shows the associated curves. Here, these coefficients are computed for a waterfall configuration with downstream Mach number $m_d = 2.9$, which is the one for which the experiment of [10] has been realized. In our case, this corresponds to an upstream Mach number $m_u = 0.59$.

We can identify two regimes in Fig. 3: below a frequency denoted ω_c the lowest of the three parameters is a_1 ; above this frequency, the minimum value becomes a_0 . The value of this frequency is determined numerically and is equal to $\omega_c \approx 0.56 g n_u / \hbar$ for $m_u = 0.59$. We observe that the ratio ω_c / Ω (where Ω is the frequency (9) at which mode 2 vanishes and also depends on m_u) decreases when m_u decreases. The local mixednesses a_0 , a_1 and a_2 go to 1 when $\omega \rightarrow \Omega$, which means that the populations of all modes vanish.

Using Eqs. (60) one may rewrite expressions (54) and (58) in terms of the a_i as

$$\sigma_i = a_i \mathbb{1}_2, \quad i = 0, 1, 2,$$

$$\varepsilon_{ij} = \sqrt{a_i - 1} \sqrt{a_j - 1} \mathbb{1}_2, \quad i, j = 0, 1 \quad (i \neq j),$$

$$\varepsilon_{i2} = \sqrt{a_i - 1} \sqrt{a_2 + 1} \sigma_z, \quad i = 0, 1. \quad (62)$$

The 6×6 covariance matrix defined by Eqs. (41) and (62) is no longer the covariance matrix associated with modes \mathbf{c} , but the covariance matrix associated with modes \mathbf{e} defined by Eq. (36); since \mathbf{c} and \mathbf{e} differ only by phases, the entanglement properties are the same. When considering entanglement in Sec. V we will therefore use the standard form (62). In the case of a pure three-mode Gaussian state, the three local symplectic invariants a_i fully determine the entanglement content of any given bipartition [66]. As we shall see in Sec. V, the blocks of the covariance matrix σ in the form of expressions (62) are the key ingredients to compute the amount of bipartite and tripartite entanglement.

As mentioned in Sec. IV B, σ_i is the covariance matrix of the reduced state $\rho^{(i)}$ of mode i . Given its diagonal form, one gets from Sec. IV C that $\rho^{(i)}$ is a thermal state with local mixedness a_i . It can also be considered as a reduced state of a two-mode squeezed state with squeezing parameter r_i

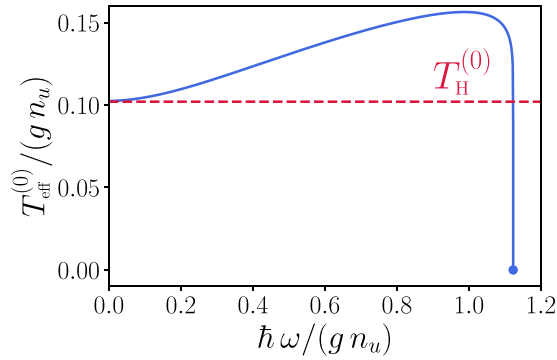


FIG. 4. Blue continuous curve: Effective temperature $T_{\text{eff}}^{(0)}$ defined in Eq. (64) plotted as a function of the frequency ω for a waterfall configuration with $m_u = 0.59$. The dashed red line is the Hawking temperature $T_H^{(0)}$ given by (65).

[56,67,68]. In this respect, the study of the reduced state $\rho^{(0)}$ is of particular interest in the context of analog gravity, since the number of emitted quanta in the 0 mode gives access to the Hawking radiation spectrum. In the context of general relativity, this spectrum is exactly Planckian⁴ [48,49], with a temperature which is called the ‘‘Hawking temperature.’’ For the analog model we consider, dispersive effects significantly affect this result. Indeed, if one defines an effective temperature $T_{\text{eff}}^{(0)}$ such that

$$\bar{n}_0(\omega) = \frac{1}{\exp(\hbar\omega/T_{\text{eff}}^{(0)}) - 1}, \quad (63)$$

one finds from (51), (59), and (60) that $T_{\text{eff}}^{(0)}$ is frequency-dependent:

$$T_{\text{eff}}^{(0)}(\omega) = \frac{\hbar\omega}{2 \ln\{\coth[r_0(\omega)]\}} = \frac{\hbar\omega}{\ln[1 + |S_{02}(\omega)|^{-2}]}. \quad (64)$$

Figure 4 represents $T_{\text{eff}}^{(0)}(\omega)$ for a waterfall configuration with $m_u = 0.59$. We note here that the same type of results has been obtained numerically in [13]. In the long wavelength limit the effective temperature tends to a constant analog Hawking temperature $T_H^{(0)} = \lim_{\omega \rightarrow 0} T_{\text{eff}}^{(0)}(\omega)$. Based on the expansion (C1) and on the formula (C2) one gets

$$\frac{T_H^{(0)}}{gn_u} = 2 \frac{m_u(1 - m_u)^{\frac{3}{2}}(1 + m_u^2)^{\frac{3}{2}}}{(1 + m_u)^{\frac{1}{2}}(1 + m_u + m_u^2)^2}. \quad (65)$$

This long wavelength determination of the analog Hawking temperature is physically sound, since the reduced density matrix of mode 0 is indeed thermal (in the sense of Sec. IV C). However, it has the drawback of depending of the mode considered (here the outgoing Hawking mode). The reduced density matrices of modes 1 and 2 are also thermal, and on the basis of the present reasoning there is another, different Hawking temperature for the Companion (which could be denoted as $T_H^{(1)}$), and still another one for the Partner ($T_H^{(2)}$). In Sec. V C we use a different reasoning and argue that $T_H^{(2)}$ gives

a more satisfactory definition of the Hawking temperature, valid for the whole system.

V. ENTANGLEMENT IN THREE-MODE GAUSSIAN STATES

Entanglement detection and characterization has attracted a great deal of effort in the past two decades, as it has been identified as a key resource for quantum information processing [69]. A quantum state is entangled if it is not separable, i.e., if it cannot be written as a convex sum of product states [70]. One of the simplest necessary separability criteria is given by the positivity of the partial transpose (PPT), first proposed for discrete variables [71,72] and extended to the continuous case in [73]. A wealth of entanglement measures were discussed in the literature, for both discrete and continuous variables. For bipartite pure states, quantitative measures of entanglement include the entanglement entropy (which can be shown to be unique if some additional natural requirements are imposed) [74], or the concurrence [75]. In the mixed state case, it is possible to construct ‘‘good’’ entanglement measures in many different ways, which are inequivalent in the sense that they lead to different orderings of entangled states [69]. A possible way is to extend measures for pure states via a convex roof construction: entanglement of a mixed state is then defined by a minimization over all its possible pure state decompositions. For instance, entanglement entropy generalizes for mixed states to the entanglement of formation [76].

A striking difference between classical correlations and quantum entanglement is that the latter is monogamous [77,78]. This means that a particle which is maximally entangled with a Partner cannot be entangled with a third party, or in other words that any amount of entanglement shared with a particle limits the entanglement that can be shared with another particle. In the case of three qubits, this limitation to bipartite entanglement was expressed in [79] through an inequality that must be satisfied by an entanglement measure called the concurrence, or more precisely by its square, the tangle. This monogamy inequality was later generalized to an arbitrary number of qubits [80], to three-qutrit systems [81] and to continuous variables [82,83], as we now discuss.

In the case of continuous variables, to which the situation of black hole analogs pertains, Gaussian states are the most natural objects with which one is led to deal. From a qualitative point of view, entanglement can be detected by the PPT criterion, which is a necessary and sufficient separability condition for $1 \times N$ -mode Gaussian states [73]; the three-mode case, which is relevant to our situation, was investigated in [84], and will be considered in Sec. V A. From a quantitative point of view, entanglement can be measured by the logarithmic negativity, which quantifies by which amount the PPT criterion is violated [85].⁵ In [82] it was proposed to construct

⁵For continuous variables it is generally highly difficult to make use of the convex roof construction, both analytically and numerically, as the optimization has to take place over all pure state decompositions. To circumvent this issue, Gaussian entanglement of formation was defined in [86], restricting the convex roof construction to Gaussian pure state decompositions. This quantity provides an upper bound for

⁴We do not consider here possible effects of a gray-body factor. These will be accounted for in Sec. V C.

a specific measure of entanglement, the *contangle* (continuous tangle), defined as the convex roof extension of the square of the logarithmic negativity. In that manner, the monogamy inequality expressed by this measure also holds for Gaussian states. The amount by which both sides of the monogamy inequality differ provides an estimate for multipartite entanglement. In the present section, we will make use of this measure of entanglement to quantify tripartite entanglement in our analog black hole system. For consistency purposes we shall also quantify bipartite entanglement using the contangle.

In the domain of analog gravity, previous approaches have already considered quantitative measures of entanglement. Using a relation [89] between entanglement entropy and cumulants of the full counting statistics, Ref. [28] expresses the (long wave-length limit of the) entanglement entropy of a pure two-mode Gaussian state in terms of number fluctuations in a given region. Although this approach bears some similarity with the one we discuss at the end of Sec. VI C we cannot directly compare it with ours because for our three-mode Gaussian state the reduced two-body state is mixed. Reference [30] studies the dynamical Casimir effect in a BEC and quantifies the nonseparability after a quench by means of the entanglement of formation, which takes an exact analytic expression for symmetric two-mode Gaussian states [90]. Although we cannot directly compute this quantity,⁶ the spirit of our approach is similar to theirs and to the one of Refs. [29,31], which use the symplectic spectrum to construct quantitative measures of entanglement in the context of ion rings and nonlinear optics analog, respectively.

A. Bipartite entanglement

The criterion usually used to detect entanglement in bipartite systems is the Peres-Horodecki (or PPT) criterion [71,72]. It is a necessary and sufficient separability condition for bipartite $1 \times (N - 1)$ -mode Gaussian states [73]. This corresponds to all possible bipartitions occurring in three-mode states: indeed, we will have to consider either bipartitions $i|jk$ or, after tracing out mode k , bipartitions $i|j$. This criterion states that a state ρ is separable if and only if its partial transpose ρ^{PT} with respect to the first mode (mode i in the above notation) is positive. Partial transposition of an N -mode Gaussian state is equivalent to mirror reflection in phase space for the Wigner function [73]. The covariance matrix of ρ^{PT} is given by

$$\sigma^{\text{PT}} = \Lambda \sigma \Lambda, \quad \text{with} \quad \Lambda = \sigma_z \oplus \mathbb{1}_{2N-2}. \quad (66)$$

According to the criteria (49), the necessary and sufficient separability criterion $\rho^{\text{PT}} \geq 0$ is equivalent to

$$v_j^{\text{PT}} \geq 1, \quad j = 1, \dots, N, \quad (67)$$

where v_j^{PT} are the symplectic eigenvalues of σ^{PT} .

In our case $N = 3$. Let us investigate bipartite entanglement of two-mode states obtained by tracing out the third one.

the entanglement of formation and is more amenable to calculations. In [87,88] it was shown that Gaussian entanglement of formation and entanglement measured by negativity are inequivalent measures.

⁶In our case the reduced state of modes i and j is nonsymmetric, since in general $a_i \neq a_j$ (i and j in $\{0, 1, 2\}$).

As discussed in Sec. IV B, the covariance matrix associated with the two-mode state i, j obtained by tracing out mode k is σ_{ij} given by (45). Its symplectic eigenvalues v_{\pm} are given by

$$2v_{\pm}^2 = \Delta_{ij} \pm \sqrt{\Delta_{ij}^2 - 4 \det \sigma_{ij}}, \quad (68)$$

with $\Delta_{ij} = \det \sigma_i + \det \sigma_j + 2 \det \varepsilon_{ij}$ [91]. The symplectic eigenvalues v_{\pm}^{PT} of σ_{ij}^{PT} associated with the partial transpose are given by

$$2(v_{\pm}^{\text{PT}})^2 = \Delta_{ij}^{\text{PT}} \pm \sqrt{(\Delta_{ij}^{\text{PT}})^2 - 4 \det \sigma_{ij}}, \quad (69)$$

with $\Delta_{ij}^{\text{PT}} = \det \sigma_i + \det \sigma_j - 2 \det \varepsilon_{ij}$. For a two-mode state, the PPT criterion is in fact equivalent to condition $v_{-}^{\text{PT}} \geq 1$ only, since v_{+}^{PT} is always larger than 1 [64].

From (62) one readily derives the expressions for v_{-}^{PT} in our case. Note that, again, since the local mixednesses appearing in Eq. (62) depend on the frequency ω , the lowest symplectic eigenvalue v_{-}^{PT} also depends on ω . By using the fact that $a_i \geq 1$, $i = 0, 1, 2$ and the relation (61), one can prove easily that $v_{-}^{\text{PT}} \geq 1$ for the bipartition $0|1$, independently of the frequency. Therefore, the reduced state of modes $0|1$ is always separable: the Hawking quantum and the Companion are not entangled. On the other hand, the eigenvalues v_{-}^{PT} of the reduced covariance matrices σ_{02}^{PT} and σ_{12}^{PT} are lower than 1, which implies that the reduced state of modes $0|2$ (Hawking-Partner) and $1|2$ (Companion-Partner) is entangled for all frequencies ω ; see, for instance, Fig. 9(a), where the blue curve represents $1 - v_{-}^{\text{PT}}(\omega)$ computed for the reduced state of modes $0|2$.

The same results are obtained with the ‘‘Cauchy-Schwarz criterion’’ (see, e.g., Ref. [92]), which has been often used in the context of analog gravity [20–22,24,26,27]. According to this criterion modes i and j are entangled if the following inequality is verified:

$$\begin{aligned} |\langle \hat{c}_i \hat{c}_j \rangle|^2 &> \langle \hat{c}_i^\dagger \hat{c}_i \rangle \langle \hat{c}_j^\dagger \hat{c}_j \rangle, \quad \text{for } i \in \{0, 1\}, j = 2, \\ \langle \hat{c}_i \hat{c}_j^\dagger \rangle|^2 &> \langle \hat{c}_i^\dagger \hat{c}_i \rangle \langle \hat{c}_j^\dagger \hat{c}_j \rangle, \quad \text{for } i \neq j \in \{0, 1\}. \end{aligned} \quad (70)$$

Using Eqs. (58) and (62), one finds $\langle \hat{c}_i^\dagger \hat{c}_i \rangle \langle \hat{c}_j^\dagger \hat{c}_j \rangle = \sinh^2 r_i \sinh^2 r_j$, $|\langle \hat{c}_i \hat{c}_2 \rangle|^2 = \sinh^2 r_i \cosh^2 r_2$ ($i \neq 2$) and $|\langle \hat{c}_0 \hat{c}_1^\dagger \rangle|^2 = \sinh^2 r_0 \sinh^2 r_1$. Therefore, when considering the bipartition $0|1$, one concludes immediately that the second inequality of (70) is never true; one has instead the equality $|\langle \hat{c}_0 \hat{c}_1^\dagger \rangle|^2 = \langle \hat{c}_0^\dagger \hat{c}_0 \rangle \langle \hat{c}_1^\dagger \hat{c}_1 \rangle$ for all frequencies ω . Therefore, the reduced state $0|1$ is separable. For bipartitions $0|2$ and $1|2$, since $\tanh(r_2) < 1$ (with $r_2 > 0$, finite), the first inequality of (70) is always true. The criterion of violation of the Cauchy-Schwarz inequality thus leads to the same conclusion as the PPT criterion for the reduced states $0|2$ and $1|2$: these states are always entangled.

However, the Cauchy-Schwarz criterion does not give any clue about the amount of entanglement shared by each bipartition. Indeed, as will be discussed in Sec. VI C, in an experimental setup for which the temperature of the system cannot be exactly equal to zero, a stronger violation of the Cauchy-Schwarz inequality does not necessarily imply a greater amount of entanglement.

B. Tripartite entanglement

1. Monogamy inequality

Monogamy is a fundamental property of entanglement correlations. It can be described by monogamy inequalities, which in the case of a tripartite system with subsystems labeled by (i, j, k) takes the form

$$E^{(ijk)} - E^{(ij)} - E^{(ik)} \geq 0, \tag{71}$$

where $E^{(A|B)}$ is a proper measure of bipartite entanglement between subsystems A and B [nonnegative on separable states and monotonic under (G)LOCC]. This inequality expresses the fact that the total amount of entanglement that can be shared between i and j and between i and k is upper bounded by the amount of entanglement between i and jk taken as a whole. The left-hand side of inequality (71) provides a quantifier of genuine tripartite entanglement.

Not all entanglement measures satisfy a monogamy inequality. However, it is possible to find and construct proper measures of entanglement which satisfy these relations, both in the qubit case and in the continuous-variable case. In the case of qubits, the monogamy inequality holds for entanglement measured by the square of the concurrence. For Gaussian states a measure satisfying (71) was constructed in [82]; it is called the contangle E_τ and it corresponds to the squared logarithmic negativity. For an arbitrary pure state $\rho = |\psi\rangle\langle\psi|$ with covariance matrix σ^p (p stands for pure), it is defined as

$$E_\tau(\sigma^p) = (\ln \|\rho^{\text{PT}}\|_1)^2, \tag{72}$$

where $\|\hat{O}\|_1 = \text{tr}\sqrt{\hat{O}^\dagger\hat{O}}$ is the trace norm.

The state considered in our case is a pure three-mode Gaussian state; thus, any bipartition $i|jk$ is a pure state, for which the term $E^{(ijk)}$ in (71) can be computed easily (see Sec. VB 2 below). On the contrary, the two other terms of (71) correspond to reduced two-mode states, which are mixed. The squared logarithmic negativity can be extended to mixed states by taking the infimum over all convex decompositions of ρ in terms of pure states $\{|\psi_i\rangle\}$. In order to get a quantity more amenable to computations, the Gaussian contangle G_τ was defined by restricting this convex-roof construction to decompositions over pure Gaussian states only. The Gaussian contangle can be expressed as

$$G_\tau(\sigma) = \inf_{\sigma^p \leq \sigma} E_\tau(\sigma^p), \tag{73}$$

where the notation $\sigma^p \leq \sigma$ means that the matrix $\sigma - \sigma^p$ is positive semidefinite. It is an upper bound to the true contangle E_τ obtained from unrestricted pure-state decompositions, but for pure states both coincide.

For three qubits the residual tangle (or three-way tangle) $E^{(ijk)} - E^{(ij)} - E^{(ik)}$ provides a measure of tripartite entanglement. It has an explicit expression [79], which is symmetric in the three qubits. The corresponding quantity in the continuous case is no longer symmetric in the three modes. One can however define a permutation-invariant quantity by minimizing it over all permutations of the modes [82]. This measure of tripartite entanglement shared among Gaussian modes was

called residual contangle [66]. Its explicit expression reads

$$G_\tau^{\text{res}} = G_\tau^{(ijk)} = \min_{i,j,k} (G_\tau^{(ijk)} - G_\tau^{(ij)} - G_\tau^{(ik)}). \tag{74}$$

2. Pure-state contangle

Let us consider first a bipartition $i|jk$. For a pure state, the Gaussian contangle $G_\tau^{(ijk)}$ coincides with the true contangle $E_\tau^{(ijk)}$. In general, for a multimode Gaussian state $|\psi\rangle$ with covariance matrix σ^p and generic bipartition $i_1 \dots i_{N-1}|i_N$ ($N = 3$ in our case), the squared logarithmic negativity can be written as [82]

$$E_\tau^{i_1 \dots i_{N-1}|i_N}(\sigma^p) = \left(\sum_{j: v_j^{\text{PT}} < 1} \ln v_j^{\text{PT}} \right)^2, \tag{75}$$

where v_j^{PT} are the symplectic eigenvalues associated with the partial transpose state ρ^{PT} .

It is actually possible to write Eq. (75) in terms of the local mixedness a_{i_N} associated with mode i_N . Indeed, for any covariance matrix σ associated with a pure multimode Gaussian state and generic bipartition $i_1 \dots i_{N-1}|i_N$, there exists a local symplectic transformation \mathcal{S} such that [93]

$$\mathcal{S} \sigma \mathcal{S}^T = \mathbb{1}_{2(N-2)} \oplus \sigma_{\text{sq}}, \tag{76}$$

where σ_{sq} is the covariance matrix of a two-mode squeezed state and reads

$$\begin{pmatrix} a_{i_N} & 0 & \sqrt{a_{i_N}^2 - 1} & 0 \\ 0 & a_{i_N} & 0 & -\sqrt{a_{i_N}^2 - 1} \\ \sqrt{a_{i_N}^2 - 1} & 0 & a_{i_N} & 0 \\ 0 & -\sqrt{a_{i_N}^2 - 1} & 0 & a_{i_N} \end{pmatrix}. \tag{77}$$

In the case of a tripartite system ($N = 3$), a direct proof of Eqs. (76) and (77), as well as explicit expressions of the symplectic matrix \mathcal{S} for each bipartition, $12|0$ and $02|1$ and $01|2$, can be found in Appendix D.

The symplectic eigenvalues of σ^{PT} (corresponding to taking the partial transpose with respect to mode i_N) are then readily obtained from (69), using the form (77); the symplectic eigenvalue 1 has degeneracy $2(N - 2)$, while the ones associated with (77) are $e^{\pm 2r_{i_N}}$, with twofold degeneracy. They can be related to the local mixedness a_{i_N} through the relations $a_{i_N} = \cosh(2r_{i_N})$. Equation (75) then gives

$$E_\tau^{i_1 \dots i_{N-1}|i_N}(\sigma^p) = \text{arsinh}^2(\sqrt{a_{i_N}^2 - 1}) = 4r_{i_N}^2, \tag{78}$$

which only depends on the local mixedness of mode i_N and has a simple expression in terms of r_{i_N} . We will perform explicit calculations for our system in the next section.

3. Residual contangle

Equation (78) provides an explicit expression for the first term $G_\tau^{(ijk)}$ in (74). For a pure three-mode Gaussian state, an explicit expression of $G_\tau^{(ij)}$ and $G_\tau^{(ik)}$ can also be obtained. Indeed, in this specific case, any reduced two-mode state saturates the uncertainty relation (44) and belongs to a class of states called Gaussian least entangled mixed states (GLEMS).

For GLEMS, one has [66]

$$G_{\tau}^{(ij)} = \operatorname{arsinh}^2[\sqrt{m^{\text{GLEMS}}(a_i, a_j, a_k) - 1}], \quad (79)$$

where m^{GLEMS} can be explicitly calculated as a function of the three local mixednesses, as shown in Appendix E. In our case [see Eqs. (E24)–(E27)], we obtain

$$\begin{aligned} G_{\tau}^{(01)} &= 0, \\ G_{\tau}^{(j2)} &= \operatorname{arsinh}^2\left[\frac{2}{1+a_k}\sqrt{(a_2+1)(a_j-1)}\right] \\ &= \operatorname{arsinh}^2\left(\frac{2|\langle\hat{c}_j\hat{c}_2\rangle|}{1+\langle\hat{c}_k^\dagger\hat{c}_k\rangle}\right), \end{aligned} \quad (80)$$

with $j = 0, k = 1$ or $j = 1, k = 0$. Let us now introduce the quantity

$$G_{\tau}^{\text{res}(i)} = G_{\tau}^{(ijkl)} - G_{\tau}^{(ij)} - G_{\tau}^{(ik)}, \quad (81)$$

such that the residual contangle is given by

$$G_{\tau}^{\text{res}} = \min_{i \in \{0,1,2\}} [G_{\tau}^{\text{res}(i)}]. \quad (82)$$

Using (78) and (80), Eq. (81) yields

$$\begin{aligned} G_{\tau}^{\text{res}(0)} &= \operatorname{arsinh}^2(\sqrt{a_0^2 - 1}) \\ &\quad - \operatorname{arsinh}^2\left[\frac{2}{1+a_1}\sqrt{(a_2+1)(a_0-1)}\right], \end{aligned} \quad (83)$$

$$\begin{aligned} G_{\tau}^{\text{res}(1)} &= \operatorname{arsinh}^2(\sqrt{a_1^2 - 1}) \\ &\quad - \operatorname{arsinh}^2\left[\frac{2}{1+a_0}\sqrt{(a_2+1)(a_1-1)}\right], \end{aligned} \quad (84)$$

and

$$\begin{aligned} G_{\tau}^{\text{res}(2)} &= \operatorname{arsinh}^2(\sqrt{a_2^2 - 1}) \\ &\quad - \operatorname{arsinh}^2\left[\frac{2}{1+a_1}\sqrt{(a_2+1)(a_0-1)}\right] \\ &\quad - \operatorname{arsinh}^2\left[\frac{2}{1+a_0}\sqrt{(a_2+1)(a_1-1)}\right]. \end{aligned} \quad (85)$$

The residual contangle only depends on the three local mixednesses a_0, a_1 and a_2 (this is no longer true at finite temperature; see Sec. VIB and Appendix B). The minimum over all possible permutations of i, j , and k in Eq. (82) can be obtained by choosing as reference mode i the one with smallest local mixedness [66].

We can then compute the residual Gaussian contangle for our three-mode Gaussian state using the expression of the a_i 's given in (60). The results for $m_u = 0.59$ are shown⁷ in Fig. 5. Tripartite entanglement naturally emerges from quantum fluctuations around a sonic horizon and diverges when the energy goes to zero. This divergence always comes from the first term in Eqs. (83), (84), and (85). Indeed, this term diverges as $\ln^2 \omega$ (see discussion in Sec. VB 4). On the other hand, it may be proven that $G_{\tau}^{(j2)}$ given by expressions (80)

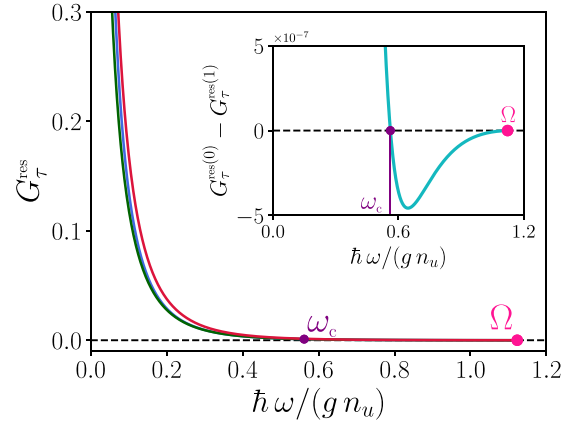


FIG. 5. Residual contangles $G_{\tau}^{\text{res}(0)}$ (blue), $G_{\tau}^{\text{res}(1)}$ (green), $G_{\tau}^{\text{res}(2)}$ (red). The upper-bound frequency Ω corresponds to the vanishing of the mode 2. The frequency ω_c is the value above which a_0 becomes lower than a_1 (see Fig. 3) and coincides with the point above which $G_{\tau}^{\text{res}(0)} < G_{\tau}^{\text{res}(1)}$. The inset displays the difference $G_{\tau}^{\text{res}(0)} - G_{\tau}^{\text{res}(1)}$ (cyan).

for $j = 0, 1$ is bounded at zero energy for any $m_u < 1$. Indeed, for $j = 0, k = 1$ or $j = 1, k = 0$,

$$G_{\tau}^{(j2)} \underset{\omega \rightarrow 0}{=} \operatorname{arsinh}^2\left(\frac{2|F_{22}F_{j2}|}{|F_{k2}|^2}\right), \quad (86)$$

where the explicit expressions of the constant coefficients $|F_{i2}|^2$, $i \in \{0, 1, 2\}$ are given in Appendix C. It means in particular that the entanglement of bipartitions $j|2$, $j \in \{0, 1\}$ remains finite at zero energy, while the tripartite entanglement becomes infinite. Then, for higher frequencies, the residual contangle decreases rapidly to zero and vanishes at the upper-bound frequency Ω .

Moreover, we show in the inset of Fig. 5 (cyan curve) that while at low frequency $G_{\tau}^{\text{res}(1)} < G_{\tau}^{\text{res}(0)}$ the situation is reversed for $\omega > \omega_c$, i.e., when $a_0 < a_1$ (the difference is anyway quite small). We note that this result may be different for Mach numbers different from the value $m_u = 0.59$ we consider here. In particular, based on the estimate (87) below, one can show that, when $m_u < 0.17$, at low frequency $G_{\tau}^{\text{res}(0)}$ becomes the contribution which minimizes (82).

4. Experimental perspectives

The waterfall model we use has proven to provide a fairly good description of the experimental setting [16]. In this section we use the relevance of our model to assess what is the best choice of parameters for an experimental measure of tripartite entanglement. Figure 6 displays the amount of genuine tripartite entanglement G_{τ}^{res} expected in our 1D analog black hole as a function of frequency (horizontal axis) and upstream Mach number m_u (vertical axis). For most cases, as proved by this two-dimensional graph, the entanglement is indeed shared among the Hawking, the Partner, and the Companion quanta. Therefore, the Companion plays an important role in the distribution of entanglement within the emitted quanta.

From Fig. 6 one sees that the amount of tripartite entanglement is maximal for $m_u = 0.14$, in the sense that the integral of $G_{\tau}^{\text{res}}(\omega)$ over all frequencies is maximal for this value of

⁷These results have been previously presented in [94].

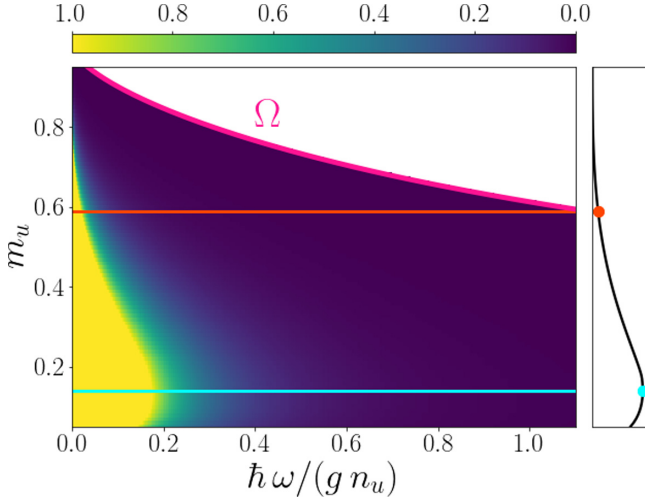


FIG. 6. Measure of tripartite entanglement G_τ^{res} as a function of the (dimensionless) energy $\hbar\omega/(gn_u)$ and of the upstream Mach number $m_u \in [0.05, 0.95]$ defined in Eq. (7). The pink curve corresponds to the upper bound frequency Ω (9). For a fixed value m_u mode 2 exists only for a frequency ω lower than $\Omega(m_u)$. Beyond this value the tripartite system $\{0, 1, 2\}$ no longer exists; this is the reason why the corresponding area is left blank. The horizontal red line corresponds to the value $m_u \simeq 0.59$, corresponding to $m_d = 2.9$ as realized in the experiment of [10]. The right plot shows the integral $\int G_\tau^{\text{res}} d\omega$ over frequencies $\omega \in [0, \Omega]$ for each value of m_u . The red dot pinpoints the numerical estimate of the integral for the specific value $m_u \simeq 0.59$, while the blue dot locates the maximum of the black curve reached for $m_u = 0.14$. The light blue horizontal line on the left graph corresponds to this value.

upstream Mach number. This specific value of m_u is indicated by the light blue horizontal cut on the graph. It has been determined by numerical integration of the residual contangle (82). One can also obtain an analytic estimate of this value of m_u , as we now explain. From the low-frequency behavior (C1) of the components of the S -matrix involved [through Eq. (60)] in (83), (84), and (85), one obtains the following expression for the low-frequency residual contangle:

$$G_\tau^{\text{res}}(\omega) \simeq \min_{\omega \rightarrow 0} \min_{i \in \{0,1,2\}} \left[\ln^2 \left(\frac{4|F_{i2}|^2}{\hbar\omega/gn_u} \right) \right]. \quad (87)$$

The value of m_u for which $G_\tau^{\text{res}}(\omega)$ in (87) is the largest is thus simply the value for which the minimum of $|F_{02}|$, $|F_{12}|$ and $|F_{22}|$ reaches a maximum. From the analytic expressions (C2), (C3), and (C4) of these coefficients one obtains $m_u = 0.17$. Although this value has been determined using a different criterion than the numerical estimate $m_u = 0.14$ plotted in Fig. 6 (the former is based on the low ω behavior and the latter on the integrated signal) the fact that both are quite close confirms their relevance.

C. Entanglement localization

The tripartite entanglement of our system can be concentrated in a two-mode state by applying a local linear Bogoliubov transformation [95,96]; this is called entanglement localization. This transformation can be obtained by means of the symplectic transformation S given by (76). To

the mapping (76) between σ and its three-mode localized version $\mathbb{1}_2 \oplus \sigma_{\text{sq}}$ one can associate the Bogoliubov transformation $\mathcal{T} = U^\dagger S U$ [see Eq. (48)]. The modes \mathbf{e} defined in (35) (which coincide with the modes \mathbf{c} up to a phase) are mapped through this Bogoliubov transformation to new modes \mathbf{f} . The Bogoliubov transformation from \mathbf{e} to $\mathbf{f} = (\hat{f}_0, \hat{f}_1, \hat{f}_2, \hat{f}_0^\dagger, \hat{f}_1^\dagger, \hat{f}_2^\dagger)^\top$ is denoted $\mathcal{T}_{\mathbf{e} \rightarrow \mathbf{f}}$, and thus we have $\mathbf{f} = \mathcal{T}_{\mathbf{e} \rightarrow \mathbf{f}} \mathbf{e}$. This transformation is such that the tripartite entanglement $e_0|e_1|e_2$ gets completely localized in a two-mode squeezed state.

Let us consider in turn the different cases. If we consider bipartitions $ij|k = 12|0$ and $02|1$ for modes \mathbf{e} , as derived explicitly in Appendix D [see in particular Eq. (D22)], the new operators \hat{f}_i and \hat{f}_2 correspond to a mixing of annihilation and creation operators \hat{e}_i, \hat{e}_2 and $\hat{e}_i^\dagger, \hat{e}_2^\dagger$. In the case of bipartition $ij|k = 01|2$ of modes \mathbf{e} , entanglement can also be localized but without mixing annihilation and creation operators. The corresponding Bogoliubov transformation is given by Eq. (D25) and corresponds to a change of basis from $\{\hat{e}_0, \hat{e}_1, \hat{e}_2\}$ to $\{\hat{f}_0, \hat{f}_1, \hat{f}_2\}$ given by

$$\hat{f}_0 = -\sin\theta \hat{e}_0 + \cos\theta \hat{e}_1, \quad (88a)$$

$$\hat{f}_1 = \cos\theta \hat{e}_0 + \sin\theta \hat{e}_1, \quad (88b)$$

$$\hat{f}_2 = \hat{e}_2, \quad (88c)$$

where (see Appendix D 4)

$$\cos\theta = \frac{\sinh r_0}{\sinh r_2} \quad \text{and} \quad \sin\theta = \frac{\sinh r_1}{\sinh r_2}. \quad (89)$$

The transformation leading to entanglement localization is thus particularly simple in the case of bipartition $01|2$. Inserting (88) into Eq. (38) leads to

$$|0\rangle_b = T |0\rangle_f, \quad \text{where} \quad T = \exp[r_2(\hat{f}_1^\dagger \hat{f}_2^\dagger - \hat{f}_1 \hat{f}_2)]. \quad (90)$$

The operator T is a two-mode squeezing operator [compare with the generic form (22)] between \hat{f}_1 and \hat{f}_2 , with squeezing parameter $r_2(\omega)$ defined in (59). Note that the modes \hat{e}_0 and \hat{e}_1 that are combined in (88a) and (88b) are those of positive norm; this leads to a squeezed state between the only mode of negative norm (mode 2) and a combination of the modes of positive norm (modes 0 and 1), exactly as occurs in the gravitational case [97].

To summarize, the tripartite entanglement in our system can be unitarily localized by linearly combining modes \hat{e}_0 and \hat{e}_1 as in Eqs. (88a) and (88b) to obtain mode \hat{f}_1 , which forms a two-mode squeezed state with $\hat{f}_2 = \hat{e}_2$. Besides, using the definition (89) and noticing that $\langle \hat{e}_1^\dagger \hat{e}_0 \rangle = |\langle \hat{e}_1^\dagger \hat{e}_0 \rangle|$ one obtains

$$\begin{aligned} \langle \hat{f}_0^\dagger \hat{f}_0 \rangle &= \sin^2\theta \langle \hat{e}_0^\dagger \hat{e}_0 \rangle + \cos^2\theta \langle \hat{e}_1^\dagger \hat{e}_1 \rangle - 2\sin\theta \cos\theta |\langle \hat{e}_1^\dagger \hat{e}_0 \rangle| \\ &= (\sin\theta |S_{02}| - \cos\theta |S_{12}|)^2 = 0. \end{aligned} \quad (91)$$

This means that mode f_0 is not occupied. This comes as no surprise since the corresponding local mixedness is equal to 1 in the transformed covariance matrix given by (76), which entails from (59) that the mean particle number is equal to 0. One can thus schematically describe the Bogoliubov transformation (88) operating in our analog black hole by means of the equivalent optical setup represented in Fig. 7: nondegenerate parametric down-conversion in a nonlinear crystal creates a

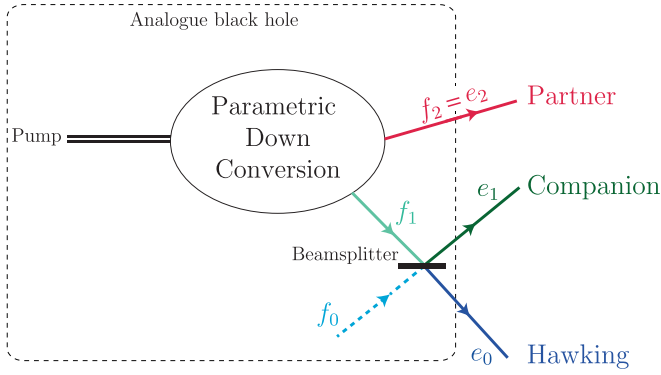


FIG. 7. Schematic representation of an optical process equivalent to the Hawking emission in the transonic BEC system we consider. Entanglement is localized in the two-mode squeezed state $f_1|f_2$. The mode f_0 being empty is represented by a dashed line.

two-mode squeezed state.⁸ One of the modes is the Partner $\hat{f}_2 = \hat{e}_2$. The other one, \hat{f}_1 , is directed to a beamsplitter that generates the two other outgoing channels \hat{e}_1 and \hat{e}_0 which are, up to a phase, the Companion and the Hawking mode, respectively.

We note that various theoretical proposals and experimental works have addressed the issue of generating and measuring tripartite entangled states for continuous variables, based on different setups of nonlinear optical parametric oscillators [96,98–100]. The analog black hole we consider here is another such setup. It is quite peculiar in the sense that genuine tripartite entanglement is realized although two of the outgoing modes (0 and 1) are not entangled.

An interesting outcome of the present study is a redefinition of the analog Hawking temperature, associated to a so-called gray-body factor. Redoing for the f_1 and f_2 modes at the output of the parametric down conversion process the analysis done for the Hawking mode at the end of Sec. IV D, it is clear that these two modes have the same occupation number

$$\langle \hat{f}_2^\dagger \hat{f}_2 \rangle = \langle \hat{f}_1^\dagger \hat{f}_1 \rangle = \sinh^2 r_2, \quad (92)$$

and the same effective temperature

$$\begin{aligned} T_{\text{eff}}^{(2)}(\omega) &= \frac{\hbar\omega}{2 \ln\{\coth[r_2(\omega)]\}} \\ &= \frac{\hbar\omega}{\ln\left[\frac{|S_{22}(\omega)|^2}{|S_{22}(\omega)|^2 - 1}\right]}. \end{aligned} \quad (93)$$

The f_1 mode being sent to the beamsplitter is transmitted onto the Hawking mode with a transmission coefficient $\cos^2 \theta$, and indeed one can easily check that

$$\langle \hat{e}_0^\dagger \hat{e}_0 \rangle = \cos^2 \theta \langle \hat{f}_1^\dagger \hat{f}_1 \rangle. \quad (94)$$

We saw in Sec. IV D that the Hawking mode could be considered as a thermal state with temperature $T_{\text{eff}}^{(0)}(\omega)$. Equation (94) shows that it can also be considered as a thermal

⁸We note here that the relevance of a nondegenerate parametric amplifier model has already been pointed out in Ref. [25].

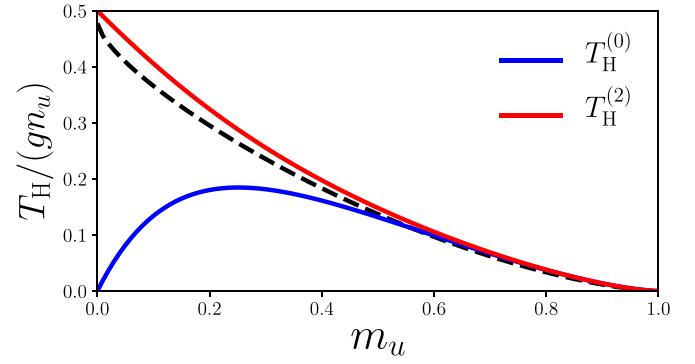


FIG. 8. Hawking temperature as a function of the upstream Mach number in the waterfall configuration. The blue solid line is the result (65), and the red solid line comes from expression (95). The dashed line is the semiclassical expectation (C8).

state of temperature $T_{\text{eff}}^{(2)}(\omega)$ affected by a gray-body factor $\Gamma(\omega) = \cos^2 \theta$. Such a factor is invoked in general relativity for explaining that the Hawking radiation is subject to an effective potential at the horizon which affects its thermal character [101]. The introduction of a gray-body term in the present analysis has the advantage to ascribe a single, global effective temperature to the analog system: $T_{\text{eff}}^{(2)}$. In this framework, the difference in population of the modes is explained by the transmission coefficients $\cos^2 \theta$ and $\sin^2 \theta$ of the beamsplitter, not by a difference in temperature. In the long wavelength limit it yields an analog Hawking radiation $T_{\text{H}}^{(2)} = \lim_{\omega \rightarrow 0} T_{\text{eff}}^{(2)}(\omega)$ which explicit expression in the waterfall configuration reads (from Appendix C)

$$T_{\text{H}}^{(2)} = \frac{1}{2} \frac{(1 - m_u^4)^{\frac{3}{2}}}{(1 + m_u + m_u^2)^2}, \quad (95)$$

and a gray-body factor

$$\Gamma_0 = \lim_{\omega \rightarrow 0} \Gamma(\omega) = \lim_{\omega \rightarrow 0} \frac{|S_{02}|^2}{|S_{22}|^2 - 1} = \frac{4m_u}{(1 + m_u)^2}. \quad (96)$$

It is satisfactory to note that the present approach yields a result for Γ_0 identical to the universal limit obtained in Refs. [102–104] by means of a different technique.

Another advantage of the present definition of the Hawking temperature over the one introduced at the end of Sec. IV D, is that $T_{\text{H}}^{(2)}$ defined in Eq. (95) is in good agreement with the semiclassical result (C8). This is to be contrasted with $T_{\text{H}}^{(0)}$, defined in Eq. (65) by studying the thermal character of the reduced mode 0 state. The discrepancy between the two behaviors is illustrated in Fig. 8. $T_{\text{H}}^{(0)}$ has the unpleasant property of vanishing at $m_u \rightarrow 0$, although in this limit the “surface gravity” is the largest. For the model sketched in Fig. 7 instead, the disappearance of Hawking radiation when $m_u \rightarrow 0$ is due to a vanishing gray-body factor, which is physically more satisfactory. One sees also in Fig. 8 that in the limit $m_u \rightarrow 1$ all definitions of the Hawking temperature coalesce to zero: in this regime $\Gamma_0 \rightarrow 1$ hence $T_{\text{H}}^{(0)} = T_{\text{H}}^{(2)}$. Also, in this limit the density profile is smoother, the semiclassical approach is more legitimate (cf. the discussion at the end of Appendix C), and the surface gravity vanishes: the semiclassical estimate of the Hawking temperature thus vanishes as $T_{\text{H}}^{(2)}$

does. However, the behavior near $m_u = 1$ is not exactly the same: whereas $T_H^{(2)}/(gn_u) \sim \frac{4}{9}(1 - m_u)^{3/2}$ the semiclassical expression (C8) behaves as $\frac{2}{\pi\sqrt{3}}(1 - m_u)^{3/2}$. In this limit, the reasoning leading to expression (95) is not at question because, as stated above, the behavior of the traditional estimate (65) is identical to that of $T_H^{(2)}$. The discrepancy between expressions (C8) and (95) when $m_u \rightarrow 1$ rather suggests that the semiclassical evaluation leading to Unruh expression (C8) should be modified in the presence of a nonanalyticity of the potential (in the waterfall configuration we consider the second derivative is discontinuous at $x = 0$).

VI. FINITE TEMPERATURE

We previously considered the zero-temperature case, where all the averages $\langle \dots \rangle$ in Sec. IV A are taken over the vacuum state $|0\rangle_b$. In the present section we study a finite-temperature system.

A. Finite-temperature states

Because of the existence of negative-energy modes, the transonic flow we consider is energetically unstable and cannot support a thermal state. However, one can define a finite-temperature configuration [13,14,26] as follows: One considers a uniform BEC (with density n_u) initially flowing at constant velocity V_u , at thermal equilibrium at temperature T_{BEC} in the frame moving along with the fluid. Then the potential $U(x)$ of Eq. (2) is slowly ramped up until the system reaches the configuration described in Sec. II A and Fig. 1. At the end of this adiabatic branching process one can define an occupation number $\bar{n}_i(\omega, T_{\text{BEC}})$ for each of the incoming modes \hat{b}_i . As explained, e.g., in [26], for a fixed frequency ω these occupation numbers are given by

$$\langle \hat{b}_i^\dagger(\omega)\hat{b}_i(\omega) \rangle = \bar{n}_i(\omega, T_{\text{BEC}}) = n_{\text{th}}\{\omega_{\text{B},\alpha}[q_{i\text{in}}(\omega)]\}, \quad (97)$$

where $n_{\text{th}}(\varpi) = [\exp(\hbar\varpi/T_{\text{BEC}}) - 1]^{-1}$ is the thermal Bose occupation distribution. In this expression $\omega_{\text{B},\alpha}(q_{i\text{in}})$ is the Bogoliubov dispersion relation (6), with $\alpha = u$ if $i = 0$ and $\alpha = d$ if $i = 1$ or 2 , and the functions $q_{i\text{in}}(\omega)$ are defined above [just after Eq. (9)].

The regime in which the separation (1) between a classical field and quantum fluctuations is valid and where the Bogoliubov treatment of the fluctuations applies has been denoted as the “weakly interacting quasiconsensate regime” in [105]. It is valid up to a temperature $T_{\text{BEC}} \simeq gn_u$ [16], where g is the coefficient of the nonlinearity in the Gross-Pitaevskii equation (2). For typical experimental parameters $gn_u \simeq 3$ nK [10]. While it is difficult to precisely determinate the experimental temperature, we note that the agreement between the experimental results of [10] and the theoretical expectations [16] suggests that the temperature of the condensate in the analog black hole realized by Steinhauer and collaborators is possibly lower than 3 nK.

At a finite temperature T_{BEC} , the vacuum state $|0\rangle_b$ is replaced by a product of thermal states of b modes given by

$$\rho_{a^b} = \bigotimes_{i=0}^2 \rho^{\text{th}}(a_i^b), \quad a_i^b = 1 + 2\bar{n}_i(\omega, T_{\text{BEC}}), \quad (98)$$

where \bar{n}_i is given by Eq. (97). We recall that we use the term “thermal” to designate that state in a loose sense, since, as explained in the beginning of this section, the occupation numbers (97) do not correspond to an equilibrium distribution in the transonic configuration we consider. The covariance matrix associated with this state is given by $\sigma_b^{\text{th}} = \text{diag}(a_0^b, a_0^b, a_1^b, a_1^b, a_2^b, a_2^b)$. After the Bogoliubov transformation $\mathbf{c} = \mathcal{S} \mathbf{b}$, the covariance matrix becomes $\sigma_c^{\text{th}} = \mathcal{S} \sigma_b^{\text{th}} \mathcal{S}^T$ [see Eq. (48)]. The 2×2 matrices σ_i and ε_{ij} in the block decomposition (41) of σ_c^{th} are given by expressions (54) and (55) where the averages $\langle \dots \rangle$ should be replaced by

$$\langle \dots \rangle_{\text{th}} = \text{Tr}[\rho_{a^b} \dots]. \quad (99)$$

In particular,

$$\sigma_i = a_{i,\text{th}} \mathbb{1}_2, \quad (100)$$

where

$$a_{i,\text{th}} = 1 + 2 \langle \hat{c}_i^\dagger \hat{c}_i \rangle_{\text{th}}, \quad i \in \{0, 1, 2\} \quad (101)$$

is the corresponding local mixedness [compare to (54) and to the first of Eqs. (62)].

We conclude this short section by noting that the optical analog proposed in Fig. 7 remains relevant at finite temperature. The difference with the zero-temperature case is just the occupation number of the f -modes: they now acquire an incoherent contribution. In particular the occupation $\langle \hat{f}_0^\dagger \hat{f}_0 \rangle$ is no longer zero as in Eq. (91). This suggests a possible experimental study of the effects of temperature on tripartite entanglement: one could realize the optical setup of Fig. 7, send a noncoherent beam along the mode f_0 , and evaluate the associated effect on entanglement in the system.

B. Detection of entanglement

Contrary to the zero-temperature case, $\sigma_c^{\text{th}} = \mathcal{S} \sigma_b^{\text{th}} \mathcal{S}^T$ is associated with a mixed state with no special symmetry, and it cannot be put in a standard form where the matrices ε_{ij} are all diagonal [66]. In this section we thus restrict our study to bipartite entanglement. In this case, the 4×4 covariance matrix associated with the reduced two-mode state ij can always be brought by LLUBOs to its standard form [65]. One easily proves that matrices ε_{ij} have, *mutatis mutandis*, the same form as those in the zero-temperature case, namely

$$\begin{aligned} \varepsilon_{ij} &= 2 |\langle \hat{c}_i \hat{c}_j^\dagger \rangle_{\text{th}}| \mathbb{1}_2, \quad i, j = 0, 1, \quad i \neq j, \\ \varepsilon_{i2} &= 2 |\langle \hat{c}_i \hat{c}_2 \rangle_{\text{th}}| \sigma_z, \quad i = 0, 1. \end{aligned} \quad (102)$$

As a consequence, the lowest symplectic eigenvalue associated with the partial-transposed reduced two-mode state ij takes the same form as in the zero-temperature case. Eq. (69) still holds, and in particular

$$2(v_{-}^{\text{PT}})^2 = \Delta_{ij}^{\text{PT}} - \sqrt{(\Delta_{ij}^{\text{PT}})^2 - 4 \det \sigma_{ij}}, \quad (103)$$

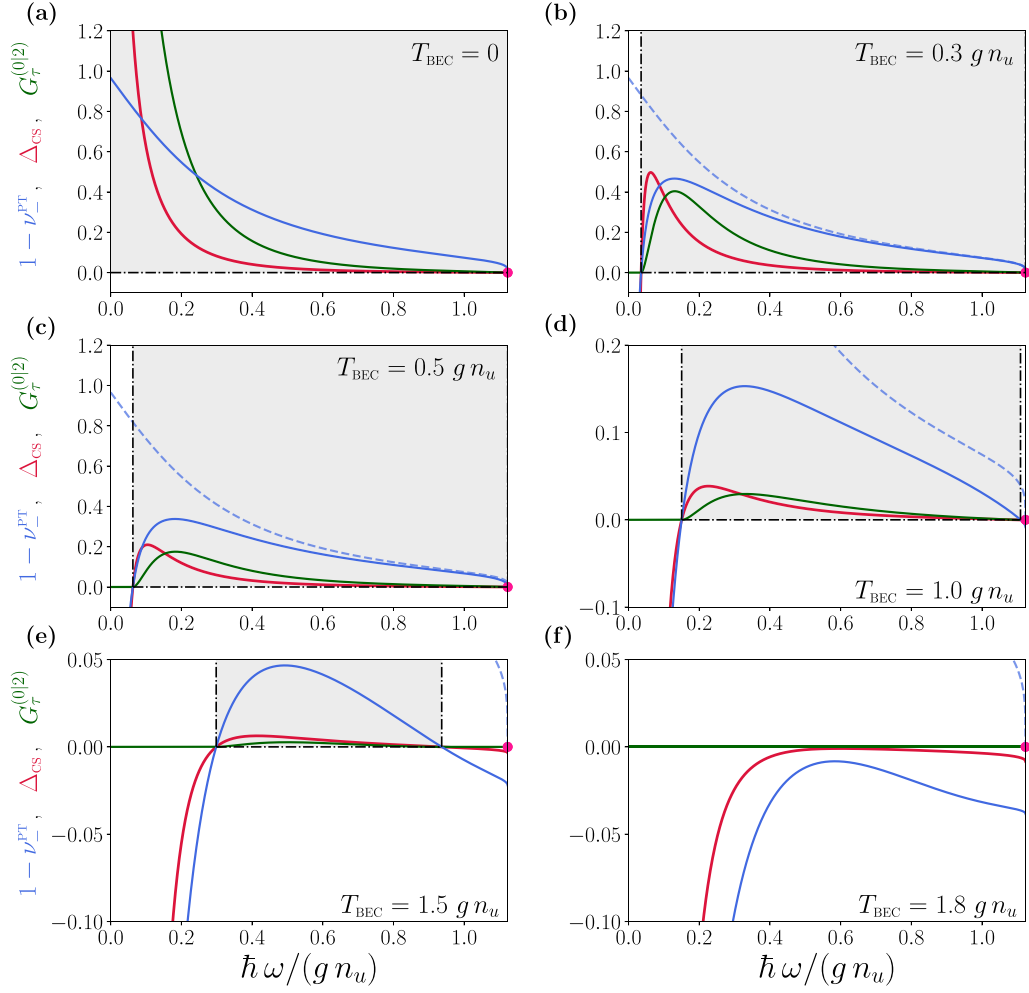


FIG. 9. Evolution of the PPT measure $1 - \nu_-^{\text{PT}}$ (blue), of the Cauchy-Schwarz parameter Δ_{CS} (red) and of the Gaussian contangle $G_\tau^{(0|2)}$ (green) for the bipartite system $0|2$ (i.e., the analog Hawking pair) as functions of the dimensionless frequency $\hbar\omega/(gn_u)$ and for different temperatures of the system, denoted by T_{BEC} , ranging from 0 (a) to $1.8 gn_u$ (f). All the plots are obtained for an upstream Mach number $m_u = 0.59$. The dashed blue curves in panels (b)–(f) correspond to the zero-temperature value of $1 - \nu_-^{\text{PT}}$. The gray areas indicate the range of frequencies for which the bipartite system is entangled [see text and Eqs. (105) and (107)]. The purple dots locate the upper-bound frequency Ω at which mode 2 vanishes.

with here

$$\begin{aligned}
 \det \sigma_{01} &= (a_{0,\text{th}} a_{1,\text{th}} - 4 |\langle \hat{c}_0 \hat{c}_1^\dagger \rangle_{\text{th}}|^2)^2, \\
 \Delta_{01}^{\text{PT}} &= a_{0,\text{th}}^2 + a_{1,\text{th}}^2 - 8 |\langle \hat{c}_0 \hat{c}_1^\dagger \rangle_{\text{th}}|^2, \\
 \det \sigma_{i2} &= (a_{i,\text{th}} a_{2,\text{th}} - 4 |\langle \hat{c}_i \hat{c}_2 \rangle_{\text{th}}|^2)^2, \quad i = 0, 1, \\
 \Delta_{i2}^{\text{PT}} &= a_{i,\text{th}}^2 + a_{2,\text{th}}^2 + 8 |\langle \hat{c}_i \hat{c}_2 \rangle_{\text{th}}|^2, \quad i = 0, 1. \quad (104)
 \end{aligned}$$

Note that the above expressions only involve moduli of mean values, so that we could equivalently use operators \hat{e}_i instead of \hat{c}_i since the transformation defined by Eqs. (36) and (37) is diagonal. The explicit form of the quantities appearing in Eqs. (104) is given in Eqs. (B2). At variance with the zero-temperature case they do not depend only on the local mixednesses. They should be experimentally accessible through the measurement of the structure form factor and of real space density correlations [106], meaning that the PPT criterion can be used to experimentally detect entanglement (cf. the discussion at the end of Sec. VIC).

The PPT criterion asserts that the bipartite state is entangled iff

$$1 - \nu_-^{\text{PT}} > 0. \quad (105)$$

In the following we denote this quantity as the ‘‘PPT measure.’’ It is of particular interest to focus on the bipartition $0|2$ since it corresponds to the Hawking-Partner pair. In this case expression (103) leads to

$$\begin{aligned}
 \nu_-^{\text{PT}} &= \frac{a_{0,\text{th}} + a_{2,\text{th}}}{2} \\
 &\quad - \sqrt{\left(\frac{a_{0,\text{th}} - a_{2,\text{th}}}{2}\right)^2 + 4 |\langle \hat{c}_0 \hat{c}_2 \rangle_{\text{th}}|^2}. \quad (106)
 \end{aligned}$$

The corresponding value of the PPT measure $1 - \nu_-^{\text{PT}}$ is represented in Fig. 9 as a function of the frequency ω of the elementary excitations and for different temperatures ranging from 0 to $1.5 gn_u$ (blue curves). In each plot the dashed blue curves display the same quantity at zero temperature for comparison.

It is instructive to compare the conclusions drawn from the study of the PPT measure with those obtained using the criterion of violation of the Cauchy-Schwarz inequality (70). According to this criterion, the analog Hawking-Parker pair $|0\rangle|2\rangle$ is entangled iff

$$\Delta_{\text{CS}} \equiv |\langle \hat{c}_0 \hat{c}_2 \rangle_{\text{th}}|^2 - \frac{(a_{0,\text{th}} - 1)(a_{2,\text{th}} - 1)}{4} > 0. \quad (107)$$

In the following we denote Δ_{CS} as the ‘‘Cauchy-Schwarz parameter.’’ It is represented by the red curves in Fig. 9 which confirm the results obtained with the PPT criterion: the blue and red curves are positive in the same region and cross zero exactly at the same frequency. This means, as expected, that both criteria lead to the same qualitative result for entanglement detection. However, as we shall see in Sec. VIC, they lead to different quantitative estimation of the amount of entanglement.

The analog Hawking pair is entangled in the range of frequencies for which inequalities (105) and (107) hold. This corresponds to the gray shaded regions bounded by two vertical black dot-dashed lines in Fig. 9. The range of parameters over which entanglement can be observed decreases when the temperature of the Bose gas increases. In agreement with the findings of Refs. [23,30], we observe that when T_{BEC} increases entanglement first disappears at low ω . It eventually completely disappears when $T_{\text{BEC}} \gtrsim 1.8 g n_u$; cf. Fig. 9(f). Therefore the temperature of the experimental system should not exceed this limiting value to be able to observe entanglement. It is interesting to compare this value to the one obtained in Ref. [23], which studies an analog black hole configuration different from the waterfall we consider here (it had been denoted as ‘‘flat profile’’ in Ref. [15]) with values of the upper and lower Mach numbers not significantly different from ours.⁹ The authors of Ref. [23] find a disappearance of entanglement for $T_{\text{BEC}} \gtrsim 0.195 g n_u$, i.e., at much lower temperature than what is observed here. This is in agreement with the findings of Ref. [26] where entanglement was shown to be much less resilient to temperature in the flat profile configuration than in the waterfall configuration.

In order to perform a more detailed discussion of the effects of temperature on entanglement, we represent in Fig. 10(a) the PPT measure $1 - \nu_{-}^{\text{PT}}$ of the Hawking pair $|0\rangle|2\rangle$ at temperature $T_{\text{BEC}} = 0.5 g n_u$ for different configurations parameterized by the upstream Mach number m_u . As already seen in Fig. 9, which corresponds to the specific case $m_u = 0.59$, a finite temperature reduces the range of frequencies for which entanglement occurs. One observes in this new plot that the entanglement of the Hawking pair persists for a larger fraction of the available frequency domain when the parameter m_u is closer to unity. This is in agreement with the results obtained in [22]; it was noticed that not only the temperature T_{BEC} destroys the entanglement of the analog Hawking pair, but also that a strong ‘‘coupling’’ of mode 1 with the other modes can affect their entanglement. This coupling is measured through the squared modulus of the scattering matrix coefficients $|S_{01}(\omega)|^2$ and $|S_{21}(\omega)|^2$. One finds numerically

⁹They have $m_u = 0.75$ and $m_d = 1.5$, whereas here $m_u = 0.59$ and $m_d = 2.9$.

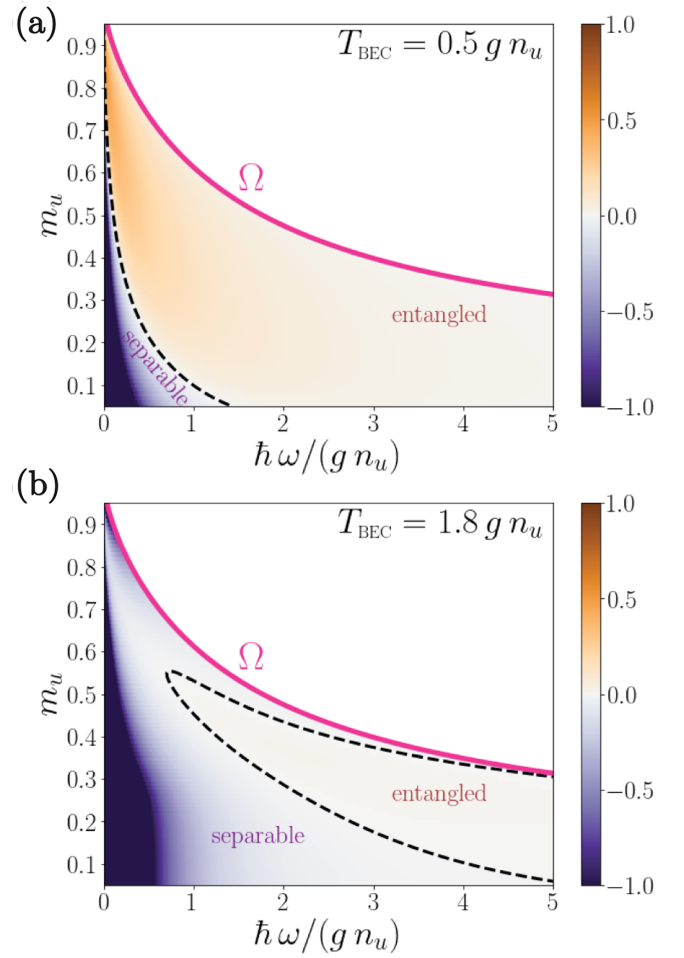
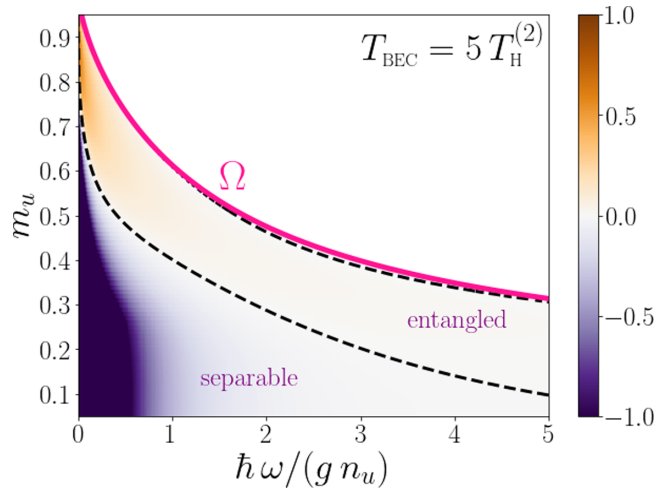


FIG. 10. PPT measure $1 - \nu_{-}^{\text{PT}}$ of the Hawking pair $|0\rangle|2\rangle$ plotted as a function of the upstream Mach number m_u and of the frequency ω , for temperatures (a) $T_{\text{BEC}} = 0.5 g n_u$ and (b) $T_{\text{BEC}} = 1.8 g n_u$. The pink curve corresponds to the upper-bound frequency Ω (9). For a fixed value m_u , i.e., along a horizontal cut on the graph, mode 2 only exists for a frequency ω lower than $\Omega(m_u)$ (see Fig. 2). The dashed black curve corresponds to $1 - \nu_{-}^{\text{PT}} = 0$ and thus delimits the region where the analog Hawking pair is entangled.

(and analytically in the low- ω sector [15]) that these two quantities decrease when m_u increases. This exactly corresponds to the results presented in Fig. 10(a): when m_u increases, the coupling between $|0\rangle|1\rangle$ and $|1\rangle|2\rangle$ decreases, and indeed leads to a stronger violation of PPT criterion for a larger fraction of frequencies. However, it is important to note that this phenomenon is valid only at low enough temperatures. This is illustrated in Fig. 10(b): for a temperature as large as $T = 1.8 g n_u$ the region where the pair is entangled greatly diminishes and entanglement only survives at moderate values of m_u (at variance with the conclusion of the above discussion). Likewise, at this temperature, even in the region where entanglement is present, the PPT measure is significantly lower than in the equivalent regions in Fig. 10(a).

It is also interesting to study the entanglement of the Hawking pair, not as a function of the absolute temperature, but as a function of the Hawking temperature $T_{\text{H}}^{(2)}$ (95). There is no obvious reason why entanglement between modes should


 FIG. 11. Same as Fig. 10 for $T_{\text{BEC}} = 5 T_{\text{H}}^{(2)}$.

disappear when the temperature of the system exceeds the Hawking temperature. This is indeed what is observed in Fig. 11: entanglement persists in sizable regions even when $T_{\text{BEC}} = 5 T_{\text{H}}^{(2)}$.

We can conclude from the above discussion that whereas entanglement persists for temperatures noticeably larger than $T_{\text{H}}^{(2)}$, it is significantly reduced when T_{BEC} becomes larger than the chemical potential $g n_u$.

C. Measurement of entanglement

The violation of the Cauchy-Schwarz inequality is often used to study the entanglement between the elementary excitations in the context of analog gravity [20–22,24,26,27]. However, while this criterion tells us whether the bipartite system is entangled or not, the Cauchy-Schwarz parameter Δ_{CS} it is not a good measure of the amount of entanglement at finite temperature.

To clarify this point, we compute the amount of entanglement at finite temperature for the bipartition $0|2$, as measured by the Gaussian contangle $G_{\tau}^{(0|2)}$ defined in Eq. (73). This computation is slightly more difficult here than in the zero-temperature case, where it is given by Eq. (80). In the presence of temperature the reduced two-mode state $0|2$ is not a GMEMMS, a GMEMS, or a GLEMS, for which analytic expressions hold [87]. Nevertheless, the Gaussian contangle can be put under the form [87]

$$G_{\tau}^{(0|2)} = \text{arsinh}^2 \left\{ \sqrt{\min_{\theta} [m(\theta)] - 1} \right\}, \quad (108)$$

where $m(\theta)$ is explicitly given by Eq. (E23). In Fig. 9 we represent by a green solid line the value of $G_{\tau}^{(0|2)}$ in the range of frequencies for which the system is entangled [the minimum over the angle θ in Eq. (108) is obtained numerically]. The results for $G_{\tau}^{(0|2)}$ confirm that the PPT and Cauchy-Schwarz criteria correctly determine the region where entanglement exists.

As expected, entanglement decreases as the temperature increases. In the zero-temperature case [Fig. 9(a)], both $1 - \nu_{-}^{\text{PT}}$ and Δ_{CS} vary in the same way as $G_{\tau}^{(0|2)}$. The situation at finite

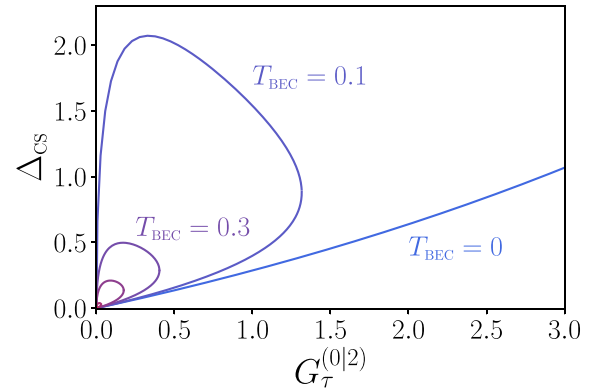


FIG. 12. Evolution of Δ_{CS} given by Eq. (107) as a function of the measure of bipartite entanglement $G_{\tau}^{(0|2)}$ given by expressions (108) and (E23), for the same set of temperatures as in Fig. 9, ranging from $T_{\text{BEC}} = 0$ (blue curve) to $T_{\text{BEC}} = 1.5 g n_u$ (red curve), with $m_u = 0.59$. When possible, the corresponding temperature for each curve is indicated on the graph (we dropped the factor $g n_u$ for readability). Note that for $T_{\text{BEC}} > 0$, the curves describe a loop.

temperature is different: while the quantities $1 - \nu_{-}^{\text{PT}}$ and $G_{\tau}^{(0|2)}$ appear to behave similarly, being increasing and decreasing in the same regions and having a maximum at the same value of ω , this is not the case for Δ_{CS} whose maximum is shifted with respect to the two others; see Figs. 9(b)–9(f).

In order to illustrate this phenomenon, in Fig. 12 we plotted Δ_{CS} as a function of $G_{\tau}^{(0|2)}$ for several temperatures. These are parametric curves obtained from expressions (107) and (108), ω playing the role of the parameter. Except at $T_{\text{BEC}} = 0$, Δ_{CS} is not a monotonous function of $G_{\tau}^{(0|2)}$, as demonstrated by the closed loops with regions of negative slope observed for each finite temperature. Another way to note the same point is to remark that the maximal violation of Cauchy-Schwarz inequality (Δ_{CS} maximal) is not reached when $G_{\tau}^{(0|2)}$ is maximal. This confirms that the parameter Δ_{CS} is not an entanglement monotone.

In Fig. 13 we underline the difference between the behaviors of the Cauchy-Schwarz parameter and the PPT measure by plotting $1 - \nu_{-}^{\text{PT}}$ as a function of $G_{\tau}^{(0|2)}$.

The difference with Fig. 12 is striking. For each temperature, $1 - \nu_{-}^{\text{PT}}$ is a monotonous increasing function of $G_{\tau}^{(0|2)}$. It is not easily seen in the figure, but for finite T_{BEC} the relation between the two quantities is not one to one: for each $G_{\tau}^{(0|2)}$ there are two (close) values of $1 - \nu_{-}^{\text{PT}}$ which coalesce at the common maximum of the two quantities, marked with a point on Fig. 13. This confirms without ambiguity that the PPT measure is still an entanglement monotone at finite temperature. We also note that all the curves in Fig. 13 almost superimpose, meaning that relation between the two quantities $1 - \nu_{-}^{\text{PT}}$ and $G_{\tau}^{(0|2)}$ is very weakly dependent on temperature, which makes the PPT measure an even better candidate for quantifying entanglement.

In view of the results presented in Figs. 12 and 13, it is of interest to also discuss the generalized Peres-Horodecki (GPH) parameter, which has been used in [23,25] for witnessing entanglement in analog systems. As shown by Simon [73], nonseparability of modes 0 and 2 can be defined as $\mathcal{P} < 0$,

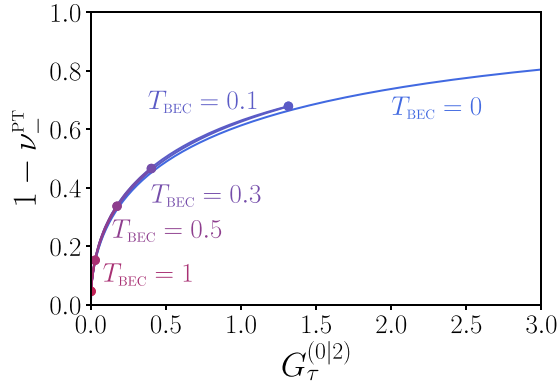


FIG. 13. Evolution of $1 - \nu_-^{\text{PT}}$ given by Eq. (106) as a function of the measure of bipartite entanglement $G_\tau^{(0|2)}$ given by expressions (108) and (E23), for the same set of temperatures as in Fig. 9, ranging from $T_{\text{BEC}} = 0$ (blue curve) to $T_{\text{BEC}} = 1.5 g n_u$ (red curve), with $m_u = 0.59$. When possible, the corresponding temperature for each curve is indicated on the graph (we dropped the factor $g n_u$ for readability). For each temperature the common maximal value of $1 - \nu_-^{\text{PT}}$ and $G_\tau^{(0|2)}$ is marked with a point.

where, using our conventions, the GPH parameter reads

$$\mathcal{P} = \det \sigma_0 \det \sigma_2 + (1 - |\det \varepsilon_{02}|)^2 - \text{tr}(\sigma_0 J \varepsilon_{02} J \sigma_2 J \varepsilon_{02}^\top J) - \det \sigma_0 - \det \sigma_2, \quad (109)$$

and the matrix J is defined in (40). This yields

$$\mathcal{P} = (1 - 4|\langle \hat{c}_0 \hat{c}_2 \rangle_{\text{th}}|^2 + a_{0,\text{th}} a_{2,\text{th}})^2 - (a_{0,\text{th}} + a_{2,\text{th}})^2. \quad (110)$$

As is clear from expressions (106), (107), and (110), negativity of \mathcal{P} is equivalent to the positivity of $1 - \nu_-^{\text{PT}}$ and to that of Δ_{CS} : these three criteria are equivalent in terms of qualitative assessment of nonseparability. This being ascertained, we want to check if $-\mathcal{P}$ is a good *quantitative* measure of entanglement. To this end, we plot it as a function of $G_\tau^{(0|2)}$ in Fig. 14. It appears clearly that, as Δ_{CS} , $-\mathcal{P}$ is not an entanglement monotone at finite temperature.

We would like to insist on the positive aspects of using the PPT measure in future experimental studies of analog black hole configurations: (1) as just seen, contrary to the Cauchy-Schwarz and GPH parameters, the PPT measure is

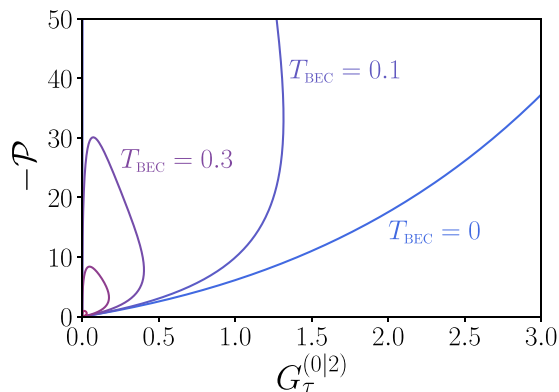


FIG. 14. Same as Figs. 12 and 13 for the GPH parameter $-\mathcal{P}$ defined in Eqs. (109) and (110).

a good quantitative measure of entanglement, whatever the temperature of the system is; (2) from Fig. 13 it appears that $1 - \nu_-^{\text{PT}}$ is almost as good a measure of entanglement as $G_\tau^{(0|2)}$, but it has a much simpler expression in terms of the local mixednesses and mode correlation functions [compare Eq. (106) with Eqs. (108) and (E23)]; and (3) the calculations of Sec. VIB show that the computation of the lowest symplectic eigenvalue requires essentially the knowledge of the same quantities (104) as Δ_{CS} and \mathcal{P} [compare Eqs. (106), (107), and (110)]. This means that the value of ν_-^{PT} is experimentally accessible and can be measured, for instance, from the density correlations along the acoustic black hole, as we now demonstrate.

An experimental evaluation of the quantities used in the present work for characterizing bipartite and tripartite entanglement necessitates to experimentally determine the coefficients of the covariance matrix (41). For our three-mode Gaussian state this matrix is 6×6 , and its coefficients are all expressed in terms of correlation functions of the c -operators [see, e.g., Eqs. (100), (101), and (102)]. Steinhauer [106] has devised a clever method for determining such quantities from the knowledge of the static structure factor and the density-density correlation function, which are both experimentally accessible quantities. This technique has been used in Refs. [9,10] and can be in principle extended for evaluating all the relevant averages of c -operators. Note, however, that there are potential practical difficulties: the method necessitates the computation of windowed Fourier transforms of the real space density-density correlation function and this quantity has to be accurately determined over a large spatial range in order to correctly perform all the necessary Fourier transforms. Also the windows used to evaluate these Fourier transforms have to be selected with special care, as discussed in Refs. [16,25,26].

In order to give a proof of concept of the method, we performed the following computation: considering a zero-temperature system we neglected the occupation of the Companion mode, which, from Eq. (61) yields $a_0 \simeq a_2$. This makes it possible, through (58) and (62), to express the symplectic eigenvalue (69) as

$$\nu_-^{\text{PT}} \simeq \sqrt{1 + 4|\langle \hat{c}_0 \hat{c}_2 \rangle|^2} - 2|\langle \hat{c}_0 \hat{c}_2 \rangle|. \quad (111)$$

The corresponding value of $1 - \nu_-^{\text{PT}}$ is reported in Fig. 15. We determined the quantity $|\langle \hat{c}_0 \hat{c}_2 \rangle|$ appearing in (111) by combining the results of the experimental analysis of [10] with the theoretical value of the structure form factor. A self-contained experimental analysis should resort to the experimentally determined value of this quantity. Also, as discussed in Ref. [16], (1) neglecting the occupation number of the Companion mode is too crude an approximation, or at least necessitates an independent experimental confirmation and (2) the windowed Fourier analysis of the experimental density-density correlation function deserves a careful analysis. This is the reason why Fig. 15 does not provide an experimental signature of bipartite entanglement in the BEC analog realized in Ref. [10], but is rather a proof of concept, demonstrating that the theoretical techniques employed in the present work provide valuable tools for analyzing experimental data.

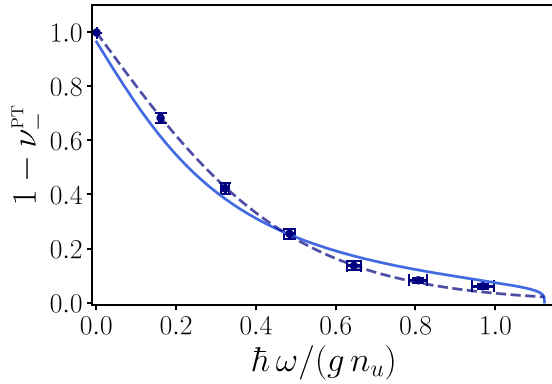


FIG. 15. Zero-temperature PPT measure as a function of energy in a waterfall configuration with $m_u = 0.59$. The blue solid curve is the same as in Fig. 9(a). The points with error bars are evaluated from Eq. (111), extracting the value of $|\langle \hat{c}_0 \hat{c}_2 \rangle|$ from the experimental data of Ref. [10] as discussed in the text. The dashed line represents the result of Eq. (111) obtained by assuming that $|\langle \hat{c}_0 \hat{c}_2 \rangle| \simeq \frac{1}{2} \sqrt{a_0^2 - 1} \simeq \sqrt{\bar{n}_0(\bar{n}_0 + 1)}$, where $\bar{n}_0(\omega)$ is a thermal Bose occupation evaluated at the Hawking temperature $T_H = 0.124 g n_u$ determined in [10].

VII. CONCLUSION

In the present work, we have investigated entanglement properties of modes emitted from an analog black hole realized in the flow of a Bose-Einstein condensate. The ground state of the system is seen by an external observer as a three-mode Gaussian state. Gaussian states are entirely characterized by their first and second moments. Thus, their entanglement properties can be expressed in terms of their covariance matrix. We have characterized bipartite and tripartite entanglement in the system using tools developed in the field of continuous-variable entanglement. We identified the best configuration for the experimental measurement of tripartite entanglement: the Gaussian residual entanglement G_{τ}^{res} is larger for waterfall configurations with moderate upstream Mach number ($m_u \simeq 0.15$) and at small frequencies. An interesting result is the finiteness of bipartite entanglement (for instance, between the Hawking and the Partner) at zero energy, while the tripartite entanglement diverges. This point sheds light on the importance of the Companion particle, which is sometimes discarded when studying entanglement in analog black holes. We also showed that, quite counter-intuitively, while there is no bipartite entanglement between two of the outgoing modes (tracing out the third one), there is nevertheless genuine tripartite entanglement between the three modes.

Our detailed investigation of the distribution of entanglement in the system in Sec. V enabled us to propose a table top optical setup modeling the physical process we study. This, in turn, suggested an alternative manner to define the analog Hawking temperature and the associated gray-body factor, in better agreement with the gravitational paradigm.

In Sec. VI we studied the effect of temperature on bipartite entanglement and obtained several results. The Cauchy-Schwarz and the GPH criteria which have been studied in previous studies of analog systems merely give a qualitative assessment of whether the system is entangled or not. In this paper, we go beyond this qualitative approach by evaluating

the amount of entanglement in the Hawking pair using the Gaussian contangle. We assess the capability of several parameters to correctly quantify the amount of entanglement between the Hawking pair by comparing them with our measure of entanglement. Our results should be relevant in future experiments: as a main message, we advise to use the PPT measure $1 - \nu_{-}^{\text{PT}}$ instead of the Cauchy-Schwarz or the generalized Peres-Horodecki parameters as a good quantifier of entanglement. We have also observed that the connection between the PPT measure and the contangle is weakly affected by thermal effects, which strengthens even more its relevance in the context of analog black holes in BEC.

Extensions of the present work include the investigation of zero-norm modes, which were shown in [16] to play an important role in the correct quantum description of Bogoliubov excitations. The study of the influence of thermal effects on the amount of tripartite entanglement also constitutes a natural continuation of the present study.

During the completion of this work, we became aware of the preprint [107] which studies tripartite entanglement in an analog system thanks to the residual contangle, as done in the present paper. The model in [107] corresponds to a “subluminal” dispersion relation, whereas in the BEC case we consider, the dispersion is rather “superluminal.” Also, the authors of the recent preprint [108] use a quantum description of an analog black hole similar to the one we present in Sec. VC and define the Hawking temperature from the squeezing parameter of the associated parametric amplifier, as done in Eq. (93).

ACKNOWLEDGMENTS

We thank M. Jacquet for inspiring discussions on entanglement in analog gravity. We also acknowledge fruitful exchanges with A. Aspect, T. Bienaimé, A. Fabbri, Q. Glorieux, F. Sols, and C. Westbrook. We thank J. Steinhauer for providing us with experimental data. We acknowledge financial support from the DIM SIRTEQ (Science et Ingénierie en Région Île-de-France pour les Technologies Quantiques), EML 2020 project HydroLive. LPTMS is a member of the QUANTUM center of Université Paris-Saclay.

APPENDIX A: BOGOLIUBOV TRANSFORMATIONS

In this Appendix we detail some intermediate steps useful for establishing the results presented in Sec. III A.

The form (13) and (16) of vectors \mathbf{b} and \mathbf{c} implies that the $2N \times 2N$ matrix \mathcal{T} defining the unitary Bogoliubov transformation (15) has a block structure given by (17). In order that the \hat{c}_i defined in Eq. (15) satisfy bosonic commutation relations, the matrix \mathcal{T} must verify

$$\mathcal{T} \tilde{\mathbb{J}} \mathcal{T}^{\text{T}} = \tilde{\mathbb{J}}, \quad (\text{A1})$$

where $\tilde{\mathbb{J}}$ is defined in Eq. (14). Equation (A1) means that \mathcal{T} belongs to the symplectic group $\text{Sp}(2N, \mathbb{C})$. As a consequence, one has

$$\mathcal{T}^{-1} = -\tilde{\mathbb{J}} \mathcal{T}^{\text{T}} \tilde{\mathbb{J}} = \begin{pmatrix} \alpha^{\text{T}} & \beta^{\dagger} \\ \beta^{\text{T}} & \alpha^{\dagger} \end{pmatrix}. \quad (\text{A2})$$

Condition (A1) can be reexpressed in terms of the two $N \times N$ matrices α and β as

$$\begin{aligned} \alpha \alpha^\dagger - \beta \beta^\dagger &= \mathbb{1}_N, & \alpha \beta^\top - \beta \alpha^\top &= 0, \\ \alpha^\dagger \alpha - \beta^\top \beta^* &= \mathbb{1}_N, & \alpha^\top \beta^* - \beta^\dagger \alpha &= 0. \end{aligned} \quad (\text{A3})$$

The matrix \mathcal{T} being symplectic, it can be written as

$$\mathcal{T} = \exp(\tilde{\mathcal{J}} Q), \quad (\text{A4})$$

with Q a $2N \times 2N$ symmetric matrix.

The unitary operator T relating operators \hat{c}_i and \hat{b}_i according to (18) is defined as

$$T = \exp\left(\frac{1}{2} \mathbf{b}^\top Q \mathbf{b}\right), \quad (\text{A5})$$

as can be shown by using the Baker-Campbell-Hausdorff formula [42]. Note that using Eqs. (15) and (A4) one has $\mathbf{b}^\top Q \mathbf{b} = \mathbf{c}^\top (\mathcal{T}^{-1})^\top Q \mathcal{T}^{-1} \mathbf{c} = \mathbf{c}^\top Q \mathbf{c}$. This indicates that T has the same expression in term of the c 's and in term of the b 's.

It is possible to show [47,54,109] that T can be uniquely decomposed into the product

$$T = (\det \alpha)^{-1/2} \exp\left[\frac{1}{2} \sum_{i,j=1}^N X_{ij} \hat{c}_i^\dagger \hat{c}_j^\dagger\right] \exp\left[\sum_{i,j=1}^N Y_{ij} \hat{c}_i^\dagger \hat{c}_j\right] \exp\left[\frac{1}{2} \sum_{i,j=1}^N Z_{ij} \hat{c}_i \hat{c}_j\right], \quad (\text{A6})$$

where X, Y, Z are $N \times N$ matrices defined by

$$X = -\beta^* \alpha^{-1}, \quad e^{-Y^\top} = \alpha, \quad Z = \alpha^{-1} \beta. \quad (\text{A7})$$

The interest of the decomposition (A6) lies in the fact that all annihilation operators have been put to the right. Therefore, when applied to the vacuum $|0\rangle_c$, T only acts through matrix X . This directly yields Eq. (21).

APPENDIX B: EXPLICIT EXPRESSION OF THE COVARIANCE MATRIX

In this Appendix we give a useful formula for the covariance matrix, present explicit expressions necessary for evaluating its finite-temperature form, and discuss their zero-temperature limit.

The decomposition (34) makes it possible to write the covariance matrix σ_c of Eq. (53) under the form

$$\sigma_c = \begin{pmatrix} 1 + 2v_{02}^2 & 0 & 2v_{02}v_{12} \cos(\phi_{01}) & -2v_{02}v_{12} \sin(\phi_{01}) & 2v_{22}v_{02} \cos(\phi_{02}) & 2v_{22}v_{02} \sin(\phi_{02}) \\ 0 & 1 + 2v_{02}^2 & 2v_{02}v_{12} \sin(\phi_{01}) & 2v_{02}v_{12} \cos(\phi_{01}) & 2v_{22}v_{02} \sin(\phi_{02}) & -2v_{22}v_{02} \cos(\phi_{02}) \\ 2v_{02}v_{12} \cos(\phi_{01}) & 2v_{02}v_{12} \sin(\phi_{01}) & 1 + 2v_{12}^2 & 0 & 2v_{22}v_{12} \cos(\phi_{12}) & 2v_{22}v_{12} \sin(\phi_{12}) \\ -2v_{02}v_{12} \sin(\phi_{01}) & 2v_{02}v_{12} \cos(\phi_{01}) & 0 & 1 + 2v_{12}^2 & 2v_{22}v_{12} \sin(\phi_{12}) & -2v_{22}v_{12} \cos(\phi_{12}) \\ 2v_{22}v_{02} \cos(\phi_{02}) & 2v_{22}v_{02} \sin(\phi_{02}) & 2v_{22}v_{12} \cos(\phi_{12}) & 2v_{22}v_{12} \sin(\phi_{12}) & -1 + 2v_{22}^2 & 0 \\ 2v_{22}v_{02} \sin(\phi_{02}) & -2v_{22}v_{02} \cos(\phi_{02}) & 2v_{22}v_{12} \sin(\phi_{12}) & -2v_{22}v_{12} \cos(\phi_{12}) & 0 & -1 + 2v_{22}^2 \end{pmatrix}, \quad (\text{B1})$$

where v_{ij} and ϕ_{ij} are defined in Eq. (34) and $\phi_{ij} = \varphi_{i2} - \varphi_{j2}$.

Also, for explicitly computing the finite-temperature entanglement properties studied in Sec. VIB [see Eqs. (104) and (107)] one uses the formulas:

$$\begin{aligned} \langle \hat{c}_0 \hat{c}_1^\dagger \rangle_{\text{th}} &= S_{00} S_{10}^* (1 + \bar{n}_0) + S_{01} S_{11}^* (1 + \bar{n}_1) + S_{02} S_{12}^* \bar{n}_2, \\ \langle \hat{c}_i^\dagger \hat{c}_i \rangle_{\text{th}} &= |S_{i0}|^2 \bar{n}_0 + |S_{i1}|^2 \bar{n}_1 + |S_{i2}|^2 (1 + \bar{n}_2), \quad i = 0, 1, \\ \langle \hat{c}_i \hat{c}_2 \rangle_{\text{th}} &= S_{i0} S_{20}^* (1 + \bar{n}_0) + S_{i1} S_{21}^* (1 + \bar{n}_1) + S_{i2} S_{22}^* \bar{n}_2, \quad i = 0, 1, \\ \langle \hat{c}_2^\dagger \hat{c}_2 \rangle_{\text{th}} &= |S_{20}|^2 (1 + \bar{n}_0) + |S_{21}|^2 (1 + \bar{n}_1) + |S_{22}|^2 \bar{n}_2, \end{aligned} \quad (\text{B2})$$

where the quantities \bar{n}_0 , \bar{n}_1 and \bar{n}_2 are defined in Eq. (97), and, as in Eq. (B1), we do not write the explicit ω dependences for legibility.

At zero temperature the above equations reduce to

$$\begin{aligned} \langle \hat{c}_0 \hat{c}_1^\dagger \rangle &= S_{00} S_{10}^* + S_{01} S_{11}^* = S_{12}^* S_{02}, \\ \langle \hat{c}_i^\dagger \hat{c}_i \rangle &= |S_{i2}|^2, \quad i = 0, 1, \\ \langle \hat{c}_i \hat{c}_2 \rangle &= S_{i0} S_{20}^* + S_{i1} S_{21}^* = S_{i2} S_{22}^*, \quad i = 0, 1, \\ \langle \hat{c}_2^\dagger \hat{c}_2 \rangle &= |S_{20}|^2 + |S_{21}|^2 = -1 + |S_{22}|^2, \end{aligned} \quad (\text{B3})$$

where use has been made of property (11). Using Eqs. (B3) and expressions (60), one may show that the finite-temperature components (100) and (102) of the covariance matrix reduce at $T_{\text{BEC}} = 0$ to the form (62) as they should. However, at finite temperature, Eq. (B2) holds instead of (B3), implying that, contrarily to the zero-temperature case, the covariance matrix, its symplectic eigenvalues, and thus the

entanglement properties of the system, do not depend only on the local mixednesses.

APPENDIX C: LONG WAVELENGTH LIMIT OF THE SCATTERING AMPLITUDES

In the long wavelength limit, the S_{i2} coefficients of the S -matrix (12) behave as

$$S_{i2}(\omega) = F_{i2} \sqrt{\frac{gn_u}{\hbar\omega}} + O(\omega^{1/2}), \quad i \in \{0, 1, 2\}, \quad (\text{C1})$$

where the F_{i2} are dimensionless constant coefficients. For the waterfall configuration we consider here, analytic expressions of their moduli have been determined in [15]:

$$|F_{02}|^2 = 2 \frac{m_u(1-m_u)^{\frac{3}{2}}(1+m_u^2)^{\frac{3}{2}}}{(1+m_u)^{\frac{1}{2}}(1+m_u+m_u^2)^2}, \quad (\text{C2})$$

$$|F_{12}|^2 = \frac{1}{2} \frac{(1-m_u)^{\frac{7}{2}}(1+m_u^2)^{\frac{3}{2}}}{(1+m_u)^{\frac{1}{2}}(1+m_u+m_u^2)^2}, \quad (\text{C3})$$

and

$$|F_{22}|^2 = \frac{1}{2} \frac{(1-m_u^4)^{\frac{3}{2}}}{(1+m_u+m_u^2)^2}, \quad (\text{C4})$$

where m_u is the upstream Mach number.

From the low-frequency behavior of the scattering coefficients it is possible to evaluate the analog Hawking temperature of the waterfall configuration; see Eqs. (65) and (95). An alternative way to evaluate the Hawking temperature is to use the semiclassical analog surface gravity expression [1,110]

$$T_{\text{H}} = \frac{\hbar}{2\pi} \left(\frac{dv}{dx} - \frac{dc}{dx} \right)_{x_{\text{H}}}, \quad (\text{C5})$$

where $v(x)$ is the velocity of the flow, $c(x) = \sqrt{gn(x)/m}$ is the local sound velocity and x_{H} is the position of the horizon, defined as the point at which

$$v(x_{\text{H}}) = c(x_{\text{H}}). \quad (\text{C6})$$

However, as argued in Sec. II A the definition (C5) is not expected to apply in the case we consider because, strictly speaking, the local sound velocity is ill-defined for the waterfall profile around $x = 0$. A blindfolded use of Eqs. (C6) and (C5) leads to

$$\frac{x_{\text{H}}}{\xi_u} = -\frac{1}{\sqrt{1-m_u^2}} \operatorname{arcosh} \sqrt{\frac{1-m_u^2}{1-m_u^{2/3}}} \quad (\text{C7})$$

and

$$\frac{T_{\text{H}}}{gn_u} = \frac{3}{2\pi} (1-m_u^{2/3}) \sqrt{1-m_u^{4/3}}. \quad (\text{C8})$$

This expression is compared with alternative definitions of the Hawking temperature in Fig. 8. Note that when m_u increases, x_{H} goes deeper in a region of smooth density profile where the concept of local sound velocity becomes relevant: $x_{\text{H}} \ll -\xi_u$ when $m_u \rightarrow 1$. In this regime expression (C5) and the corresponding result (C8) are mathematically sound.

APPENDIX D: ENTANGLEMENT LOCALIZATION IN A TRIPARTITE SYSTEM

In this Appendix we present the specifics of the process of entanglement localization discussed in Sec. V C. Let σ be a covariance matrix associated with a pure three-mode Gaussian state. We want to determine the explicit form of the symplectic matrix \mathcal{S} which transforms σ according to

$$\mathcal{S} \sigma \mathcal{S}^{\text{T}} = \mathbb{1}_2 \oplus \sigma_{\text{sq}}, \quad (\text{D1})$$

where σ_{sq} is the covariance matrix of a two-mode squeezed state [see Eq. (77)].

1. General form of the symplectic matrix

Consider a bipartition $ij|k$. The covariance matrix associated with the subsystem k is denoted as σ_k and the one associated with subsystem ij reads

$$\sigma_{ij} = \begin{pmatrix} \sigma_i & \varepsilon_{ij} \\ \varepsilon_{ij}^{\text{T}} & \sigma_j \end{pmatrix}. \quad (\text{D2})$$

The whole covariance matrix associated with the tripartite system is then

$$\sigma = \begin{pmatrix} \sigma_i & \varepsilon_{ij} & \varepsilon_{ik} \\ \varepsilon_{ij}^{\text{T}} & \sigma_j & \varepsilon_{jk} \\ \varepsilon_{ik}^{\text{T}} & \varepsilon_{jk}^{\text{T}} & \sigma_k \end{pmatrix}. \quad (\text{D3})$$

Consider the case where the covariance matrix is in its standard form (62), i.e., $\sigma_k = a_k \mathbb{1}_2$ and either

$$\sigma_{ij} = \begin{pmatrix} a_i & 0 & c & 0 \\ 0 & a_i & 0 & -c \\ c & 0 & a_j & 0 \\ 0 & -c & 0 & a_j \end{pmatrix}, \quad c = \sqrt{a_i - 1} \sqrt{a_j + 1} \quad (\text{D4})$$

for bipartitions $ij|k = 02|1$ and $12|0$ (for which $\varepsilon_{i2} = c\sigma_z$) or

$$\sigma_{ij} = \begin{pmatrix} a_i & 0 & c & 0 \\ 0 & a_i & 0 & c \\ c & 0 & a_j & 0 \\ 0 & c & 0 & a_j \end{pmatrix}, \quad c = \sqrt{a_i - 1} \sqrt{a_j - 1} \quad (\text{D5})$$

for the bipartition $01|2$ (for which $\varepsilon_{01} = c\mathbb{1}_2$). The difference in the sign in front of c between (D4) and (D5) is actually of great importance and leads to two different types of symplectic transformations in Eq. (D1). Note that we also impose $a_i < a_j$ in (D4); in fact, the order of the local mixednesses does not matter in (D5), as shall be clear at the end of this section.

The symplectic eigenvalues $\sigma_k = a_k \mathbb{1}$ are $\nu_k = a_k$. Using Williamson theorem, we can bring σ_{ij} to a diagonal matrix

$$(\sigma_{ij})' = \mathcal{S}_{ij} \sigma_{ij} (\mathcal{S}_{ij})^{\text{T}} = \operatorname{diag}\{\nu_i, \nu_i, \nu_j, \nu_j\}, \quad (\text{D6})$$

where we ordered the symplectic eigenvalues such that $\nu_i < \nu_j$. Easy calculations lead to

$$\mathcal{S}_{ij} = \begin{pmatrix} a & 0 & b & 0 \\ 0 & a & 0 & \eta b \\ \eta b & 0 & -a & 0 \\ 0 & b & 0 & -a \end{pmatrix}, \quad (\text{D7})$$

with

$$a = -\sqrt{\frac{a_j v_j - a_i v_i}{v_j^2 - v_i^2}}, \quad b = \sqrt{\frac{a_i v_j - a_j v_i}{v_j^2 - v_i^2}}, \quad (\text{D8})$$

and $\eta = -1$ for bipartitions $ij|k = 02|1$ and $12|0$, and $\eta = 1$ for bipartition $01|2$. The coefficients a and b satisfy the identity

$$a^2 + \eta b^2 = \frac{a_i + \eta a_j}{v_i + \eta v_j} = 1. \quad (\text{D9})$$

The last equality is valid only if \mathcal{S}_{ij} is a symplectic matrix.

Expressions (D7) and (D8) are valid for any covariance matrix σ_{ij} of the form (D4) and (D5). In our case, we can further simplify these expressions using the purity constraint of the three-mode Gaussian state under consideration. Indeed, one can easily prove that for any reduced two-mode states ij of a pure three-mode Gaussian state, $\Delta_{ij} = \det \sigma_{ij} + 1 = \det \sigma_k + 1$ [66]. Therefore, considering the reduced state jk , Eq. (68) immediately gives $v_i = 1$ and $v_j = \sqrt{\det \sigma_{ij}} = a_k$, which imply from the last equality of (D9) that $a_i + \eta a_j = v_i + \eta v_j = 1 + \eta a_k$. This expression is true for the case (D4) iff $a_i < a_j$, because $\eta = -1$. For (D5), the order is not important because $\eta = 1$. Thus, (D8) simplifies to

$$a = -\sqrt{\frac{(a_j - \eta)(a_k + \eta)}{a_k^2 - 1}}, \quad b = \sqrt{\frac{(a_i - 1)(a_k + \eta)}{a_k^2 - 1}}. \quad (\text{D10})$$

2. Standard form

The symplectic matrix defined by

$$\mathcal{S} = \mathcal{S}_{ij} \oplus \mathcal{S}_k, \quad (\text{D11})$$

with $\mathcal{S}_k = a_k \mathbb{1}_2$, transforms the covariance matrix (D3) to

$$\sigma' = \mathcal{S} \sigma \mathcal{S}^\top = \begin{pmatrix} \sigma'_{ij} & \mathbf{K} \\ \mathbf{K}^\top & \sigma'_k \end{pmatrix}, \quad (\text{D12})$$

with \mathbf{K} some matrix and

$$\sigma'_{ij} = \begin{pmatrix} 1 & 0 & 0 & 0 \\ 0 & 1 & 0 & 0 \\ 0 & 0 & a_k & 0 \\ 0 & 0 & 0 & a_k \end{pmatrix}, \quad \sigma'_k = \begin{pmatrix} a_k & 0 \\ 0 & a_k \end{pmatrix}. \quad (\text{D13})$$

Following [93], we first notice that

$$-(\mathbb{J} \sigma)^2 = \mathbb{1}_6, \quad (\text{D14})$$

where we recall that \mathbb{J} is given by Eq. (40). The previous expression is not difficult to prove: the Williamson theorem ensures the existence of a symplectic matrix \mathcal{O} mapping the covariance matrix σ to the identity (for a pure state all the symplectic eigenvalues are equal to one); thus, one obtains $-(\mathbb{J} \sigma)^2 = -\mathbb{J} \mathcal{O} \mathcal{O}^\top \mathbb{J} \mathcal{O} \mathcal{O}^\top = \mathbb{1}_6$. Note that one also has $-(\mathbb{J} \sigma')^2 = \mathbb{1}_6$. Then, inserting expression (D12) in Eq. (D14) and using the fact that σ'_{ij} and σ'_k are diagonal, it is easy to

prove the following conditions for the matrix \mathbf{K} :

$$\begin{aligned} (\sigma'_{ij})^2 - J_{ij} \mathbf{K} J_k \mathbf{K}^\top &= \mathbb{1}_4, \\ (\sigma'_k)^2 - J_k \mathbf{K}^\top J_{ij} \mathbf{K} &= \mathbb{1}_2, \\ -\sigma'_{ij} \mathbf{K} + J_{ij} \mathbf{K} J_k \sigma'_k &= 0, \end{aligned} \quad (\text{D15})$$

where J_k is defined in Eq. (40) and $J_{ij} = J_i \oplus J_j$. The last condition in (D15) implies that a given coefficient $\mathbf{K}_{mn} \neq 0$ iff $(\sigma'_{ij})_{mm} = (\sigma'_k)_{mm}$, i.e., if and only if the symplectic eigenvalue on the row m of the subsystem ij matches with the one on the column n of the subsystem k . Therefore, one can rewrite expression (D12) in the form

$$\sigma' = \begin{pmatrix} \mathbb{1}_2 & 0 \\ 0 & \tilde{\sigma} \end{pmatrix}, \quad \text{with} \quad \tilde{\sigma} = \begin{pmatrix} a_k \mathbb{1}_2 & \tilde{\mathbf{K}} \\ \tilde{\mathbf{K}}^\top & a_k \mathbb{1}_2 \end{pmatrix}, \quad (\text{D16})$$

where we introduced a new 2×2 matrix $\tilde{\mathbf{K}}$. Then, noticing that $-(J_{ij} \tilde{\sigma})^2 = \mathbb{1}_4$, one obtains

$$\begin{aligned} \tilde{\mathbf{K}} J_k \tilde{\mathbf{K}}^\top &= (1 - a_k^2) J_k, \\ J_k \tilde{\mathbf{K}} J_k &= \tilde{\mathbf{K}}. \end{aligned} \quad (\text{D17})$$

The above conditions lead to

$$\tilde{\mathbf{K}} = \begin{pmatrix} a & \sqrt{\lambda^2 - a^2} \\ -\sqrt{\lambda^2 - a^2} & -a \end{pmatrix}, \quad (\text{D18})$$

where $\lambda = \sqrt{a_k^2 - 1}$. Then, given that σ is in its standard form [meaning that ε_{ik} and ε_{jk} are diagonal matrices; see Eq. (D3)] and remembering that \mathcal{S}_{ij} is given by expression (D7), one can see easily that $\tilde{\mathbf{K}}$ must be diagonal; therefore, $a = \lambda$. As a result, one finds that

$$\tilde{\sigma} = \begin{pmatrix} a_k \mathbb{1}_2 & \sqrt{a_k^2 - 1} \sigma_z \\ \sqrt{a_k^2 - 1} \sigma_z & a_k \mathbb{1}_2 \end{pmatrix}, \quad (\text{D19})$$

which exactly corresponds to the covariance matrix of a squeezed state with squeezing parameter $r_k > 0$, with $\cosh(2r_k) = a_k$ [see Eq. (77)]. This statement ends the proof: the symplectic matrix \mathcal{S} given by expression (D11), with \mathcal{S}_{ij} explicitly written in Eqs. (D7) and (D8) and $\mathcal{S}_k = \mathbb{1}_2$, indeed lead to the transformation (D1).

3. Bipartitions 02|1 and 12|0

For bipartitions $ij|k = 02|1$ and $12|0$ of modes e , the symplectic transformation (D11) involves the matrix \mathcal{S}_{ij} (with $j = 2$) given by Eq. (D7) with $\eta = -1$. Using the identity (D9), we introduce a parameter γ , such that $a = \cosh \gamma$ and $b = \sinh \gamma$, where a and b are the coefficients of the \mathcal{S}_{ij} matrix. In this case, one finds

$$\mathcal{S}_{i2} = \begin{pmatrix} -\cosh \gamma & 0 & \sinh \gamma & 0 \\ 0 & -\cosh \gamma & 0 & -\sinh \gamma \\ -\sinh \gamma & 0 & \cosh \gamma & 0 \\ 0 & \sinh \gamma & 0 & \cosh \gamma \end{pmatrix}, \quad (\text{D20})$$

with $\cosh \gamma = \cosh r_2 / \cosh r_k$, $\sinh \gamma = \sinh r_i / \cosh r_k$, computed from expressions (D10).

To this symplectic transformation $\mathcal{S}\sigma\mathcal{S}^\dagger$ at the level of the covariance matrix corresponds a Bogoliubov transformation

$$\mathbf{f} = \mathcal{T}_{\mathbf{e} \rightarrow \mathbf{f}} \mathbf{e}, \quad \text{with } \mathcal{T}_{\mathbf{e} \rightarrow \mathbf{f}} = U^\dagger \mathcal{S} U \quad (\text{D21})$$

[see Eqs. (46) and (48)]. Using the explicit expression of the symplectic matrix (D20), one finds

$$\begin{aligned} \hat{f}_i &= -\cosh \gamma \hat{e}_i + \sinh \gamma \hat{e}_j^\dagger, \\ \hat{f}_j &= -\sinh \gamma \hat{e}_i^\dagger + \cosh \gamma \hat{e}_j, \\ \hat{f}_k &= \hat{e}_k. \end{aligned} \quad (\text{D22})$$

Therefore, entanglement can be localized in the subsystem $f_2|f_k$ with $k = 0$ or 1 only through a Bogoliubov transformation which mixes annihilation and creation operators.

4. Bipartition 01|2

For the bipartition $ij|k = 01|2$ the matrix \mathcal{S}_{01} is given by Eq. (D7) with $\eta = 1$. One finds

$$\mathcal{S}_{01} = \begin{pmatrix} -\sin \theta & 0 & \cos \theta & 0 \\ 0 & -\sin \theta & 0 & \cos \theta \\ \cos \theta & 0 & \sin \theta & 0 \\ 0 & \cos \theta & 0 & \sin \theta \end{pmatrix}, \quad (\text{D23})$$

with $\cos \theta = \sinh r_0 / \sinh r_2$, $\sin \theta = \sinh r_1 / \sinh r_2$, using again the identity (D9) and expressions (D10). The associated Bogoliubov transformation

$$\mathcal{T}_{\mathbf{e} \rightarrow \mathbf{f}} = U^\dagger (\mathcal{S}_{01} \oplus \mathcal{S}_2) U \quad (\text{D24})$$

leads to the new set of operators

$$\begin{aligned} \hat{f}_0 &= -\sin \theta \hat{e}_0 + \cos \theta \hat{e}_1, \\ \hat{f}_1 &= \cos \theta \hat{e}_0 + \sin \theta \hat{e}_1, \\ \hat{f}_2 &= \hat{e}_2, \end{aligned} \quad (\text{D25})$$

where, as in the previous subsection, f_0 and f_1 are new combinations of modes e_0 and e_1 , and $f_2 = e_2$. Here there is no mixing of annihilation and creation operators, and the matrix $\mathcal{S}_{01} \oplus \mathcal{S}_2$ is unitary.

APPENDIX E: COMPUTATION OF THE FINITE-TEMPERATURE GAUSSIAN CONTANGLE

In this Appendix we explain how to obtain expression (E23) used in Eq. (108) for evaluating the Gaussian contangle at finite temperature. We could not find a derivation of this formula in the literature, and since the explicit form given in [87] appears to contain some missprints, we find it useful to give the whole proof, following the same path as in [87]. For a general (mixed or pure) two-mode Gaussian state, a measure of bipartite entanglement is given by the Gaussian contangle $G_\tau(\sigma)$ defined in Eq. (73). It has been proven in [87] that finding the infimum over pure Gaussian states amounts to minimize

$$m(x_0, x_1, x_3) = 1 + \frac{x_1^2}{\det \Gamma}, \quad (\text{E1})$$

with $\det \Gamma = x_0^2 - x_1^2 - x_3^2$, where x_0 , x_1 , and x_3 must belong to the following cones:

$$\begin{aligned} x_0 &= \frac{a+b}{2} - \sqrt{(x_1 - c_+)^2 + \left(x_3 - \frac{a-b}{2}\right)^2}, \\ x_0 &= \frac{a+b}{2d} + \sqrt{\left(x_1 + \frac{c_-}{d}\right)^2 + \left(x_3 + \frac{a-b}{2d}\right)^2}, \end{aligned} \quad (\text{E2})$$

where a , b , c_+ , and c_- are the coefficients of the covariance matrix σ written in the standard form and associated with a given two-mode Gaussian state:

$$\sigma = \begin{pmatrix} a & 0 & c_+ & 0 \\ 0 & a & 0 & c_- \\ c_+ & 0 & b & 0 \\ 0 & c_- & 0 & b \end{pmatrix}. \quad (\text{E3})$$

In Eqs. (E2), $d = ab - c_-^2$. The minimum of expression (E1) is located at the intersection of both cones (E2) [87]. Therefore, in the following, we aim at finding this intersection, which corresponds to an ellipse. To find the equation of this ellipse, we first make a change of coordinates (Lorentz boost):

$$\begin{aligned} x'_0 &= \gamma(x_0 - v x_3), \\ x'_3 &= \gamma(x_3 - v x_0), \\ x'_1 &= x_1, \end{aligned} \quad (\text{E4})$$

with

$$\begin{aligned} v &= \frac{a-b}{a+b} \frac{d+1}{d-1} \quad (<1 \text{ for } d > 1), \\ \gamma &= \frac{(a+b)(d-1)}{2\sqrt{(ad-b)(bd-a)}}. \end{aligned} \quad (\text{E5})$$

We find after simplifications:

$$\begin{aligned} (x'_0 - \alpha_1)^2 - (x'_1 - \beta_1)^2 - (x'_3 - \gamma_1)^2 &= 0, \\ (x'_0 - \alpha_2)^2 - (x'_1 - \beta_2)^2 - (x'_3 - \gamma_2)^2 &= 0, \end{aligned} \quad (\text{E6})$$

with

$$\begin{aligned} \alpha_1 &= \frac{\gamma(a-b)}{2} \left(\frac{a+b}{a-b} - v \right), \quad \beta_1 = c_+, \\ \alpha_2 &= \frac{\gamma(a-b)}{2d} \left(\frac{a+b}{a-b} + v \right), \quad \beta_2 = -\frac{c_-}{d}, \end{aligned} \quad (\text{E7})$$

and

$$\gamma_1 = \gamma_2 = -\frac{\gamma(a-b)}{d-1}. \quad (\text{E8})$$

Note that α_1 and α_2 simplify to

$$\begin{aligned} \alpha_1 &= \frac{2abd - a^2 - b^2}{2\sqrt{(ad-b)(bd-a)}}, \\ \alpha_2 &= \frac{d(a^2 + b^2) - 2ab}{2d\sqrt{(ad-b)(bd-a)}}. \end{aligned} \quad (\text{E9})$$

Let us now make another change of variables:

$$\begin{aligned} x''_0 &= x'_0 - L_+, \\ x''_1 &= x'_1 - H_+, \\ x''_3 &= x'_3 - \gamma_1 = x'_3 - \gamma_2, \end{aligned} \quad (\text{E10})$$

with

$$L_+ = \frac{\alpha_1 + \alpha_2}{2} = \frac{ab(d^2 - 1)}{2d\sqrt{(ad-b)(bd-a)}},$$

$$H_+ = \frac{\beta_1 + \beta_2}{2} = \frac{c_+d - c_-}{2d}. \tag{E11}$$

This leads to

$$(x''_0 - L_-)^2 - (x''_1 - H_-)^2 - x''_3{}^2 = 0,$$

$$(x''_0 + L_-)^2 - (x''_1 + H_-)^2 - x''_3{}^2 = 0, \tag{E12}$$

with

$$L_- = \frac{\alpha_1 - \alpha_2}{2} = \frac{\sqrt{(ad-b)(bd-a)}}{2d},$$

$$H_- = \frac{\beta_1 - \beta_2}{2} = \frac{c_+d + c_-}{2d}. \tag{E13}$$

Looking at Eqs. (E12), one sees that the changes of coordinates (E4) and (E10) make it possible to eliminate one variable (x''_3) and to symmetrize the equations. Note that both cone tops belong to the plane $x''_3 = 0$.

The intersection of the cones (E12) is now simple to find. By combining Eqs. (E12), one can first eliminate x''_3 to find the relation between x''_0 and x''_1 :

$$x''_0 = \frac{H_-}{L_-} x''_1. \tag{E14}$$

Inserting this relation in one of Eqs. (E12) yields

$$\left(1 - \frac{H_-^2}{L_-^2}\right) x''_1{}^2 + x''_3{}^2 = L_-^2 - H_-^2, \tag{E15}$$

which exactly corresponds to the equation of an ellipse. Let us define the angle θ such that

$$x''_0 = H_- \cos \theta,$$

$$x''_1 = L_- \cos \theta,$$

$$x''_3 = \sqrt{L_-^2 - H_-^2} \sin \theta. \tag{E16}$$

At this stage, we have everything needed to express Eq. (E1) only in terms of the parameter θ and coefficients of the covariance matrix. Since the Lorentz boost preserves the relations between both cones, one can find the minimum of the function

$$m(\theta) = 1 + \frac{1}{2d} [\sqrt{(ad-b)(bd-a)} \cos \theta + c_+d - c_-]^2$$

$$\times \left\{ (a^2 + b^2 + 2c_-c_+) - \cos \theta \frac{2abc_-^3 + (a^2 + b^2)c_+c_-^2 + c_-[a^2(1 - 2b^2) + b^2] - abc_+(a^2 + b^2 - 2)}{\sqrt{(ad-b)(bd-a)}} \right.$$

$$\left. + (a^2 - b^2) \sin \theta \sqrt{1 - \frac{(c_+d + c_-)^2}{(ad-b)(bd-a)}} \right\}^{-1}. \tag{E23}$$

The explicit expressions of a , b , c_+ , c_- , and $d = ab - c_-^2$ used for evaluating $G_r^{(0|2)}$ in Eq. (108) are $a = a_{2,\text{th}}$,

m in the basis (x'_0, x'_1, x'_3) , that is to say

$$m = 1 + \frac{x'_1{}^2}{x'_0{}^2 - x'_1{}^2 - x'_3{}^2}. \tag{E17}$$

Using Eqs. (E10), (E11), (E13), and (E16), one finds

$$x'_0 = H_- \cos \theta + L_+,$$

$$x'_1 = L_- \cos \theta + H_+$$

$$= \frac{1}{2d} [c_+d - c_- + \sqrt{(ad-b)(bd-a)} \cos \theta],$$

$$x'_3 = \sqrt{L_-^2 - H_-^2} \sin \theta + \gamma_1. \tag{E18}$$

This gives

$$x'_0{}^2 - x'_1{}^2 - x'_3{}^2$$

$$= \alpha_1\alpha_2 - \beta_1\beta_2 - \gamma_1^2 - 2(L_-H_+ - H_-L_+) \cos \theta$$

$$- 2\gamma_1 \sqrt{L_-^2 - H_-^2} \sin \theta. \tag{E19}$$

After some simplifications, the first right-hand side term of Eq. (E19) reads

$$\alpha_1\alpha_2 - \beta_1\beta_2 - \gamma_1^2 = \frac{a^2 + b^2 + 2c_-c_+}{2d}. \tag{E20}$$

Expanding the coefficient of $-\cos \theta$ in the second right-hand side term of Eq. (E19) leads to

$$2(L_-H_+ - H_-L_+)$$

$$= \alpha_1\beta_2 - \beta_1\alpha_2$$

$$= \{2abc_-^3 + (a^2 + b^2)c_+c_-^2 + c_-[a^2(1 - 2b^2) + b^2]$$

$$- abc_+(a^2 + b^2 - 2)\}$$

$$\times [2d\sqrt{(ad-b)(bd-a)}]^{-1}. \tag{E21}$$

The coefficient of $-\sin \theta$ in the last right-hand side term of Eq. (E19) reads

$$2\gamma_1 \sqrt{L_-^2 - H_-^2}$$

$$= -\frac{a^2 - b^2}{2d} \sqrt{1 - \frac{(c_+d + c_-)^2}{(ad-b)(bd-a)}}. \tag{E22}$$

The last step consists of inserting expressions (E20), (E21), and (E22) in Eq. (E19); then Eq. (E19) in expression (E17). This leads to the final result

$b = a_{0,\text{th}}$, $c_+ = 2|\langle \hat{c}_0 \hat{c}_2 \rangle_{\text{th}}|$, $c_- = -c_+$, and $d = a_{0,\text{th}} a_{2,\text{th}} - 4|\langle \hat{c}_0 \hat{c}_2 \rangle_{\text{th}}|^2$.

Let us finally consider the case of a pure state (i.e., the zero-temperature case) and compute the explicit expressions of the Gaussian contangles $G_\tau^{(j|2)}$ given by (79). We need to evaluate

$$G_\tau^{(j|2)} = \operatorname{arsinh}^2 \left\{ \sqrt{\min[m(\theta)] - 1} \right\}, \quad (\text{E24})$$

where $m(\theta)$ is given by Eq. (E23) and $j = 0, 1$. First, by noticing that any reduced two-mode state of a pure three-mode Gaussian state belongs to the class of GLEMS [66], expression (E23) simplifies to [87]

$$m^{\text{GLEMS}}(\theta) = 1 + \frac{(A \cos \theta + B)^2}{2d[(g^2 - 1) \cos \theta + g^2 + 1]}, \quad (\text{E25})$$

where $g = \sqrt{\det \sigma}$, with σ given by (E3), $A = c_+ d + c_-$ and $B = c_+ d - c_-$. Using our notations and the explicit expres-

sion of the covariance matrix written in the standard form (62), for a given bipartition $j|2$, one has $a = a_2$, $b = a_j$, $c_+ = -c_- = \sqrt{a_j - 1} \sqrt{a_2 + 1}$, $d = g = a_k$; we recall that $j = 0$ or 1 and that the remaining (third) mode (1 or 0) is denoted as k . One proves in this case that the minimum over θ in expression (E25) is reached when $\theta = \theta^*$, with [87]

$$\cos \theta^* = -1 + \frac{2}{1 + a_k}. \quad (\text{E26})$$

Inserting this expression in Eq. (E25) leads to

$$m^{\text{GLEMS}}(\theta^*) = \left(\frac{-1 + 2a_j + a_k}{1 + a_k} \right)^2. \quad (\text{E27})$$

Using this result in Eq. (E24) and remembering that $a_j + a_k = a_2 + 1$ yields immediately expressions (80).

-
- [1] W. G. Unruh, Experimental Black-Hole Evaporation? *Phys. Rev. Lett.* **46**, 1351 (1981).
- [2] T. Torres, S. Patrick, A. Coutant, M. Richartz, E. W. Tedford, and S. Weinfurter, Rotational superradiant scattering in a vortex flow, *Nat. Phys.* **13**, 833 (2017).
- [3] P. Chen and G. Mourou, Accelerating Plasma Mirrors to Investigate the Black Hole Information Loss Paradox, *Phys. Rev. Lett.* **118**, 045001 (2017).
- [4] S. Liberati, G. Tricella, and A. Trombettoni, The information loss problem: An analogue gravity perspective, *Entropy* **21**, 940 (2019).
- [5] M. J. Jacquet, S. Weinfurter, and F. König, The next generation of analogue gravity experiments, *Philos. Trans. R. Soc. London A* **378**, 20190239 (2020).
- [6] L. J. Garay, J. R. Anglin, J. I. Cirac, and P. Zoller, Sonic Analog of Gravitational Black Holes in Bose-Einstein Condensates, *Phys. Rev. Lett.* **85**, 4643 (2000).
- [7] O. Lahav, A. Itah, A. Blumkin, C. Gordon, S. Rinott, A. Zayats, and J. Steinhauer, Realization of a Sonic Black Hole Analog in a Bose-Einstein Condensate, *Phys. Rev. Lett.* **105**, 240401 (2010).
- [8] J. Steinhauer, Observation of self-amplifying Hawking radiation in an analogue black-hole laser, *Nat. Phys.* **10**, 864 (2014).
- [9] J. Steinhauer, Observation of quantum Hawking radiation and its entanglement in an analogue black hole, *Nat. Phys.* **12**, 959 (2016).
- [10] J. R. M. de Nova, K. Golubkov, V. I. Kolobov, and J. Steinhauer, Observation of thermal Hawking radiation and its temperature in an analogue black hole, *Nature (London)* **569**, 688 (2019).
- [11] V. I. Kolobov, K. Golubkov, J. R. Muñoz de Nova, and J. Steinhauer, Observation of stationary spontaneous Hawking radiation and the time evolution of an analogue black hole, *Nat. Phys.* **17**, 362 (2021).
- [12] U. Leonhardt, T. Kiss, and P. Öhberg, Theory of elementary excitations in unstable Bose-Einstein condensates and the instability of sonic horizons, *Phys. Rev. A* **67**, 033602 (2003).
- [13] J. Macher and R. Parentani, Black-hole radiation in Bose-Einstein condensates, *Phys. Rev. A* **80**, 043601 (2009).
- [14] A. Recati, N. Pavloff, and I. Carusotto, Bogoliubov theory of acoustic Hawking radiation in Bose-Einstein condensates, *Phys. Rev. A* **80**, 043603 (2009).
- [15] P.-E. Larré, A. Recati, I. Carusotto, and N. Pavloff, Quantum fluctuations around black hole horizons in Bose-Einstein condensates, *Phys. Rev. A* **85**, 013621 (2012).
- [16] M. Isoard and N. Pavloff, Departing from Thermality of Analogue Hawking Radiation in a Bose-Einstein Condensate, *Phys. Rev. Lett.* **124**, 060401 (2020).
- [17] J. Drori, Y. Rosenberg, D. Bermudez, Y. Silberberg, and U. Leonhardt, Observation of Stimulated Hawking Radiation in an Optical Analogue, *Phys. Rev. Lett.* **122**, 010404 (2019).
- [18] L.-P. Euvé, S. Robertson, N. James, A. Fabbri, and G. Rousseaux, Scattering of Co-Current Surface Waves on an Analogue Black Hole, *Phys. Rev. Lett.* **124**, 141101 (2020).
- [19] L.-P. Euvé, F. Michel, R. Parentani, T. G. Philbin, and G. Rousseaux, Observation of Noise Correlated by the Hawking Effect in a Water Tank, *Phys. Rev. Lett.* **117**, 121301 (2016).
- [20] J. R. M. de Nova, F. Sols, and I. Zapata, Violation of Cauchy-Schwarz inequalities by spontaneous Hawking radiation in resonant boson structures, *Phys. Rev. A* **89**, 043808 (2014).
- [21] X. Busch, I. Carusotto, and R. Parentani, Spectrum and entanglement of phonons in quantum fluids of light, *Phys. Rev. A* **89**, 043819 (2014).
- [22] X. Busch and R. Parentani, Quantum entanglement in analogue Hawking radiation: When is the final state nonseparable?, *Phys. Rev. D* **89**, 105024 (2014).
- [23] S. Finazzi and I. Carusotto, Entangled phonons in atomic Bose-Einstein condensates, *Phys. Rev. A* **90**, 033607 (2014).
- [24] D. Boiron, A. Fabbri, P.-E. Larré, N. Pavloff, C. I. Westbrook, and P. Ziñ, Quantum Signature of Analog Hawking Radiation in Momentum Space, *Phys. Rev. Lett.* **115**, 025301 (2015).
- [25] J. R. M. de Nova, F. Sols, and I. Zapata, Entanglement and violation of classical inequalities in the Hawking radiation of flowing atom condensates, *New J. Phys.* **17**, 105003 (2015).
- [26] A. Fabbri and N. Pavloff, Momentum correlations as signature of sonic Hawking radiation in Bose-Einstein condensates, *SciPost Phys.* **4**, 019 (2018).

- [27] A. Coutant and S. Weinfurter, Low-frequency analogue Hawking radiation: The Bogoliubov-de Gennes model, *Phys. Rev. D* **97**, 025006 (2018).
- [28] S. Giovanazzi, Entanglement Entropy and Mutual Information Production Rates in Acoustic Black Holes, *Phys. Rev. Lett.* **106**, 011302 (2011).
- [29] B. Horstmann, R. Schützhold, B. Reznik, S. Fagnocchi, and J. I. Cirac, Hawking radiation on an ion ring in the quantum regime, *New J. Phys.* **13**, 045008 (2011).
- [30] D. E. Bruschi, N. Friis, I. Fuentes, and S. Weinfurter, On the robustness of entanglement in analogue gravity systems, *New J. Phys.* **15**, 113016 (2013).
- [31] M. J. Jacquet and F. Koenig, The influence of spacetime curvature on quantum emission in optical analogues to gravity, *SciPost Phys. Core* **3**, 5 (2020).
- [32] L. P. Pitaevskii and S. Stringari, *Bose-Einstein Condensation and Superfluidity*, International Series of Monographs on Physics (Oxford University Press, Oxford, 2016).
- [33] C. Menotti and S. Stringari, Collective oscillations of a one-dimensional trapped Bose-Einstein gas, *Phys. Rev. A* **66**, 043610 (2002).
- [34] M. Olshani, Atomic Scattering in the Presence of an External Confinement and a Gas of Impenetrable Bosons, *Phys. Rev. Lett.* **81**, 938 (1998).
- [35] R. Balbinot, A. Fabbri, S. Fagnocchi, A. Recati, and I. Carusotto, Nonlocal density correlations as a signature of Hawking radiation from acoustic black holes, *Phys. Rev. A* **78**, 021603(R) (2008).
- [36] I. Carusotto, S. Fagnocchi, A. Recati, R. Balbinot, and A. Fabbri, Numerical observation of Hawking radiation from acoustic black holes in atomic Bose-Einstein condensates, *New J. Phys.* **10**, 103001 (2008).
- [37] I. Zapata, M. Albert, R. Parentani, and F. Sols, Resonant Hawking radiation in Bose-Einstein condensates, *New J. Phys.* **13**, 063048 (2011).
- [38] A. Parola, M. Tettamanti, and S. L. Cacciatori, Analogue Hawking radiation in an exactly solvable model of BEC, *Europhys. Lett.* **119**, 50002 (2017).
- [39] W. G. Unruh, Sonic analogue of black holes and the effects of high frequencies on black hole evaporation, *Phys. Rev. D* **51**, 2827 (1995).
- [40] R. Brout, S. Massar, R. Parentani, and P. Spindel, Hawking radiation without trans-Planckian frequencies, *Phys. Rev. D* **52**, 4559 (1995).
- [41] S. Corley and T. Jacobson, Hawking spectrum and high frequency dispersion, *Phys. Rev. D* **54**, 1568 (1996).
- [42] J.-P. Blaizot and G. Ripka, *Quantum Theory of Finite Systems* (MIT Press, Cambridge, MA, 1986).
- [43] A. L. Fetter, Theory of a dilute low-temperature trapped Bose condensate, in *Bose-Einstein Condensation in Atomic Gases, Proceedings of the International School "Enrico Fermi," Course CXL*, edited by M. Inguscio, S. Stringari, and C. E. Wieman (IOS Press, Amsterdam, 1999), pp. 201–263.
- [44] C. Barceló, L. J. Garay, and G. Jannes, Two faces of quantum sound, *Phys. Rev. D* **82**, 044042 (2010).
- [45] S. J. Robertson, The theory of Hawking radiation in laboratory analogues, *J. Phys. B: At. Mol. Opt. Phys.* **45**, 163001 (2012).
- [46] A. Fabbri and J. Navarro-Salas, *Modeling Black Hole Evaporation* (Imperial College Press, London, 2005).
- [47] R. Balian and E. Brézin, Nonunitary Bogoliubov transformations and extension of Wick's theorem, *Nuovo Cimento B* **64**, 37 (1969).
- [48] S. W. Hawking, Black hole explosions?, *Nature (London)* **248**, 30 (1974).
- [49] S. W. Hawking, Particle creation by black holes, *Commun. Math. Phys.* **43**, 199 (1975).
- [50] B. S. DeWitt, Quantum field theory in curved spacetime, *Phys. Rep.* **19**, 295 (1975).
- [51] P. C. W. Davies and S. A. Fulling, Radiation from moving mirrors and from black holes, *Proc. R. Soc. London A* **356**, 237 (1977).
- [52] R. M. Wald, On particle creation by black holes, *Commun. Math. Phys.* **45**, 9 (1975).
- [53] L. Parker, Probability distribution of particles created by a black hole, *Phys. Rev. D* **12**, 1519 (1975).
- [54] K. Takayanagi, Utilizing group property of Bogoliubov transformation, *Nucl. Phys. A* **808**, 17 (2008).
- [55] B. L. Schumaker and C. M. Caves, New formalism for two-photon quantum optics. II. Mathematical foundation and compact notation, *Phys. Rev. A* **31**, 3093 (1985).
- [56] G. S. Agarwal, *Quantum Optics* (Cambridge University Press, Cambridge, 2012).
- [57] C. Weedbrook, S. Pirandola, R. García-Patrón, N. J. Cerf, T. C. Ralph, J. H. Shapiro, and S. Lloyd, Gaussian quantum information, *Rev. Mod. Phys.* **84**, 621 (2012).
- [58] R. Simon, E. C. G. Sudarshan, and N. Mukunda, Gaussian-Wigner distributions in quantum mechanics and optics, *Phys. Rev. A* **36**, 3868 (1987).
- [59] R. Simon, N. Mukunda, and B. Dutta, Quantum-noise matrix for multimode systems: $U(n)$ invariance, squeezing, and normal forms, *Phys. Rev. A* **49**, 1567 (1994).
- [60] G. K. Giedke, Quantum information and continuous variable systems, Ph.D. thesis, Universität Linz Bibliothek, 2001.
- [61] J. Williamson, On the algebraic problem concerning the normal forms of linear dynamical systems, *Amer. J. Math.* **58**, 141 (1936).
- [62] A. Serafini, Multimode Uncertainty Relations and Separability of Continuous Variable States, *Phys. Rev. Lett.* **96**, 110402 (2006).
- [63] G. Adesso, A. Serafini, and F. Illuminati, Quantification and Scaling of Multipartite Entanglement in Continuous Variable Systems, *Phys. Rev. Lett.* **93**, 220504 (2004).
- [64] G. Adesso, A. Serafini, and F. Illuminati, Extremal entanglement and mixedness in continuous variable systems, *Phys. Rev. A* **70**, 022318 (2004).
- [65] L.-M. Duan, G. Giedke, J. I. Cirac, and P. Zoller, Inseparability Criterion for Continuous Variable Systems, *Phys. Rev. Lett.* **84**, 2722 (2000).
- [66] G. Adesso, A. Serafini, and F. Illuminati, Multipartite entanglement in three-mode Gaussian states of continuous-variable systems: Quantification, sharing structure, and decoherence, *Phys. Rev. A* **73**, 032345 (2006).
- [67] K. Mølmer, A. Perrin, V. Krachmalnicoff, V. Leung, D. Boiron, A. Aspect, and C. I. Westbrook, Hanbury Brown and Twiss correlations in atoms scattered from colliding condensates, *Phys. Rev. A* **77**, 033601 (2008).
- [68] M. Perrier, Z. Amodjee, P. Dussarrat, A. Dureau, A. Aspect, M. Cheneau, D. Boiron, and C. I. Westbrook, Thermal count-

- ing statistics in an atomic two-mode squeezed vacuum state, *SciPost Phys.* **7**, 2 (2019).
- [69] R. Horodecki, P. Horodecki, M. Horodecki, and K. Horodecki, Quantum entanglement, *Rev. Mod. Phys.* **81**, 865 (2009).
- [70] R. F. Werner, Quantum states with Einstein-Podolsky-Rosen correlations admitting a hidden-variable model, *Phys. Rev. A* **40**, 4277 (1989).
- [71] A. Peres, Separability Criterion for Density Matrices, *Phys. Rev. Lett.* **77**, 1413 (1996).
- [72] M. Horodecki, P. Horodecki, and R. Horodecki, Separability of mixed states: Necessary and sufficient conditions, *Phys. Lett. A* **223**, 1 (1996).
- [73] R. Simon, Peres-Horodecki Separability Criterion for Continuous Variable Systems, *Phys. Rev. Lett.* **84**, 2726 (2000).
- [74] S. Popescu and D. Rohrlich, Thermodynamics and the measure of entanglement, *Phys. Rev. A* **56**, R3319 (1997).
- [75] S. Hill and W. K. Wootters, Entanglement of a Pair of Quantum Bits, *Phys. Rev. Lett.* **78**, 5022 (1997).
- [76] C. H. Bennett, D. P. DiVincenzo, J. A. Smolin, and W. K. Wootters, Mixed-state entanglement and quantum error correction, *Phys. Rev. A* **54**, 3824 (1996).
- [77] B. M. Terhal, Is entanglement monogamous? *IBM J. Res. Dev.* **48**, 71 (2004).
- [78] M. Koashi and A. Winter, Monogamy of quantum entanglement and other correlations, *Phys. Rev. A* **69**, 022309 (2004).
- [79] V. Coffman, J. Kundu, and W. K. Wootters, Distributed entanglement, *Phys. Rev. A* **61**, 052306 (2000).
- [80] T. J. Osborne and F. Verstraete, General Monogamy Inequality for Bipartite Qubit Entanglement, *Phys. Rev. Lett.* **96**, 220503 (2006).
- [81] Q. Li, J. Cui, S. Wang, and G.-L. Long, Entanglement monogamy in three qutrit systems, *Sci. Rep.* **7**, 1946 (2017).
- [82] G. Adesso and F. Illuminati, Continuous variable tangle, monogamy inequality, and entanglement sharing in Gaussian states of continuous variable systems, *New J. Phys.* **8**, 15 (2006).
- [83] L. Rosales-Zárate, R. Y. Teh, B. Opanchuk, and M. D. Reid, Monogamy inequalities for certifiers of continuous-variable Einstein-Podolsky-Rosen entanglement without the assumption of Gaussianity, *Phys. Rev. A* **96**, 022313 (2017).
- [84] G. Giedke, B. Kraus, M. Lewenstein, and J. I. Cirac, Separability properties of three-mode Gaussian states, *Phys. Rev. A* **64**, 052303 (2001).
- [85] G. Vidal and R. F. Werner, Computable measure of entanglement, *Phys. Rev. A* **65**, 032314 (2002).
- [86] M. M. Wolf, G. Giedke, O. Krüger, R. F. Werner, and J. I. Cirac, Gaussian entanglement of formation, *Phys. Rev. A* **69**, 052320 (2004).
- [87] G. Adesso and F. Illuminati, Gaussian measures of entanglement versus negativities: Ordering of two-mode Gaussian states, *Phys. Rev. A* **72**, 032334 (2005).
- [88] T. Hiroshima, G. Adesso, and F. Illuminati, Monogamy Inequality for Distributed Gaussian Entanglement, *Phys. Rev. Lett.* **98**, 050503 (2007).
- [89] I. Klich and L. Levitov, Quantum Noise as an Entanglement Meter, *Phys. Rev. Lett.* **102**, 100502 (2009).
- [90] G. Giedke, M. M. Wolf, O. Krüger, R. F. Werner, and J. I. Cirac, Entanglement of Formation for Symmetric Gaussian States, *Phys. Rev. Lett.* **91**, 107901 (2003).
- [91] A. Serafini, F. Illuminati, and S. D. Siena, Symplectic invariants, entropic measures and correlations of Gaussian states, *J. Phys. B: At. Mol. Opt. Phys.* **37**, L21 (2004).
- [92] D. Walls and G. J. Milburn, *Quantum Optics* (Springer-Verlag, Berlin, 2008).
- [93] A. Botero and B. Reznik, Modewise entanglement of Gaussian states, *Phys. Rev. A* **67**, 052311 (2003).
- [94] M. Isoard, Theoretical study of quantum correlations and nonlinear fluctuations in quantum gases, Ph.D. thesis, Université Paris-Saclay, 2020.
- [95] A. Serafini, G. Adesso, and F. Illuminati, Unitarily localizable entanglement of Gaussian states, *Phys. Rev. A* **71**, 032349 (2005).
- [96] D. Daems, F. Bernard, N. J. Cerf, and M. I. Kolobov, Tripartite entanglement in parametric down-conversion with spatially structured pump, *J. Opt. Soc. Am. B* **27**, 447 (2010).
- [97] N. D. Birrell and P. C. W. Davies, *Quantum Fields in Curved Space* (Cambridge University Press, Cambridge, 1982).
- [98] T. Aoki, N. Takei, H. Yonezawa, K. Wakui, T. Hiraoka, A. Furusawa, and P. van Loock, Experimental Creation of a Fully Inseparable Tripartite Continuous-Variable State, *Phys. Rev. Lett.* **91**, 080404 (2003).
- [99] A. S. Villar, M. Martinelli, C. Fabre, and P. Nussenzveig, Direct Production of Tripartite Pump-Signal-Idler Entanglement in the Above-Threshold Optical Parametric Oscillator, *Phys. Rev. Lett.* **97**, 140504 (2006).
- [100] A. S. Coelho, F. A. S. Barbosa, K. N. Cassemiro, A. S. Villar, M. Martinelli, and P. Nussenzveig, Three-color entanglement, *Science* **326**, 823 (2009).
- [101] D. N. Page, Particle emission rates from a black hole: Massless particles from an uncharged, nonrotating hole, *Phys. Rev. D* **13**, 198 (1976).
- [102] P. R. Anderson, A. Fabbri, and R. Balbinot, Low frequency gray-body factors and infrared divergences: Rigorous results, *Phys. Rev. D* **91**, 064061 (2015).
- [103] A. Fabbri, R. Balbinot, and P. R. Anderson, Scattering coefficients and gray-body factor for 1D BEC acoustic black holes: Exact results, *Phys. Rev. D* **93**, 064046 (2016).
- [104] M. F. Linder, R. Schützhold, and W. G. Unruh, Derivation of Hawking radiation in dispersive dielectric media, *Phys. Rev. D* **93**, 104010 (2016).
- [105] P. Deuar, A. G. Sykes, D. M. Gangardt, M. J. Davis, P. D. Drummond, and K. V. Kheruntsyan, Nonlocal pair correlations in the one-dimensional Bose gas at finite temperature, *Phys. Rev. A* **79**, 043619 (2009).
- [106] J. Steinhauer, Measuring the entanglement of analogue Hawking radiation by the density-density correlation function, *Phys. Rev. D* **92**, 024043 (2015).
- [107] Y. Nambu and Y. Osawa, Tripartite entanglement of Hawking radiation in dispersive model, *Phys. Rev. D* **103**, 125007 (2021).
- [108] I. Agullo, A. J. Brady, and D. Kranas, Stimulating the quantum aspects of an optical analog white-black hole, [arXiv:2107.10217](https://arxiv.org/abs/2107.10217) [gr-qc].
- [109] X. Ma and W. Rhodes, Multimode squeeze operators and squeezed states, *Phys. Rev. A* **41**, 4625 (1990).
- [110] M. Visser, Acoustic black holes: Horizons, ergospheres and Hawking radiation, *Classical Quantum Gravity* **15**, 1767 (1998).